Chromosome segregation errors: a double-edged sword

Aniek Janssen

ISBN: 9789088915383

Printed by: Proefschriftmaken.nl || Uitgeverij BOXPress

Published by: Uitgeverij BOXPress, ‘s-Hertogenbosch

Cover: An immunofluorescence image is shown of a cancer cell that missegregates its chromosomes (blue) in telophase upon treatment with an Mps1 inhibitor

Chromosome segregation errors: a double-edged sword

Ongelijke chromosoomverdeling: een tweezijdig fenomeen

(met een samenvatting in het Nederlands)

Proefschrift

ter verkrijging van de graad van doctor aan de Universiteit Utrecht op gezag van de rector magnificus, prof.dr. G.J. van der Zwaan, ingevolge het besluit van het college voor promoties in het openbaar te verdedigen op donderdag 20 december 2012 des middags te 12.45 uur

door

Aniek Janssen

geboren op 19 april 1983 te ’s-Hertogenbosch

Promotoren: Prof.dr. R.H. Medema

Prof.dr. G.J.P.L. Kops

Get up, stand up, stand up for your right
Get up, stand up, don't give up the fight
Get up, stand up. Life is your right
Don't give up the fight

-Bob Marley-

Contents

Chapter 1

General Introduction

Aniek Janssen[1,2,] and René H. Medema[2]

[1] Department of Medical Oncology and Cancer Genomics Center, University Medical Center Utrecht, Universiteitsweg 100, 3584 CG, Utrecht, the Netherlands

[2] Division of Cell Biology, Netherlands Cancer Institute, Plesmanlaan 121, 1066 CX, Amsterdam, the Netherlands

Accepted in adapted form for publication in Oncogene

1. Introduction

1.1 The cell cycle

Cell division, the generation of two new daughter cells from one mother cell, is an essential process for reproduction and development of organisms, but also for the maintenance and regeneration of vital tissues in the body. Eukaryotic cells, with the exception of germ cells, divide in a process called mitosis. Before two new daughter cells can be generated, mother cells need to have duplicated their DNA and essential organelles, processes which are being fulfilled in the phases preceding the mitotic phase. These phases are called the G1, S and G2 phase of the cell cycle, together termed interphase, and are sequentially initiated due to the activity of several Cyclin-dependent kinases (CDK) in complex with Cyclins, the main driving forces behind the cell cycle (reviewed in [1]). The G1, or Gap1, phase ensures that a cell has obtained sufficient size and enough growth signals to enter the synthesis or S phase, in which the DNA gets duplicated during a process called replication. The following G2, or Gap2, phase has evolved to give the cell time to repair breaks in the newly synthesized DNA before it irreversibly enters mitosis. Mitosis in mammalian cells depends on the essential activity of Cyclin B1-Cdk1 and mitotic entry will only occur in the presence of sufficient activity of this major mitotic regulator (reviewed in [2]).

1.2 Mitosis

The DNA of the eukaryotic cell is orderly folded and packed into big structures called chromosomes, which are being kept close together in the nucleus of a cell. Each duplicated chromosome, or chromatid, remains associated with its sister chromatid from the moment of synthesis in S phase until the end of mitosis. This association is accomplished by the work of cohesins, multi-protein complexes that are thought to form a ring around the DNA strands of the two sisters[3]. The different mitotic phases together ensure the proper distribution of sister chromatids over the two daughter cells (Fig.1). Mitosis starts with breakdown of the nuclear envelope and condensation of the paired chromosomes in prophase. Subsequently, chromosomes need to congress to the cell's equator (also known as the metaphase plate) in prometaphase, and remain there in metaphase until the sister chromatids can be separated to opposite sides of the cell in anaphase. Finally, to ensure full cell division, the process of cytokinesis separates the

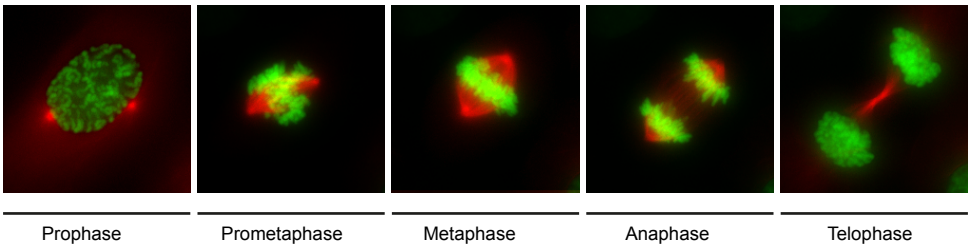

Figure 1. Mitotic phases
Mitosis starts with nuclear envelope breakdown and chromosome condensation in prophase. Bipolar spindle assembly is initiated when centrosomes move apart and start to nucleate microtubules. In prometaphase, the condensed sister chromatids each capture microtubules coming from opposite poles, which eventually leads to alignment of the chromosomes in between the two spindle poles during metaphase. Upon biorientation of all sister chromatids, anaphase is initiated and the cell's cytoplasm is divided in two compartments upon cleavage furrow ingression in telophase. Representative time-lapse images are shown of a human osteosarcoma cell line stably expressing tubulin-RFP (red) and Histone-2B-GFP (green).

cytoplasms and pinches off the membrane in between the two daughter cells during abscission. In order to align chromosomes in such a way that each daughter cell will receive the same amount of DNA, the mitotic spindle has evolved, which is a structure mainly originating from two microtubule organizing centers at opposite sides of the cell. The mitotic spindle has a bipolar conformation and primarily consists of dynamic a- and b-tubulin polymers, called microtubules (MTs), which are associated with a variety of microtubule-associated proteins (reviewed in [4]). To create chromosome-microtubule attachments and to ensure congression of the chromosomes to the metaphase plate, MTs rapidly polymerize and depolymerize during prophase and prometaphase to ultimately achieve attachments with their plus-ends at specific, highly conserved sites on the chromosomes, called kinetochores. The initial proposed model of 'search and capture' [5], in which kinetochores randomly capture MTs originating from centrosomes (the mammalian microtubule organizing centers), has been extended with the knowledge that MT growth is strongly biased towards chromatin due to the presence of a Ran-GTP gradient [6] and the fact that MTs can also be directly nucleated from chromatin [7] and kinetochores [8] . On top of that, a gradient of Aurora B kinase activity around the chromatin is thought to also help in stabilizing MTs in the vicinity of chromatin [9].

2. Molecular mechanisms controlling mitotic progression

2.1 Centromeres, Kinetochores and Microtubule attachments

Kinetochores are big proteinaceous structures [10] , of which most of the proteins are not present during interphase and are only being assembled into the kinetochore upon mitotic entry and disassembled upon mitotic exit (Fig.2). Kinetochores are built up at specific loci on the chromatin, called centromeres, which, in humans, are long stretches of repetitive heterochromatic a-satellite DNA [11]. Centromeres contain non-coding DNA sequences ranging in size from ~125 base pairs in the budding yeast Saccharomyces cerevisiae to several tens of megabases in higher eukaryotes, such as humans [11]. Although eukaryotic centromeric DNA does not show any sequence or size conservation between species, the functionality has been conserved, i.e. marking the region where a Histone H3 variant, named CENP-A in vertebrates[12], incorporates into the nucleosomes. CENP-A is thought to be the epigenetic mark that determines centromere identity [13] and forms specific nucleosomes that serve as a building block for kinetochore formation. CENP-A nucleosomes are essential and, in some organisms, sufficient for formation of a proper centromere and kinetochore[14-17]. Since centromeric DNA was found to also consist of Histone H3 containing nucleosomes [18], a model originated in which centromeric DNA adapts a 3D conformation where only CENP-A nucleosomes are present on the side of the sister chromatid facing the spindle pole and as such create an interface for inner-kinetochore formation only on the outside of the chromatid which is facing the spindle poles [18]. The vertebrate inner kinetochore consists of multiple proteins that are closely associated to centromeric DNA and CENP-A throughout the cell cycle. Together these proteins form the Constitutive Centromere Associated Network (CCAN), which is required for proper kinetochore formation (reviewed in[19,20]). CENP-C and the CENP-W/T complex, which are part of the CCAN, have been shown to be able to form ectopic kinetochores in human cells, indicating that they function as core kinetochore assembly factors[21]. Recently, budding yeast homologues of the CCAN proteins CENP-T and CENP-W were identified, revealing that the proteins that make up the inner kinetochore structure are evolutionary conserved[22,23].

The CCAN network is thought to create a stable environment for mitotic assembly of the outer kinetochore [20,24], which consists of proteins that are important for the interaction with the plus-ends of spindle microtubules (MTs) such as the MT-binding KMN network, consisting of Knl1[25], the Mis12 complex [26] and the Ndc80 complex[27-30]. The KMN network is an evolutionary conserved network [31] of which only Knl-1 and the Ndc80 complex have direct MT-binding capacity, but the complete network acts synergistic in acquiring full MT binding capacity[31]. Another outer kinetochore component that directly controls the kinetochore microtubule interaction is the recently identified SKA complex in human cells[32-37], of which it is hypothesized that it might function as the ring-shaped Dam1 complex found at budding yeast kinetochores[38-40]. The kinesin CENP-E is another important MT-binding protein identified at the outer kinetochore and is required to move polar chromosomes to the spindle equator and promote proper kinetochore-

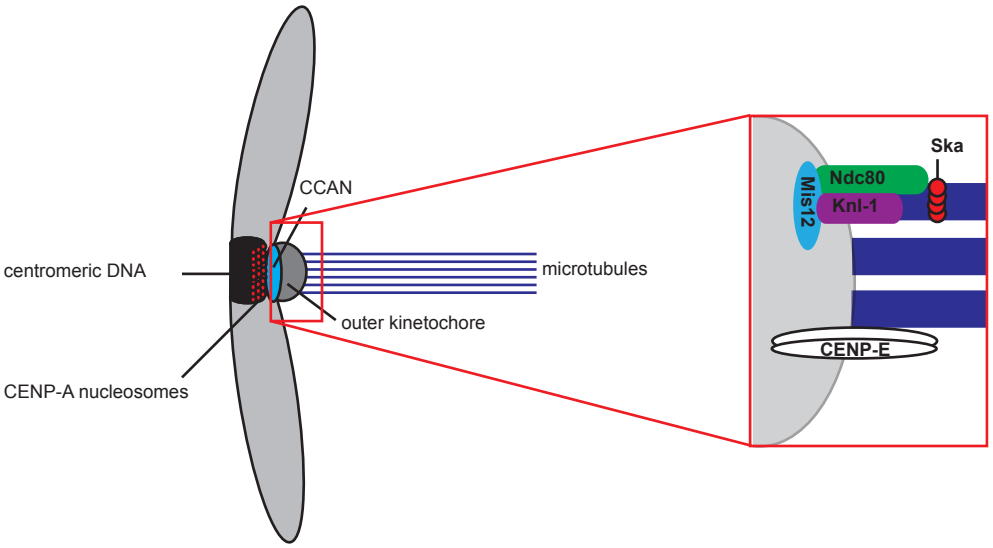

Figure 2. Build-up of centromeres and kinetochores
Centromeres are defined by the presence of CENP-A nucleosomes and form the kinetochore assembly sites on chromosomes. Kinetochores consist of an inner- and outer compartment, of which the inner kinetochore is made up of CCAN proteins and the outer kinetochore recruits a variety of microtubule binding proteins to establish stable microtubule interactions.

MT attachments[41,42]. Besides these MT-binding proteins that are thought to be directly responsible to create stable kinetochore-microtubule interactions, over 80 other outer kinetochore proteins have been identified over the years (reviewed in[19,43]). These include other microtubule-binding proteins, such as CLIP-170 [44,45], MCAK [46], Dynein [47,48]and CLASPs [49], but also non-microtubule-binding proteins such as Plk1 [50] , CENP-F [51] and all mitotic checkpoint proteins important in monitoring the kinetochore-MT attachment status (see below section 2.3). All these kinetochore proteins together create an environment that allows efficient chromosome alignment at the metaphase plate and eventually proper chromosome segregation.

2.2 Error-correction

To ensure proper chromosome segregation in anaphase, sister-kinetochores of each chromatid pair should be facing opposite spindle poles, also referred to as bi-orientation. The above described MT-nucleating and capturing events often result in 'aberrant' attachments [52], which are attachments in

which sister-chromatids are not properly bi-oriented. Several erroneous attachments can occur, such as monotelic or syntelic, in which only one or both sister kinetochores respectively are attached to one spindle pole, or merotelic attachments resulting in one sister kinetochore being attached to both spindle poles (Fig.3). To prevent anaphase onset in the presence of these aberrant attachments, an error-correction machinery has evolved in which the mitotic kinase Aurora B plays an essential role[53-56]. Aurora B is part of the chromosomal passenger complex (CPC), which localizes to the centromeric region of the kinetochore during (pro) metaphase (reviewed in [57]) and phosphorylates many (outer) kinetochore substrates, which eventually results in destabilization of erroneous kinetochore-MT interactions [53-56].

In some cases, substrate phosphorylation by Aurora B affects the static interactions between microtubule-binding proteins and the MT interface, such as phosphorylation of members of the KMN network [58-60] or CENP-E[61]. Phosphorylation of the microtubule depolymerase MCAK, however, is thought to directly affect its depolymerizing activity[62-65].

The model for Aurora B-dependent error-correction is that establishment of tension in between two sister kinetochores upon MT-binding will spatially restrict Aurora B phosphorylation of outer kinetochore substrates[66]. Bi-orientation and tension across sisters will promote the dephosphorylation of Aurora B substrates and will eventually result in stable kinetochore-MT attachments[60,61,67]. Erroneous attachments, such as merotelic or syntelic attachments, lead to incomplete establishment of tension in between the two sister-kinetochores, which gives Aurora B the opportunity to phosphorylate its targets and destabilize the faulty kinetochore-MT interactions [64,66].

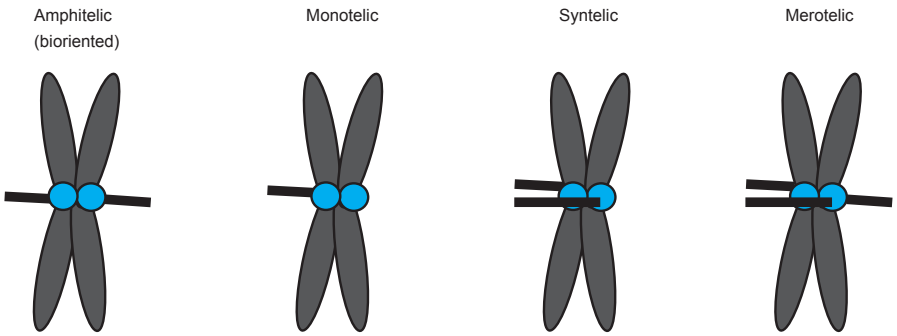

Figure 3. Schematic representation of the various types of kinetochore microtubule interactions
Normal (amphitelic) bi-orientation is achieved when each sister-kinetochore is attached to microtubules coming from one spindle pole. Erroneous interactions occur when one sister kinetochore is unattached (monotely), attached to two poles (merotely), or when both sister kinetochores are attached to one pole (syntely).

2.3 Monitoring attachment status: the Mitotic Checkpoint

Sophisticated mechanisms have evolved to organize kinetochore-MT attachments in such a way that proper bi-orientation of sister chromatid pairs is being achieved during every mitotic cycle. To allow time to fulfill these dynamic processes, the mitotic checkpoint or spindle assembly checkpoint (SAC) has evolved (Fig.4). From the initial observations that anaphase was only initiated after all kinetochores were attached to MTs [68,69] and that laser-ablating the last unattached kinetochore resulted in anaphase onset [70], it was postulated that the mitotic checkpoint consists of an inhibitory signal that originates from unattached kinetochores and delays anaphase progression [70]. A couple of

years before this experimental evidence was published, some of the components that are responsible for this mitotic checkpoint signal were identified by two independent screens for budding yeast mutants that were unable to delay mitosis in the presence of microtubule destabilizing drugs [71,72]. These identified genes included Bub1, Bub3 [71], MAD1, MAD2 and MAD3 [72] and were later found to be conserved in higher eukaryotes [73-76]. All checkpoint components are recruited to outer kinetochores in prometaphase, where they monitor MT attachment status and delay anaphase onset through inhibition of the E3 ubiquitin ligase activity of the Anaphase Promoting Complex or Cyclosome (APC/C). The APC/C is a 1.5-MDa complex which ubiquitinates various substrates important for cell cycle progression (reviewed in [77]) by collaborating with three E2 enzymes, UbcH5, UbcH10 and Ube2S [78-81]. The unattached kinetochore is thought to function as a catalytic platform for the generation of the mitotic checkpoint complex (MCC) [82], consisting of Mad2, Bub3 and the pseudo-kinase BubR1 [83] (Mad3 in budding yeast), which directly binds and sequesters the APC/C co-activator Cdc20 [84-94]. By binding Cdc20, the MCC inhibits the ubiquitination of two APC/C substrates, Securin and Cyclin B1, whose degradation by the 26S proteasome is necessary for cells to progress into anaphase [95-99] (Fig.4). The protease Separase is required to separate sister chromatids in anaphase by cleaving the cohesin complex present in between both DNA strands [99,100] and is kept inactive by its chaperone Securin [101]. Therefore, degradation of Securin in anaphase is required to allow cohesin cleavage and subsequent separation of sister chromatids to opposite sides of the cell[98-100]. Degradation of Cyclin B1 results in inactivation of the major mitotic regulator Cyclin B1- Cdk1, an event that is essential for mitotic exit[96,97]. Unattached kinetochores catalyze MCC formation through the presence of a hetero-tetrameric complex consisting of MAD2 and MAD1 [102,103] (Fig.4). MAD2 homodimerization at this kinetochore-bound complex induces a conformational change in the inactive cytoplasmic form of MAD2, called open- or O-MAD2, to the active form, termed closed- or C-MAD2 [104,105]. This closed form of MAD2 is capable of forming the MCC complex with BubR1, Bub3 and Cdc20 and therefore to inhibit APC/C activity [106]. BubR1 binds to the MCC through its conserved N-terminal KEN-box [107-110], which is a motif specifically recognized by Cdc20 [111]. Another KEN-Box motif in BubR1, more centrally located, can also directly bind the APC/C and is thought to act as a pseudosubstrate [107,108,110]. The final component of the MCC is Bub3, which is, besides MCC binding [91], required for kinetochore localization of both BubR1 and Bub1 [76].

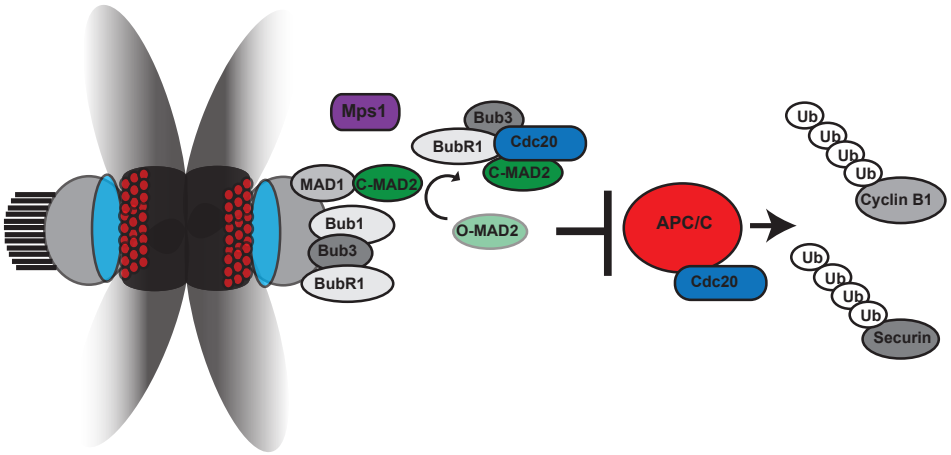

1

Figure 4. Mitotic checkpoint signaling
Mitotic checkpoint components are recruited to unattached kinetochores, thereby creating a platform for the formation of the Mitotic Checkpoint Complex (MCC) consisting of MAD2, BubR1 and Bub3, which inhibits APC/C dependent Cyclin B1 and Securin degradation through sequestration of Cdc20.

Non-MCC members, but important mitotic checkpoint proteins, are the kinases Bub1 and Mps1 (Mps1 will be discussed in more detail in section 2.4). Although conflicting data have been published on the role of Bub1 kinase activity in checkpoint activation [112-114], the presence of Bub1 protein is required to delay anaphase onset in the presence of unattached kinetochores [74,115]. In contrast to this, Mps1 kinase activity is absolutely essential for mitotic checkpoint function [116-119]. It was recently shown that Mps1 in both yeast and human cells phosphorylates Knl1 and thereby promotes Bub3 and Bub1 binding to kinetochores [120-122]. Moreover, it has been found to be required for localization of Mad1 and Mad2 to unattached kinetochores and is therefore thought to be upstream of MCC formation [118,119,123-125]. When all kinetochores are attached, the mitotic checkpoint is silenced and the cell exits mitosis [70]. Several mechanisms for mitotic checkpoint silencing have been described, one of which is dynein-dependent kinetochore-stripping of checkpoint proteins [48,126]. By walking to the minus-end of the kinetochore-MTs and simultaneously binding checkpoint proteins, dynein can reduce MCC formation. Secondly, phosphatases could help in silencing the checkpoint by counteracting phosphorylation events [127]. Thirdly, p31^{comet}-dependent inactivation of the checkpoint by structural mimicry and direct binding to C-MAD2 has been shown to be important as well [128-130]. p31^{comet} is thought to silence the checkpoint both dependently [131] and independently [132-134] of its kinetochore localization. Finally, Cdc20 ubiquitination could also contribute to MCC disassembly [132,135], although this remains controversial since Cdc20 ubiquitination has also been described to aid in keeping APC/C activity low [136].

2.4 Mps1 (Monopolar spindle 1)

Originally identified as a kinase essential for spindle pole body duplication in budding yeast [137-139], Mps1 kinase was soon after found to be important for mitotic checkpoint signaling as well [140,141]. Although its role in mitotic checkpoint functioning has been found to be conserved in higher eukaryotes [124,142,143], the effect of Mps1 on spindle pole duplication remains controversial. In budding yeast, Mps1 temperature-sensitive mutants clearly result in monopolar spindle formation [137,144]. In line with this, Mps1 has been shown to localize to centrosomes [145,146] and overexpression of Mps1 in human and mouse cells resulted in overduplication of centrosomes [145-147]. However, other studies could not reproduce these effects of Mps1 on centrosome duplication as well as its centrosome localization [119,143,148]. Mps1 localizes to outer kinetochores via its N-terminus [124,148] and its protein levels are specifically increased during G2 and mitosis [142,143,149-151]. In both budding yeast and human cells, Mps1 was found to be targeted for proteasomal degradation by the APC/C [152,153]. These data all correlate with a function for Mps1 specifically during mitosis. Indeed, on top of a role in the mitotic checkpoint [117,118,123], Mps1 kinase activity has been implicated in chromosome alignment as well [116]. By phosphorylating Borealin, Mps1 indirectly stimulates Aurora B kinase activity at the kinetochore, resulting in correction of erroneous kinetochore-MT attachments [116]. Interestingly, Aurora B has also been implicated in targeting Mps1 to the kinetochore in prophase [154], which suggests that these two kinases together influence error-correction and possibly also mitotic checkpoint activity [154,155]. Depletion of the outer kinetochore proteins Prp4 [156] or the Ndc80 complex member Hec1 [125,148,154] affects Mps1 localization to the kinetochores, which indicates that these proteins might function as its kinetochore receptors. Mps1 exchanges very rapidly at the kinetochores [157] and has been shown to promote MCC formation already in interphase, when kinetochores are not fully matured [119]. This indicates that Mps1 kinetochore localization might not be required for full checkpoint activity. However, stable targeting of Mps1 to the kinetochore has been shown to result in sustained mitotic checkpoint activity [158], which shows that Mps1 at kinetochores most likely does play a role in acquiring checkpoint activity and that release from kinetochores is necessary to exit mitosis [158].

Besides Borealin and Knl1 [116,120-122], other downstream targets of Mps1 have been described as well, but many remain controversial: some substrates have been implicated in the role of Mps1 in spindle pole duplication (reviewed in [159]), others, such as Ndc80, Mad1 or CENP-E have, until now, been identified as Mps1 substrates in only one model organism [141,160,161]. Mps1 has also been implicated in activating DNA damage signaling through phosphorylation of Chk2 [162], BLM [163] and p53 [164]. In addition, DNA damage-induced expression of p53 was also shown to suppress expression of various mitotic checkpoint proteins, including Mps1 [165]. This is in contrast to DNA damage-induced Chk2 activation, which resulted in stabilization of Mps1 protein [166]. Although a link could exist between Mps1 and the DNA damage checkpoint response, clear significance and direct mechanisms remain unknown. Contrary to its downstream substrates, auto-phosphorylation of Mps1 has been described in multiple organisms on conserved residues (reviewed in [167]). The catalytic activity of Mps1 is restricted to its C-terminus [123,168,169] and although *in vitro* reactivity towards tyrosine residues has been observed [168,170], only threonine or serine residues were found to be phosphorylated by Mps1 *in vivo* [170-175]. Threonine676 and Threonine686, two of the identified auto-phosphorylation sites on hMps1, reside in the catalytic C-terminus [170-172] and were found to play an important role in acquiring full kinase activity [170-172]. Substitution of Thr686 to alanine renders Mps1 almost completely kinase dead [170-172], whereas substituting Thr676 to an alanine resulted in a 1.4- [170] to 5-fold [172] decrease in hMps1 kinase activity. Interestingly, expressing the T676A mutant of Mps1 in human cells affected mitotic checkpoint function and resulted in mild defects in mitotic progression [171,172]. Since only structures of inactive Mps1 protein have been resolved [123,168,169,176], it remains difficult to determine how these phosphorylations precisely affect its catalytic activity *in vivo*.

2.5 Cytokinesis: full separation of daughter cells

When the duplicated chromatin has moved to opposite sides of the mother cell, cytokinesis will finish cell division by partitioning the remaining cellular material into two daughter cells. Cytokinesis in animal cells is initiated during anaphase, when the mitotic spindle reorganizes into the central spindle, a dense array of overlapping microtubules in between the two DNA packs. The central spindle forms as a consequence of the decline in Cyclin B1-Cdk1 activity, which leads to stabilization of MTs and association of several microtubule-binding proteins (reviewed in [177]). MTs of the central spindle are being bundled by proteins such as PRC1 [178] and the central spindlin complex, consisting of MKLP-1 and the Rho-family GTPase-activating protein Cyk-4 [179,180]. Cyk-4 recruits the RhoGEF Ect2 to the central spindle [181], an event that is regulated through phosphorylation of Cyk-4 by polo-like kinase 1 (Plk1) [182]. PRC1 is thought to be the main docking factor for Plk1 on the spindle midzone [183], but additional binding sites have been reported as well [184]. Another important complex involved in central spindle formation is the aforementioned chromosomal passenger complex (CPC). CPC members relocalize from centromeres to the central spindle in anaphase, which requires the two kinesins MKLP-1 and MKLP-2 in mammalian cells [185,186]. The CPC functions in central spindle formation by phosphorylating PRC1 [187] and MKLP-1[16], but might also directly mediate MT-bundling by functioning as a structural component [177]. Central spindle assembly provides cues to initiate cleavage furrow formation at the plasma membrane by promoting concentration and activation of the small GTPase RhoA at the equatorial cortex [181,188,189]. The RhoA pathway induces cleavage furrow formation by stimulating the assembly of the actomyosin ring through activation of ROCK kinase [190] and nucleation of actin filaments [191-193]. Subsequent contraction of the actomyosin ring induces ingression of the plasma membrane and actual division of the cytoplasm. Although extremely important in cell division, the actual mechanism for force-generation within this contractile ring is not well understood (reviewed in [194]). Cytokinesis is completed when abscission occurs, the process in which the two plasma membranes are

completely separated. Following cleavage furrow ingression, the two daughter cells remain attached for up to several hours through an intercellular bridge that consists of remnants of the contractile ring, MTs and more than 100 other proteins [195]. Abscission can be delayed in both budding yeast and human cells by an Aurora B-dependent checkpoint that senses the presence of chromatin in the intracellular bridge [196,197]. The persistent presence of active Aurora kinase prevents abscission, so that the intercellular bridge remains intact. This way, Aurora B can inhibit the formation of tetraploid cells in human cells [196] and inhibit chromatin damage in yeast [197] when chromosomes get trapped in the cleavage furrow. In the absence of any chromatin in the intercellular bridge, abscission will be induced and result in full physical separation of the two daughter cells. The daughter cells enter the G1 phase of the subsequent cell cycle and will, if sufficient growth signals are present, proceed with another round of cell division.

3. The DNA damage response

3.1 Repair mechanisms

Chromatin is continuously being exposed to DNA damaging insults, as a result of cell-endogenous or exogenous processes. DNA damage can be the result of normal cellular metabolism, while examples of exogenous insults are cigarette smoke, x-rays or sunlight exposure. To prevent the cell from progressing through the cell cycle when its DNA is damaged, various evolutionarily conserved responses are present in cells. These responses can lead to repair of the lesion and cell cycle arrest or apoptosis when the damage is unrepairable. Several types of DNA damage have been found, each of which is repaired by a specific DNA repair mechanism. Mispaired DNA bases are repaired through mismatch repair, intra- and interstrand crosslinks by nucleotide excision repair or interstrand crosslink repair respectively, while single-strand breaks (SSB) are resolved by single-strand break repair (reviewed in [198]). Double-strand breaks (DSB) are in general being repaired by either homologous recombination (HR) or non-homologous end joining (NHEJ), although at least two other types of DSB repair pathways have been identified as well, such as alternative-NHEJ and single strand annealing (reviewed in [199]). HR is promoted by Cdk activity and is mainly active during the S and G2 phases of the cell cycle. HR is a relatively error-free repair mechanism because it uses homologous sequences on, preferably, sister chromatids to repair DSBs. NHEJ is more error prone, since it religates two broken DNA strands independent of their homology [199]. NHEJ is active throughout the cell cycle and starts with the recruitment of the Ku heterodimer (Ku70 and Ku80), that can form a ring around the site of DNA damage [200]. This heterodimer loads and activates the catalytic subunit of DNA-PK (DNA-PKcs), the kinase activity of which is essential for NHEJ to occur [201,202]. Loading of DNA-PKcs results in recruitment of the DNA ligase XRCC4/LIG4, and this promotes religation of the two broken ends [203,204]. Although various DSB repair pathways have been identified, the initial response to DSBs almost always includes activation of the ATM kinase. Double-strand breaks are first being recognized by sensors, such as the Mre11-Rad50-Nbs1 (MRN) complex, Ku70/80 and the PARP family of proteins, which poly-ADP-ribosylate DNA surrounding the break [205]. These sensors on their turn promote the recruitment and activation of ATM [206]. ATM phosphorylates H2AX on serine 139 to form γH2AX [207,208], which acts to recruit and sustain binding of a variety of other repair proteins [209], such as MDC1, which is a direct sensor of γH2AX and binds to Serine 139 through its BRCT domain [210,211]. MDC1 indirectly stabilizes ATM binding and as such allows spreading of γH2AX to form discrete foci of up to 1-2 megabases [207,212]. 53BP1, one of the more downstream components of the DNA damage signaling pathway [213] that promotes NHEJ through inhibition of HR [214-216], binds methylated DNA surrounding the DSB [217,218].

53BP1 does not depend on γH2AX for its initial recruitment [209], although its accumulation at DNA damage foci is affected when the interaction between γH2AX and MDC1 is abrogated in cells [210,212]. 53BP1 and all other repair proteins work together to control genomic stability and loss of any of these proteins could have disastrous consequences for the damaged cell and, more importantly, for the whole organism [198].

3.2 Checkpoint activation

To be able to initiate and complete DSB repair before cells divide, a signaling cascade has evolved that halts cell cycle progression, called the DNA damage checkpoint. DNA damage checkpoint activation in G1 ultimately induces the rapid stabilization and accumulation of the tumor suppressor p53. Although p53 activation is absolutely essential for G1 checkpoint maintenance, additional pathways exist in S and G2 phase that can delay cell cycle progression [219] involving degradation of cell cycle regulators such as Cdc25A and Cyclin D1. The main downstream target for transcriptional activation by p53 is the Cdk inhibitor p21, activation of which results in inhibition of G1 cell cycle progression [220]. Besides its role in H2AX phosphorylation and recruitment of repair factors, ATM is also essential for DSB-induced checkpoint activation by phosphorylating several downstream effectors, such as p53, Chk2 and MDM2. ATM phosphorylates p53 on Serine 15, resulting in stabilization of p53 and enhanced transactivation of p53 target genes [221-224]. ATM also stabilizes p53 via the activation of its downstream kinase Chk2. ATM activates Chk2 by phosphorylating it on threonine 68 [225,226] and Chk2 on its turn phosphorylates p53 on serine 20[227-229]. Serine 20 phosphorylation was shown to directly affect the binding affinity of the E3 ubiquitin ligase MDM2 to p53, therefore resulting in p53 stabilization [227-229]. Moreover, ATM can also directly phosphorylate and inhibit MDM2 [230]. Overall, ATM activation has been shown to be crucial for G1 checkpoint activation by DSBs and is therefore essential for genomic stability.

4. Genetic instability

Despite all cell cycle checkpoints that can prevent damaged cells from entering into mitosis or help to maintain chromosome segregation fidelity, tumor cells typically become genetically unstable, and continuously undergo changes in their genetic make-up [231]. These changes can range from single base substitutions to complete chromosome gains or losses.

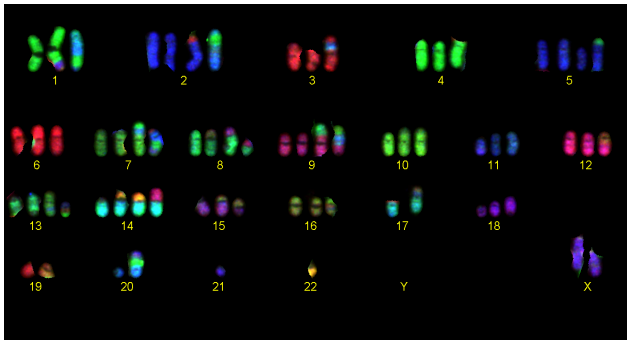

Figure 5. Typical karyotype of a cancer cell
Karyotype of a human osteosarcoma cell line (U2OS) revealing a variety of numerical and structural chromosomal abnormalities.

Two striking features of cancer cells are their abnormal chromosome number and the presence of abnormal chromosomal structures, such as inversions, duplications, deletions and fusions of two (or more) chromosomal parts, called translocations [232-236] (Fig.5). These chromosomal abnormalities in cancer cells were already identified about one century ago and it was suggested by Boveri that these abnormalities could be causal for the formation of tumors [232]. During the last decades, these genetic abnormalities have been investigated extensively and have indeed been shown to influence tumorigenesis [231,237-240].

4.1 Structural chromosomal instability

Translocations, one of the most prominent types of structural chromosomal changes, have been found in many cancer types [235]. In hematological malignancies, several translocations have been identified that contribute to specific gene fusions, which are thought to be drivers in the process of tumorigenesis [240]. The first identified translocation in human cancer was the Philadelphia chromosome [234], which results in the formation of a fusion between the BCR and Abl1 genes, and is causative in the development of chronic myeloid leukemia [241]. Some of the translocations found in cancer are balanced and homogeneously present in all tumor cells [242]. However, more often, cancer cells within a tumor display mosaic structural changes, which indicates that chromosomes continue to rearrange at a high rate in the established tumor [236,243-247]. Generally, these chromosome structure instabilities are thought to promote tumorigenesis by providing continued genetic diversification within the tumor that might help it adapt to changes in its environment, through loss of certain tumor suppressors or gain of specific oncogenes [244,248]. Also, this continued genetic diversification could help the tumor acquire resistance to drugs, cope with increased hypoxia, or escape challenges by the immune system. In line with this, an increased occurrence of structural chromosomal aberrations correlates with higher grade tumors [235,249,250]. Structural chromosomal instabilities arise through mis- or unrepaired double-strand breaks and HR and NHEJ are thought to be the two main repair pathways contributing to formation of structural aberrations [238,239,251]. Especially the error-prone NHEJ pathway, which ligates any two broken DNA ends together, is held responsible for the formation of many structural aberrations [251]. Indeed, individuals with genetic defects that cause defects in the repair of DSBs, such as patients with Nijmegen Breakage Syndrome, Bloom's syndrome, Ataxia telangiectasia or mutations in BRCA1 and 2, show an increased susceptibility to form structural chromosomal changes [252]. Cells from these patients accumulate translocations due to mutations in DNA repair proteins, such as NBS1 [253], BLM helicase [254], ATM kinase [255] or the BRCA1 [256] and BRCA2 [257] proteins, both involved in the HR pathway. Moreover, it was shown more than 40 years ago that several DSB-inducing agents, such as ionizing irradiation, UV-light and chemical mutagens, can also result in the formation of chromosomal aberrations [258]. On top of initial genetic defects or exogenous agents that increase the chance of developing chromosomal aberrations, a pathway that directly contributes to structural instability has also been described in cancer, termed the Breakage-Fusion-Bridge (BFB) cycle, first described in maize meiosis [259,260]. Chromosomes that are broken by DSBs can fuse with other broken chromosomal parts, for example through fusion at dysfunctional telomeres [261]. These telomere fusion events have been shown to cause dicentric (two centromeres) or ring chromosomes, both often found in tumors [261,262]. The presence of two centromeres on these aberrantly shaped chromosomes can result in uncoordinated microtubule attachment in mitosis, such that the two centromeres on a single chromatid become attached to opposite spindle poles (Fig.7). These attachments can subsequently induce chromatin bridging in telophase, resulting in breakage of the fused chromosome during cytokinesis [259,263]. These BFB events could go on for a prolonged period of time [259,260] and thereby increase the number of aberrant chromosomes in the offspring. BFB has indeed been correlated with an increase in intratumor

heterogeneity and might therefore be an important factor in structural instability [264].

4.2 Numerical Chromosomal Instability

Another striking hallmark of cancer cells is the presence of an abnormal chromosome number [236,265,266], termed aneuploidy, a state in which cells do not contain an exact multiple of the haploid DNA content [267]. On average 25 percent of the genome of a cancer cell is affected by numerical changes of either whole chromosomes or complete chromosomal arms [243]. Aneuploidy can be stably inherited in a population of (tumor) cells [243,268,269], but more often chromosome numbers continuously change between cancer cells and their offspring [270]. This continuous change in chromosome number is termed whole chromosomal instability (CIN) [231,270] and is associated with high-grade tumors, metastasis and poor prognosis [271-277] Moreover, CIN has been associated with resistance to chemotherapeutics, such as the widely used microtubule stabilizing agent Paclitaxel [278-280]. Various hypotheses have been postulated on how CIN and aneuploidy could contribute to tumorigenesis [281-285] (see Discussion, Chapter 8). The general idea is that whole chromosome gains and losses during cell division can, as suggested above for structural changes, result in loss and gain of tumor suppressors and oncogenes respectively [286], thereby providing a platform for cancer cells to adapt to their environment and continuously divide [287,288].

4.3 Causes of numerical CIN

Since the initial discovery of chromosomal instability in a variety of colon cancer cell lines in 1997 [270], many researchers have investigated the underlying cause of this striking phenotype, which was later found to be present in many other tumor types as well [243 231,289]. Several mechanisms have been proposed and tested using a variety of cancer cell lines and mouse models. However, it seems highly unlikely that one single mechanism can be held responsible for the CIN observed in the different types of tumors. Below we outline the different cellular causes that have been postulated and the genetic defects that could underlie these phenotypes.

4.3.1 Mitotic checkpoint defects

Defects in mitotic checkpoint signaling directly lead to chromosome missegregations (Fig.6A). Indeed, the hypothesis that has been investigated the most postulates that mitotic checkpoint defects could underlie CIN [290]. Complete mitotic checkpoint loss is lethal to all dividing cell types studied thus far and causes embryonic lethality [291-298], likely because it results in continuous missegregations. Thus, even if a viable daughter cell is generated during a first cell division, its genome is not properly propagated in the subsequent cell division, resulting in growth arrest and cell death in the respective daughter cells [291-298]. In contrast, partial checkpoint dysfunction results in mild chromosome segregation errors, which can potentially generate new viable genotypes that are relatively stable. Partial mitotic checkpoint activity could be responsible for this by allowing mitotic exit in the presence of one or more unattached kinetochores[291,298-300]. In line with this, CIN cancer cell lines were initially thought to have a weakened mitotic checkpoint due to mutations in the mitotic checkpoint kinase Bub1 [301]. However, other researchers could not reproduce these checkpoint defects in the same CIN cell lines [302], which opened up the avenue for research on other possible causes of CIN. Although many CIN lines do not show a weakened mitotic checkpoint when challenged with microtubule-targeting agents [302], reduced levels or mutations in mitotic checkpoint genes have been identified in human cancer [73,282,303-315]. In one specific syndrome, Mosaic Variegated Aneuploidy (MVA), which is linked to cancer

predisposition at a very young age, mono- and biallelic mutations in the BUB1B gene have been identified [303], which encodes for the mitotic checkpoint protein BubR1. These mutations can lead to complete absence of BubR1 mRNA or single amino acid substitutions in the BubR1 protein product [316]. In all cases, these mutations lead to lower BubR1 protein levels and decreased mitotic checkpoint activity [304,316,317], linking the cancer predisposition of MVA patients to defects in the mitotic checkpoint. Nonetheless, the occurrence of mutations in mitotic checkpoint genes in human cancers remains extremely rare [318-321] and, although seemingly paradoxical, it was found that many CIN tumors actually display enhanced levels of mitotic checkpoint proteins [272,322-327]. One explanation for this increase in expression of mitotic checkpoint genes lies in the dysfunction of the Rb pathway in many tumor cells. Indeed, deregulation of the Rb pathway can result in CIN in several organisms [328]. The Rb-E2F pathway regulates expression of various mitotic genes [151,329,330] and it has been shown that Rb dysfunction can result in overexpression of the mitotic checkpoint protein MAD2 [331]. Notably,

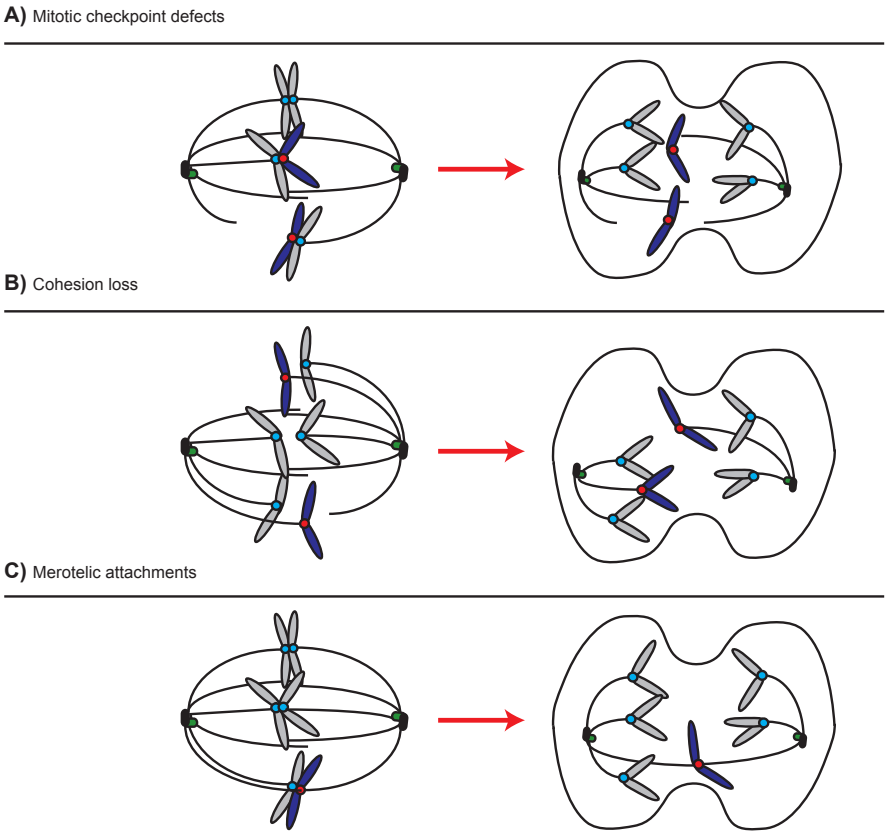

Figure 6. Various mitotic defects can lead to chromosomal instability (CIN)
A) Absence of mitotic checkpoint signaling allows anaphase initiation in the presence of unattached kinetochores, whereas cohesion loss (B) or merotelic attachments (C) induce chromosomal segregation errors by incorrect kinetochore orientation or the induction of lagging chromatids respectively

CIN induced in Rb-negative cell lines was directly dependent on increased MAD2 levels [331]. In line with this, MAD2 overexpression in mice results in aneuploidy and spontaneous tumor formation [332] (See section 4.5 and Table I) and CIN in Rb-negative tumors depends on increased MAD2 levels [333]. In summary, overexpression of mitotic checkpoint proteins, and in particular MAD2, through deregulated Rb and E2F signaling, might be a more prevalent cause in the induction of CIN in various

tumor types than mutation of mitotic checkpoint components. However, it still remains largely unknown how overexpression of mitotic checkpoint genes, such as MAD2, could result in chromosome missegregations and this will need further investigation.

4.3.2 Cohesion loss

Duplicated sister chromatids are held together until anaphase by the centromeric cohesin complex. Maintenance of cohesion between the two sister centromeres is essential for chromosome bi-orientation and hence for proper chromosome segregation [334-336]. Loss of cohesion before anaphase results in premature sister chromatid separation, which eventually results in chromosome segregation errors and aneuploidy (Fig.6B). Various genes encoding for proteins involved in cohesion establishment or maintenance have been found to be mutated in aneuploid tumors [335,337]. In addition, a recent report observed frequent deletion of an X-chromosome-linked region in genetically unstable tumor samples [338]. This locus encodes for SA2, which is a subunit of the cohesin complex. Interestingly, targeted inactivation of this locus, termed STAG2, resulted in chromosomal instability in otherwise chromosome-stable near-diploid cells. Moreover, reconstitution of STAG2 in CIN tumor cells, which harbor a deletion of the endogenous locus, reverted the CIN phenotype and enhanced chromosomal stability in these lines [338]. Defective sister chromatid cohesion as a result of somatic mutations may represent a major cause of CIN in human cancers. In line with this, overexpression of Separase, the protease that cleaves cohesin upon mitotic exit, has been observed in breast cancer samples [339] and transient overexpression of Separase can also result in anaphase bridges and aneuploidy in human cells [339]. Besides its role in sister chromatid cohesion, cohesin has also been implicated in DNA replication, DNA damage and protection of telomeres [340]. Therefore, various other mechanisms might underlie the aneuploidy observed in cells that have mutations in one of the cohesin subunits [341] and further research is needed to investigate in cohesion defects in the establishment of CIN.

4.3.3 Merotelic attachments

Although CIN cell lines do not necessarily possess a weakened mitotic checkpoint, many CIN cell lines do have an increased occurrence of lagging chromosomes due to unresolved merotelic attachments to the mitotic spindle [289,342] (Fig.6C). Because merotelic attachments link one kinetochore to two spindle poles, the sister chromatid has an increased chance of ending up in between the two packs of DNA during anaphase [343,344]. Most merotelic attachments are resolved by the error-correction machinery before anaphase [248,345,346]. However, tension can be established on a kinetochore despite merotelic attachments, causing Aurora B not to correct the erroneous attachments [344]. Moreover, since merotelic attachments do not prohibit kinetochores to obtain full microtubule occupancy, they do not necessarily activate the mitotic checkpoint [344]. Such merotelic attachments could therefore persist into anaphase and lead to chromosome missegregations and aneuploidy [289,344]. Multiple cellular, genetic and molecular causes of merotelic attachments have been hypothesized, of which the most significant ones are outlined below.

Aberrant spindle morphology

One way in which merotelic attachments could arise is through abnormal spindle assembly. Initial clues on this mechanism came from the observation that multipolar spindle assembly in kangaroo cells often led to kinetochore-binding to two spindle poles [347]. These merotelic attachments were not sensed by the mitotic checkpoint and often resulted in lagging chromosomes in anaphase [348]. These data indicate

that aberrant spindle formation increases the chance of obtaining erroneous kinetochore attachments and that proper bipolar spindle assembly is essential to obtain normal, amphitelic attachments. In line with this, it was shown that washout of drugs that affect spindle formation in prophase also increased the number of merotelic attachments and induced chromosome segregation errors [345]. Interestingly, multipolar spindles are often observed in CIN tumors [349-352], which indicates that aberrant spindle assembly might be responsible for merotelic attachments and CIN induction in vivo as well. These multipolar spindles are often the result of centrosome overduplication, a common trait of cancer cells [353]. Persistence of multipolar spindles in anaphase results in severe chromosome missegregations and the severely aneuploid daughter cells often die in the next G1 phase [354]. Tumor cells that harbor multiple centrosomes have also been shown to sometimes progress through a transient multipolar state, after which supernumerary centrosomes cluster during mitosis and eventually form a seemingly normal bipolar spindle[355,356] (Fig.7A). Mitotic entry in the presence of a multipolar spindle results in attachments of single kinetochores to multiple spindle poles[347,348,355,356]. Subsequent centrosome clustering converts these attachments to merotelic attachments, thus providing a mechanism that links multipolarity to lagging chromosomes[355,356] (Fig.7A). Supernumerary centrosomes can arise through a number of different mechanisms, such as centrosome overduplication, cytokinesis failure or virus-induced cell fusion, of which the last two also result in increased ploidy. Interestingly, tetraploidy is also frequently observed in tumor cells and has been shown to promote tumorigenesis in mice [357] and transformation *in vitro* and *in vivo* [358]. One remarkable mechanism by which tetraploidy could arise is 'entosis': the invasion of a cell into another cell, a phenotype often observed in tumors that increases with increasing tumor grade [359-361]. The mere presence of an invading cell in the host cell's cleavage plane inhibits cytokinesis and as a result causes tetraploidy and multipolarity in the next mitosis, resulting in aneuploid daughter cells [361,362]. This illustrates that one single cytokinesis failure could initiate chromosome segregation errors in the tumor cell's off-spring, ultimately leading to CIN.

Increased stability of kinetochore MT attachments

The proper control of kinetochore-microtubule stability is another crucial factor that determines the fidelity of chromosome segregation (Fig.7B). Increasing the stability of microtubules bound to kinetochores through depletion of MCAK or Kif2b, two kinetochore-localized microtubule depolymerases, results in an increased occurrence of merotelic attachments and severe chromosome missegregations in human tumor cells [363]. These results stress the importance of the error-correction machinery, because a slight decrease in kinetochore-MT turnover upon Kif2b or MCAK depletion can clearly affect Aurora B-dependent correction of misattached kinetochores [363]. A follow-up study in which the kinetochore-MT turnover was compared between an untransformed cell line and several CIN lines, revealed that CIN tumor cell lines often display an increased stability of kinetochore MTs, which could result in persistent misattachments until anaphase [364]. Importantly, increasing kinetochore-MT turnover in these CIN cell lines by overexpressing Kif2b or MCAK could partially revert the chromosomal instability phenotype [364]. A recent report revealed an unexpected link between MAD2 overexpression, often found in CIN tumors, and increased kinetochore-MT stability. Aurora B centromere localization and activity was significantly decreased upon MAD2 overexpression, which could explain the increased occurrence of chromosome segregation errors in these cells [365]. The authors observed that the effect on Aurora B localization is independent of the checkpoint function of MAD2, but the exact underlying mechanism is still unknown. This effect on Aurora B localization and activity is in line with another study, which suggested that the Aurora B-dependent error correction machinery works more efficiently in healthy cells when compared to tumor cells [366], thus providing an

explanation for the occurrence of CIN in those tumor cells. Since MAD2 overexpression results in chromosome segregation errors and tumorigenesis in mice [331,332](Table I), aberrant Aurora B localization and activation could very well explain the CIN observed in MAD2-overexpressing tumors. One other interesting possibility which could explain the increased stability of kinetochore-MTs observed in CIN cells [363], is the mutation or loss of the tumor-suppressor gene Adenomatous Polyposis Coli (APC), which frequently occurs in colon carcinomas [367]. These APC mutations are thought to be an initiating event in colon tumorigenesis through loss of APC's inhibitory role in Wnt signaling [368]. APC loss and CIN are both found in early cancer lesions [369] and APC loss-of-function has been shown to result in genetic instability [370,371], which is thought to, at least partially, be dependent on its function in kinetochore-MT stability [372-374]. APC localizes to centrosomes, kinetochores and MT plus-ends [369] and depletion of APC results in reduced inter-kinetochore tension, which is thought to be due to decreased kinetochore-MT dynamics [372,373]. Although a very interesting hypothesis, future research will have to assess the direct effects of APC loss on CIN *in vivo*, since defects in APC function also result in activation of Wnt signaling and its downstream targets, which might explain the induction of CIN as well [375,376].

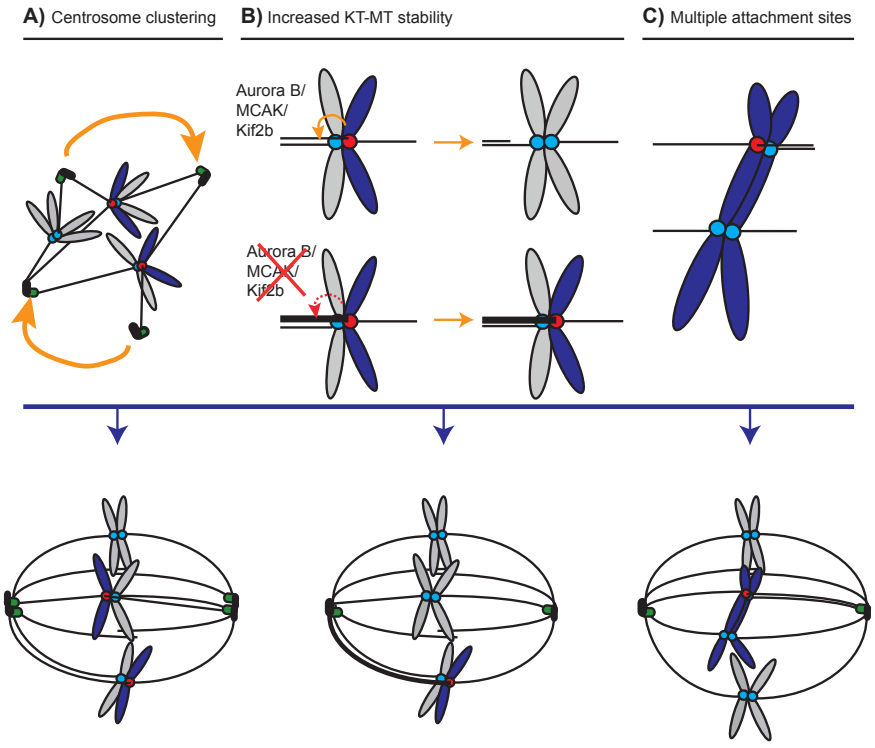

Figure 7. Schematic representation of underlying causes of merotelic attachments
A) Centrosome coalescence creates merotelic attachments by allowing clustering of centrosomes, which had already established microtubule interactions with kinetochores. B) Impaired kinetochore microtubule dynamics inhibits the release of erroneous attachments, whereas the presence of multiple centromeres (C) increases the chance of creating faulty attachments.

1

Multiple attachment sites

The presence of extra centromeres on chromosomes could be another cause of lagging chromosomes

(Fig.7C). As discussed in section 4.1, aberrantly structured chromosomes, such as ring chromosomes or fusion of multiple chromosomes have a high chance of ending up in the cleavage furrow during telophase. These chromosomes often have multiple centromeres and therefore an increased number of MT attachment possibilities due to the presence of extra kinetochores. The multiple kinetochores present on these chromosomes increase the chance of aberrant MT-binding, creating merotelic attachments [17,377,378]. The cell could therefore exit mitosis with the structurally aberrant chromosome lagging behind, resulting in whole chromosome gain or loss [17,259,263,378]. These data indicate that structural chromosomal aberrations and numerical CIN are closely linked and show that DNA damage due to for example replication defects [379,380], telomere defects [263,341,378,381] or DNA repair defects [382] could, besides structural CIN, eventually result in numerical CIN as well. Another cause of multiple centromere formation could be the random incorporation of CENP-A at heterochromatic sites, other than the core centromeric region. It has been shown in Drosophila (cells) that overexpression of CENP-A can directly result in localization of CENP-A into noncentromeric regions [17]. This leads to ectopic kinetochore formation, which results in an increase in erroneous MT attachments upon mitotic entry and ultimately anaphase bridges and severe aneuploidy in the daughter cells, indicating that CENP-A overexpression can be held responsible for CIN as well. In line with this hypothesis, enhanced levels of CENP-A and its targeting factor HJURP have been found in both breast and colon cancer [383,384]. However, in human cells, contradictory data have been obtained on the effects of ectopic localization of CENP-A. One study suggested that CENP-A presence is not sufficient to drive complete de novo kinetochore formation [385], while others have shown it can [386]. These data suggest that mere overexpression of CENP-A might not be sufficient for the induction of CIN through creation of multiple attachment sites.

4.4 Numerical CIN & DNA damage

Increased levels of aneuploidy in cells have been shown to correlate with the number of structural chromosomal aberrations [387]. Until recently, this causal relationship was ascribed to the fact that structural chromosomal aberrations can induce numerical CIN through induction of aberrant mitotic progression. However, several recent reports have shown that both aneuploidy [388] and chromosome segregation errors [389-391] can affect structural integrity of chromosomes through the induction of double-stranded breaks (See Chapter 4 and 8 for more details). Aneuploid yeast strains have been shown to undergo recombination defects which cause DSBs [388], whereas two other reports using human cells as a model system show that one mere chromosome segregation event can result in either cytokinesis-induced DNA damage [389] or micronuclei formation, of which the latter affects replication fidelity in the next S phase [390]. In line with these data, structural changes have been found in CIN mouse models and CIN tumor cells as well [236,272,332,357,389]. This reciprocal relationship complicates the ability to determine direct effects of either structural chromosomal changes or numerical CIN on tumor formation and reveals additional ways in which heterogeneity arises in tumors.

4.5 Mouse models of numerical CIN

Since the discovery of numerical CIN in human colorectal tumors [270], several CIN mouse models have been generated with deletions or hypomorphic alleles of genes important for mitotic fidelity [392]. Homozygous deletion of genes required for faithful mitotic progression leads to embryonic lethality [293,297,298,318,393-397]. Haploinsufficiency of mitotic genes, however, is tolerated in all cases and is therefore used extensively to investigate in the effects of CIN in tumorigenesis (Table 1) [398]. Following recent findings that mitotic genes are more frequently up- than downregulated in CIN tumors, various mouse

models have been generated which overexpress genes involved in mitotic progression, such as the mitotic checkpoint genes Bub1[399] and MAD2 [332] and the E2 enzyme UbcH10 [400].

4.5.1 Tumor-promoting role of numerical CIN

Haploinsufficiency, hypomorphy or overexpression of genes involved in mitotic progression can result in aneuploidy in Mouse Embryonic Fibroblasts (MEFs) and various adult tissues. Although aneuploidy levels vary between different mouse models [398], CIN generally seems to be able to enhance tumorigenesis. Treatment with carcinogens, such as DMBA, leads to increased tumor incidence in 6 out of 10 CIN models tested (see Table I) and crossing some of the CIN models with tumor-prone mouse models, such as Em-myc[332,399] or $APC^{min/+}$ [286,401] mice, results in enhanced or accelerated tumor formation (Table I). Many CIN mouse models also display an increased susceptibility to spontaneous tumor formation in lung, liver and lymph nodes, albeit at a relatively old age (Table I). Interestingly, the extent of spontaneous tumor formation does not always correlate with the level of aneuploidy found in MEFs. For example, $BubR1^{H/H}$ MEFs [297] have similar levels of aneuploidy as MEFs of $Bub1^{-/H}$ and $Bub1^{H/H}$ animals [395], but $BubR1^{H/H}$ animals do not display an increased tumor incidence, whereas Bub1 hypomorphic animals do. These discrepancies could be due to additional roles of these checkpoint proteins in other cellular processes. Indeed, BubR1 hypomorphic animals also develop severe ageing-associated phenotypes, which indicates that BubR1 has additive functions in maintaining cell homeostasis, possibly through regulation of p16 and p19 protein levels [297,402]. One striking similarity in the spectrum of spontaneously developing tumors in the various CIN models is the formation of lung tumors. This resemblance indicates that, for unknown reasons, CIN specifically enhances tumorigenesis in lung epithelial cells.

4.5.2 Tumor-suppressive role of numerical CIN

Although CIN in most models correlates with increased tumor formation, several cases of CIN-associated tumor suppression have been described as well (Table I). In particular, animals heterozygous for the motor protein CENP-E showed a significant decrease in spontaneous liver tumor formation, decreased tumor incidence in a p19 heterozygous background, but also a clear reduction in carcinogen-induced tumor formation [397]. Similarly, BubR1 heterozygosity decreased intestinal tumor incidence in the tumor-prone $APC^{min/+}$ model [401,403] and Bub1 hypomorphy reduced the number of prostate lesions when crossed with heterozygous PTEN animals [286]. In line with this, inverse correlations between CIN and patient prognosis in various tumor types have been described as well [404,405]. Overall, these data suggest that an optimal level of CIN exists, which, dependent on the tissue, results in either tumorigenesis or tumor suppression. Excessive CIN could compromise genome stability in such a way that it is incompatible with cell viability, whereas partial CIN could be promoting growth by providing the tumor cell with a level of genetic instability that is moderate enough to maintain a relatively stable cancer genome, while at the same time providing enough genetic variation in the population to allow for rapid adaptation to changes in the tumor environment. This could involve adaptation to changes in oxygen tension and altered cellular metabolism, as well as acquiring resistance to chemotherapeutics. If a maximal tolerated level of CIN does exist for tumors, this feature could be exploited in future anti-cancer strategies (See chapter 4-8). This paradoxical relationship between CIN, tumorigenesis and cell viability is a highly debated topic and future research will hopefully lead to more insight in the role of CIN in tumorigenesis, but also allow for the successful development of new anti-cancer strategies specifically targeting CIN or aneuploid tumor cells.

Thesis outline

Chromosome segregation errors are a hallmark of cancer cells. This thesis describes the effects of these mitotic chromosome missegregations on the cell's progeny. We have investigated in the consequences of mitotic errors both with regards to tumorigenesis and the development of new anti-cancer strategies. In addition, we have developed new techniques to study chromosome segregation errors in vivo.

Chromosome segregation errors are a common characteristic of chromosome unstable (CIN) tumor cells, but it remains highly debated whether this feature is contributing to the tumorigenic capacity of cancer cells. In **Chapter 2** we describe that chromosome segregation errors can cause DNA damage during cytokinesis, leading to chromosomal translocations in the next generations. These data reveal that chromosome segregation errors can provide cancer cells with additional ways to evolve and change their genetic make-up, not only by inducing aneuploidy, but also by contributing to structural chromosomal instability. To be able to determine the effects of chromosome segregation errors at an organismal level, we have generated two mouse models, discussed in **Chapter 3,** which inducibly express mutant forms of the mitotic checkpoint kinase Mps1. These mutations reduce or ablate Mps1 kinase activity and will therefore result in chromosome segregation errors upon cell division. These mouse models will allow us to induce chromosome segregation errors at specific moments and in specific tissues during adult life stages, and therefore enable us to determine the effects of CIN on tumorigenesis in vivo. Although it remains unclear whether CIN is a true contributing factor to tumorigenesis, we have hypothesized that this hallmark of cancer cells could be exploited in anti-cancer therapy, as discussed in the second part of this thesis. In **Chapter 4** we review current anti-cancer strategies that specifically target mitotic cells and discuss the potential of specifically targeting tumor cells by exploiting mitotic defects, such as CIN, already present in these cells. In **Chapter 5** we describe the possibility of enhancing chromosome segregation errors as a strategy to kill tumor cells both in vitro and in vivo (addendum). Partial depletion of the mitotic checkpoint proteins Mps1 or BubR1 synergizes with low doses of paclitaxel by inducing severe chromosome missegregations in anaphase. In addition, we characterize a previously unrecognized specific small molecule inhibitor of Mps1 in **Chapter 6**, which is active in mice and specifically kills tumor cells in vitro. We hypothesize that this selectivity towards tumor cells is due to the fact that these cells are more dependent on the chromosome alignment and checkpoint function of Mps1 than healthy cells due to the presence of an abnormal chromosome number. Data described in Chapter 5 and 6 fuel the idea of using Mps1 inhibition as a way to specifically kill tumor cells. Although interesting, it remains highly debated whether anti-mitotic drugs are truly interesting chemotherapeutics. To determine the effects of anti-mitotic drugs in vivo, we have developed a FRET based intravital imaging technique in **Chapter 7,** which allows us to simultaneously visualize both mitotic progression and apoptosis onset. Interestingly, we find that the clinically used chemotherapeutic Docetaxel, a semi-synthetic Taxane, induces apoptosis in vivo independent of its effect on mitotic progression, which shows that Taxanes might not be so successful solely due to their anti-mitotic effects. Finally, we discuss our findings in light of the recent literature in Chapter 8 and propose ideas for future research to investigate in the effects of CIN on tumorigenesis and in possible ways to exploit this prevalent phenotype in anti-cancer treatment.

Table I. Mouse models of numerical CIN

Mouse model	Spontaneous (organ)	Carcinogen induced tumors (organ)	Crossed with	Tumorigenesis in compound mice (organ)	References
$MAD2^{+/-}$	Yes (lung)	x	$p53^{+/-}$ $p53^{+/-}/MAD1^{+/-}$	Increase Increase (lung, spleen, breast)	291,406
$MAD1^{+/-}$	Yes (lung)	Increase, vincristine (lung, liver)	$p53^{+/-}$ $p53^{+/-}/MAD2^{+/-}$	Normal Increase (lung, spleen, breast)	298,406
$Bub3^{+/-}$	No	Normal, DMBA	$p53^{+/-}$ $Rb^{+/-}$ $Rae1^{+/-}$	Normal Normal Increase, DMBA (lung)	300 295,394
$BubR1^{+/-}$	No	Increase, azoxymethane (lung, colon)	$APC^{min/+}$	Increase (colon) Decrease (small intestine)	296,401
$BubR1^{+/H}$	No	x	x	x	297
$BubR1^{H/H}$	No	Increase, DMBA (lung)	x	x	297
$Bub1^{+/-}$	No	Increase, DMBA (lung)	$p53^{-/-}$ $APC^{min/+}$	Normal Increase (colon)	286,395,407

$Bub1^{H/H}$	Yes (liver, lung, lymph nodes)	x	$p53^{+/-}$ $p53^{-/-}$	Increase (thymus) Increase (thymus)	286,395,407,408
$Bub1^{-/H}$	Yes (liver, lung, lymph nodes)	x	$p53^{+/-}$ $p53^{-/-}$ $APC^{min/+}$ $Rb^{+/-}$ $PTEN^{+/-}$	Increase (thymus) Increase (thymus) Increase (colon) Increase (pituitary) Decrease (prostate lesions)	286,395,407
MAD2 ox	Yes (liver, lung, lymph nodes, intestine)	x	Eμ-myc $KRAS^{G12D}$	Increase (lymph nodes) Increased relapse (lung)	332,409
$Bub1^{T85/T264}$	Yes (liver, lymph nodes and skin)	x	Eμ-myc	Increase (lymph nodes)	399
CENP-$E^{+/-}$	Yes (lung, colon, spleen) Decrease (liver)	Decrease, DMBA (lung)	$p19^{+/-}$	Decrease (lymph nodes)	397
$Cdh1^{+/-}$	Yes (breast, lung)	x	x	x	410
Hec1 ox	Yes (lung, liver)	x	x	x	411
$Cdc20^{+/-/H/H/-/H}$	No	Normal, DMBA	x	x	412
$Cdc20^{AAA/+}$	Yes (lymph nodes, liver)	x	$p53^{-/-}$ $ATM^{-/-}$	Increase (thymus) Increase (thymus)	407,413
$UbcH10^{T1/T2}$	Yes (lung, liver, blood, skin)	Increase, DMBA (lung)	x	x	400

Chapter 2

Chromosome Segregation Errors as a Cause of DNA Damage and Structural Chromosome Aberrations

Aniek Janssen[1,4], Marja van der Burg[2], Karoly Szuhai[2], Geert J.P.L. Kops [1,3,5], René H. Medema[1,4,5.]

[1]Department of Medical Oncology and Cancer Genomics Center, University Medical Center Utrecht, Universiteitsweg 100, 3584 CG, Utrecht, the Netherlands,

[2]Department of Molecular Cell Biology, Leiden University Medical Center, Einthovenweg 20, 2300RC Leiden, the Netherlands,

[3]Department of Molecular Cancer Research and Cancer Genomics Center, University Medical Center Utrecht, Universiteitsweg 100, 3584 CG, Utrecht, the Netherlands.

[4]Division of Cell Biology, Netherlands Cancer Institute, Plesmanlaan 121, 1066 CX, Amsterdam, the Netherlands.

Science. 2011 Sep 30;333(6051):1895-8

Abstract

Various types of chromosomal aberrations, including numerical (aneuploidy) and structural (e.g. translocations, deletions), are commonly found in human tumors and are linked to tumorigenesis. Aneuploidy is a direct consequence of chromosome segregation errors in mitosis, while structural aberrations are caused by improperly repaired DNA breaks. Here we demonstrate that chromosome segregation errors can also result in structural chromosome aberrations. Chromosomes that missegregate are frequently damaged during cytokinesis, triggering a DNA double strand break response in the respective daughter cells involving ATM, Chk2 and p53. We show that these double strand breaks can lead to unbalanced translocations in the daughter cells. Our data show that segregation errors can cause translocations and provide novel insights on the role of whole-chromosome instability in tumorigenesis.

Results & Discussion

Tumor cells show two types of genetic instability: whole chromosomal instability (CIN) in which cells frequently lose and gain whole chromosomes due to chromosome segregation errors in mitosis [270,289,398] and instability at the structural level of DNA, causing small changes at the nucleotide level or larger structural aberrations at the chromosomal level, including deletions and translocations [238]. These two types of genetic instability are thought to occur independently of each other [417]. To examine the impact of chromosome segregation errors on chromosome integrity, hTert-immortalized, non-transformed human retinal pigment epithelial (RPE-1) cells were treated with Monastrol to induce formation of erroneous kinetochore-microtubule attachments, in which one kinetochore is attached to both spindle poles [289]. Subsequent release from the Monastrol block causes a high incidence of lagging chromosomes, reflecting the situation in CIN cells [289,419]. ~80% of the RPE-1 cells blocked and released in this manner improperly segregated their chromosomes, which correlated to a similar percentage of cells with abnormal nuclei (Fig.1A,B). 6 hours after release, 70% of these abnormal nuclei displayed γH2AX and 53BP1-foci, two markers for damaged DNA [207,213] (Fig.1C,D, and Fig.S1A). Conversely, only 20% of morphologically normal nuclei were positive for γH2AX (Fig.1D, S1A). Short treatments (1h) with Monastrol were sufficient to induce missegregations and foci formation (Fig.S1B), indicating this does not require an extensive mitotic delay. To exclude prolonged mitotic duration as the cause of foci formation [420-422], we provoked chromosome missegregations by inhibiting the mitotic checkpoint kinase Mps1. Cells that divided in the presence of the Mps1 inhibitor Mps1-IN-1 [123], missegregated their chromosomes and produced daughter cells with abnormal nuclei (Fig.1E). Of these, 78% was γH2AX-positive, compared to 25% in control nuclei (Fig.1E,F). Similar results were obtained with BJ-Tert fibroblasts (Fig.S1C). Taken together, these results show that an increased frequency of chromosome missegregations is associated with DNA damage foci-appearance. We next monitored chromosome segregation and DNA damage foci-appearance simultaneously in real-time in RPE-1 cells stably expressing both H2B-RFP and 53BP1-GFP (Fig.1G) (Movie S1, 2). Control RPE-1 cells showed no chromosome segregation errors and on average only one 53BP1 focus emerged per 4 daughter cells (Fig.1G). The number of cells with 53BP1 foci and the number of foci per cell increased proportionally to the severity of Mps1-IN-1-induced segregation errors (Fig.1G). ~80% of the cells accumulated 53BP1 foci within 2 hours following a missegregation event (Fig.S1D). Mps1-IN-1 also induced increased 53BP1 foci formation in U2OS human osteosarcoma cells stably expressing 53BP1-GFP (Fig.S1E). H2AX phosphorylation and 53BP1 recruitment following a segregation error were often restricted to DNA positioned in or close to the cleavage furrow (Fig.1E,G), suggesting that damage might occur as a consequence of cytokinesis. We therefore prevented cytokinesis by inhibiting myosin II activity with blebbistatin [423] or by inhibiting Aurora B kinase activity with AZD1152 or ZM447439 [424,425]. Treatment of RPE-1 cells with any of these inhibitors decreased Monastrol-induced formation of γH2AX foci in fixed cells (Fig.2A, S2A) and decreased 53BP1 foci formation from 2,4 foci to 0,7 focus per cell in live cells (Fig. S2B-D). Similarly, inhibition of cytokinesis resulted in a 2.5 fold decrease in Mps1-IN-1-induced 53BP1 foci formation (Fig.2B). Chromosome missegregations as a cause for DNA damage was also apparent after spontaneous segregation errors in the CIN tumor cell lines MCF7 and SW480 [289]. Chromosome missegregation events in these cells also produced enhanced 53BP1 foci formation (from an average of 0,3 to 1 or 0,7 to 1,5 focus per MCF7 or SW480 daughter cell respectively) (Fig.S3A-C), which was again suppressed by blocking cytokinesis (Fig.S3B,C). In line with these results, U2OS cells, which display high incidence of spontaneous segregation errors [299], have high levels of endogenous 53BP1 foci formation (average 1,2 focus/daughter cell) (Fig.S1E).

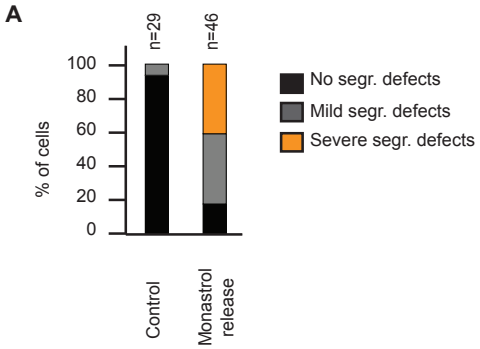
A
n=29
n=46
100
80
60
40
20
0
% of cells
No segr. defects
Mild segr. defects
Severe segr. defects
Control
Monastrol release

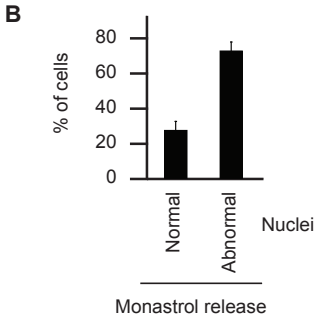
B
80
60
40
20
0
% of cells
Normal
Abnormal
Nuclei
Monastrol release

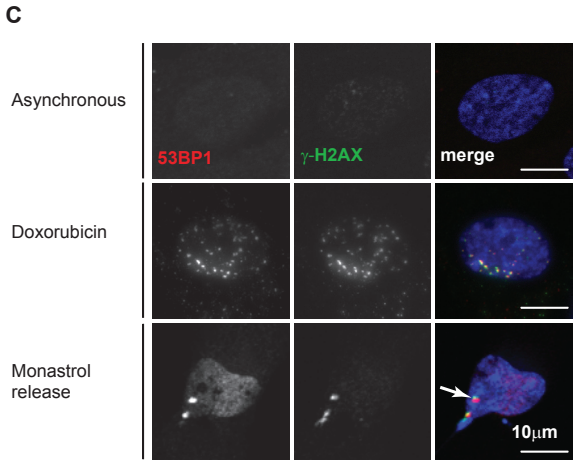
C
Asynchronous
Doxorubicin
Monastrol release
53BP1
γ-H2AX
merge
10μm

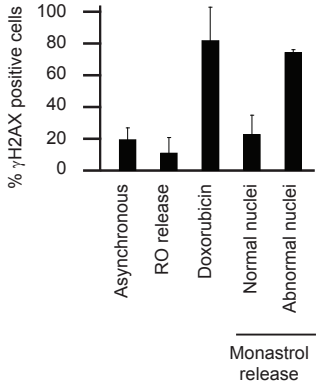
D
100
80
60
40
20
0
% γH2AX positive cells
Asynchronous
RO release
Doxorubicin
Normal nuclei
Abnormal nuclei
Monastrol release

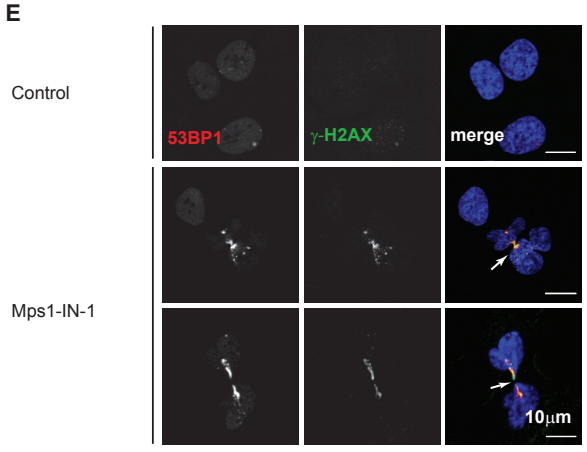
E
Control
Mps1-IN-1
53BP1
γ-H2AX
merge
10μm

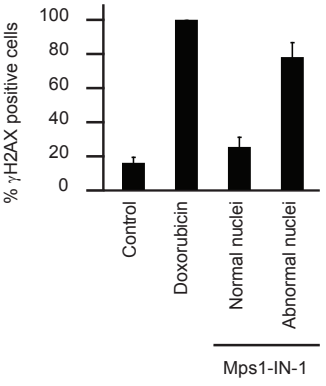
F
100
80
60
40
20
0
% γH2AX positive cells
Control
Doxorubicin
Normal nuclei
Abnormal nuclei
Mps1-IN-1

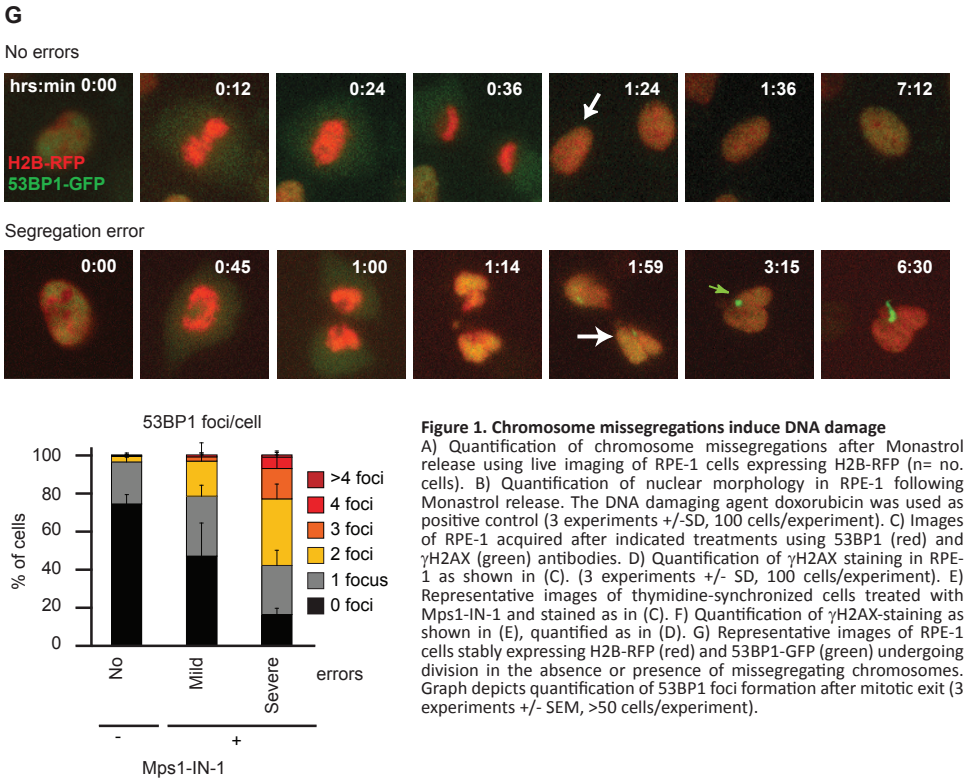

Figure 1. Chromosome missegregations induce DNA damage
A) Quantification of chromosome missegregations after Monastrol release using live imaging of RPE-1 cells expressing H2B-RFP (n= no. cells). B) Quantification of nuclear morphology in RPE-1 following Monastrol release. The DNA damaging agent doxorubicin was used as positive control (3 experiments +/-SD, 100 cells/experiment). C) Images of RPE-1 acquired after indicated treatments using 53BP1 (red) and γH2AX (green) antibodies. D) Quantification of γH2AX staining in RPE-1 as shown in (C). (3 experiments +/- SD, 100 cells/experiment). E) Representative images of thymidine-synchronized cells treated with Mps1-IN-1 and stained as in (C). F) Quantification of γH2AX-staining as shown in (E), quantified as in (D). G) Representative images of RPE-1 cells stably expressing H2B-RFP (red) and 53BP1-GFP (green) undergoing division in the absence or presence of missegregating chromosomes. Graph depicts quantification of 53BP1 foci formation after mitotic exit (3 experiments +/- SEM, >50 cells/experiment).

These data suggest that missegregating chromosomes get damaged during cytokinesis by cleavage furrow-generated forces. Indeed, 'trapped' chromosomes positioned exactly at the site of furrow ingression (Fig.S4A) stained positive for the DNA-damage markers γH2AX and MDC1 in U2OS cells, undergoing spontaneous segregation errors, as well as Mps1-IN-1-treated RPE-1 cells (Fig.2C,D and Movie S3). In comparison, foci were rarely found on missegregating chromosomes before furrow ingression, or outside the cleavage furrow (Fig.S4B, Fig.2D). In line with previously published data [426,427], we find that MDC1 and γH2AX could get recruited to DNA damage sites on mitotic chromosomes, whereas 53BP1 localization was delayed until after mitosis (Fig.2D and S1D). If daughter cells inherit parts of broken chromosomes, the observed foci should reflect double-stranded DNA breaks (DSBs). Indeed, Monastrol-induced chromosome missegregations resulted in auto-phosphorylation of ATM on serine 1981 (S1981) (Fig.3A, S5A), a hallmark of DSBs [428]. Activated ATM is known to phosphorylate Chk2 on threonine 68 (T68) [429]. Consistently, we found increased T68-phosphorylated Chk2 in Monastrol released-cells, which was reduced to background levels by inhibiting furrow ingression during the release (Fig.3C,D). pS1981-ATM and pT68-Chk2, as well as the amount of γH2AX-positive nuclei, were all diminished by the ATM inhibitors KU55933 [430] and caffeine (Fig.3A-C). Moreover, ATM inhibition reduced 53BP1 foci formation observed during time-lapse analysis of Mps1-IN-1 treated RPE-1 cells (average of 1.3 focus/cell to 0.2 focus/cell) or released from Monastrol (average of 2.4 foci/cell to 0.2 focus/cell) (Fig.3E,F, Fig.S2E, Movie S4). The observed DNA damage response therefore reflects a bona fide DSB response triggered by breakage of missegregating chromosomes during cytokinesis. Chromosome missegregation events can activate p53 and block cell proliferation [407,431]. To

assess whether cytokinesis induced-DNA damage on missegregating chromosomes can also trigger p53-activation, we determined the effects on ATM-dependent p53-phosphorylation on serine15 (S15) (Fig.S5B-D). Segregation errors caused an increase in daughter nuclei with S15-phosphorylated p53-foci co-localizing with γH2AX (Fig.S5C,D), which depended on cytokinesis and ATM activity (Fig.S5D). Together, these data demonstrate that DSBs produced by segregation errors can activate canonical DNA damage checkpoint responses involving ATM/Chk2 and p53. We found that ~70% of 53BP1 foci produced after segregation errors disappeared within 8 hours (Fig.4A), suggesting that the chromosome fragments were somehow joined together, or fused to intact chromosomes. Inhibition of Non-Homologous-End-Joining (NHEJ) by inhibition or knockdown of DNA-PK [432] blocked mitotic entry, but this could be overcome by p53 depletion. NHEJ inhibition did not affect 53BP1 foci appearance in Mps1-IN-1-treated RPE-1 cells depleted of p53, but it strongly suppressed resolution of those foci (Fig.4A, S6A-C). p53 depletion did not change the kinetics of 53BP1 foci-resolution (Fig.S6D). This indicated that cytokinesis-induced DNA damage is at least in part repaired via NHEJ, possibly resulting in chromosomal translocations.

Since chromosome missegregations caused DSBs that likely resulted in distribution of chromosome fragments between daughter cells, we next wished to assess whether this could be a cause for chromosomal translocations. To this end, we examined chromosome morphology of Mps1-IN-1-treated cells (Fig.4B) [433]. As expected, inhibition of Mps1 induced overt numerical aberrations in

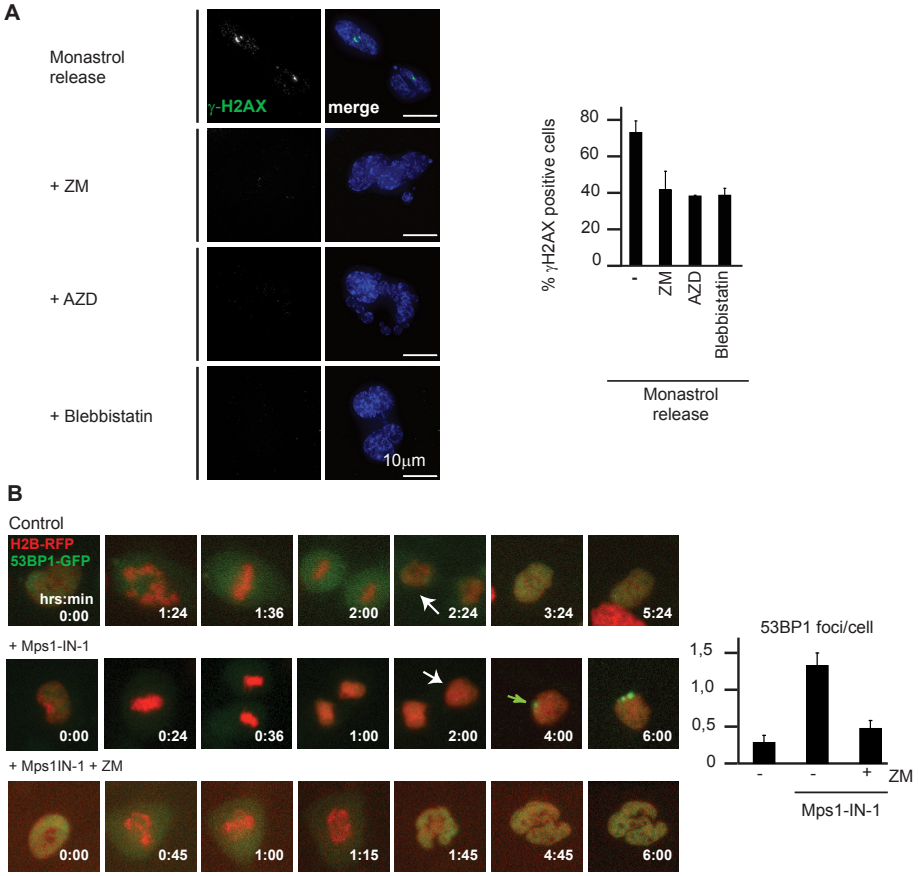

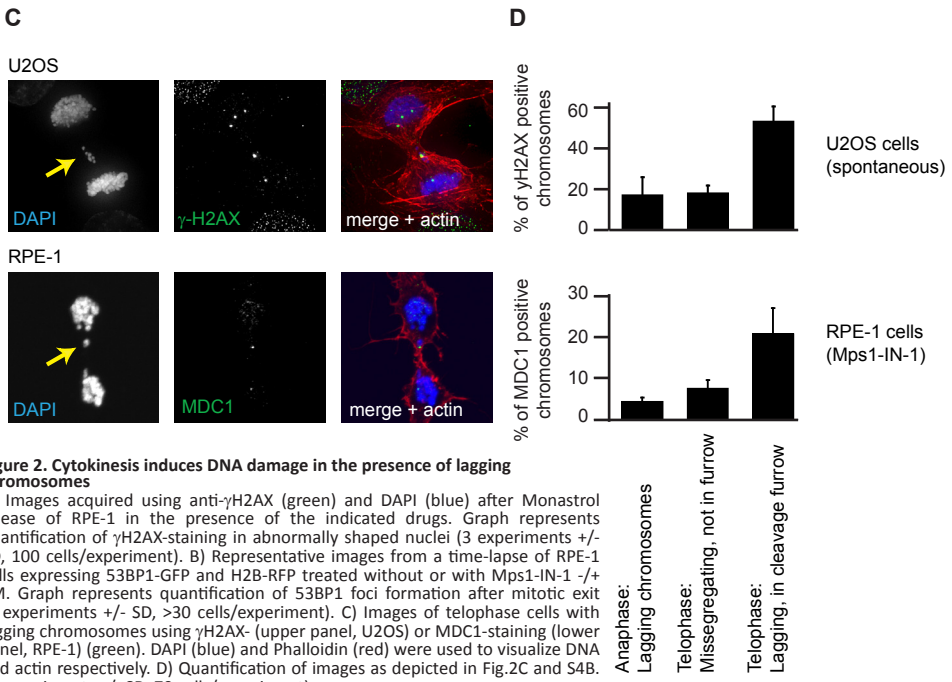

Figure 2. Cytokinesis induces DNA damage in the presence of lagging chromosomes
A) Images acquired using anti-γH2AX (green) and DAPI (blue) after Monastrol release of RPE-1 in the presence of the indicated drugs. Graph represents quantification of γH2AX-staining in abnormally shaped nuclei (3 experiments +/- SD, 100 cells/experiment). B) Representative images from a time-lapse of RPE-1 cells expressing 53BP1-GFP and H2B-RFP treated without or with Mps1-IN-1 -/+ ZM. Graph represents quantification of 53BP1 foci formation after mitotic exit (3 experiments +/- SD, >30 cells/experiment). C) Images of telophase cells with lagging chromosomes using γH2AX- (upper panel, U2OS) or MDC1-staining (lower panel, RPE-1) (green). DAPI (blue) and Phalloidin (red) were used to visualize DNA and actin respectively. D) Quantification of images as depicted in Fig.2C and S4B. (3 experiments +/- SD, 70 cells/experiment).

almost all daughter cells as a consequence of whole-chromosome missegregations [123] (Fig.S7A). We also observed an elevated occurrence of structural chromosomal aberrations in Mps1-IN-1-treated RPE-1 cells (6%) versus control cells (0,8%) (Fig.4B,C and S7B,C). These structural aberrations included both broken chromosomes (Fig.S7C) and unbalanced chromosomal translocations, which were observed in ~4% of Mps1-IN-1-treated RPE-1 cells, but never in control cells (Fig.4B,C, S7B). Consistent with previous results [431], we found that chromosome missegregations promote a p53-dependent G1-arrest (Fig.S8A,B), suggesting that p53 can suppress chromosome translocations-appearance induced by Mps1-IN-1. Indeed, p53-depletion resulted in enhanced occurrence of chromosomal aberrations (12% versus 6% in siLuciferase-treated cells) and unbalanced translocations (6% versus 4% in siLuciferase-treated cells) (Fig.4C, S8C). While 70-80% of Mps1-IN-1-treated RPE-1 cells obtained DSBs (Fig.1F, G), only 6-12% eventually contain structural chromosomal aberrations (Fig.4C). This indicates that most daughter cells either died or obtained both fragments of the damaged chromosome and were able to efficiently repair the DSBs (Fig.S9). Together, our data show that chromosomal breaks induced by segregation errors in a dividing cell can produce structural chromosomal aberrations in the subsequent daughter cells. This establishes a link between chromosome missegregations, frequently occurring in CIN cells [270,289], and structural chromosomal aberrations, including chromosomal translocations. In line with this, SW480-, MCF7- and U2OS-CIN cell lines harbor many structural aberrations (Fig.S10). Cytokinesis-induced DSBs can cause the separate parts of the broken chromosomes to end up in distinct daughter cells, providing a platform for an unbalanced translocation event (Fig.S9). Therefore, our data imply that CIN has the potential of increasing the cells' tumorigenic capacity, not only by changing the amount of whole chromosomes, but in addition by increasing the amount of structural chromosomal aberrations.

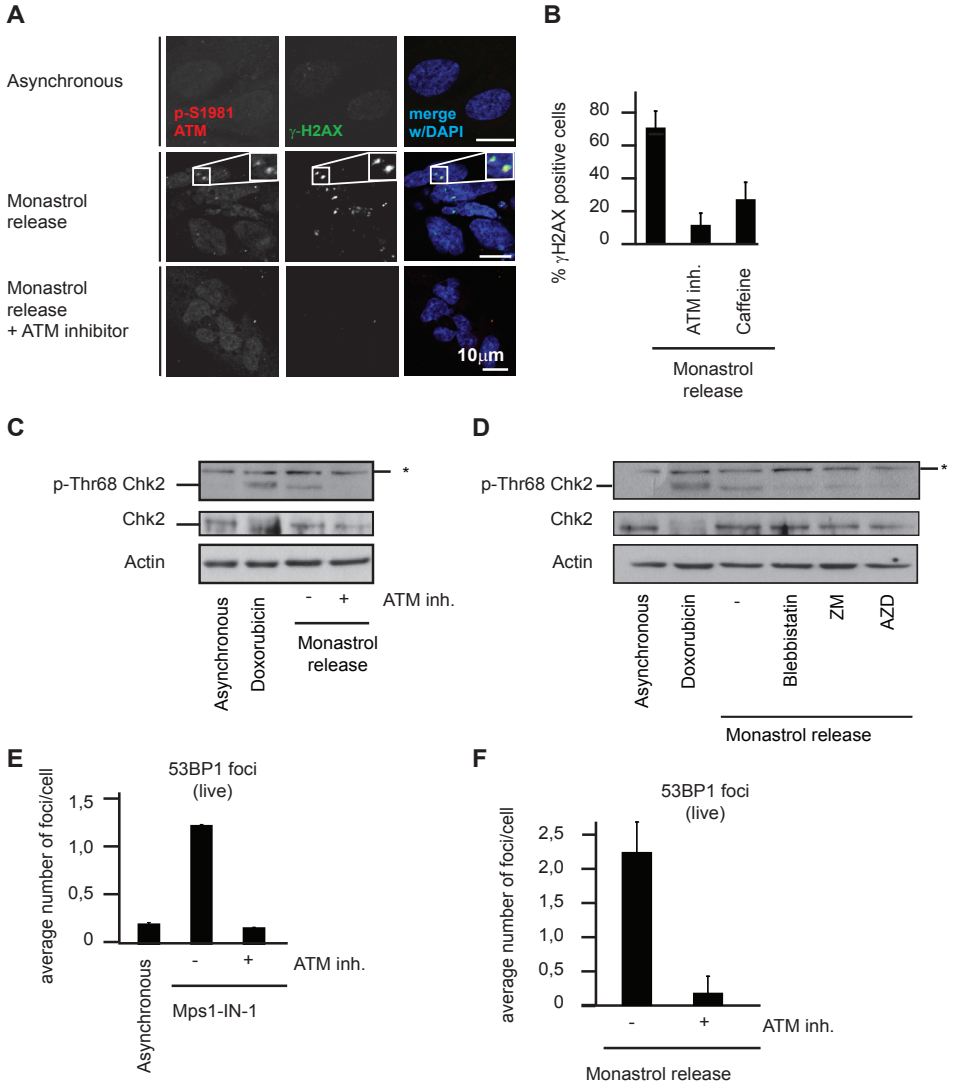

Figure 3. Missegregating chromosomes activate ATM/Chk2
A) Images acquired using anti-phospho-Serine1981-ATM (red) and γH2AX (green) after indicated treatments. B) Quantification of γH2AX-staining after indicated drug treatments (abnormal nuclei only) (3 experiments +/- SD, 100 cells/experiment). C,D) RPE-1 lysates immuno-blotted for phospho-threonine-68-Chk2, total Chk2 and actin after indicated treatments. Asterisk indicates aspecific band. E,F) Quantification of 53BP1-foci formation using RPE-1 live imaging after indicated treatments (3 experiments +/- SD, 30 cells/experiment).

Materials and Methods

2

Tissue Culture, Transductions and Treatments

Tumor cell lines were grown in DMEM (Lonza), RPE-1 cells and BJ-Tert (hTert-immortalized fibroblasts kindly provided by Dr. Roderick Beijersbergen) were grown in DMEM/F-12 + Glutamax (GIBCO) with 6% FCS (Clontech), supplemented with antibiotics (Invitrogen) and ultraglutamine (Lonza). All siRNA transfections were done using HiPerfect according to the manufacturers protocol (QIAGEN).

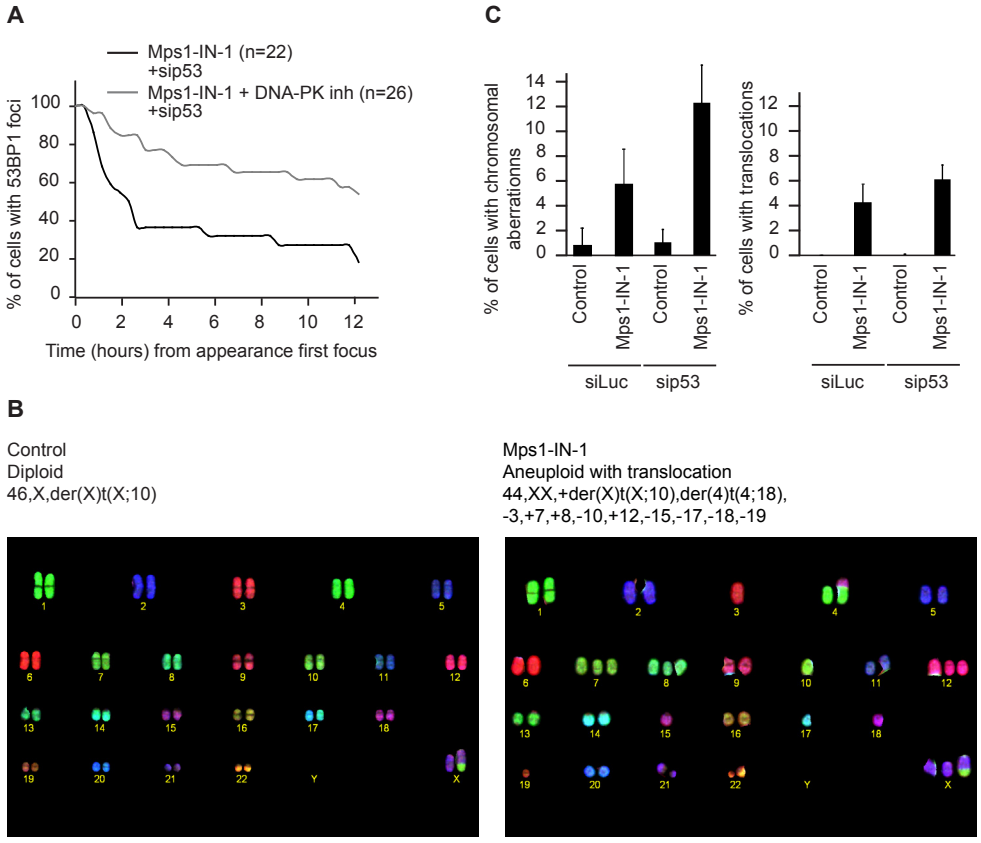

Figure 4. Chromosome missegregations cause structural chromosomal aberrations
A) Time-lapse analysis of 53BP1-foci disappearance in RPE-1 treated with Mps1-IN-1 -/+ DNA-PK inhibitor (n=no. cells). B) Representative images of chromosome spreads labeled with COBRA-FISH two days after indicated treatments. C) Quantification of all structural aberrations (left) or chromosomal translocations only (right) following indicated treatments (4 experiments +/- SD, 50 cells/experiment).

Doxorubicin (0,5μM), Monastrol (100μM) and Caffeine (5mM) were from Sigma. ZM (2μM), ATM inhibitor KU55933 (10μM) and DNA-PK inhibitor Nu7441 (5μM) were from Tocris Biosciences, AZD (100nM) from Selleck and Blebbistatin (30μM) from Omnilabo. Calyculin A (80nM) was from Biolmol, RO-3306 (7,5μM) was from Calbiochem and Mps1-IN-1 (10μM) was kindly provided by Dr. Nathanael Gray [123]. RPE-1 and U2OS lines were infected with retrovirus carrying pBabeH2B-RFP and/or pLNCX2GFP-m53BP1. Cell lines were selected with 5 μg/ml blasticidine (for H2B-RFP) and/or 500μg/ml G418 (for GFP-53BP1). Single colonies were selected after replating 1-2 cells/well. SW480 cells were infected with pLV.CMV.H2B-GFP and selected with 1 μg/ml puromycin. MCF-7 cells stably expressing 53BP1-GFP were a kind gift from Dr. Marcel van Vugt. For time-lapse analysis SW480-H2B-GFP and MCF7-53BP1-GFP cells were transiently transfected with 53BP1-mCherry and H2B-mCherry-N1 (kindly provided by Dr. Susanne Lens) respectively using FuGene HD Transfection reagent (Roche) or standard Calcium Phosphate method. Both pLNCX2-53BP1-GFP and 53BP1-mCherry were kindly provided by Dr. Marcel van Vugt.

Monastrol wash-out procedure

For Monastrol block-release experiments asynchronously growing cells were treated with Monastrol

for 14 hours (unless indicated otherwise). Monastrol is an inhibitor of the kinesin-5 motor protein Eg5 that induces monopolar spindle formation and a mitotic delay [434]. During monopolar spindle formation many erroneous kinetochore-microtubule attachments are established, (i.e. two sister kinetochores bound to one pole, one kinetochore bound to two poles) [64,289,434] that cause a high rate of chromosome missegregation upon release from the block [289]. Mitotic cells were collected by shake-off after Monastrol treatment, washed 3 times with PBS using centrifugation at 1000 rpm and replated. Cells were harvested for immuno-fluorescence or immuno-blotting 6 hours after release, or were followed by time-lapse analysis for 6 hours after mitotic exit. For the immuno-fluorescence analysis of foci formation, Monastrol-released cells were subdivided in nuclei with a normal and abnormal morphology. Normal nuclei: oval shaped with no clear aberrations. Abnormal nuclei: multilobed shape and/or DNA in cleavage furrow. Except when stated otherwise, only abnormally shaped nuclei were taken into account. In all Monastrol release experiments, inhibitors were added at the moment of replating after mitotic shake-off.

Mps1-IN-1 treatments

Unless stated differently, RPE-1 or U2OS (Fig.S1E) cells were grown asynchronously in the experiments in which Mps1-IN-1 was used to induce chromosome segregation errors. In time-lapse experiments only foci formation within 5 hours after mitotic exit was taken into account. In experiments in which Thymidine was used to synchronize the cells, Thymidine was added for 24 hours and cells were then washed 3 times with PBS to release from the thymidine block. Subsequently, Mps1-IN-1- or control-supplemented medium was added for 16 hours before harvesting (Fig.1E, F, S1C and S8B).

Doxorubicin and RO-3306 treatments

The DNA damaging agent doxorubicin was used as a positive control for immuno-fluorescence experiments and immuno-blotting. Asynchronously growing cells were treated with doxorubicin for 1 hour, washed 2 times and harvested 6 hours later. For RO-release experiments (Fig.1D, S1A,B), RPE-1 cells were treated with the Cdk1 inhibitor RO-3306 (7,5 μM) for 16 hours to arrest cells in G2 [435]. Subsequently cells were washed 3 times with warm medium to remove RO-3306. Mitotic cells were collected by mitotic shake-off one hour after RO-3306 wash-out, replated and fixed 6 hours later.

Cleavage furrow experiments

In the experiments shown in Fig.2C,D, S4A,B and Movie S3 U2OS and RPE-1 cells were synchronized in G2 using RO-3306 (7,5μM) for 3 hours (U2OS cells) or 16 hours (RPE-1 cells) and subsequently released from the RO-induced G2 arrest. U2OS cells underwent spontaneous segregation errors, while RPE-1 cells were treated with Mps1-IN-1 (added at the moment of RO-wash out) to induce segregation errors. Cells were harvested and fixed 1, 5 to 2 hours after RO release to obtain cells in ana- or telophase. As control conditions, γH2AX or MDC1 staining on lagging chromosomes in anaphase cells (before cleavage furrow ingression) or missegregating chromosomes found outside of the cleavage furrow in telophase cells (Fig.S4B, Fig.2D) were determined.

Live cell imaging

Cells were plated in 2, 4 or 8-well chambered glass bottom slides (LabTek) and imaged in a heated chamber (37ºC and 5% CO2) using a 40X/1.3NA oil objective on a Zeiss Axiovert 200M microscope equipped with a 0.55NA condenser and controlled by a lambda-DG4 (Roper Scientific) and MetaMorph software. Green fluorescent (80 msec exposure) and red fluorescent images (200msec exposure) were acquired every 12 min using a Photometrics CoolSnap HQ CCD camera (Roper Scientific) for 48-64 hours. Images were processed using MetaMorph software. For live analysis of Monastrol release (Fig.3F, S2B-E), RPE-1 cells stably expressing H2B-RFP and 53BP1-GFP were imaged using a 40X/0,75NA UPLFLN objective on an Olympus 1X-81 microscope, controlled by Cell-M software (Olympus). Green fluorescent and red fluorescent images were acquired every 12 minutes for 12 hours following release from Monastrol. Images were processed using Cell-M software. Segregation errors in daughter cells were categorized in three classes: no, mild (metaphase plate formed properly, some lagging chromosomes in anaphase) and severe (no proper metaphase plate has been formed when cells enter anaphase) (Fig.1A, G). To avoid analysis of 53BP1 foci formation that might be associated with the onset of DNA replication, we analyzed only 53BP1 foci that formed within 5 hours after mitotic exit (anaphase) in all live cell imaging experiments shown.

Immunofluorescence Microscopy

Cells were plated on 10 or 12mm coverslips. For all Monastrol release samples, mitotic cells were collected by shake-off, washed 3 times with PBS using centrifugation for 5 minutes at 1000 rpm and replated in a new well. Cells were harvested 6 hours after Monastrol release or 16 hours after Thymidine release. Fixation was done using 4% PFA in PBS. Antibodies were incubated O/N in PBS 3% BSA. Secondary antibodies and DAPI were incubated in PBS 0, 1% Tween. DAPI was used to visualize DNA. Stained coverslips were mounted with Vectashield Mounting Medium (Vector). Images were acquired on a Zeiss 510 Meta confocal laser scanning microscope with a 63X/1.4NA Plan-ApoChromat objective using the Zeiss LSM software or on a DeltaVision RT system (Applied Precision) with 100x/1.40NA UplanSapo objective (Olympus) using SoftWorx software.

Chromosome spreads and COBRA FISH

RPE-1 cells were transfected with either luciferase or p53 siRNA on day 0, treated for 2 days with or without Mps1-IN-1 and harvested on day 4 (Fig.4). CIN tumor cell lines MCF7, SW480 and U2OS were grown asynchronously (Fig.S10). Calyculin A (80nM) was added for 25 minutes to the medium to enrich for G2 and Mitotic cells with condensed chromosomes. Cells were treated with 0.075 M KCl at 37ºC for 10 minutes and centrifuged at 750 rpm for 8 minutes. Cells were fixed with Methanol: Acetic Acid (4:1) and centrifuged at 750 rpm for 8 minutes. The fixation procedure was repeated 3 times. Samples were collected in Methanol: Acetic Acid (4:1). Chromosome spreads were created by allowing the drops to fall from 30 cm height onto glass slides. Spreads were left at room temperature for 2 days before hybridization. COBRA-FISH staining and analysis was performed as described before [433]. Structural chromosomal aberrations include all aberrations; breaks, deletions and translocations. RPE-1 cells harbor an endogenous translocation derived from chromosome X and 10. Therefore, this specific translocation has been left out of the quantifications shown in Fig.4C.

Immuno Blotting

Cells were lysed in Laemmli buffer. Samples were separated by SDS-page and transferred to Nitrocellulose membrane (Whatman). The membranes were blotted with anti-p53, anti-phospho-threonine68-chk2, anti-chk2 or anti-actin. Peroxidase-coupled secondary antibodies and ECL (GE healthcare) were used to visualize protein bands.

Automated analysis of EdU incorporation

Cells were grown in 96 wells plates in 100µl culture medium. After release from thymidine or Monastrol, EdU was added to the culture medium and cells were fixed using 4% PFA at indicated time-points. siRNA transfections were performed 24 hours prior to Thymidine or Monastrol addition. EdU incorporation was visualized by staining with 100mM Tris 1mM CuSO4 buffer pH 8.5 in the presence of 100mM Vitamin C and Alexafluor 488-Azide. Image acquisition was performed using a Cellomics ArrayScan VTI (Thermo Scientific) using a 10x 0.5NA objective. 10 images were acquired per well, which contained around 4000 cells in total. Image analysis was performed using Cellomics ArrayScan HCS Reader (Thermo Scientific). The percentage of S phase entry was calculated by the amount of EdU positive cells over the total DAPI positive cells.

Antibodies and siRNAs

The following antibodies have been used for Western Blot and Immunofluorescence: α-p53 (126) and α-53BP1 (22760), α-chk2 (9064) (Santa Cruz), α-phospho-thr68-chk2 (2661), pS15-p53 (9286) and pS1981-ATM (4526), γH2AX (2577) (Cell Signaling), α-tubulin (5168) (Sigma), actin (1616) (TeBu), γH2AX (05-636) (Upstate), MDC1 (11171) (Abcam), CREST (1058) (Cortex Biochem), Alexa-Fluor-Phalloidin-633, anti-mouse Alexafluor647, anti-rabbit/mouse Alexafluor488, anti-rabbit/mouse Alexafluor568, anti-human-Alexafluor568, Alexafluor-488-azide (Invitrogen). Rabbit anti-Goat-PO, Goat anti-Mouse-PO and Goat anti-Rabbit-PO were all from DAKO. For Luciferase, p53, ATM and DNA-PK knockdown ON-TARGETplus SMARTpools (Dharmacon) were used at a final concentration of 20 µM.

Acknowledgements

The authors thank Livio Kleij for technical assistance and the Medema, Lens and Kops labs for discussions. We thank Jonne Raaijmakers, Marvin Tanenbaum, André Maia and Saskia Suijkerbuijk for critically reading the manuscript. We are grateful to Marcel van Vugt and Roderick Beijersbergen for sharing plasmids and cell lines. This work was supported by the Netherlands Organisation for Scientific Research (NWO) (R.H.M. and A.J.: ZonMw 918.46.616; G.J.P.L.K.: VIDI-91776336), TI Pharma (R.H.M and A.J.: T3-105) and the ERC (G.J.P.L.K.: ERC-StG KINSIGN). R.H.M. was additionally funded by the Netherlands Genomic Initiative of NWO.

Supplemental data

Supplemental text

Chromosome missegregations induce DNA damage

Monastrol is an inhibitor of the kinesin-5 motor protein Eg5 that induces monopolar spindle formation and a subsequent delay in mitosis [434]. During monopolar spindle formation many erroneous kinetochore-microtubule attachments are established, (i.e. two sister kinetochores bound to one pole, one kinetochore bound to two poles) [64,289,434] that are responsible for the high rate of chromosome segregation errors upon release from the Monastrol block. To rule out the possibility that γH2AX and 53BP1 foci formation are a consequence of a prolonged arrest in mitosis, we performed shorter treatments with Monastrol. Treatment with Monastrol for only 1 or 2 hours also resulted in abnormal nuclei formation and enhanced γH2AX-foci formation (Fig.S1B), indicating this occurs independently of the length of the mitotic delay. To rule out that γH2AX and 53BP1 foci formation occurs as a consequence of cell synchronization, cell were synchronized in mitosis by an alternative protocol. Mitotic cells obtained by shake-off after release from a G2 arrest induced by the Cdk1 inhibitor RO-3306 [436], did not produce G1 daughters with increased γH2AX and 53BP1 foci (Fig.S1A). This indicates that enhanced foci formation is not simply due to synchronization of cells in mitosis.

Supplemental Movies

S1-S4 can be found online at http://www.sciencemag.org.proxy.library.uu.nl/content/333/6051/1895/suppl/DC1

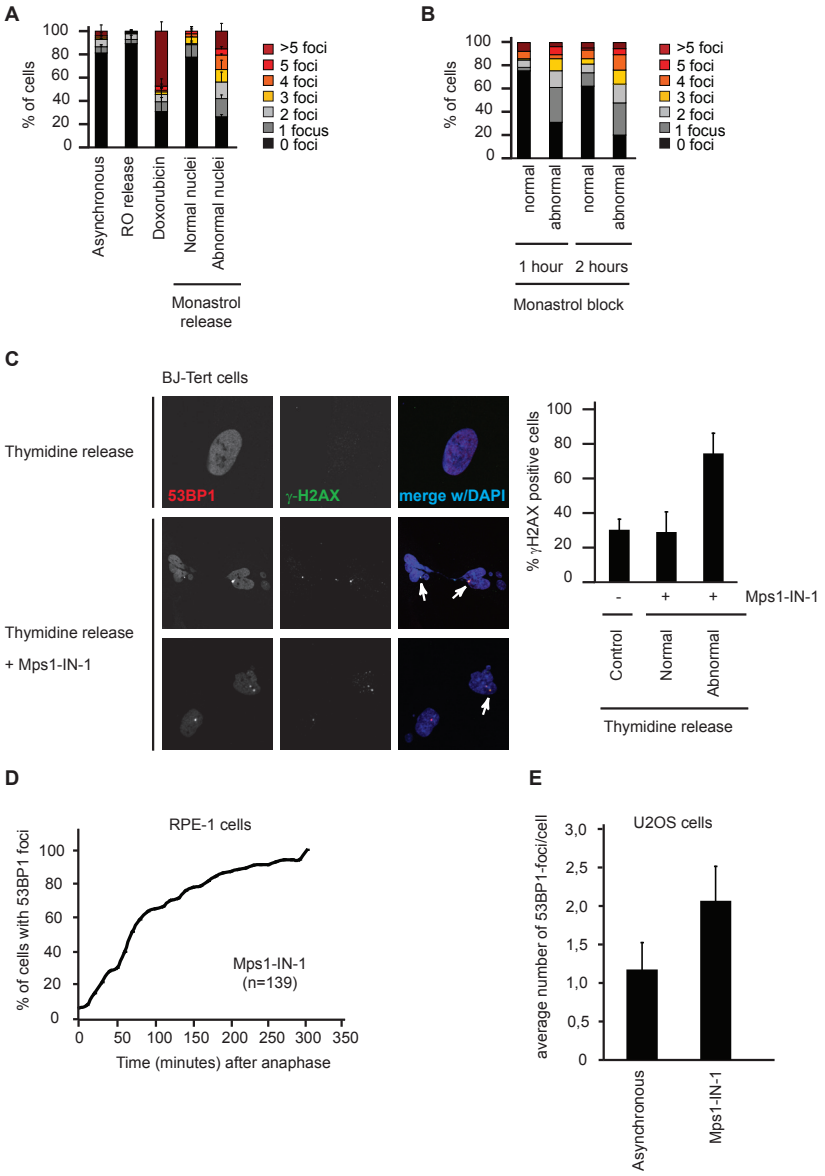

Figure S1.
A) Quantification of the amount of γH2AX foci per nucleus. RPE-1 cells were treated as described in Fig.1C, D. Average percentage of cells with indicated amount of foci is shown of 3 independent experiments +/- SD. At least 100 cells were counted per condition/experiment. B) Quantification of γH2AX immunostaining of RPE-1 cells treated with Monastrol for 1 or 2 hours. After this treatment, mitotic cells were collected by shake-off, washed, replated and fixed 6 hours later. Normal: oval shaped nuclei with no clear aberrations. Abnormal: cells that underwent chromosome missegregations; multilobed nuclei and/or DNA in cleavage furrow. n=at least 75 cells/condition. C) Left: Representative images of untransformed, immortalized BJ-Tert cells released from a thymidine block treated without or with 10μM Mps1-IN-1 and harvested at t=16 hours after release. 53BP1 is shown in red and γH2AX in green. DAPI (blue) was used to visualize DNA. Right: Quantification of images shown in left panel. Average of 3 independent experiments is shown +/- SD, with n=100 cells per condition/per experiment. D) Timing of 53BP1 foci formation in Mps1-IN-1 treated RPE-1 cells stably expressing H2B-RFP and 53BP1-GFP. Only cells which obtained 53BP1 foci were included in this graph. N indicates the amount of cells filmed. E) Quantification of 53BP1 foci formation using live cell imaging of U2OS cells stably expressing 53BP1-GFP. U2OS cells were treated with or without Mps1-IN-1 and foci formation was determined within 5 hours after mitosis. Average of 4 independent experiments +/- SD is shown with n=at least 50 cells per condition/per experiment.

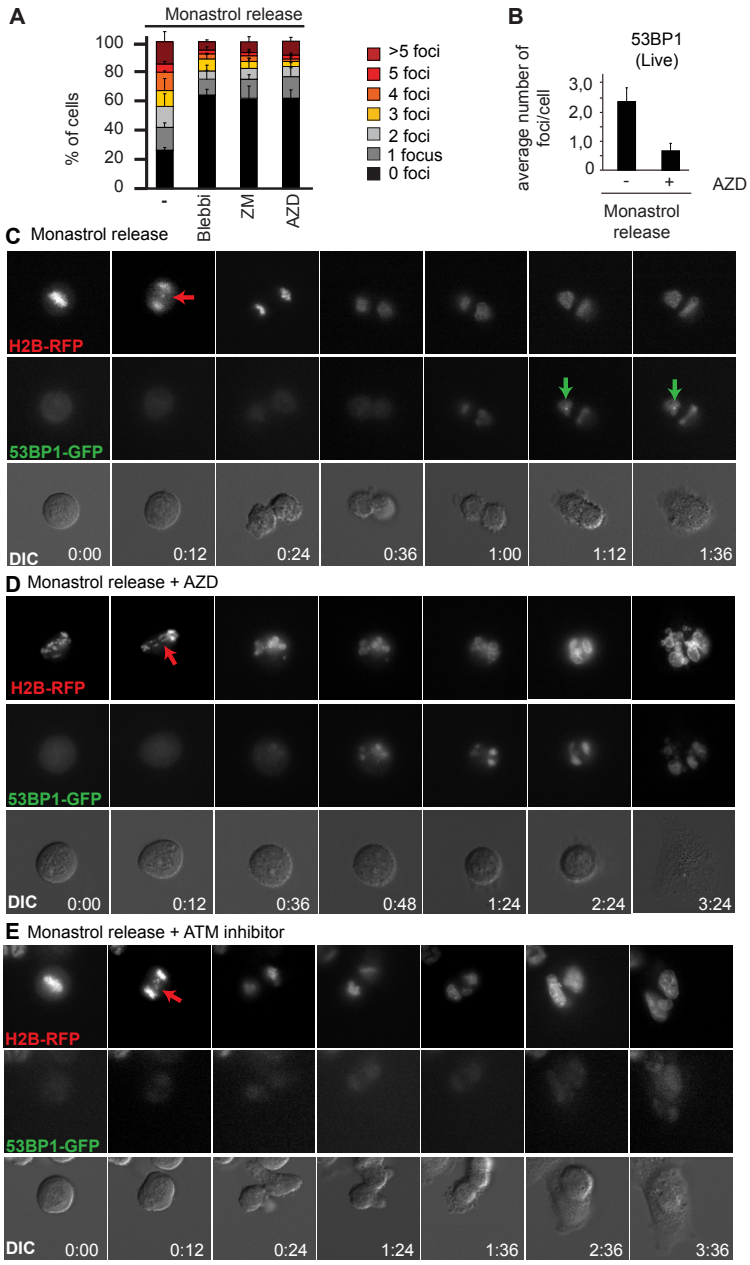

Figure S2.
A) Quantification of the amount of γH2AX foci per cell. RPE-1 cells were treated as described in Fig.2A. Average percentage of cells with indicated amount of foci is shown of 3 independent experiments +/- SD. At least 100 cells were counted per condition/experiment. B) Quantification of 53BP1 foci formation using live cell imaging after indicated treatments as shown in (C, D). Average of 3 independent experiments is shown +/- SD. n= at least 50 cells per condition/per experiment. C) Representative images of RPE-1 cells stably expressing H2B-RFP and 53BP1-GFP filmed using time-lapse microscopy following release from Monastrol. After treatment with Monastrol, mitotic cells were collected, washed and replated on a glass-bottom well to allow time-lapse analysis. D) As (C), AZD was added at the moment of replating. E) As (C), ATM inhibitor was added at the moment of replating.

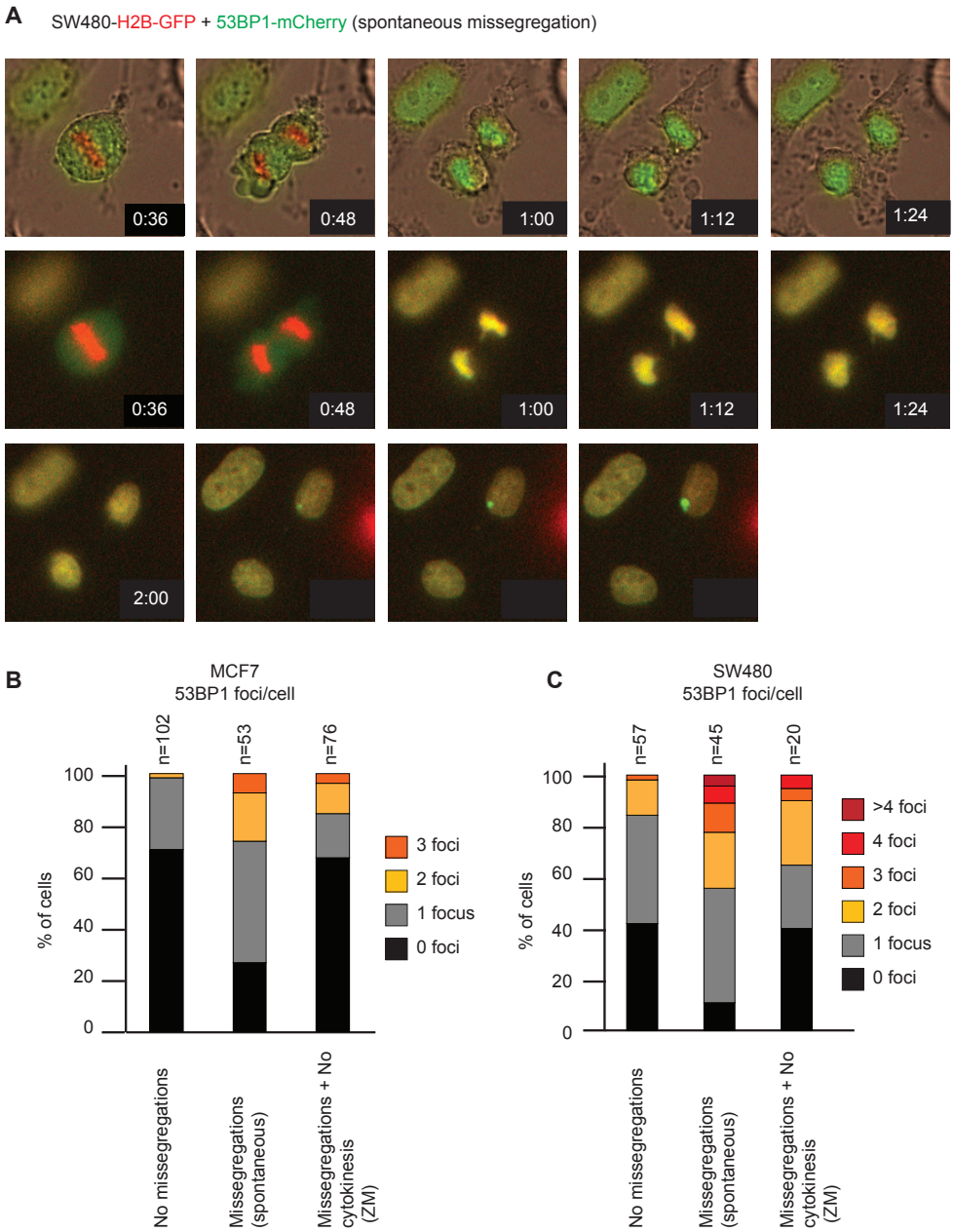

Figure S3.
A) Representative images of asynchronously growing SW480 cells stably expressing H2B-GFP (red) and transiently expressing 53BP1-mCherry (green) filmed using time-lapse microscopy. B) Quantification of 53BP1 foci formation in asynchronously growing MCF7 cells stably expressing 53BP1-GFP and transiently expressing H2B-RFP. 'No missegregations': normal metaphase plate, no clear aberrations. 'Spontaneous missegregations': chromosome missegregations in the presence of cytokinesis. 'Missegregations + no cytokinesis: cells were treated with the Aurora B inhibitor ZM, which results in chromosome missegregations and failed cytokinesis. 53BP1 foci formation was determined upon mitotic exit. Only foci formation within 5 hours after mitotic exit was taken into account. N indicates amount of cells filmed in each condition. C) Quantification of 53BP1 foci formation of asynchronously growing SW480 cells stably expressing H2B-GFP and transiently expressing 53BP1-mCherry as in (B).

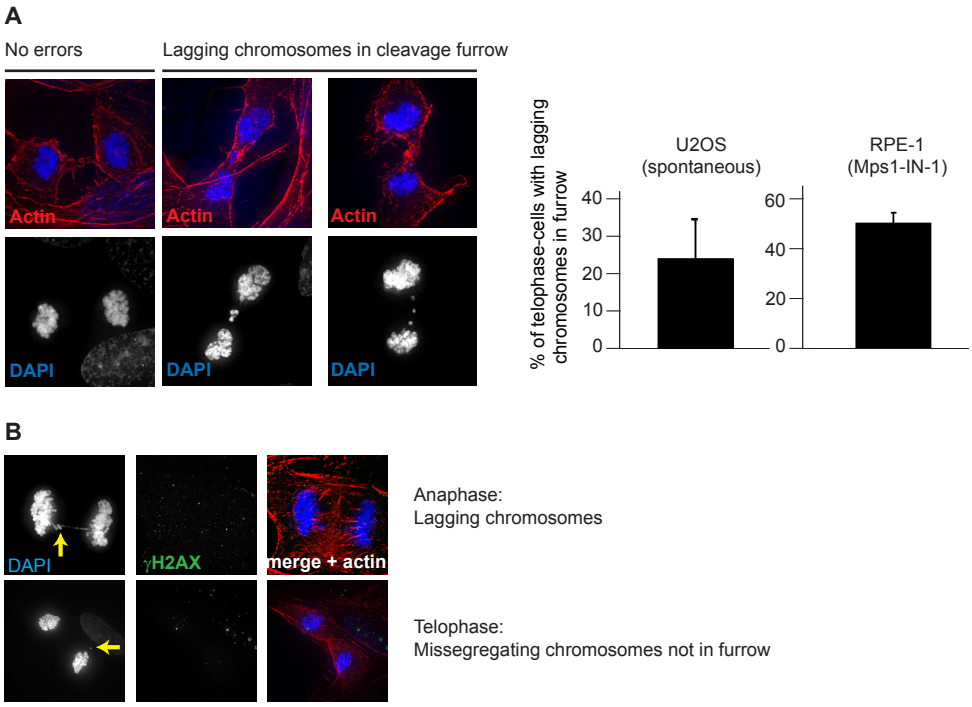

Figure S4.
A) Left: Immunofluorescence images of RPE-1 cells acquired using DAPI (blue) to visualize the chromosomes and Phalloidin (red) to visualize the actin cytoskeleton. Right: Quantification of representative images shown on the left. The percentage of telophase cells with lagging chromosomes in the cleavage furrow was determined over all telophase cells. U2OS cells were released from a 3 hour RO block and fixed at the moment of telophase. RPE-1 cells were released from a 16 hour RO block, treated with Mps1-IN-1 and fixed at the moment of telophase. Average of 3 independent experiments is shown +/- SD. At least 100 cells were counted per experiment. B) Immunofluorescence images acquired using an antibody against γH2AX (green), DAPI (blue) and Phalloidin (red) in U2OS cells released from a 3 hour RO block and fixed at the moment of anaphase (upper panel) or telophase (lower panel).

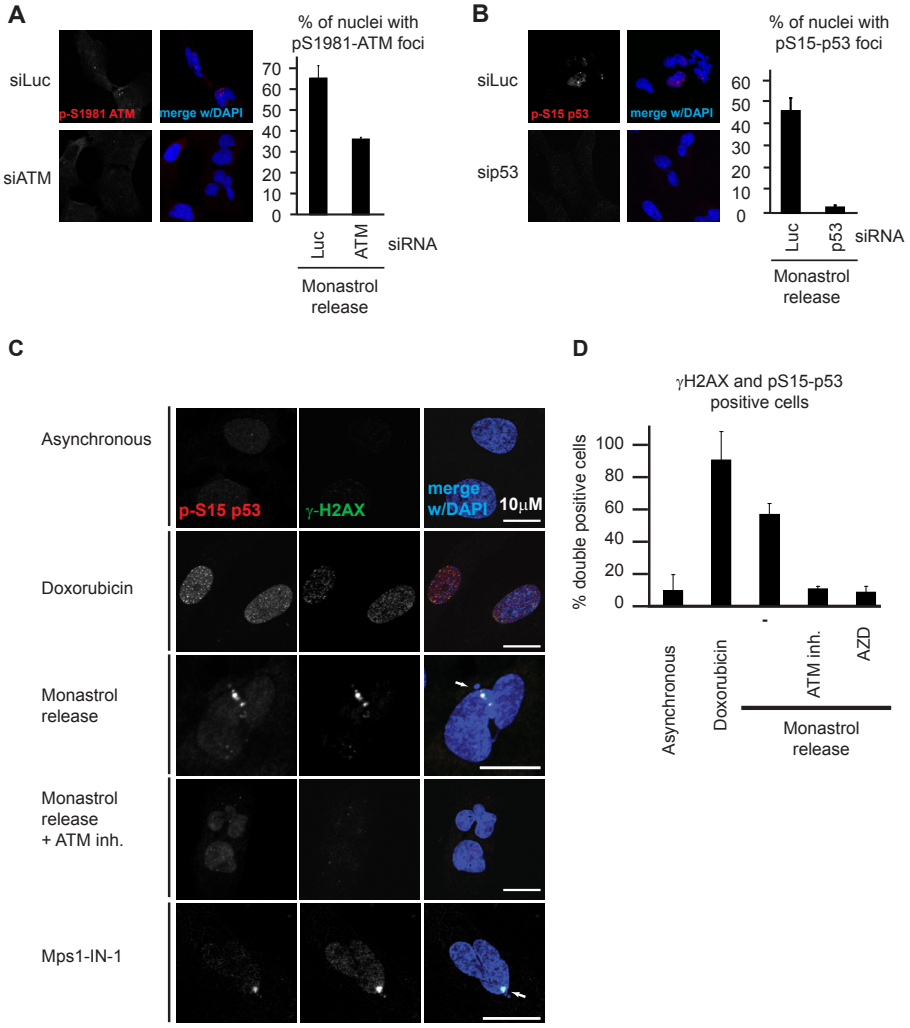

Figure S5.
A,B) Left: RPE-1 cells were transfected with indicated siRNAs for 2 days, released from Monastrol as described before and stained for phospho-Serine-1981 on ATM (A) or phospho-Serine 15 on p53 (B) (red) and DAPI (blue) to visualize the DNA. Right: Quantification of immunofluorescence images shown in (A) and (B). n= at least 100 cells/experiment/condition. C) RPE-1 cells were treated as indicated and stained for phospho-Serine 15 on p53 (p-S15-p53) (red), γH2AX (green) and DAPI (blue). D) Quantification of immunofluorescence images shown in (C). Percentage of cells positive for both γH2AX and p-S15-p53 (double positive) was determined after treating RPE-1 cells with indicated conditions. In the Monastrol released samples (-, ATM inhibitor, AZD), only abnormal nuclei were quantified. Indicated inhibitors were added at the moment of release. For all experiments average of 3 independent experiments is shown +/- SD. n=at least 75 cells/condition.

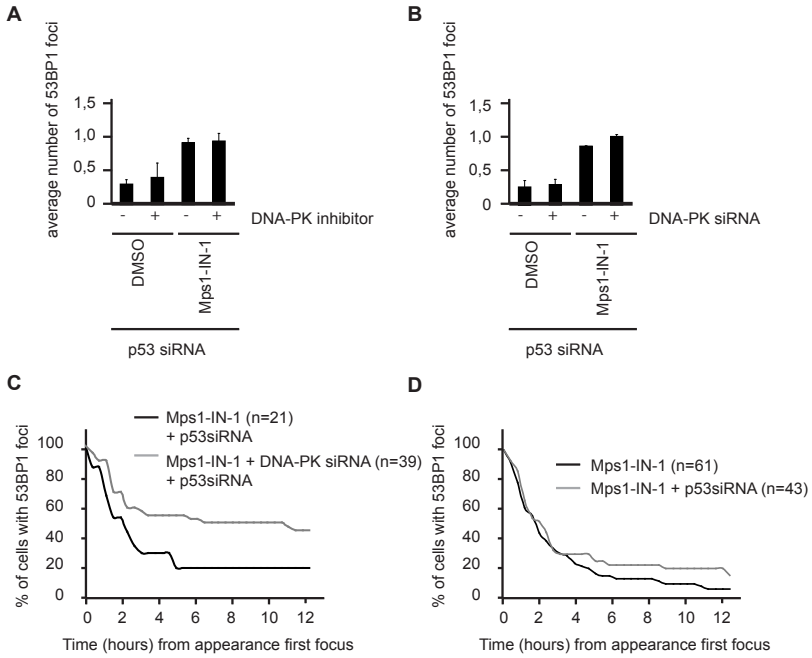

Figure S6.
A,B) Quantification of 53BP1 foci formation using live cell imaging of asynchronously growing RPE-1 cells in the presence of indicated treatments. n=3 independent experiments +/- SD, in which at least 20 cells were analyzed per condition. All cells were transfected with p53 siRNA and (where indicated) with DNA-PK siRNA for 1 day prior to filming. Indicated inhibitors were added at the start of the movie. C, D) Timing (in hours) of 53BP1 foci disappearance in RPE-1 cells filmed in the presence of indicated treatments. N indicates the amount of cells analyzed.

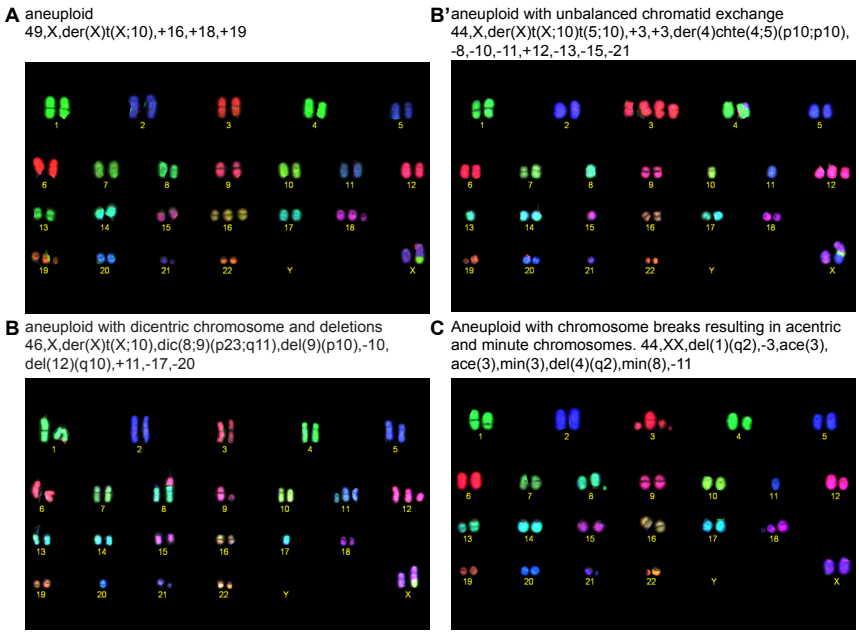

Figure S7.
Representative COBRA FISH images are shown of chromosome spreads of RPE-1 cells treated with Mps1-IN-1 in the presence of p53 knockdown reflecting different phenotypes: A) aneuploidy, B) aneuploidy + translocations and C) aneuploidy + chromosomal breakage.

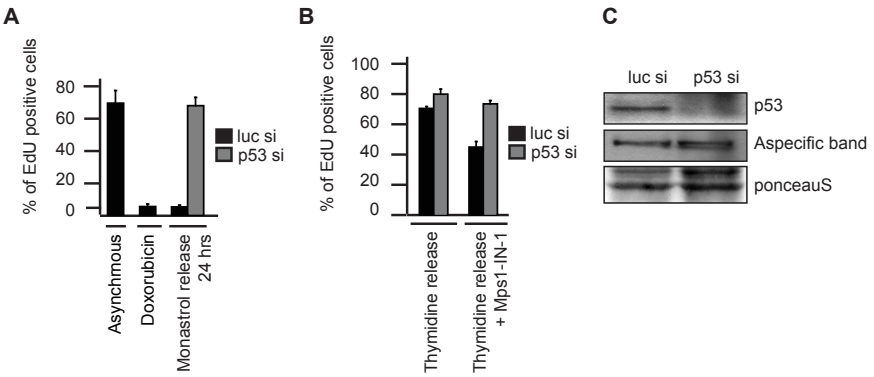

Figure S8.
A,B) EdU incorporation was used to determine the amount of cells that have entered S phase in RPE-1 cells 24 hours after indicated treatments. % of EdU positive cells was determined over the amount of nuclei using Cellomics software. C) RPE-1 lysates were immuno-blotted for p53 after indicated siRNA treatments for 2 days. PonceauS and an aspecific band are shown as loading controls.

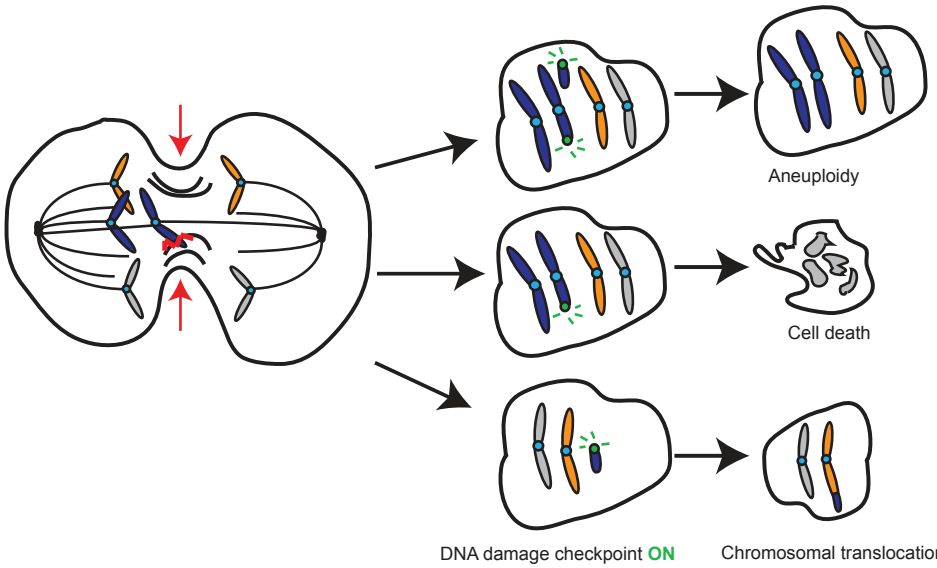

Figure S9.
Model for cleavage furrow induced DNA double strand breaks. Cleavage furrow ingression damages a missegregating chromosome, which results either in one daughter cell inheriting both chromosomal fragments or in two daughter cells that both inherit parts of the broken chromosome. This activates a DNA damage checkpoint response. In the upper case, the daughter cell will be able to repair the damage and becomes an aneuploid cell without any structural aberrations. In most cases, the daughter cell will die. However, in a small percentage of cells, the broken chromosome will fuse to another chromosome and form a translocation.

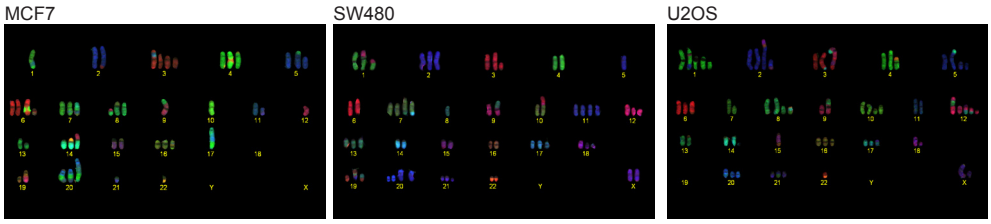

Figure S10.
Representative COBRA FISH images are shown of chromosome spreads of asynchronously growing MCF7, SW480 and U2OS cells.

Chapter 3

Studying Chromosomal instability *in vivo* using a Cre inducible Mps1 knock-in mouse model (CiMKi)

Aniek Janssen[1,2,*], Nannette Jelluma[1,*], René H. Medema[1,2,†], Geert J.P.L. Kops [1,3 †]

[1] Department of Medical Oncology and Cancer Genomics Center, University Medical Center Utrecht, Universiteitsweg 100, 3584 CG, Utrecht, the Netherlands

[2] Division of Cell Biology, Netherlands Cancer Institute, Plesmanlaan 121, 1066 CX, Amsterdam, the Netherlands

[3] Department of Molecular Cancer Research, University Medical Center Utrecht, Universiteitsweg 100, 3584 CG, Utrecht, the Netherlands

[*]These authors contributed equally

[†]These authors contributed equally

Abstract

Chromosomal instability (CIN), the loss and gain of whole chromosomes during cell division, is one of the hallmarks of solid tumors and has been described to influence tumor formation. Both tissue context and the level of CIN are thought to determine whether CIN has a tumor promoting or tumor suppressive function. Moreover, excessive CIN has been described to specifically kill tumor cells *in vitro.* Here, we describe the generation of a mouse model in which we will be able to test the effects on tumor growth of various levels of CIN in different tissues. We have generated two Cre-inducible-Mps1-Knock-in (CiMKi) mouse models that inducibly express mutant forms of the mitotic checkpoint kinase Mps1; kinase dead Mps1 (D637A) or an Mps1 point mutant with reduced kinase activity (T649A). These models will gives us the opportunity to test the effect of different levels of CIN in both tumorigenesis and tumor growth inhibition in a tissue-specific and temporal manner.

Introduction

Aneuploidy is a common genetic alteration in solid human cancers and refers to an abnormal chromosome number [236]. The main underlying phenotype that causes aneuploidy is known as chromosomal instability (CIN), which is the frequent gain and loss of whole chromosomes during cell division[270,289]. The widespread occurrence of aneuploidy in cancers has led to the hypothesis that CIN may contribute to tumor formation and/or progression[287]. In support of this, CIN occurs at an early stage of colorectal tumorigenesis and has been shown to occur in cell cultures of colon, prostate, oropharynx, lung and breast tumors[289,312,437-439]. Moreover, a strong correlation of CIN with aggressiveness of the tumor, resistance to chemotherapeutics and poor patient prognosis has been reported[271-273,275-280,283], and a striking correlation was observed between a CIN signature and different grades of primary breast cancers and derivative lung metastases[275]. Such observations have spurred extensive investigations into the potential role of CIN in tumor formation and progression, and several mouse models have resulted in important advances in our understanding of this [398]. Errors in mitotic chromosome segregation are the predominant cause of CIN. Such errors are normally prevented by the error-correction and mitotic checkpoint machineries. The mitotic or spindle assembly checkpoint is a safeguarding mechanism that delays mitotic exit until error-correction has ensured that all chromosomes are attached and aligned correctly on the mitotic spindle [440]. The mitotic checkpoint is a robust signalling cascade that originates from the chromosomal anchor points of mitotic spindle microtubules, termed kinetochores, whenever these kinetochores are not interacting with microtubules [441]. The core conserved components of the mitotic checkpoint are Mad1, Mad2, Bub3, BubR1, Bub1, and Mps1. Depletion or inactivation of any one of these components abrogates mitotic checkpoint activity, resulting in chromosome missegregations and thus aneuploidy [441]. On top of their role in the mitotic checkpoint, Mps1, BubR1 and Bub1 have also been shown to be important players in error-correction[116,442,443]. Although yet to be shown for human cancers, defects in both error correction and mitotic checkpoint functioning have been hypothesized to cause CIN in tumor cells and experimental weakening of either has supported this [290]. Additional defects that have been hypothesized to contribute to CIN are sister chromatid cohesion defects, cytokinesis defects and centrosome overduplication[335,338,353,355,356,444]. Various mouse models for chromosomal instability have been generated[392]. These mouse models mainly target proteins which have a role in mitotic progression, such as CENP-E, UbcH10 and Cdc20 and the mitotic checkpoint proteins Mad2, Mad1, Bub1, Bub3, BubR1, [332,392,400,413]. Homozygous deletion of all studied mitotic checkpoint components causes early embryonic lethality[392]. The effects of heterozygous deletion, however, depend on the gene and tissue examined. For instance, Mad2$^{+/-}$ and Mad1$^{+/-}$ mice develop tumors at long latency [291,298], while on the other hand, heterozygous deletion of Bub1, Bub3 or BubR1 did not lead to spontaneous tumor formation, despite development of aneuploidy [295-297,300]. However, treating some of these models with carcinogens or crossing them with tumor prone mouse models did increase the extent and speed of tumor formation[286,295,296,401]. In contrast to heterozygous deletion, reducing levels of Bub1 using hypomorphic mice resulted in spontaneous tumorigenesis[395], indicating that different levels of CIN may have different outcomes, depending on the genetic context. In contrast to the tumor promoting roles of CIN, excessive CIN and aneuploidy are not tolerated at the cellular level[292,445,446]. Indeed, CIN may also confer a tumor suppressive function in certain mouse models[286,397] and more importantly, in human patients[404]. In line with this, enhancing chromosome segregation errors through mitotic checkpoint inhibition has been suggested as a useful anti-cancer strategy[292,299,447].

The abovementioned studies suggest that the contribution of CIN to tumor formation or progression

may be quite complex, and may depend on the level of CIN reached in a given tissue in a given genetic model. However, the fact that in currently available mouse models CIN is already present during early development and in most cases cannot be induced in the adult mouse poses a significant problem in interpreting its effects on tumor formation and inhibition. Therefore, we have designed and tested a genetic strategy to inducibly reduce or ablate Mps1 activity in mice. In this model, named CiMKi (*Cre-inducible Mps1 Knock-in*), timed and local induction of Cre-mediated recombination using the Cre-ER^{T2} system will result in knock-in of two activity-reducing Mps1 point mutations in the endogenous Mps1 locus. This will allow us to control when and where and to what extent Mps1 activity will be reduced, and therefore what level of CIN will be induced. As expected from our previous work[172,299] and predicted from our experiments with the CiMKi^{T649A} strain, different activities of Mps1 will cause diverse levels of CIN. This makes CiMKi a suitable model to test the influence of various levels of CIN on tumor initiation, progression and tumor growth inhibition (Fig.1).

Results

To study the contributions of mild CIN to tumorigenesis as well as to assess whether inducing excessive CIN is a feasible anti-cancer strategy, we have developed the CiMKi (Cre-inducible Mps1 Knock-in) model. Inspired by a recently published conditional V600E mutation in the BRAF locus[448], CiMKi allows conditional mutation of the endogenous allele of Mps1 to one that encodes D637A (equivalent of human D664; CiMKi^{D637A}) or T649A (equivalent of human T676; CiMKi^{T649A}). Both the D664A and T676A mutation have been shown to reduce kinase activity of human Mps1 to 0% and 20% respectively. D664 is one of the catalytic aspartates, which is required for ATP positioning via Mg^{2+} binding, and substitution of this residue renders the kinase inactive[143]. T676 is an autophosphorylation site present in the activation loop of Mps1 and substitution for alanine reduces Mps1 kinase

Mps1	WT/WT	WT/T649A	WT/D637A	T649A/T649A	T649A/D637A	D637A/D637A
% kinase activity (expected)	100	60	50	20	10	0
Phenotype (expected)	No CIN	?	?	Mild CIN	Moderate CIN	Severe CIN

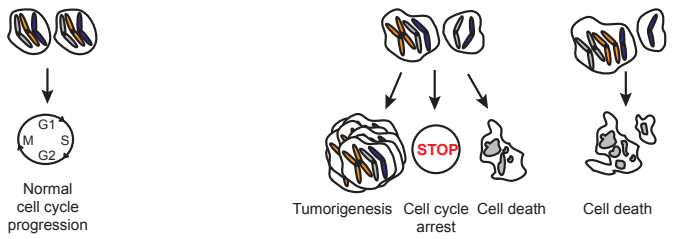

Figure 1
Schematic overview of the CiMKi mouse models that will be generated. Expected residual Mps1 kinase activity of each mouse model is indicated as well as the phenotype expected in the specific genotypes. The absence of CIN will produce two identical daughters after each cell division and normal cell cycle progression. The presence of mild CIN will lead to mild chromosome missegregations (~1-2 chromosomes/cell division), which will lead to intermediate levels of aneuploidy. This mild CIN could lead to cell death, cell cycle arrest or tumorigenesis. Severe CIN will induce severe chromosome segregation errors upon mitotic exit (>3 chromosomes/cell division) causing enhanced genomic instability, which is incompatible with cell viability.

activity by ~80%[170-172]. With the use of these two different Mps1 mutations we create a panel of mice with graded reductions in Mps1 kinase activity (100%, 60%, 50%, 20%, 10% and 0%) and as a result with various levels of CIN (Fig. 1). This way we will be able to test the hypothesis that different levels of CIN will have different effects on tumor-initiation, -enhancement or –inhibition. Using homologous recombination in mouse embryonic stem cells (ES cells) we have inserted a cDNA sequence encompassing exons 17-22 followed by the polyA sequence and stop codon of Mps1 mRNA, into intron 16 of the genomic sequence coding for Mps1 (Fig.2A). This results in transcription of wild-type Mps1, but with the sequences of exons 17-22 being transcribed from the inserted intron-less cDNA. The inserted cDNA is flanked by LoxP sites, and the targeting vector included a right

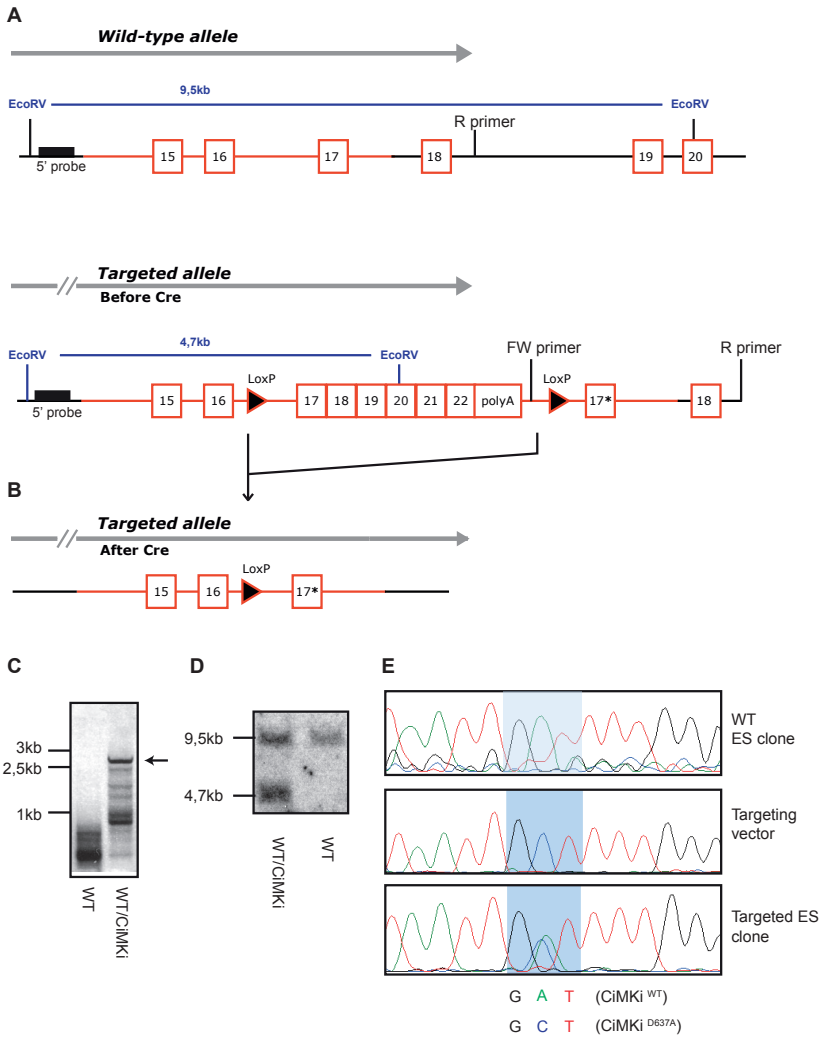

Figure 2
A) CiMKi gene targeting strategy. Part of the wildtype (upper panel) and targeted (lower panel) Mps1 locus, EcoRV restriction sites, 5' Southern probe, PCR primers and loxP sites are indicated. B) The targeted Mps1 locus following Cre recombinase addition. C) PCR-based genotype analysis of CiMKi ES clones. Positions of PCR primers (FW/R) are indicated in A and B. D) Southern blot analysis of CiMKi ES clones. EcoRV restriction sites and 5' Southern probe are indicated in A and B. E) Sequences of the D637 position in the Mps1 allele of a wildtype ES cell clone, the CiMKi^{D637A} targeting vector and a CiMKi^{D637A} targeted ES cell clone.

recombination arm carrying the desired point mutation in exon 17. Cre-mediated recombination of the LoxP sites will therefore result in excision of the cDNA sequence and restoration of the original allelic organization, but now with a mutated exon 17 (Fig. 2B). As such, Cre activity will switch expression of Mps1 protein from wild-type to mutant. ES-cell targeting and subsequent analysis of clones by PCR (Fig.2C) and Southern blot using a 5' probe upstream of the recombined fragment (Fig. 2A,D) verified integration at the correct site for several clones of each point mutant. Sequencing revealed the presence of the point mutations in one Mps1 allele of the ES cells (example shown for D637A in Fig.2E). After confirming a diploid content in ~80% of the cells (Fig.3A), the CiMKi ES clones, originating from agouti 129/Ola mice, were injected into blastocysts of black C57BL/6 mice (Fig.3B). Implantation of the embryos in surrogate mothers resulted in the generation of chimeric males (Fig.3B). Crossing these chimeric males with C57BL/6 females gave rise to agouti offspring carrying the targeted Mps1 allele (CiMKi^{D637A} or CiMKi^{T649A}) (Fig.3C).

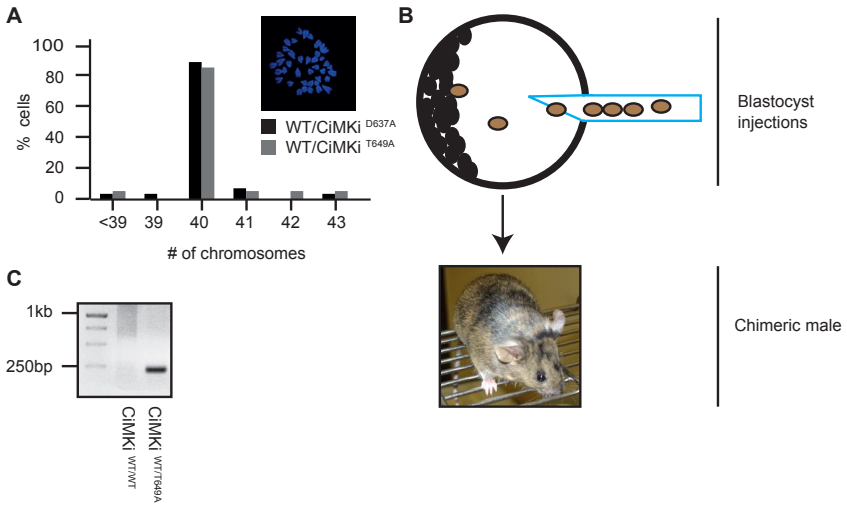

Figure 3
A) Chromosome spread analysis of indicated ES clones. Representative picture is shown. B) Schematic overview of blastocyst injection and the generation of CiMKi chimeric mice. C) PCR-based genotype analysis of F1 CiMKi^{T649A} mice.

CiMKi^{D637A} and CiMKi^{T649A} mice have been generated and back-crossed three (D637A) and six times (T649A) on a C57BL/6 background. Genotyping of Mouse Embryonic Fibroblasts (MEFs) isolated from day 13-17 embryos generated by CiMKi$^{WT/T649A}$ crosses resulted in a distribution of 25% CiMKi$^{WT/WT}$ (n=2), 50% CiMKi$^{WT/T649A}$ (n=4) and 25% homozygous CiMKi$^{T649A/T649A}$ (n=2) animals (Fig.4A). This distribution indicates that introduction of the cDNA into intron 16 does not result in any lethal hypomorphic effects on Mps1 protein expression. To further test the functionality of the CiMKi allele, we isolated mRNA from Adeno-GFP or Adeno-Cre-GFP infected MEFs and determined the presence of the T649A mutation by sequencing of reverse-transcriptase synthesized cDNA (Fig.4B-D). Infection of heterozygous CiMKi$^{WT/T649A}$ MEFs with Cre-GFP virus resulted in the induction of expression of the T649A mutation (ACA to GCA) in ~25% of the sequenced cDNA (Fig.4C). As expected, the induction of the T649A expression was more evident (~50%) in the homozygous Cre-GFP-transduced MEFs (Fig.4D). Recombination was not complete in these experiments, as 75% of the cDNA in heterozygous MEFs and 50% in homozygous MEFs was still wildtype (Fig.4C, D). This is not uncommon when using Adeno-based viruses in primary MEFs, and therefore this does not necessarily translate into poor recombination in the whole animal. Importantly, these results show

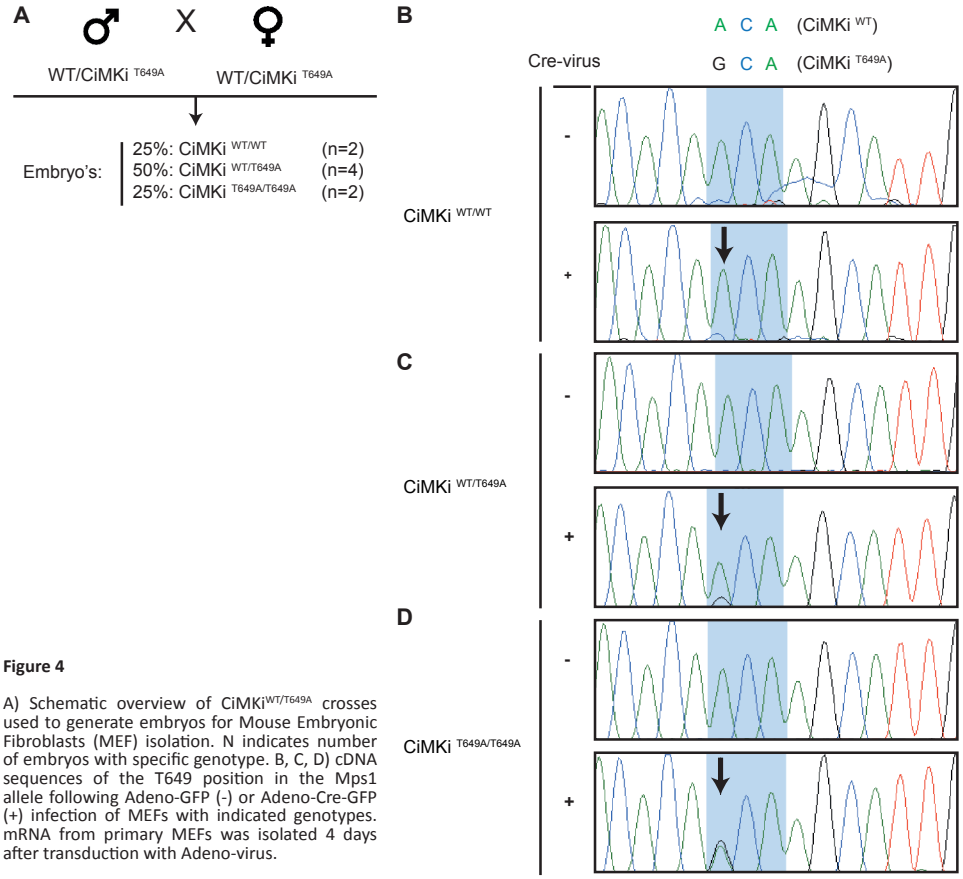

Figure 4

A) Schematic overview of CiMKi$^{WT/T649A}$ crosses used to generate embryos for Mouse Embryonic Fibroblasts (MEF) isolation. N indicates number of embryos with specific genotype. B, C, D) cDNA sequences of the T649 position in the Mps1 allele following Adeno-GFP (-) or Adeno-Cre-GFP (+) infection of MEFs with indicated genotypes. mRNA from primary MEFs was isolated 4 days after transduction with Adeno-virus.

that Cre expression can promote recombination and induce transcription of mutant Mps1 mRNA. Western Blot analysis of Cre-GFP infected MEFs showed that expression of the mutant Mps1 mRNA most likely does not affect Mps1 protein levels, as protein levels were comparable between all three phenotypes in both asynchronous and mitotic (nocodazole treated) cultures (Fig.5A). Interestingly, immunofluorescence with an anti-pT649 antibody (previously used to detect pT676 in human Mps1 [172] but recognizing the identical epitope in mouse Mps1) showed that Cre-GFP-infected homozygous CiMKi$^{T649A/T649A}$ MEFs contained significantly reduced pT649 kinetochore signals (Fig.5B).Auto-phosphorylation of human Mps1 on Threonine 676 is essential to obtain full Mps1 kinase activity[171,172], which is required for mitotic checkpoint activation[143]. Previous experiments have shown that exogenous expression of mutated Mps1-T676A cDNA in human osteosarcoma cells (depleted of endogenous Mps1) resulted in an increase in mild chromosome segregation errors in unperturbed mitotic progression, but did not affect cell viability [172]. These data indicated that the mitotic checkpoint function of Mps1 is only mildly affected when T676 cannot be autophosphorylated. To evaluate the effects of Mps1-T649A expression on mitotic checkpoint efficiency in our CiMKi system we treated MEFs for 6 hours with the microtubule destabilizing drug Nocodazole and determined the amount of mitotic cells by FACS analysis of MPM2 staining. In line with human Mps1-T676A studies[171,172], homozygous expression of Mps1-T649A did affect the efficiency of cells to delay mitosis upon spindle perturbation. Although Cre-GFP infection somewhat affected the number of mitotic cells in both WT and heterozygous CiMKi MEFS (28% and 19% in GFP controls to 22% and 16% in Cre-GFP infected cells

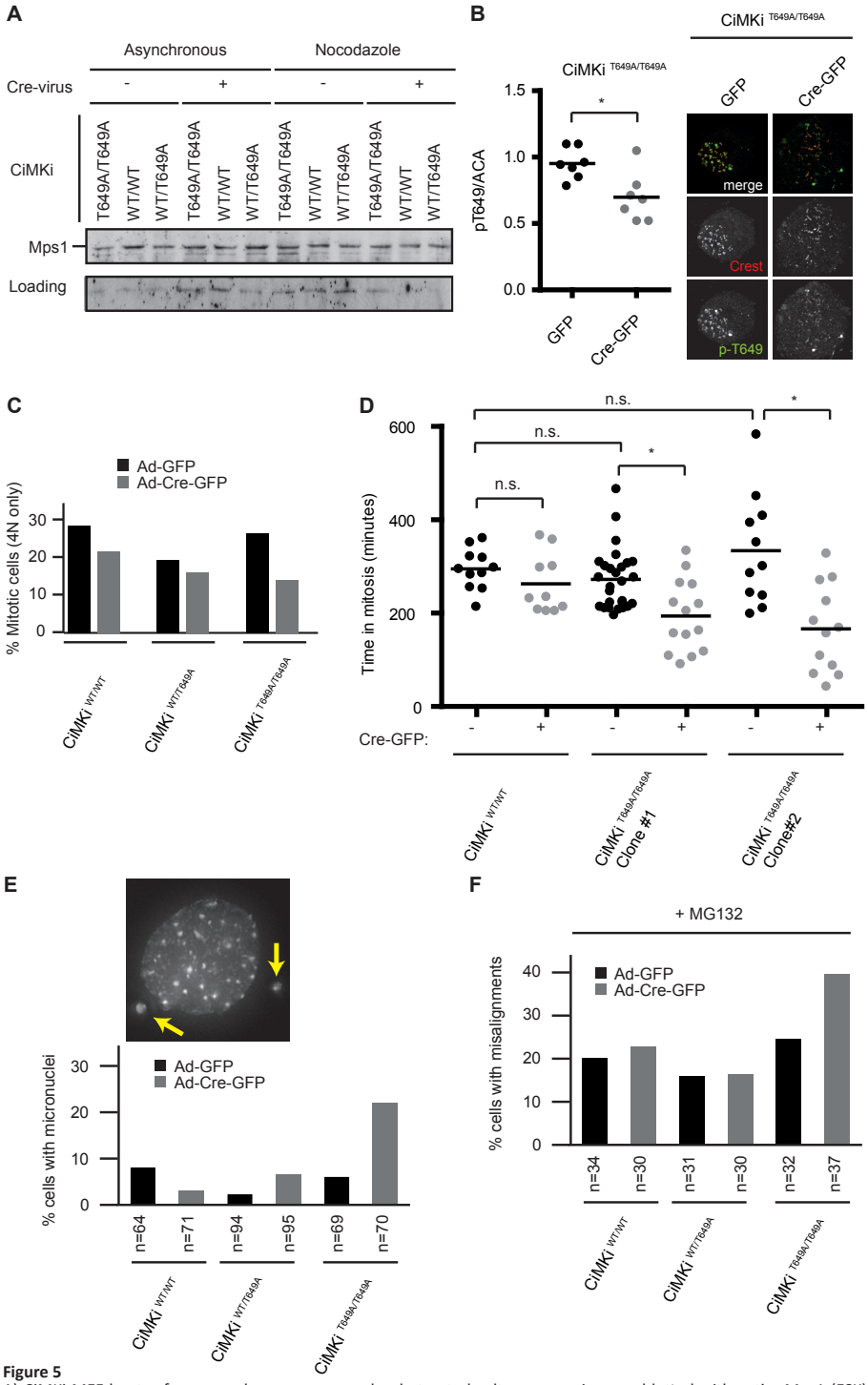

Figure 5

A) CiMKi MEF lysates from asynchronous or nocodazole treated cultures were immunoblotted with anti-mMps1 (ESK). Aspecific band was used as a loading control. B) (Left) Quantification of phospho-T649 kinetochore staining after 2 hours nocodazole treatment (MG132 was added the last 60 minutes to prevent exit from mitosis). Intensity of p-T649 was determined relative to CREST (kinetochore marker) signal. Each dot represents the average intensity of 36 kinetochores of one cell. *, p=0.01 versus

control treated MEFs (unpaired t test). Line indicates average of each condition. (Right) Representative images of pT649 (green) and Crest staining (red) of GFP or Cre-GFP transduced CiMKi$^{T649A/T649A}$ MEFs. C) Quantification of the percentage of mitotic cells after 6 hours nocodazole treatment. The amount of MPM2 positive cells with 4N DNA content was determined using FACS analysis of CiMKi$^{WT/WT}$, CiMKi$^{WT/T649A}$ and CiMKi$^{T649A/T649A}$ MEFs four days after transduction with Adeno-GFP or Adeno-Cre-GFP. D) Live cell analysis (DIC) of the mitotic duration of indicated MEF lines in the presence of nocodazole four days after Adeno-GFP or Adeno-Cre-GFP transduction. Mitotic duration was determined as the time in minutes from cell rounding to mitotic exit (cell flattening). Dot plot is shown with each dot representing one cell. Average is indicated. n.s., no significant difference between indicated conditions (p>0, 05 (unpaired student t-test)), *, statistically significant difference (p<0,002 (unpaired student t-test)). E) Representative image of a cell with two micronuclei (upper panel). DAPI was used to visualize DNA. Quantification of the number of cells with micronuclei 4 days after transduction with GFP or Cre-GFP of indicated cell lines. F) Quantification of the number of cells with chromosome misalignments (>1 chromosome outside of the metaphase plate) following 1 hour MG132 treatment and transduction with either GFP or Cre-GFP virus of indicated MEFs.

respectively), Cre-GFP infection of homozygous CiMKi$^{T649A/T649A}$ MEFs reduced the percentage of mitotic cells in response to nocodazole with almost 50% (26% in controls to 14% upon Cre infection) (Fig.5C). In agreement with this, time-lapse imaging of two independent CiMKi$^{T649A/T649A}$ MEF clones showed that Cre-GFP expression significantly reduced the time spent in mitosis, from 300 minutes on average to ~200 minutes, while CiMKi$^{WT/WT}$ MEFs were not affected (Fig.5D). We did observe a relatively big spread in mitotic timing in the Cre-GFP-infected hetero- and homozygous CiMKi MEFs (50-300 minutes), consistent with our previous observation that the CiMKi allele is only recombined in a fraction of the MEFs. Next we wished to determine the effects of Mps1-T649A expression on mitotic progression in the absence of any microtubule targeting drugs. Abnormally shaped nuclei or the presence of micronuclei (Fig.5E) are indicative of prior chromosome missegregations. Analysis of nuclear morphology in CiMKi$^{T649A/T649A}$ MEFs infected with Cre-GFP indeed revealed a three-fold increase in cells with micronuclei (21%) when compared to control GFP-infected cells (6%). This effect of Cre-GFP infection was absent in both CiMKi$^{WT/WT}$ and heterozygous CiMKi$^{WT/T649A}$ MEFs (Fig.5E). Overall, these data indicate that Mps1-T649A affects mitotic checkpoint signalling in both unperturbed mitosis and in response to mitotic spindle disruption. Independent from its role as a mitotic checkpoint kinase, Mps1 is also required for proper chromosome alignment[116]. Indeed, analysis of chromosome congression revealed that homozygous expression of Mps1-T649A decreased the efficiency of chromosome alignment in the presence of the proteasome inhibitor MG132: 40% of Cre-GFP-infected CiMKi$^{T649A/T649A}$ MEFs showed chromosome alignment defects compared to 25% in GFP controls, while both wildtype and heterozygous CiMKi MEFs were not affected (from 21% and 16% in GFP controls respectively to 23% and 17% upon Cre infection) (Fig.5F). Collectively, these data show that decreased Mps1 activity in our CiMKi^{T649A} mouse model results in mitotic checkpoint deficiency, chromosome missegregations and alignment errors, which are all in line with data obtained from human cells [171,172].

Discussion

We have developed a CIN mouse model (CiMKi), in which one of two different point mutations that render Mps1 completely (D637A) or partially inactive (T649A) can be introduced into the endogenous Mps1 locus in a timed and tissue-specific manner. In line with studies performed in human cells [172], we find that substituting the autophosphorylation site T649 for an alanine results in decreased mitotic checkpoint efficiency and chromosome segregation errors, already in an otherwise unperturbed mitosis. This makes CiMKi^{T649A} a very powerful model to study chromosomal instability at an organismal level. Future studies will be performed to determine whether the mutated D637A allele affects mitotic progression as well. Since Mps1 kinase activity is absolutely essential for mitotic checkpoint function [148], it is expected that homozygous induction of the kinase-dead version of Mps1 will lead to higher levels of CIN due to (near) complete mitotic checkpoint deficiency resulting in severe chromosome segregation errors. In contrast to current CIN mouse models, our aim is to induce various levels of CIN (Fig.1) in specific tissues of adult mice of various ages and monitor its effect on (spontaneous) tumor formation. In this way we expect these mouse models to better resemble the development of CIN

in human tissues when compared to current CIN mouse models. To accomplish this timely and spatial induction of mutant Mps1 expression we have crossed our CiMKi mouse model with Cre-ER^{T2} mice, which express Cre-ER^{T2} under the ubiquitous and endogenous Rosa26 locus[449]. Cre-ER^{T2} is a system in which heat shock proteins directly bind the ER^{T2} moiety (mutated ligand binding domain of the human Estrogen Receptor) of the constitutively expressed Cre-ER^{T2} fusion protein. This binding inhibits the activity of the Cre-ER^{T2} protein until exogenous addition of 4-hydroxy tamoxifen (4-OHT, modified form of tamoxifen that specifically binds ER^{T2}, but not wildtype ER) releases the binding of heat-shock proteins to ER^{T2} and thus permits Cre driven LoxP recombination [449,450]. Treatment of tissues expressing both CiMKi and Cre-ER^{T2} with 4-OHT will therefore lead to recombination of the CiMKi allele and transcription of the mutated Mps1 allele (Fig.2A, B). Furthermore, to determine both the efficiency of Cre activation following 4-OHT treatment and the effect of mutant Mps1 expression on healthy tissues in the mouse, we have crossed our CiMKi/CreER^{T2} mouse model with Lox-stop-Lox-LacZ (LsL-LacZ) reporter mice, which express LsL-LacZ under the Rosa26 locus [451]. In this reporter strain, release of Cre will lead to recombination of the LsL-LacZ allele, which will result in expression of LacZ. Using X-gal staining, which visualizes LacZ activity, this system gives us the opportunity to identify tissues and single cells in which Cre has been activated and simultaneously evaluate the effects of mutant Mps1 expression on 4-OHT-treated tissues. Data obtained using Cre-GFP-infected CiMKi MEFs indicate that recombination of the CiMKi allele is only successful in a fraction of the cells (4C, D and 5D). These effects are most likely due to an incomplete Cre-GFP-transduction efficiency in our CiMKi MEFs. Nevertheless, we will need to repeat these experiments using 4-OHT-treated CreER-CiMKi MEFs to rule out the possibility that the partial recombination is due to intrinsic recombination defects present in the CiMKi allele. If this would be the case, we will need to be very careful in interpreting effects on tumor growth and always determine CiMKi recombination efficiency *in vivo*. Although effects of CIN on spontaneous tumor development have been reported [291,298,397,400,413], many studies using CIN models in combination with carcinogen treatments or crosses with tumor prone mouse models have shown that CIN is more likely to be an enhancer of tumor formation [286,295,296,400,401]. In apparent contradiction to these reports, tumorsuppressive functions of CIN have also been suggested[286,397]. One explanation for this discrepancy is that there is a fine balance between having enough CIN to enhance tumorigenesis and acquiring too high levels of CIN resulting in severe aneuploidy and cell death (Fig. 1). In line with this idea, we have recently shown *in vitro* that mild CIN does not affect cell viability, while high levels of CIN are detrimental to tumor cells[299]. To test this hypothesis in adult mice, we will apply DMBA/TPA [452] carcinogen-treatments on the skin of our 'CIN titration panel' of CiMKi/CreER^{T2} animals and assess the effects of various levels of CIN on tumor growth by simultaneously inducing the expression of mutant Mps1 through topical 4-OHT treatment [453]. Our aims are to identify how much reduction of Mps1 activity and what level of CIN cells is needed to kill tumor cells, what level of CIN will promote tumor formation, and how early or late induction of CIN relative to tumor initiation impacts tumor development. In parallel with these carcinogen treatments we will cross our CiMKi/CreER^{T2} models with hemizygously expressing MMTV-Neu mice[454], which develop mammary tumors after ~7-10 months of age. To determine the effects of different levels of CIN on either mammary tumor-formation or -growth inhibition, we will induce mutant Mps1 expression specifically in the breast epithelium of these compound mice through intraductal 4-OHT injections. Using the described experiments and crosses with our CiMKi mouse model we hope to be able to address the question what the effects of increasing levels of CIN are on tumor development and, more importantly, whether we can use the induction of elevated levels of CIN as a way to inhibit tumor growth.

Materials and Methods

Cloning targeting vector (D637A=kinase-dead and T649A=Hm676)
Targeting vector; pAC16 (based on pFlexible [455]) (kind gift from Dr. Jos Jonkers):
F=FRT site L=loxP site

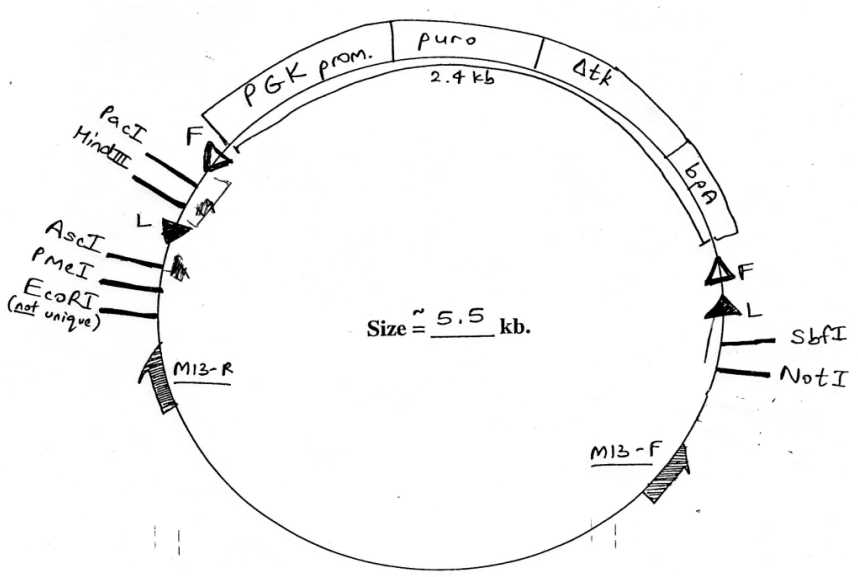

1) Ligate conditional part (fragment#2) into HindIII-PacI (between loxP sites)

2) Ligate 5' recombination arm (fragment#1) into PmeI-AscI (upstream of 5' loxPsite)

3) Ligate 3' recombination arm, including point mutation (fragment#3) into SbfI-NotI (downstream of 3' loxP site)

Fragment#1 **Fragment#2** **Fragment#3**

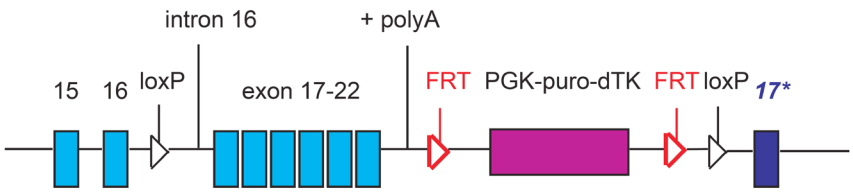

1) Ligate conditional part (fragment#2) into HindIII-PacI (between loxP sites)

Fragment#2 was assembled from 3 parts:

#2-1=*HindIII*-(lastpartof)intron16-*XhoI* (600 bp)

#2-2=*XhoI*-**exon17-exon18-exon19-exon20-exon21-exon22**-*BamHI* (1000 bp)

#2-3=*BamHI*-intron22(polyAsignal)-*PacI* (600 bp)

*AAGCTT*ATGGCCAGTTTTTCAGTCTCCAAAGGATTTTCTCTTTGGAGCCCGGTGTGAGAGTTGGTCTGTTCTTGCTGTTTTCT-
GTTTCATTATTTGTTTGTTCTTGTTCTCTCCAGTTTCCTCTGCCTTTCCCTTGTCTTTTAAACAGATGTGTTCAATCTCATGC-
GCTTCCTCTGCTTCTCCTTTTAGAAGCAGTAACTAAGCAGAGGATAGGACTCTTTGGGGGTGAGGGAGGCCTTGCGATCT-
TATTGTCTGACAGTTCTTGGTGGTGCTTTCCTGGCCTGTGCATGGCAGTGTGCAGCACACACTGACAGGCTAGGCCTG-
GAATCCTGAACAGTTCACTTCAACTCAAATCACATTGAGTGTCCTCACCCTGAAAATGATGATGATAATGGGACTTATTTGC-
TATGCATTGCTATAGAATGGTACCTGGCCCACAACATTTGCTAAGAAAGTGTAGAATGTATAATAACTAAATATTAATGTGTT-
GCCTAATTGAAAGGATAAGCCTGACCTAAAGATTATGAAATGCTTTTTTGTCCCCTGGCCATAGAATGTTTTTCTTCATCTAA-
CAGAACGGATTTTATTTTGAAG**GTATTGTTCATAGTGATCTGAAGCCTGCTAACTTTGTGATAGTGGATGGAATGCTAAAGC-
TAATTGATTTTGGGATTGCAAACCAAATGCAGCCAGACACAACAAGCATTGTTAAAGATTCTCAGGTTGGCACAGTTAAC-
TATATGGCCCCAGAAGCAATCAGAGACATGTCTTCTTCAAGAGAAAATTCGAAAATCAGAACCAAGGTAAGTCCCAGAAGT-
GATGTCTGGTCCTTGGGGTGCATTTTGTACTACATGACTTATGGGAGGACGCCATTTCAGCACATCATCAATCAGGTCTCTA-
AACTGCACGCCATAATCAACCCTGCTCATGAGATTGAATTTCCCGAGATTTCGGAAAAAGATCTTCGAGACGTGCTAAAGT-
GCTGTTTAGTGAGGAACCCTAAAGAGAGGATATCTATCCCTGAGCTCCTCACACATCCGTATGTTCAAATTCAGCCCCATC-
CAGGCAGCCAAATGGCTAGGGGAGCCACTGATGAAATGAAATATGTGTTGGGTCAACTTGTTGGTCTGAATTCTCCTA-
ACTCCATCTTGAAAACTGCAAAAACTTTGTATGAACGTTATAATTGTGGTGAAGGTCAAGATTCTTCGTCATCCAAGACTTTT-
GACAAAAAGAGAGAAAGAAAGTGATGCACAGCTACGTACAAACCAAGAACACTAGATTGTTTCCTCTGCCATACTCTT-
GAATCTCTGAGGAAATCTACCAGTTGGAAACAACCTCACCTGGATTTTATCAGTTAAAAAAACAAACAAACAAAACTTCAG-
TAGATTATCCTCAAAAGAAAGCTGTAAAGTTAACCACTCATAGCACTGTGTATATTAAATTATAGAGTTGTGCTTTTCTTT-
TATGCTTTTCTGTAAATCTGCTAATGTTTTACGTTTGGAACAGTGAATGATAGCTGGAATGTTGAAGAGCTCTGTAAATA-
AAGCGTCACCACAGTTCC**AGAACTGTACAGTGGTCAGTTTCTTCAATCAAATGTGTTCTTGGCATGATAGCAAAATTTT-
TAGAAAAACGGGATTAAGAATAGACCGTAGTAAATAAAGTTTAACAATTAAATTTCCAAAGGATTTAGGACTGTAAA-
CAGGCTCACACCTTTAGTCCCAGCACTTGGGAGGCAGAGGCAGGCAGATTTCTGAGTTCGAGGCCAGCCTGGTCTA-
CAGAGTGAGTTCCAGGACAGCCAGGGCTACACAGAGAAACCCTGTCTTGGCGGGGAGGGGCCGGGGAGGGGGGGA-
GATCCAAAGGATGTAGGAGGCAGAGACAGGTGGATCTCTGTGATTCTGAAGCCAGCCTGGTCTACAGAACTAGTTC-
TAGGATAGCCAAGGCTATACAGACACTTTCTCCCCACCACCATCCTGCCCTCAAAAAAATTGTAAATAAATTTCCTA-
ATTGTGTACAGCCATGATACCATCTATAGTATTTGGTCTGCAAGTGGCTTTTTCAGTTCTCCCTTTGACTCTTCAAAGTA-
CATATGGGGTTTGGTGTTCTAAATATTGTGCTGGAGTTTGTGATTTAATGTCTATAGTTAATACATGCCATTATTGAG*TTAATTAA*

PCRs performed to obtain fragment #2-1, #2-2, #2-3 *(Italic is overhang, in Capitals/Italic the restriction sites):*

- PCR #2-1 from genomic DNA (from 129/Ola-derived IB10 ES cells, (kind gift from Dr. Hans Clevers))

Primers used: #2-1Forward:*cggcgAAGCTT*ATGGCCAGTTTTTCAG
#2-1 Reverse: *cgccgCTCGAG*CTTCAAAATAAAATCCGTC

- PCR #2-2 from mouse cDNA (ordered from Imagenes, Germany, BC 058851, ID: 30023533)

Primers used: #2-2long Forward: *ccggcCTCGAGgcgctactctggtg*GTATTGTTCATAGTG
#2-2long Reverse: *ccgcgGGATCCgcgctactctggtg*CTGGAACTGTGGTGAC

- PCR #2-3 from genomic DNA (from 129/Ola-derived IB10 ES cells, Clevers lab)

Primers used: #2-3 Forward: *ccgccGGATCC*AACTGTACAGTGGTC
#2-3 Reverse: *ccgccgTTAATTAA*CTCAATAATGGCATG

Ligation steps to assemble 3 fragments:

- Ligate #2-1 & #2-2 simultaneously into pCDNA3 (>>pCDNA-#2-12)

- Loop out XhoI site with site-directed mutagenesis:

Primers used: #2-1_#2-2-(XhoI) loopF: GACGGATTTTATTTTGAAGGTATTGTTCATAGTGATC
#2-1_#2-2-(XhoI) loopR: GATCACTATGAACAATACCTTCAAAATAAAATCCGTC

- Ligate #2-3 (from pGEM-Teasy) into pCDNA-#2-12 (>>pCDNA-#2-123)

- Loop out BamHI site with site-directed mutagenesis

Primers used: #2-2_#2-3-(BamHI) loopF: GCGTCACCACAGTTCCAGAACTGTACAGTGGTCAG
#2-2_#2-3-(BamHI) loopR: CTGACCACTGTACAGTTCTGGAACTGTGGTGACGC

- Ligate #2-123 from pCDNA into pAC16 (HindIII/PacI) (pAC16-#2-123)

2) Ligate 5' recombination arm (fragment#1) into PmeI-AscI (upstream of 5' loxPsite):

Fragment#1=*PmeI*-(lastpartof) intron14-**exon15**-intron15-**exon16**-(firstpartof)intron16-*ApaI-AscI* (2kb):

*GTTTAAAC*TCGAAGGCCTCAACCTCACAGAGATCTTTCTGCTTCTGCCTCTCTCCTGAGTGCTGAGATTAAAGGTGTGTG-
CAGCCATGCCTAGCTGTGTGTGGCTTTCCTGTTACCACATTCTGTGGATAGCTTATCTGTTGTTTGTGCCCCACCTTGTACT-
TAATATCAAGATGAGATGTTTGGCTGTTCGGTGATACTAGCTCTGGTGACTAAAACTGAATAGGACCTTTATTCCTTTGCT-
GAGTGTTCCTCCTTGGCTATCAGGCTGTTTTATGTTATGGTGATACATGAACAGAGATAAAGGGCTTATTTTAAGTTTACTG-
TAATTCTCTAAGCCAGCTAGCTGTAATTAGACTTGCTTCTGGCTATTTTATTAACTTATAGCAAGTAATTGGAAAGCATCCCAT-
CAGACCCATTTGTATAATTCCTGCACACAGTACGCTGAGGCGGGATGATTGCCTGGGCTACATACATGCACTGTATAG-
GCTGCTGCTATGGCTTTGGTGCAGGGCCCTGGCTTTAATCTCTTAACATAAAAACCATAAGCAAAAGACAAAATAGGTAG-
GAGTGTATATTTCCACATGGAGCATGTCTTCCCATAAATATTTTCCTTTTCACGCTCCCCTTATTAGATTTTCAGTTATGAG-
CATAAGGAAGAAGGTGGGGTAAGAGTGATTGAACAAGAGTGACAGGGAAGAGGATTCGTGCAGGGGAGGGAAGT-
GCATGCATGTTCTAGGCACTGAGTGATGGGTGTGCTGGAAGCTGTAAACTGCGTGGGGGCCTCTTCCTCAGTGCTT-
TAAGAAATTGATTCATAGGAACATCATTGCTCCTGCCAACCTAACTCAACTGTGACTTGCGCTGCTTTCCACAAATGAAT-
GTAGTGATGGCTTACAATTACTGTGATTTTTAAAAATATTCCCTATCAGAGAAATGAATTGGTTGATAGTAGGCACAAT-
GAAAAGGTGGGAGTTGGTGGGGAGAGGGGTCTAGGAAGTGAACTGTCAAATCACAGCCTTAGTCATCCTTATCGTCTTC-
GAATGTCTTTTCCTTGATGTTTTCTCCCTGGATAAGAAAGGCATCCCTAGAATTTTGTGGATATAGCAACATCATATT-
TAAGTTGGTTTTCTTAGACACTGATGTAGAAAACCTTTGAATTATTTGAATGTCCATTGTTATAGGGGCTGGAAATG-
GATACTTAGCTTCTCATGTTGGTATTTCTTTAGGAATATCCTCAGCCTGAGACTGTTAGTGTTAAATGGAAAGGTACTGCTC-
CAGTTTTCAGAGGGAGACATGTCCTAAGCTCTTTCTCCACTTTTTATGTAG**GTGTTTCAGGTATTGAATGAGAAAAAA-**
CAGATAAACGCTATCAAATATGTGAACCTAGAAGACGCCGATAGCCAAACTATTGAGAGCTACCGCAACGAGATAGC-
GTTTTTGAACAAACTACAGCAACACAGTGATAAGATCATCCGCCTCTATGATTAGTATGAATTCATTTTTATTTTAAAAATA-
AAAGTTTGTTCTTGCCATAATTCTTAGGCAAAGAGTAAATCCTTAATGACATAATGTGGGCATTTATTGTTTTGTTGTGTCTGTT-
TATCTTTAATTGCAG**TGAAATCACCGAGCAGTACATCTACATGGTAATGGAATGTGGAAACATTGACCTAAATAGTTGGCT-**
TAAAAAGAAAAAATCCATCAATCCATGGGAACGCAAGAGCTACTGGAAAAACATGTTGGAGGCAGTACACATAATCCAT-
CAGCATGGTATTTTCATATCTCTTCATACACGTAAAGTTAAAATAGTTGTTAATTGTGCCATTTTAGAAACATACCCTTAACTG-
GAAGTTCATTAGAGGTGAAGGCACTCTTAAGAGTGGTTATACACAGGCTACAGAACACAAACAAGCACAGGATGTAGAA-
CAGAAATGGCCACATGTACAATGTAAACTTACCCTCCTCTGGTACCTGGGGATTCCTATCTTCAAGTCCTGAGGATTTGGA-
CATCCTACAGATAGGAGGAGA*GGGCCCGGCGCGCC*

- PCR fragment#1 from genomic DNA (from 129/Ola-derived IB10 ES cells, (kind gift from Dr. Hans Clevers)) (Italic is overhang, in Capitals/Italic the restriction sites):

Primers used: #1Forward-Short2kb2: ctagcgGTTTAAACTCGAAGGCCTCAACCTCACAGAGATCTTTC
#1 Reverse: *atcttaGGCGCGCCGGGCCC*TCTCCTCCTATCTGTAGGATG

- Ligate into pAC16 (>>pAC16-fragment#1) (PmeI&AscI)

- Ligate into pAC16-#2-123 (>>pAC16- #1-#2-123) (PmeI&AscI)

3) Ligate 3' recombination arm, including point mutation (*) (fragment#3) into SbfI-NotI (downstream of 3' loxP site)

Fragment#3=*SbfI*-(lastpartof) intron16-**exon17***-intron17-*NotI* (2.2kb): (***GCT*** **=D637A,** ***GCA*** **=T649A)**

*CCTGCAGG*ATGGCCAGTTTTTCAGTCTCCAAAGGATTTTCTCTTTGGAGCCCGGTGTGAGAGTTGGTCTGTTCTTGCT-
GTTTTCTGTTTCATTATTTGTTTGTTCTTGTTCTCTCCAGTTTCCTCTGCCTTTCCCTTGTCTTTTAAACAGATGTGTTCAATCT-
CATGCGCTTCCTCTGCTTCTCCTTTTAGAAGCAGTAACTAAGCAGAGGATAGGACTCTTTGGGGGTGAGGGAGGCCTTGC-
GATCTTATTGTCTGACAGTTCTTGGTGGTGCTTTCCTGGCCTGTGCATGGCAGTGTGCAGCACACACTGACAGGCTAGGCCTG-
GAATCCTGAACAGTTCACTTCAACTCAAATCACATTGAGTGTCCTCACCCTGAAAATGATGATGATAATGGGACTTATTTGCTAT-
GCATTGCTATAGAATGGTACCTGGCCCACAACATTTGCTAAGAAAGTGTAGAATGTATAATAACTAAATATTAATGTGTTGCCTA-
ATTGAAAGGATAAGCCTGACCTAAAGATTATGAAATGCTTTTTTGTCCCCTGGCCATAGAATGTTTTTCTTCATCTAACAGAAC-

GGATTTTATTTTGAAG**GTATTGTTCATAGTGATCTGAAGCCTGCTAACTTTGTGATAGTGGATGGAATGCTAAAGCTAATT**
***GCT*TTTGGGATTGCAAACCAAATGCAGCCAGACACA*GCA*AGCATTGTTAAAGATTCTCAG**GTAGGAGTTTTGCT-
GTCTTGGTTGTATTTTAGTGTTTTGAACCAGGGTTTTGCATCAGGGTTTTGCATAACCTAGAATGCTCTTGACTTTGATCAGTG-
GCCTTCAGCTCCTGATCCTGCTGCCTGTGCATCCCAGGTGTGGGCTTATAGGTGTCAGCCCCGACACCCGACTTCAGGTAG-
GATTTTAATGATGGCTGGTTACTACAAGGCTTAGTTCATTTTTATCTGTTAAATATGTTGCCAATATTATATTTTTACCAACCATGT-
TATTCCAAAAATTTGAAGTCTTTTTAAAGAATAGAAACTATGTTTATAAAAGACCATGGTCAAAGCCATGGTCAATTTGATT-
TATAAAAGCAGTTCAAGATCAGACAAGTATATTTATGAATTTTGGATGATTTTCTCATAGCTGAGGCAGGGCAGAGAGTAATTG-
CACCTTCATGTTCTCCACTGTCCTGTTTCTTTTTCTTACTGCTTAAATTTGGGAGAAAGTTTTAAGAGAGCCTTATTGGGAATACT-
GAAGCGTTCCACTCAGCTACGCGTTAAAAAGGAAATATTTTACTTACTGTTTGGGGGGCGGTGTGCGGATTCCAGATGTA-
AGTGTGCCATTGTGGAGGTGTGGGGATGGCTTCGGTAAACCACTTCTCTCCTACTGTGGGCCCTGGGAGCCAAAGTCA-
GATTGTGTGTGCAGCAAGCTCTACAGCCCAGCTGTGCTTTGTAGTAACATTTGCTGTGGTAAATCTCATGAAGCTGAAG-
TAGTGAGGGGAAAACAGAGCTGAAAGGTGATGTCGACTGCACCTCGCAGGCTGTGTCCAGGGATGGAGATAAATCAGAA-
GATAAATTACCATGCACGTAGAAAGTCATTCTTCTTGACAGCCATTCATTGTTTTTTGTTTCAGAAGTACAGATGATGAACAGT-
GAGTGTAGATGAGACTGAAGTTTTCTATGGCAAGGTCTTAGCAGGCCGACATTTTGTTACCTTAGAACTAAAGGATTTT-
GCGTATTATCTCCATGCCCAGCTAGAGAAGCTCTTCTCTGATATAGGTTTCCAACCCATCTTGATCTGCACATGGAGC-
CGAAGAATATTGGGAGATAAAGCTAGCTGGTTCCTTTTATTCATGTATTAATTTGTTGCTTGGTTTATTGAGGGAAGAATAT-
GTTGAATTTATTGGAACATGAAAGTGAATGAAAGGCCAAGTTCAGAATCCGCCTACGCAGTTGTAAAGACTTAGTACTTAG-
TACTTAGTACTTAGCACTAGCTCTCCAGCACAGCTGCAGACAGCACAGTGCTCCCTGTGCTCCAGACGGAGCCCGTTCATTCT-
CAGCCCAGCTCATCTGATTGTACCTGGGATGGGATAGTACATACATTCTTATATTGTTAGCAGTTATTTGAATTTTTCAAGTCTGT-
CATTTAAATCATTAGTTATTCAAATTTCCAAGAATCTGACATTTACATATTTACAAATCTAGAAAGATATTCTCATTGATTTCTTTGT-
GATTTGCAAATAG*GCGGCCGC*

- PCR fragment#3 from genomic DNA (from 129/Ola-derived IB10 ES cells, (kind gift from Dr. Hans Clevers)) (*Italic* is overhang, in *Capitals/Italic* the restriction sites):

Primers used: #3 Forward: *ccgccCCTGCAGG*ATGGCCAGTTTTTCAG
#3 Reverse: *ctagcgGCGGCCGC*CTATTTGCAAATCACAAAG

- Ligate into pAC16 (>>pAC16-#3) *(PmeI&AscI)*

- Introduce point mutations with site-directed mutagenesis

Primers used: mMps1-T649A-F: CAAATGCAGCCAGACACA*gca*AGCATTGTTAAAGATTC
mMps1-T649A-R: GAATCTTTAACAATGCTTGCTGTGTCTGGCTGCATTTG
mMps1-D637A (KD)-F: GAATGCTAAAGCTAATT*gct*TTTGGGATTGCAAAC
mMps1-D637A (KD)-R: GTTTGCAATCCCAAAAGCAATTAGCTTTAGCATTC

- Ligate into pAC16- #1-#2-123 (>>pAC16-#1-#2-123-#3) *(PmeI&AscI):*
(=CIMKI-D637A & CIMKI-T649A)

Cell culture & reagents

ES cells were grown in G-MEM supplemented with L-Glutamine, Sodium Pyruvate, NonEssential Amino Acids (all from GIBCO Invitrogen), 10% Foetal Calf Serum (Greiner), β-Mercaptoethanol and LIF (CHEMICON international). ES cells were grown on either 0.1% gelatin coated dishes or a layer of irradiated MEFS and transfected with the Not1 linearized targeting construct pAC16-D637A or T649A using electroporation with a Biorad gene pulser. Electroporated ES cells were selected with 1mg/ml puromycin (Sigma) to obtain stable transfectants. Single colonies were subsequently picked and grown in 96-wells plates before genotype analysis. MEFs were cultured in DMEM (4,5 g/L glucose) (Lonza) supplemented with antibiotics, ultraglutamine (Lonza) and 15% FCS. Ad-Cre-GFP and Ad-GFP (both from Vector Biolabs) were used to infect MEF cells at 100 MOI. Nocodazole (250ng/ml), MG132 (2μM) and DAPI (1mg/ml) were all from Sigma.

PCR analysis ES clones

ES cell clones were grown in 96 wells plates, lysed using Hotshot lysis buffer [456] and analyzed using PCR. DNA from targeted ES cells yielded a band of ~2.8 kb.

Primers: pGH_pA_FW#2: TCTATGGCTTCTGAGGCGG
Intron18_Reverse#1: AAGGGACATCAGGGAAGCAA

Southern analysis

Probe design
5' probe (500bp) was obtained from genomic DNA (from 129/Ola-derived IB10 ES cells, (kind gift from Dr. Hans Clevers)) by PCR using the following primers:
FW_EcoRV_1: CTTTCTCCTCCAATTTACCATTTTGTTCAC
Rev_EcoRV_1: GGTCAAATCCAGAGTCCTAAGGCAAGGTAC

500 bp fragment was ligated into pGEM-T-easy to further increase DNA yield.
Digestion of genomic DNA from ES cells with EcoRV and hybridization with the 5' probe resulted in a 9,5 kb band (when wildtype) or 4, 7 kb band (when targeted with CiMKi allele) (see below):

Wildtype allele:

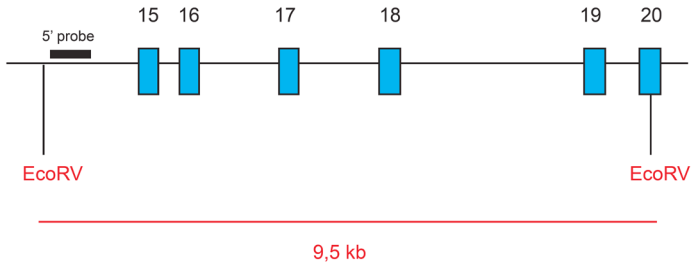

Targeted allele:

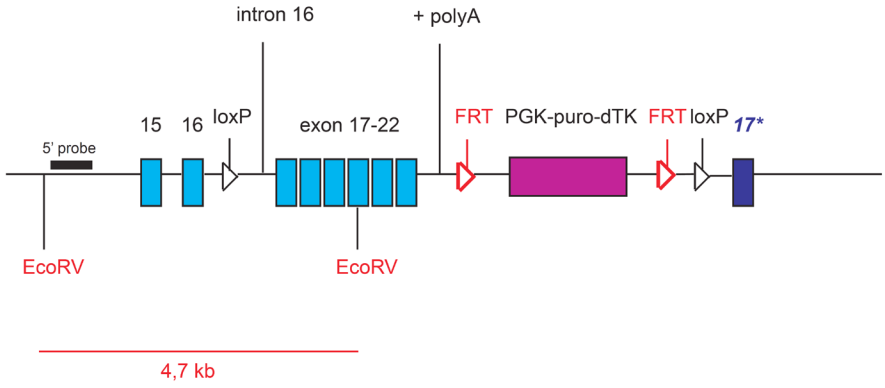

DNA purification

ES cells were lysed using 10mM Tris (pH 7.5), 10mM EDTA,10mM NaCl, 0.5% Sarkosyl and 2mg/ml Proteinase K (added freshly), dissolved in dH2O. ES cell DNA was precipitated using NaCl (50mM) mixed with ice-cold Ethanol (100%) and subsequently restricted using EcoRV.

Southern blot

DNA was separated on size at 80V in a 1% Agarose gel for 4 hours. The DNA gel was washed in denaturalizing solution (0,5 M NaOH and 1.5M NaCl) 2 times for 15' and Southern blotting was performed for 14-16 hours using a Hybond-N+ membrane (GE healthcare) in 0,5 M NaOH and 1.5M NaCl. After blotting the membrane was washed for 5' in 40mM NaPi and subsequently cross-linked using UV irradiation. Probe labeling was performed using a standard Rediprime II Random Prime labeling system (GE healthcare) and radioactive [a-32P] dCTP after linearizing the 5' probe. Hybridization of the membrane was performed in 0,5M NaPi, 7%SDS, 1mM EDTA pH8.0 overnight at 65 °C and was washed using 40mM NaPi, 1% SDS.

Generation of CiMKi mice

129/Ola-derived IB10 ES embryonic stem (ES) cells were selected in medium containing puromycin and correct recombination was confirmed by PCR, Southern blots and sequencing as described above. Targeted ES clones were injected into C57BL/6 blastocysts to generate chimeric mice, which were bred with C57BL/6 females to obtain germline transmission. CiMKi mice were backcrossed six times on a C57BL/6 background. Genotypic analysis of offspring was performed using PCR and sequencing with allele-specific primers as described below. CiMKi-CreER^{T2} mice were obtained by crossing heterozygous CiMKi females with homozygous CreER^{T2} males (B6.129-Gt(ROSA)26Sor$^{tm1(Cre/ERT2)Tyj}$/J) [449] purchased at the Jackson laboratory (stock number 008463). CiMKi/CreER^{T2}/LsL LacZ mice were obtained by crossing heterozygous CiMKi/CreER^{T2} females with homozygous LsL-LacZ males (B6.129S4-Gt(ROSA_26Sor^{tm1Sor}/J)[451] (a kind gift from Dr.Annemieke Kavelaars) originally purchased at the Jackson laboratory (stock number 003474). All animals were bred and housed at the animal facility of the Gemeenschappelijk Dieren Laboratorium (GDL), Utrecht, the Netherlands.

Genotypic analysis

Tails of 3-4 weeks old mice were lysed with Hotshot lysis buffer [456] and PCR was performed to determine the presence of the CiMKi allele using the following primers:
Exon 21 FW#4: CCAAATGGCTAGGGGAGCCACTGATG
Exon 22 R#4: GGTGAGGTTGTTTCCAACTGGTAG

DNA from CiMKi mice harboring the mutant allele will yield a band of 250bp.
To determine whether mice or embryos were heterozygous or homozygous for the CiMKi allele, tail DNA was subjected to PCR and sequencing to determine the presence of one or two mutant alleles (T649A (ACA à GCA) or D637A (GAT à GCT) in exon 17) using the following primers:

PCR:	Intron16_Seq_FW#1: CACCCTGAAAATGATGATGATAATG
	Intron17_R#: GCCATCCCCACACCTCCACAATGGC
Sequencing:	Intron16_Seq_FW#3: GGTACCTGGCCCACAACATTTGC

Genotypic analysis of (CiMKi) CreER^{T2} and (CiMKi) CreER^{T2}/LsL-LacZ mice for the presence of the CreER^{T2} or LsL LacZ allele was performed using standard primers (sequences can be found on the Jackson laboratory website).

PCR analysis of Cre-infected MEFs

mRNA from MEFs subjected to Cre-infection was isolated using an RNeasy minikit (Qiagen). cDNA

was prepared using standard procedures, subjected to PCR and subsequently sequenced to determine the presence of T649A or D637A using the following primers:

PCR	Exon15_FW#1: CCTAGAAGACGCCGATAGCC
	Exon18_R#1: GTCTCTGATTGCTTCTGGGGC
Sequencing:	Exon 15_FW#2: GATAAGATCATCCGCCTCTATG

Isolation of mouse embryonic fibroblasts

Pregnant females were sacrificed at day 13-17 p.c. by cervical dislocation. The uterine horns were dissected out and placed in tubes containing PBS. Embryos were separated from their placenta and surrounding membranes. Red organs, brains and tail (for genotyping) were removed. Embryos were finely minced using razor blades and the remaining cells/tissues were resuspended in a tube containing 2 ml Trypsin and kept at 37°C for 15 minutes. Two volumes of medium were added and remaining tissues were removed by allowing them to settle down at the bottom of the tube. Supernatant was subjected to centrifugation for 5 minutes at 1000 rpm; cell pellet was resuspended in medium and plated in 10 cm dishes.

Western Blot analysis

Cells were lysed in Laemmli buffer. Samples were separated by SDS-page and transferred to Nitrocellulose membrane (Immobilin FL, Millipore). The membranes were incubated with anti-ESK (mMps1). Peroxidase-coupled secondary antibodies and ECL (GE healthcare) were used to visualize protein bands.

FACS analysis

Mouse embryonic fibroblasts were treated with 250ng/ml nocodazole for 6 hours (4 days after transduction with Adeno-(Cre) GFP virus), harvested and fixed in 70% ice-cold ethanol for 24 hours. Cells were incubated with α-MPM2 for 1 hour in PBS-2% BSA-0, 1% Tween and α-Mouse Cy5 for 1 hour in PBS-0, 1% Tween. Stained cells were collected in PBS containing RNAse and Propidium Iodide. Fluorescence was measured on a FACSCalibur and analyzed with Cell Quest Pro software (BD Biosciences).

Immunofluoresence microscopy

Cells plated on 12mm coverslips were pre-extracted with 0.2% Triton X-100 in PEM (100 mM PIPES (pH 6.8), 1 mM $MgCl_2$ and 5 mM EGTA) for one minute at 37°C before fixation with 4% paraformaldehyde in PEM. Coverslips were blocked with 3% bovine serum albumin in PBS/0.1% Triton for 30 minutes, incubated with primary antibody (CREST or phospho-T649) for 16h at 4°C, washed with PBS, and incubated with secondary antibodies and DAPI (Sigma) for an additional 2 hours at room temperature. Coverslips were washed and mounted using ProLong antifade (Molecular Probes). All images were acquired on a DeltaVision RT system (Applied Precision) with a ×100/1.40NA UPlanSApo objective (Olympus) using SoftWorx software. Images are maximum intensity projections of deconvolved stacks.

Time lapse analysis

For live cell imaging, cells were plated in four-well or eight-well chambered glass-bottom slides

(LabTekII) and imaged after addition of nocodazole in a heated chamber (37°C and 5% CO_2) using a ×20/0.5NA UPLFLN objective on a Olympus IX-81 microscope, controlled by Cell-M software (Olympus). Images were acquired using a Hamamatsu ORCA-ER camera and processed using Cell-M software.

Antibodies

Rabbit-Anti-phospho-Threonine 676 (Msp1) was described before [172]. Rabbit-anti-ESK (sc541) was from Santa Cruz. Mouse anti-MPM2 was from Millipore, Human ACA (Crest) was from Fitzgerald Industry and Mouse anti-GFP from Roche. Anti-human Alexafluor647 and anti-rabbit Alexafluor568 were from DAKO, anti-mouse cy-5 from Jackson.

Acknowledgements

We want to thank Patrick Derksen, Jos Jonkers, Alain de Bruin, Tobias Dansen and Miranda van Amersfoort for valuable input. We are also grateful to Hans Clevers for providing ES cell targeting facilities and Stieneke van den Brink for help with the ES cell recombination. We thank Livio Kleij for assistance with the microscopes, the personnel of the animal facilities of the Gemeenschappelijk Dieren Laboratorium (GDL) in Utrecht for animal husbandry and Rika Kramer and Marco Hoekman from the Transgenesis Facility at the GDL for performing the blastocyst injections and generation of the CiMKi chimeric mice. We also want to thank all members of the Medema, Kops and Lens labs for their input during lab meetings. This work was supported by the Netherlands Organisation for Scientific Research (NWO) (R.H.M. and A.J.: ZonMw 918.46.616; G.J.P.L.K.: VIDI-91776336), TI Pharma (R.H.M and A.J.: T3-105) and the ERC (G.J.P.L.K. and N.J.: ERC-StG KINSIGN). R.H.M. was additionally funded by the Netherlands Genomic Initiative of NOW and N.J. by the Dutch Cancer foundation (KWF): UU 2012-5321.

Chapter 4

Mitosis as an anti-cancer target

Aniek Janssen[1,2] and René H Medema[1,2]

[1] Department of Medical Oncology and Cancer Genomics Center, University Medical Center Utrecht, Universiteitsweg 100, 3584 CG, Utrecht, the Netherlands

[2] Division of Cell Biology, Netherlands Cancer Institute, Plesmanlaan 121, 1066 CX, Amsterdam, the Netherlands

Oncogene, 2011 Jun 23;30(25):2799-809

Abstract

Most of the current drugs used to treat cancer can be classified as anti-proliferative drugs. These drugs perturb the proliferative cycle of tumor cells at diverse stages of the cell cycle. Examples of such drugs are DNA-damaging agents and inhibitors of cyclin-dependent kinases that arrest cell cycle progression at different stages of interphase. Another class of anti-proliferative drugs is the so-called anti-mitotic drugs, which selectively perturb progression through mitosis. Mitosis is the shortest and final stage in the cell cycle and has evolved to accurately divide the duplicated genome over the two daughter cells. This review deals with the different strategies that are currently considered to perturb mitotic progression in the treatment of cancer.

1) Delaying Mitosis

1.1 Need for the mitotic checkpoint

One way to kill mitotic cells is to increase the duration of mitosis by perturbing correct formation of the mitotic spindle that is needed for chromosome alignment and segregation. Two well established classes of anti-cancer drugs which induce a severe delay in mitotic progression are taxanes and vinca alkaloids [457,458]. These drugs affect microtubule dynamics and cause abnormal spindle formation [459-461]. Perturbation of spindle assembly precludes proper alignment of the chromosomes and as a consequence the mitotic checkpoint or spindle assembly checkpoint (SAC) maintains cells in mitosis, to provide the cell time to resolve these errors in alignment. This checkpoint comprises a large number of proteins, which together create a 'wait-anaphase' signal that delays mitotic progression [440]. Thus, any drug that induces erroneous chromosome alignment will prevent silencing of the mitotic checkpoint and will result in an extensive mitotic arrest, eventually leading to cell death.

1.2 Mitosis-specific targets

The two conventional microtubule-targeting drugs; the Vinca alkaloids and the taxanes, have been shown to be effective in the treatment of different types of cancer. One newly described family of microtubule-stabilizing drugs consists of Epothilones, which bind at the taxane-binding site on microtubules (reviewed in [462]). This drug is currently being evaluated in clinical trials for the use in several types of cancer and might be useful in the treatment of paclitaxel-resistant tumors in the future [457; 463]. Besides many clinical success stories, anti-microtubule targeting drugs have severe side-effects, which are in part caused by general perturbation of cell proliferation, resulting in myelosuppression. However, the dose-limiting toxicities of these drugs are largely a consequence of the general disturbance of microtubule dynamics that they induce, causing serious neurotoxicity. Also, acquisition of resistance is quite common in patients treated with anti-microtubule drugs [457,464,465]. Thus, while the induction of a mitotic delay does seem to have a relatively specific cytotoxic effect on cancerous tissue, the side-effects unrelated to the anti-mitotic effects of these drugs restrict their application. This has instigated a search for more mitosis-selective drugs. More specific details on the mechanism of action of the different families of microtubule-targeting drugs has been reviewed elsewhere [457,463,466]. In this review, we will focus more on recently identified mitotic targets and the possibility of exploiting these targets in anti-cancer treatment. One of the targets that was proposed for a mitosis-selective approach is the plus end-directed motor protein Eg5 (kinesin-5). Eg5 has the capacity to drive centrosome separation in prophase, which initiates bipolar spindle assembly [467,468]. Inhibition of Eg5 motor activity results in assembly of a monopolar spindle, causing a defect in chromosome congression and consequently chronic mitotic checkpoint activity [434,468,469]. Eg5 inhibition has been shown to effectively kill taxol-resistant cell lines [470], making it an attractive anti-cancer target. Indeed, a variety of potent and selective Eg5 inhibitors have been generated over the last couple of years and some of them have entered clinical trials (Table I). Although limited cytotoxicities have been found in patients treated with Eg5 inhibitors, only partial responses have been reported so far [471]. In addition, several reports have shown that mutations in Eg5 occur which can confer resistance to these compounds [472-474]. On top of that, other motor proteins can act redundantly with Eg5 and increased expression of Kif15 allows cancer cells to overcome a mitotic delay induced by Eg5 inhibition [475,476]. Nonetheless, since Eg5 inhibitors are expected to have a mitosis-specific effect and partial patient-responses have been reported, clinical trials will continue with a focus on combination therapies [471].

Two other interesting mitotic targets, for which inhibitors are currently under investigation, are the kinases Aurora A and Polo-like kinase-1 (Plk-1) [184]. Both are overexpressed in cancer [477,478] and both have important roles in G2 and mitosis [479,480]. Inhibition of either Aurora A or Plk1 results in monopolar spindle formation, due to their roles in centrosome maturation and separation in G2 [479,480]. As such, the most profound effects after inhibition of Plk1 or Aurora A are perturbation of mitotic progression, making both of these kinases attractive and possibly specific anti-mitotic targets. Many inhibitors have been produced that target these kinases, and several have already entered clinical trials [477,478] (Table I). The kinesin motor protein CENP-E is the most recent addition to potential anti-mitotic targets. It is a kinetochore-associated kinesin, whose function appears to be restricted to mitosis. Upon absence or inhibition of its activity, cells are delayed in mitosis for a prolonged period of time with unaligned chromosomes [481]. Inhibition of CENP-E function has been shown to elicit anti-tumor effects in mouse models of spontaneous tumor formation [397] as well as in mice bearing xenografts of human tumor cells [482]. Moreover, inhibitors of CENP-E are currently being tested in phase I clinical trials [471,483] (Table I).

1.3 Why does a mitotic delay result in cell death?

Cells treated with classical anti-mitotic drugs will delay mitotic progression for an extensive period of time due to the action of the mitotic checkpoint. This prolonged mitotic delay is often followed by cell death in mitosis (mitotic cell death). However, a subset of cells can escape mitotic cell death and exit [342]. Remarkably, there is a great variation in the timing of cell death amongst cells within a genetically identical population. Thus, as a consequence of a mitotic checkpoint-dependent delay, cells either die in mitosis or they exit mitosis in a tetraploid state despite an active mitotic checkpoint, a process called mitotic checkpoint slippage [342,484,485] (Fig.1). In several independent studies, no clear correlation was found between the duration of the mitotic delay and cell fate, indicating that the time a cell arrests in mitosis does not dictate whether a cell will die in mitosis, slip from the mitotic arrest and die in the next G1 phase or slip out and continue to proliferate [342,486,487]. However, it has become clear that during the mitotic arrest, cyclin B levels slowly drop despite an active mitotic checkpoint (Brito et al., 2006). This has led to a model for drug-induced mitotic death in which two independent processes are active during the arrest [342]. In this model a slow but progressive loss of cyclin B is paralleled by a slow but steady rise in caspase activity. This predicts that once cyclin B levels have dropped below a certain threshold before caspase activation has reached its critical threshold to induce apoptosis, cells will exit mitosis without undergoing cell death in mitosis. However, when cyclin B levels have not dropped sufficiently low to exit mitosis and caspase activation has already reached its death threshold, cells will die in mitosis [342]. This model, however, does not provide an answer to the question how a prolonged delay in mitosis could result in caspase activation. Mitosis is a phase in which several high energy consuming processes are active, such as chromosome condensation, mitotic spindle formation, chromosome congression and segregation, while several other cellular processes, such as vesicle transport and transcription are inhibited. A prolonged mitosis could therefore easily result in energy deprivation. Moreover, the cell is extremely vulnerable during mitosis. The chromosomes are in a highly condensed state and not protected by the nuclear membrane. In fact, it has been shown that mitotic cells have an enhanced sensitivity to for example radiation treatment, [488,489]. Therefore, cells could have evolved an intrinsic pro-apoptotic pathway that is responsible for clearance of cells that spend too much time in mitosis. Indeed, recent data show that a mitotic delay of only two hours can already result in p53 activation, indicating that a prolonged duration of the mitotic phase can directly activate a stress response in mitotic cells [490]. Interestingly, Cyclin B-cdk1 is thought to have a central role in controlling both mitotic duration and the apoptotic machinery. It can phosphorylate and inhibit caspase 9 during mitosis [491]. This suggests that, during a prolonged mitosis, a slow but steady drop in Cyclin B levels could be paralleled by a

slow but steady rise in caspase 9 activity. Recently it has also been shown that a prolonged mitosis induces CyclinB-cdk1-dependent Mcl-1 degradation, an important anti-apoptotic protein [492]. Some other reports have also suggested interplay between CyclinB-cdk1 activity and the activity of the anti-apoptotic proteins BclxL and Bcl-2 [493,494]. Moreover, activity of certain mitotic kinases can inhibit or activate p53, suggesting that cells that are delayed in mitosis are tipping the balance when it comes to p53 activation [495];[496,497]. Together, these findings show that a prolonged mitosis can result in both

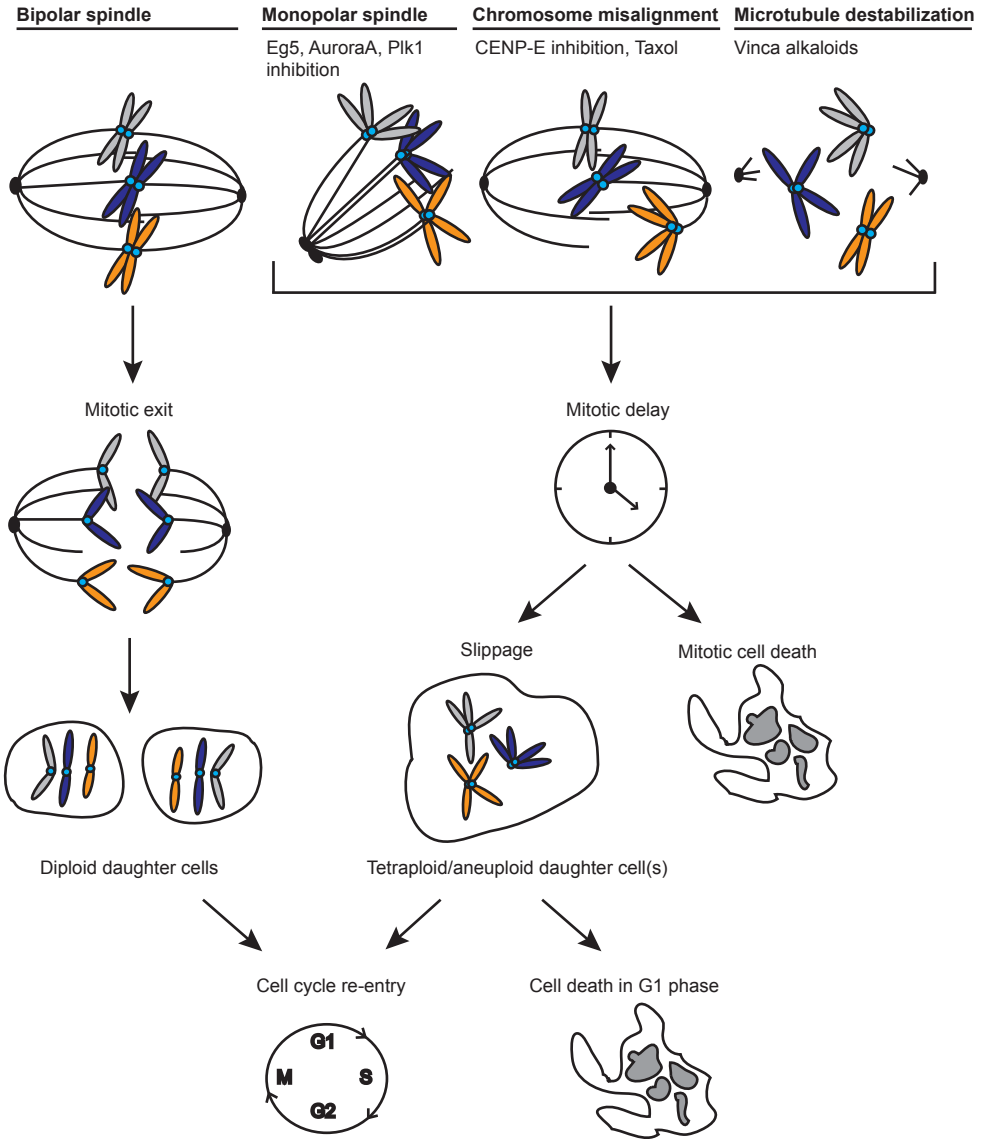

Figure 1. Model for delaying mitosis as an anti-cancer strategy
Treatment with anti-mitotic drugs can lead to a variety of phenotypes; formation of monopolar spindles, aberrant spindles due to (de)stabilization of microtubules, or a normal spindle architecture with misattached chromosomes. All of these distinct effects will lead to a delay in mitosis for an extensive period of time. This mitotic delay is either followed by cell death in mitosis (mitotic cell death) or slippage from the mitotic state. The tetraploid daughter cells arising from mitotic slippage will either die in the subsequent G1 phase or re-enter the cell cycle to produce aneuploid progeny.

inhibition of the anti-apoptotic machinery and activation of a pro-apoptotic pathway, which provides a plausible mechanism to explain a cells' sensitivity to a delay in mitosis.

1.4 Inhibiting mitotic exit

According to the current model for mitotic cell death, one way of pushing the balance towards tumor cell death in mitosis would be to inhibit cyclin B degradation. This way cells will not be able to slip out of mitosis and will be able to reach the threshold for apoptosis induction before mitotic exit is allowed. Indeed, inhibition of cyclin B degradation results in enhanced mitotic cell death when compared to treatment with spindle drugs [498]. Moreover, inhibition of mitotic exit has led to tumor regression in a recently described conditional mouse model [499]. These findings indicate that inhibition of mitotic slippage could enhance the efficacy of the anti-mitotic drugs that were mentioned earlier in this review [498,500,501] (Table I).

2) Inducing tetraploidy

2.1 Targeting Aurora B

Targeting the cytokinetic machinery is another way of specifically disturbing mitotic cells. Cytokinesis is essential for a mitotic cell to be physically separated into two daughter cells [502]. Therefore, inhibition of cytokinesis leads to the formation of one tetraploid daughter cell containing twice as much DNA. A particularly important kinase that acts during cytokinesis is Aurora B [503]. It plays an essential role in diverse processes in mitosis [418], but the final outcome of Aurora B inhibition is the generation of a tetraploid cell. This inhibition results in efficient cell killing in a variety of tumor cell lines [54,425,504;505] and does not seem to have a prominent effect on non-dividing cells, which makes it an interesting, proliferation-specific anti-cancer target [425]. Several Aurora B inhibitors have been generated and some have entered clinical trials [506]. Promising effects of these inhibitors, some of which also target Aurora A, have been seen in mouse tumor models [504,507,508] and patients with various types of tumors [477,506] (Table I).

2.2 Advantages and disadvantages of inducing tetraploidy

Once a tetraploid cell has formed, several things can happen; the tetraploid cell can arrest or die in the following G1, or it can reduplicate its tetraploid genome and divide again [425,444,509-511]. The lethality induced by Aurora B inhibition is thought to be mainly caused by the polyploidy that arises as a result of several rounds of endoreduplication and failed cell divisions [425]. This polyploidy can increase the burden on the cells' metabolism, resulting in activation of stress pathways [511,512]. Another possible cause for the observed lethality is the presence of an extra pair of centrosomes in the tetraploid cells. Centrosomes are the predominant microtubule-organizing centers of animal cells and play an important role during spindle assembly [513]. Live cell imaging has shown that tetraploid cells harboring multiple centrosomes can end up with a multipolar spindle in the subsequent mitosis [354]. This multipolar spindle causes many chromosomes to missegregate, generating severely aneuploid off-spring with limited cell viability (Fig.2). Introducing tetraploid cells in both cancerous and healthy tissue could, however, have major drawbacks. Although cytokinesis failure often results in cell death, xenograft models have revealed that tetraploidy can increase the tumorigenic capacity of untransformed cells [357,514]. Consistent with this, tetraploid cells have been found in several early malignant tissues [515,516].

A number of alternative models for the contribution of tetraploidy to the tumorigenic capacity of cells have been suggested [444]. As proposed over 100 years ago, the multipolarity often seen in tetraploid cells could, in some cases, lead to viable aneuploid progeny, which ultimately may underlie cancer formation [232,354]. Recently, two independent studies put forward another concept; mitotic cells harboring a multipolar spindle can, after achievement of chromosome attachments to the spindle,

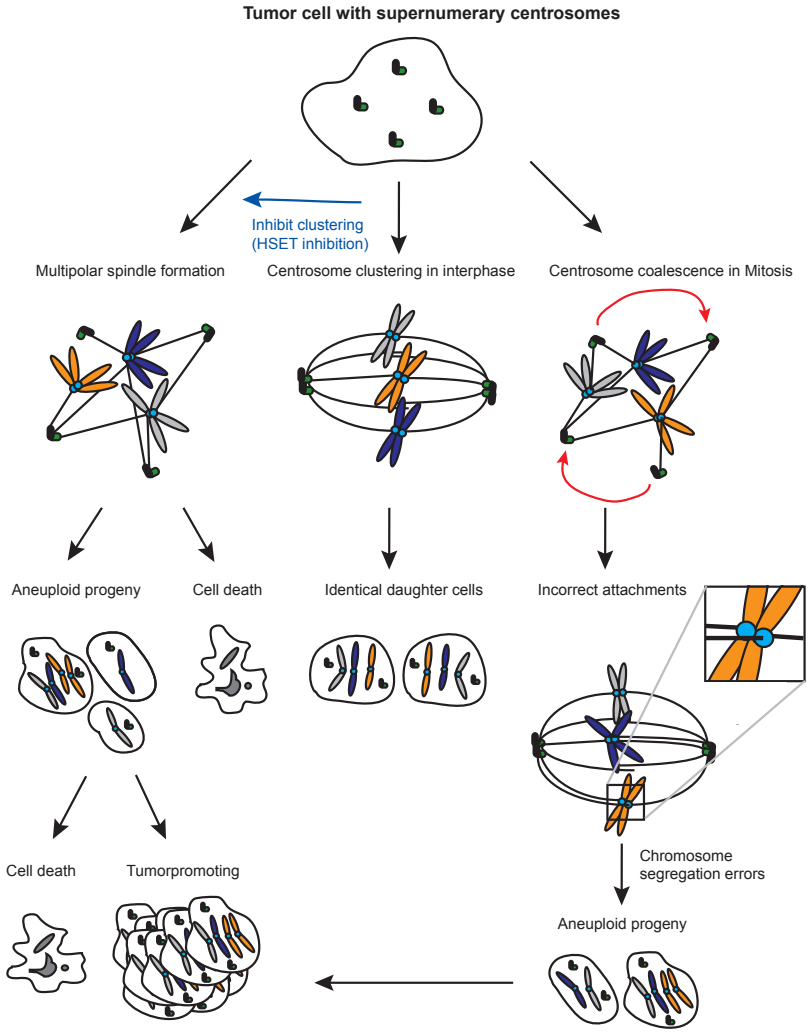

Figure 2. Supernumerary centrosomes: a specific anti-cancer target?
Multiple centrosomes can cause different mitotic defects. Extra centrosomes can promote the formation of multipolar spindles, possibly resulting in mitotic cell death. Alternatively, these multipolar spindles could give rise to aneuploid progeny. This progeny most often dies due to the massive genomic imbalance that is produced. Nonetheless, a subset of the aneuploid progeny could escape cell death and promote further tumorigenesis. What's more, tumor cells have evolved different ways to cluster supernumerary centrosomes to produce a bipolar spindle; Supernumerary centrosomes can cluster in interphase, which will lead to normal mitotic progression producing genetically identical daughter cells. Alternatively, the extra centrosomes can initially promote formation of a multipolar spindle that is converted into a bipolar spindle upon centrosome coalescence (red arrows). This centrosome clustering produces many incorrectly attached chromosomes, which will missegregate upon mitotic exit. This mis-segregation event yields aneuploid daughter cells, which eventually could promote tumor growth. Inhibition of centrosome clustering (blue arrow) will promote stable multipolar spindle formation and can increase tumor cell death.

cluster their centrosomes. This 'centrosome coalescence' can convert the multipolar spindle into a bipolar spindle, but fails to resolve all of the incorrect attachments that have occurred in the multipolar spindle, resulting in frequent missegregations upon mitotic exit and, as a consequence, aneuploid daughter cells [355,356] (Fig.2). Although plausible, it is unknown whether these two mechanisms actually explain the tumorigenic capacity of tetraploid cells *in vivo* as well.

Exploiting mitotic defects of cancer cells

Cancer cells exhibit differences in cell cycle progression when compared to normal cells. The last decennium much effort has been put in finding a way to exploit these differences in order to specifically target cancer cells. In the last part of this review we will focus on two major hallmarks of tumor cells: supernumerary centrosomes and chromosomal instability (CIN) and we will discuss the various possibilities that have been proposed of exploiting these cancer-associated phenotypes.

3) Multiple centrosomes: Achilles' heel of tumor cells?

Supernumerary centrosomes are commonly found in tumor cells and are clearly associated with increased genetic instability and tumorigenesis [350,351,517-519]. As mentioned above, tetraploidization is one mechanism by which cells can end up with multiple centrosomes [520]. Other suggested mechanisms that could lead to supernumerary centrosomes are de novo centrosome formation, cell fusion or centrosome over-duplication [353,521-523]. Tumor cells harboring multiple centrosomes often end up in an aberrant mitosis [354-356]. However, since multipolar spindles often result in cell death rather than viable aneuploid progeny [354], it is expected that tumor cells have evolved ways to suppress multipolar mitoses. Indeed, supernumerary centrosomes have been shown to cluster and form a seemingly normal bipolar spindle in various types of cells [524-526] (Fig.2).

3.1 Targeting the centrosome clustering machinery

The fact that many tumor cells can cluster their centrosomes and most likely depend on centrosome clustering to produce viable daughter cells, opens the door for anti-cancer strategies. Indeed, specific inhibition of centrosome clustering has been shown to increase the number of cells going through a multipolar mitosis, and induces enhanced cell death [527]. Using a screening-based approach, both actin-dependent forces and cell adhesion were found to be essential for bipolar spindle formation in human cells harboring multiple centrosomes. More importantly, the conserved minus-end directed motor protein HSET was identified as an essential component for cell viability specifically in cells containing supernumerary centrosomes [527]. As kinesins have been shown to be druggable targets [469], HSET could prove to be a useful target for the treatment of cancer cells with supernumerary centrosomes (Fig.2).

4) Chromosomal instability: tipping the balance

4.1 CIN and cancer

In a high percentage of human tumors chromosomes frequently missegregate, causing recurrent

chromosome losses and gains, a phenotype referred to as chromosomal instability (CIN). This chromosomal instability leads to aneuploid cells that contain an abnormal number of chromosomes [270]. Over the last decennium, extensive research has been directed at understanding the precise cause of CIN and aneuploidy in human tumors [282,528]. Although numerous mutations in genes required for normal mitotic progression have been found, none of these mutations appear to be present in a large percentage of human tumors [282,303,335,337,369,528]. This suggests that it is unlikely that CIN is solely caused by mutational inactivation of genes that control chromosome segregation. In fact, gene profiling of CIN tumors demonstrated that many genes are differentially expressed in CIN cancers [272,282]. These results have led to the hypothesis that altered expression of a large variety of proteins that are involved in safeguarding the genome could provide the driving force for CIN, rather than mutational inactivation of a small set of defined CIN-suppressive genes [528,529]. Nevertheless, a causal link does exist between CIN and cancer. Various mouse models have been generated to mimick chromosomal instability, by changing the expression of genes required for faithful mitosis [530]. These models have revealed the tumor-promoting capacity of CIN, but do not resolve the long-standing question whether CIN alone is sufficient to drive tumorigenesis or whether additional mutations in other genes are required as well [286,531,532].

4.2 The downside of being CIN

Despite our lack of understanding of the exact causes of CIN, it could nonetheless provide a useful means to specifically target tumor growth [290,533]. Since all CIN tumor cells repetitively lose and gain chromosomes, one might be able to increase the rate of missegregations to such a level that the majority of cell divisions will produce non-viable daughter cells. If the frequency of missegregations is sufficiently high, this will cause all cells within the tumor to eventually undergo an aberrant cell division resulting in inviable progeny, possibly serving as a selective strategy to eradicate CIN tumors [292,299] (Fig.3). In line with such a possible negative impact of CIN on tumor cell viability, various mouse models of enhanced chromosomal instability have also revealed a possible tumor suppressive role for CIN. For example, while reducing levels of CENP-E leads to an increase in spleen and lung tumor formation, crossing these mice with p19 knock-out mice or treating them with carcinogens resulted in decreased tumor formation [397]. Similar results were found in Bub1-insufficient mice; increased tumorigenesis has been observed when crossing these mice with p53 or Rb heterozygous mice, but a reduction in tumor formation in the prostate was observed when Bub1 insufficiency was combined with a reduction in PTEN [286]. Importantly, this latter reduction correlated with increased cell death. These results all argue in favor of the hypothesis that the level of CIN needs to be tightly regulated in tumors: mild CIN can facilitate tumorigenesis, but severe CIN is incompatible with tumor cell viability.

4.3 Targeting the chromosome segregation machinery

If enhancement of chromosome segregation errors can specifically eradicate CIN tumor cells, then what would be the optimal targets to achieve this? Obvious candidates are proteins that ensure the fidelity of chromosome segregation. For example, inhibition of mitotic checkpoint function has been shown to cause severe chromosome segregation errors and is incompatible with human cell viability [292,294], suggesting it could represent a suitable target [290]. Indeed, inhibition of the mitotic checkpoint kinase Mps1 has recently been shown to partially inhibit tumor growth in mouse models with xenografted human tumors [176] (Table I). However, full mitotic checkpoint inhibition could be detrimental to normal cells as well, and this might defeat the tumor-selective basis of the approach [291]. Also, it is improbable that full inhibition

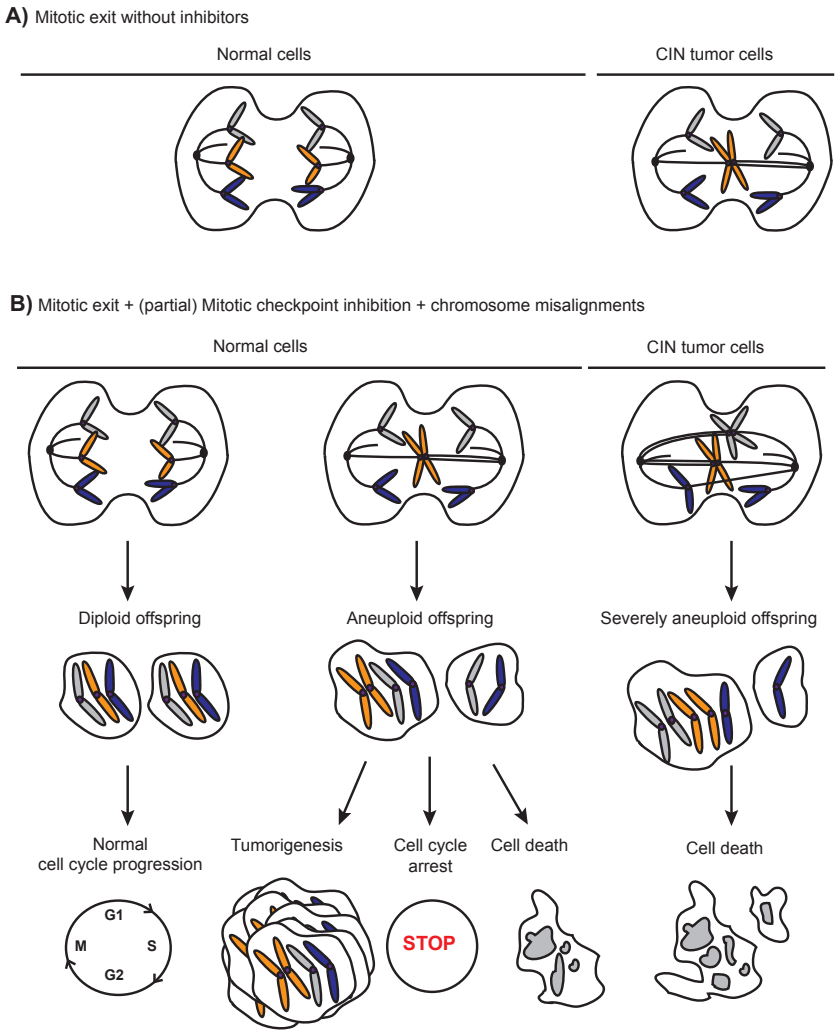

Figure 3. Model for mitotic checkpoint inhibition as a specific anti-CIN cancer strategy
A) Chromosomally unstable (CIN) tumor cells often missegregate chromosomes upon mitotic exit when compared to healthy proliferating cells. B) Enhancing chromosome alignment defects in combination with (partial) mitotic checkpoint inhibition will result in severe chromosome missegregations in CIN tumor cells and promote cell death. In contrast, in normal healthy cells (partial) mitotic checkpoint inhibition can lead to two alternative outcomes: the cell division is unaffected and cells exit mitosis normally, resulting in healthy diploid daughter cells, or aneuploid progeny is produced. This progeny has a high probability to either arrest or die. Some aneuploid daughter cells could escape the cell cycle arrest and might eventually become tumorigenic.

of checkpoint function can be achieved in clinical settings. Nonetheless, partial inhibition of mitotic checkpoint function combined with an approach that perturbs proper chromosome alignment could enhance chromosome segregation errors above the threshold required to kill tumor cells. In line with this, work from our own lab has shown that partial mitotic checkpoint inhibition in combination with sub-lethal doses of paclitaxel can produce a synergistic effect in tumor cell death that is not observed in non-transformed cells [299] (Fig.3). Inhibition of centrosome clustering, as mentioned above, could be another approach to enhance chromosome segregation errors in CIN cells harboring multiple centrosomes (Fig.2). The multipolarity resulting from this strategy

will inevitably lead to severe aneuploidy, which strongly compromises tumor cell viability [527]. Presumably the enhanced chromosomal instability kills tumor cells because the genetic imbalance that is produced as a result of error prone chromosome segregation is too severe to produce a viable daughter cell. Obviously, segregation errors that result in loss of one or more chromosomes that contain essential genes will not produce two viable daughter cells [534]. In fact, aneuploidy is in most cases incompatible with embryonic viability [535]. On the other hand, aneuploid tumor cells can proliferate without difficulty, so the coupling between aneuploidy and cell viability is not so that aneuploidy is never tolerated. How exactly does aneuploidy compromise cell viability? Recent work in yeast has shown that introduction of as much as a single extra chromosome leads to an extra burden on the cells' transcription machinery, since most genes on the extra chromosome are being transcribed [446]. Together with the increase in transcriptional activity, increased protein synthesis and proteasomal degradation produce a higher demand on the cellular metabolism and results in increased energy consumption [445,446]. The presence of extra chromosomes can trigger the activation of stress pathways, owing to protein imbalances, proteotoxic stress and presumably higher levels of Reactive Oxygen Species (ROS) [407,431,445,446]. Due to activation of these stress pathways, aneuploidy will lead to a decrease in the speed of cell growth and enhanced lethality in an otherwise healthy population of cells [445,446]. In line with this, it has been hypothesized that another specific strategy to kill aneuploid tumor cells could be to enhance proteotic stress, for example by inhibiting the proteasome machinery [446]. The actual molecular pathways underlying the initial cell cycle delay following single chromosome missegregations and aneuploidy are starting to emerge. Chromosome missegregation events have been shown to inhibit cell cycle progression through activation of p38 and eventually p53 [431]. Interestingly, inhibition of p38 function selectively targets aneuploid or tetraploid cells [536]. Moreover, recent data suggest that ATM also plays a role in the observed p53 activation following acquisition of an aneuploid state [407]. Presumably, due to the increase in oxidative stress ATM can get directly activated in the aneuploid cell [537] and in turn can activate p53 [407]. Whether other upstream pathways could contribute to the observed p53 activation is still unknown. Thus, it would seem that chromosome segregation errors and gene imbalances result in the activation of a variety of stress pathways that restrict the proliferative capacity of the newly formed aneuploid cells. The fact that aneuploid tumor cells can readily proliferate indicates that cells can adapt to this acute stress response [538]. Clearly the success of a strategy that enhances chromosome imbalances in the tumor will heavily depend on the ease at which the aneuploid cell can adapt to the newly acquired genetic imbalance it is confronted with.

4.4 Specificity of exploiting CIN

The question remains how the tumor specificity of the diverse strategies to exploit CIN can be maximized and how adverse effects on healthy dividing tissue can be minimized. Normal cells have a defined diploid content of chromosomes, while tumor cells mostly contain a much larger number of chromosomes. As a consequence, the time required for healthy cells to correctly align their chromosomes in mitosis is much shorter when compared to aneuploid tumor cells that typically harbor many extra chromosomes [539]. Thus, decreasing the duration of mitosis by mitotic checkpoint inhibition is likely to have more disastrous effects on aneuploid tumor cells than normal diploid cells. In fact, mitotic checkpoint inhibition in healthy cells does not necessarily cause segregation errors [299,540] (Fig.3). Moreover, since CIN cells already start off with massive genome imbalances, they may perhaps be more sensitive to chromosome missegregation events when compared to healthy cells [290]. More research is needed to determine whether CIN cells will reach the critical threshold of segregation errors more easily than healthy cells following disturbance of chromosome segregation.

4.5 Disadvantages of exploiting mitotic defects of cancer cells

Taken together it seems plausible that preexisting mitotic defects of cancer cells can be exploited in novel anti-cancer strategies, but more research is needed to validate these therapeutic interventions. For one, it remains largely unknown what the long-term effect of inhibition of the centrosome clustering machinery is on normal dividing cells [541]. What's more, due to the random clustering of centrosomes, cells with supernumerary centrosomes will frequently give rise to daughter cells that inherit only a single centrosome. Thus, within a population of tumor cells with supernumerary centrosomes, a subset of cells will exist or arise that contains the right number of centrosomes. This means that a fraction of the tumor cells within the population will not be sensitive to this strategy and can drive a relapse (Fig.2). Whether this will be a serious limitation of this approach will depend on the frequency at which these "normal" daughter cells acquire extra centrosomes. Increasing the amount of CIN will also inevitably lead to adverse side-effects when used as an anti-cancer therapy. For example, introduction of chromosome missegregations will affect the viability of normal diploid cells as well [431]. Moreover, as mentioned above, CIN has been implicated in promoting tumorigenesis and therefore, exploiting CIN could produce secondary tumors in the long term by inducing chromosomal rearrangements that provide a growth advantage for the aneuploid cells over their diploid counterparts (Fig.3). However, it has also been shown that aneuploidy inducing treatments have a negative impact on cell cycle progression and viability in an otherwise healthy population of cells (Fig.3). This leads to selection for cells with a diploid karyotype [289,299,431]. Moreover, it has been shown that aneuploid cells need to acquire additional (genetic) defects in order to overcome the decrease in cell growth [538]. Together, these mechanisms decrease the probability of 'healthy' aneuploid cells to become tumorigenic. Whether inhibition of mitosis-specific proteins or exploiting supernumerary centrosomes and chromosomal instability could sort any clinical efficacy remains to be tested in xenografts and tumor-prone mouse models. All in all, exploiting cancer-specific phenotypes deserves further attention as these could lead to new therapeutic interventions, which are possibly less harmful for healthy dividing tissues.

Table I. Overview of (Pre-)clinical mitotic targets currently being evaluated.

Target	Clinically used inhibitors	Cell cycle effect	Mouse model	Clinical Trials	Refs
Eg5	Ispinesib, SB743921, MK-0731,AZD-4877, ARRY-520, LY2523355	Mitotic delay (monopolar spindle)	Xenografts	I,II	[542,543] and reviewed in [471]
Plk1	BI2536, BI6727, GSK-461363,ON 01910.Na, HMN-241, NMS-1286937, TAK-960, TKM-080301 (RNAi)	Mitotic delay (monopolar spindle)	Xenografts	I,II	[544,545] and reviewed in [184,546, 547]
Aurora A	MLN8054, MLN8237, ENMD-2076	Mitotic delay (monopolar spindle)	Xenografts	I,II	[548], reviewed in [184,504 549]
Aurora B	AZD1152, GSK1070916A	Polyploidy	Xenografts	I,II	Reviewed in [184,504,506,549]
CENP-E	Lonafarnib, GSK923295A	Mitotic delay (chromosome misalignment)	Xenografts, conditional mouse model	I	[397,482,483] and reviewed in [471]
Future target	**Inhibitors (pre-clinical)**	**Cell cycle effect**	**Mouse model**	**Clinical trials**	**References**
APC/C (Cdc20)	TAME	Mitotic delay	Conditional knock out model	None	[499,501]
Mps1 (mitotic checkpoint)	Mps1 IN-1, Reversine, NMS-P715	Chromosome missegregations	Xenografts	None	[176,550, 123]

Chapter 5

Elevating the frequency of chromosome missegregation as a strategy to kill tumor cells

Aniek Janssen[1,2] Geert J.P.L. Kops[1,3,‡] and René H. Medema[1,2,‡]

[1] Department of Medical Oncology and Cancer Genomics Center, University Medical Center Utrecht, Universiteitsweg 100, 3584 CG, Utrecht, the Netherlands

[2] Division of Cell Biology, Netherlands Cancer Institute, Plesmanlaan 121, 1066 CX, Amsterdam, the Netherlands

[3] Department of Molecular Cancer Research, University Medical Center Utrecht, Universiteitsweg 100, 3584 CG, Utrecht, the Netherlands

‡ These authors contributed equally to this work.

+ Addendum

Proc. Natl. Acad. Sci. USA, 2009 Nov 10;106(45):19108-13

Abstract

The mitotic checkpoint has evolved to prevent chromosome missegregations by delaying mitosis when unattached chromosomes are present. Inducing severe chromosome segregation errors by ablating the mitotic checkpoint causes cell death. Here we have analyzed the consequences of gradual increases in chromosome segregation errors on the viability of tumor cells and normal human fibroblasts. Partial reduction of essential mitotic checkpoint components in four tumor cell lines caused mild chromosome missegregations, but no lethality. These cells were, however, remarkably more sensitive to low doses of taxol, which enhanced the amount and severity of chromosome segregation errors. Sensitization to taxol was achieved by reducing levels of Mps1 or BubR1, proteins having dual roles in checkpoint activation and chromosome alignment, but not by reducing Mad2, functioning solely in the mitotic checkpoint. Moreover, we find that untransformed human fibroblasts with reduced Mps1 levels could not be sensitized to sub-lethal doses of taxol. Thus, targeting the mitotic checkpoint and chromosome alignment simultaneously may selectively kill tumor cells by enhancing chromosome missegregations.

Introduction

Error-free chromosome segregation is vital for embryonic development and tissue homeostasis in multicellular organisms. Whereas during development the vast majority of single missegregation events is not tolerated [535], aneuploidy is a common genetic alteration in solid human tumors [551]. In ex-vivo cultures, such aneuploid tumor cells display low but significant frequencies of chromosome missegregations (chromosomal instability, CIN) [231]. The mitotic checkpoint is one of the cell cycle checkpoints that have evolved to safeguard cells from CIN [282, 290]. This checkpoint ensures the fidelity of sister chromatid segregation over the two daughter cells by inhibiting progression to anaphase until all sister chromatids are attached to microtubules of the mitotic spindle (reviewed in [441]). Defects that lead to reduced mitotic checkpoint signaling cause aneuploidy and may eventually contribute to tumorigenesis in humans (reviewed in [290,532]). Although an intriguing hypothesis and a clear causative link in experimental animal models (reviewed in [392]), it has never been shown that compromised checkpoint signaling directly underlies CIN in malignant human tissue or cultured human tumor cells [289,342]. In contrast, complete inactivation of the mitotic checkpoint results in gross chromosome missegregations and is not compatible with cell viability[292,294]. This has led to the suggestion that inhibition of the mitotic checkpoint could have therapeutic potential in cancer treatment [290]. A widely-used anti-mitotic drug is paclitaxel (taxol), which induces a mitotic checkpoint-dependent delay at high dose by inhibiting microtubule dynamics[342,552,553]. At low, clinically relevant concentrations, taxol treatment induces aneuploidy without severely delaying cells in mitosis[553-555]. Controversial results have been reported on the effect of mitotic checkpoint inhibition on taxol-induced cell death. Incomplete functioning of the checkpoint has been suggested to induce resistance to high doses of taxol[556-559], which is in line with the observation that CIN also correlated with taxol resistance[280]. However, others have shown that inhibition of the mitotic checkpoint increases the effectiveness of taxol[560]. Here, we have explored the relationship between the level of chromosome mis-segregation and cell death in two severely aneuploid tumor cell lines, two diploid tumor cell lines and one immortalized fibroblast line. We show that reducing levels of the essential mitotic regulators Mps1 and BubR1 sensitizes human tumor cells but not normal cells to death by clinically relevant doses of taxol. This sensitization is directly due to the ability of the combined treatments to cause severe chromosome segregation errors in tumor cells.

Results and Discussion

Partial knockdown of Mps1 or BubR1 weakens the mitotic checkpoint but does not affect tumor cell viability

Absence of essential mitotic checkpoint components such as BubR1 or Mps1 causes cell death within 6 cell divisions[116,172,292]. To further examine the therapeutic potential of inhibition of these proteins, we generated panels of cancer cells with reduced expression of Mps1 and BubR1. To test the effect on different types of cells, we created monoclonal lines of two aneuploid tumor cell lines (U2OS and HeLa) that expressed doxycycline-inducible Mps1 or BubR1 shRNA and two (near-) diploid tumor cell lines (HCT-116 and LS174-T) that expressed doxycycline-inducible Mps1 shRNA. Cell lines were selected in which Mps1 or BubR1 expression was reduced between 60-88% upon doxycycline addition (Fig.1A, C). The effects on cell viability and chromosome segregation of the shRNA's used in this study were specific for knockdown of the respective proteins (Fig.S3 and[116,292]). In contrast to cell lines that have an almost complete removal of Mps1 or BubR1 protein (Fig.S1A and [292 116]), partial depletions of Mps1 or BubR1 had no severe effect on cell viability (Fig 1A, C). We only observed a moderate

increase in cell death (18% vs. 4% in control) as observed by live cell imaging of propidium iodide (PI) uptake after partial depletion of Mps1 in U2OS-TetRMps1 cells (Fig.S2A-B; 0nM taxol). Despite the ability of the different cell lines to survive with significantly reduced levels of Mps1 or BubR1, their ability to delay in mitosis in response to spindle disruption was clearly affected. When U2OS-TetRMps1 cells were treated with 10μM STLC, an Eg5 inhibitor that causes a checkpoint-dependent mitotic delay by preventing bipolar spindle assembly (Fig.S1B) [561], they were delayed in mitosis for 13,2 hours on average (Fig.1B). However, upon partial depletion of Mps1 (+ doxycycline) the mean duration of the mitotic arrest was reduced to 3,7 hours (Fig.1B). With the possible exception of HeLa-TetRMps1 cells, the ability of the other inducible cell lines to prolong the duration of mitosis upon treatment with STLC was similarly affected when Mps1 or BubR1 protein levels were reduced (Fig.1B, D). To examine the effect of reduced mitotic checkpoint activity in cells partially depleted of Mps1 or BubR1 on the fidelity of chromosome segregations in an unperturbed mitosis, anaphase progression was followed by time-lapse microscopy (Fig.S1C). The percentage of U2OS-TetRMps1 cells that displayed mild chromosome segregation defects in anaphase increased from 13% in control cells to 40% upon partial Mps1 depletion. The percentage of cells that severely missegregated their chromosomes increased from 0 to 18% (Fig.1E). A similar increase in chromosome missegregations was observed in the other Mps1 and BubR1 clones, where the percentage of mild mis-segregations increased from ~10% to ~55%, while severe mis-segregations increased from ~4% to ~30% (Fig.1E). Interestingly, as colony formation was not affected (Fig.1A, C), increasing the percentage of chromosome segregation errors to more than 50% (around a third of which were severe missegregations), appeared to be well tolerated by the cell population as a whole in the four tumor cell lines tested.

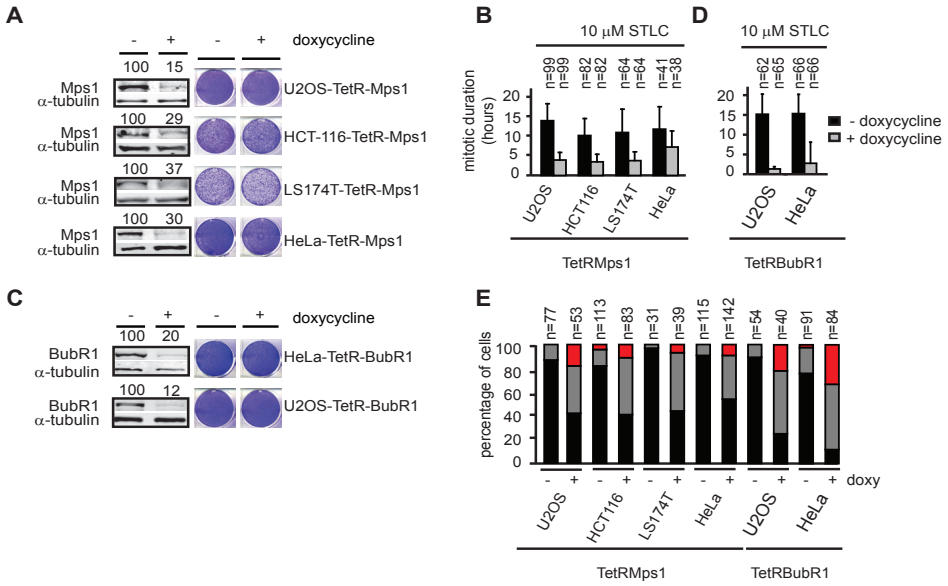

Figure 1. Partial inactivation of Mps1 or BubR1 leads to chromosome segregation defects but fails to compromise tumor cell viability.
A+ C) Left: Indicated cell lines, treated without (-) and with (+) doxycycline (dox) for 3 days, were immuno- blotted for Mps1 or BubR1 and α-tubulin. Values above blots represent relative amount of Mps1 or BubR1 protein levels. Right: Colony formations of indicated cell lines, treated with and without dox for 11 days. B+D) Live cell analysis (DIC) of the mean mitotic duration (+SD) in the presence of 10μM STLC of indicated cell lines treated with or without doxycycline for 3 days. Mitotic duration was determined as the time from nuclear envelope breakdown (NEB) to the first attempt of cytokinesis (membrane blebbing). n=amount of cells filmed per condition. E) Quantification of time-lapse movies as performed in representative images in Fig.S1C. Dox was added 3 days prior to filming. n=amount of cells filmed per condition.

Partial depletion of Mps1 or BubR1 sensitizes tumor cells to clinically relevant doses of taxol.

The observed correlation between the level of Mps1 or BubR1 depletion, the severity of chromosome missegregations and the extent of cell death pressed us to investigate if increasing the amount of segregation errors beyond that obtained by partial depletion of Mps1 or BubR1 would now impact tumor cell viability. To this end we introduced low, clinically relevant doses of taxol (1-10nM) that are known to cause aneuploidy [554,555] without causing the severe mitotic delay that occurs at high doses of taxol (50nM-10uM) [342,484,553]. We found that in U2OS-, HCT-116-, LS174- and Hela-TetRMps1 cells with normal Mps1 levels, viability as well as the fidelity of chromosome segregation was only marginally compromised at 2nM taxol (Fig.2A-H –doxycycline, 2nM taxol). However, viability was drastically reduced by this low dose of taxol when Mps1 expression was additionally partially suppressed (Fig.2A,C,E,G + doxycycline, 2nM taxol): The number of colonies was reduced 2- to 10-fold when compared to doxycycline treatment alone in U2OS-, HCT-116-, LS174T and Hela-TetRMps1 cells (Fig.2A,C,E,G). This lethality correlated strongly with an increase in the frequency and severity of segregation errors (Fig.2B, D, F, H +doxycycline, 2nM taxol). A slight increase in the dosage of taxol in U2OS-TetRMps1 cells (from 2 to 5 nM) or in LS174-T-TetRMps1 cells (from 2 to 3 nM) induced a moderate increase in chromosome missegregations when Mps1 levels were kept high, but only a partial reduction in colony formation was observed (Fig.2A,B,E,F). Nonetheless, additional partial depletion of Mps1 at these slightly higher taxol concentrations completely blocked colony formation (Fig.2A, E and S2D), which correlated with an even further increase in the amount and severity of segregation errors (Fig.2B, F). We confirmed that the observed reduction in colony formation capacity was due to cell death, and not due to a post-mitotic arrest, by filming U2OS-TetRMps1 cells in the presence of PI on day 4, 5 and 6 after treatment (Fig.S2A, B). The frequency of severe segregation errors correlated well with increased aneuploidy after 4 divisions as determined by chromosome spreads (Fig.S4A). LS174T-TetRMps1 cells were near-diploid in the absence of any treatment. After treatment with doxycycline or 3nM taxol the karyotype resembled that of control cells. This is in line with previous observations in which aneuploid cells in (near-) diploid cell lines are removed from the population[289]. Nevertheless, upon combined treatment of LS174T-TetRMps1 cells with taxol and doxycycline, the observed chromosome segregation errors (Fig.2F, 3nM taxol) induced a clear increase in aneuploidy and multinucleated cells (Fig.S4A, C). Although untreated U2OS-TetRMps1 cells were already significantly aneuploid, a clear increase in the breadth of distribution in the karyotypes was observed upon combining low doses of taxol and partial Mps1 knockdown (Fig.S4A), a combination that leads to the demise of the population (Fig.2A). The synergistic effect with low doses of taxol was not specific for partial Mps1 depletion, since reduced BubR1 levels also sensitized Hela and U2OS cells to low doses of taxol (Fig.2I, K, S2C and S3). This correlated with an increase in severe chromosome missegregations and enhanced aneuploidy as revealed by the karyotypes of the Hela-TetRBubR1 cells (Fig.2J, L and S4A). To rule out the possibility that the synergy in cell killing by low taxol and reduction of Mps1 or BubR1 was due to clonal variations within one cell type, we used titration of doxycycline in the U2OS clone in which high doxycycline addition (1μg/ml) causes almost full depletion of Mps1 (U2OS-TetRMps1-clone #2, see Fig.S1A). Such titrations enabled us to reach a reduction of Mps1 levels to 22% by adding only 2ng/ml doxycycline (Fig.S5A, B). In agreement with results obtained with the 'partial reduction' clone U2OS-TetRMps1 (Fig.1A), the reduced levels of Mps1 achieved by 2ng/ml doxycycline addition did not cause lethality on its own, whereas additional administration of 5nM taxol did (Fig.S5A, D). This again correlated with the amount of chromosome segregation errors (Fig. S5C). Unexpected side-effects of doxycycline administration on cell viability were also ruled out, as we observed no toxicity of simultaneous addition of doxycycline and low doses of taxol in the different founder cell lines (Fig.S6). Finally, the sensitization to low taxol we observed was not due to

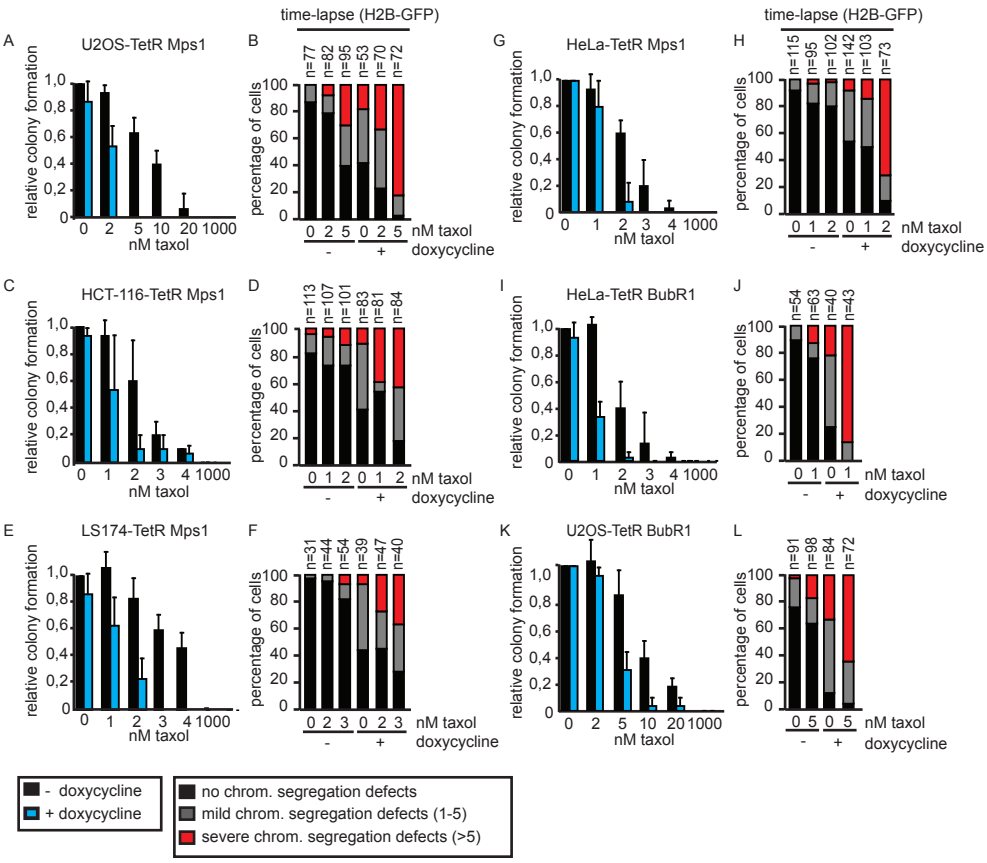

Figure 2. Low doses of taxol reduce the viability of Mps1 or BubR1 depleted tumor cells.
A, C, E, G, I, K). Quantification of colony formations of indicated cell lines treated with and without dox for 11 days. Indicated taxol concentrations were added 1 day after dox administration. Colony formation capacity of control cells (no taxol treatment) was set at 1. Average of three independent experiments is shown. B, D, F, H, J, L) Quantification of time-lapse movies performed as in Fig. S1C. Indicated taxol concentrations were added 1 hour prior to filming. n=amount of cells filmed.

a general sensitization to cytotoxic drugs, since partial depletion of Mps1 or BubR1 did not synergize with low doses of doxorubicin, a drug resulting in induction of double-strand DNA breaks (Fig.S7). To further address our hypothesis that cell death in our experiments was caused by inducing a certain threshold level of chromosome missegregations and not, for instance, by cytotoxic effects of taxol, we introduced siRNA's against CENP-E, KIF18A or HEC-1, all known to cause chromosome congression defects upon knockdown in human cells [125,562]. Knockdown of these proteins mimicked the effects of low taxol: Simultaneous reduction of Mps1 and RNAi of CENP-E, KIF18A or HEC-1 in U2OS-TetRMps1 cells increased cell death compared to siRNA transfected controls (Fig.S8A). Importantly, cell death in CENP-E RNAi cells partially depleted of Mps1 correlated with an increase in severe segregation errors (Fig.S8B, C). The differential sensitivity to low taxol when reducing Mps1 or BubR1 was no longer observed when using very high doses of taxol (Fig.2, 1000nM taxol). Although this is in apparent contradiction with reports suggesting that depletion of mitotic checkpoint components can rescue the lethality induced by high doses of taxol (50nM -10uM)[557-559], in those studies cell death was analyzed within 48 hours after taxol treatment. Indeed we have previously also observed that compromising the mitotic checkpoint causes resistance to high doses of spindle poisons in the short term[292], most likely because mitotic checkpoint inhibition prevents mitotic catastrophe in the presence of those high doses. Cell

death is not induced in the short term in those analyses because the deleterious effects of severe chromosome missegregations are not expected to become apparent before 2-6 divisions have occurred[292]. In support of this, the present study determined the effect on cell viability after 4 to 11 days and we find that high doses of taxol are equally toxic to parental as well as Mps1- or BubR1-depleted cells (Fig.2, 1000nM taxol).

The apparent resistance of CIN cells to high taxol treatment [280] and chromosome missegregations [289] has led to the hypothesis that these cells have obtained a survival mechanism that protects them against cell death induced by aneuploidy. In contrast, stable diploid (tumor) cells, which have become aneuploid, are sensitive to the genome unbalances and are removed from the cell population[289]. To address the question whether such aneuploidy-tolerance mechanisms would allow CIN cells to also tolerate simultaneous Mps1 depletion and taxol treatment, we tested the effect of this combined treatment on the CIN cell line SW480. As expected [270], these cells displayed frequent chromosome missegregations in the absence of any treatment (Fig.S8G untreated). Similar to what was observed with the other four tumor cell lines (Fig.2), simultaneous treatment of SW480 cells with low taxol (10nM) and partial depletion of Mps1 (Fig.S8D) enhanced the frequency and severity of chromosome segregation errors (Fig.S8G) and caused cell death (Fig.S8E,F). It is important to note that the level of chromosome missegregations induced by this combined treatment reached far beyond the level of missegregations found in CIN tumor cells ([270] and Fig. S8G). In all likelihood, therefore, the tolerance to aneuploidy of CIN tumor cells is insufficient to cope with the severity of chromosome segregation errors induced by our treatments. Together, our data show that substantial reduction of Mps1 or BubR1 leads to an increase in mild chromosome segregation errors but fails to induce massive tumor cell death. However, combining reduction in Mps1 or BubR1 with low, non-lethal doses of taxol increases the level and severity of segregation errors and severely compromises viability in all tumor cell lines tested.

Synergy in cell killing with low taxol depends on inefficient chromosome alignment in Mps1- or BubR1-depleted cells

In addition to their function in the mitotic checkpoint, both Mps1 and BubR1 have been shown to control chromosome alignment by influencing the stability of the kinetochore-microtubule interaction or error-correction[116,425,442]. In contrast, Mad2 is a protein which is critical for the mitotic checkpoint but has no apparent role in efficient chromosome alignment[73,442]. To examine if the mitotic checkpoint deficiency caused by reduction in Mps1 or BubR1 levels is sufficient to cause cell killing with low doses of taxol, we created an inducible monoclonal U2OS-TetRMad2 cell line in which the mitotic checkpoint was compromised to a similar extent after doxycycline addition as compared to the U2OS cells in which Mps1 or BubR1 were partially reduced (Fig.3A and S9A, C). Assessment of the time spent in mitosis in the presence or absence of low doses of taxol did also not reveal any difference between U2OS cells with partial Mps1, BubR1 or Mad2 knockdown (Fig.S9B). Importantly, partial Mad2 depletion did not lead to synergistic lethality with low doses of taxol (Fig.3B), which contrasts the effects seen with partial reduction of Mps1 or BubR1 (Fig.2A,K). This lack of synergy in cell killing correlated with a lack of synergy in severe chromosome missegregations (Fig.3C) and aneuploidy (Fig.S4B) in these cells. The rate of severe segregation errors was significantly lower than in cells with reduced Mps1 or BubR1 (40%, 85% and 65% respectively) (Fig.3C, compare with Figs.2B and 2L). In addition, in the partial Mps1- or BubR1-depleted U2OS cells almost all of the remaining cell divisions display mild missegregations, while 50% of all divisions in cells with partial Mad2 knockdown and 5nM taxol show no segregation errors at all. The previous observations indicated that inducing chromosome missegregations to a level sufficient to cause cell killing was substantially more efficient when chromosome alignment was disturbed

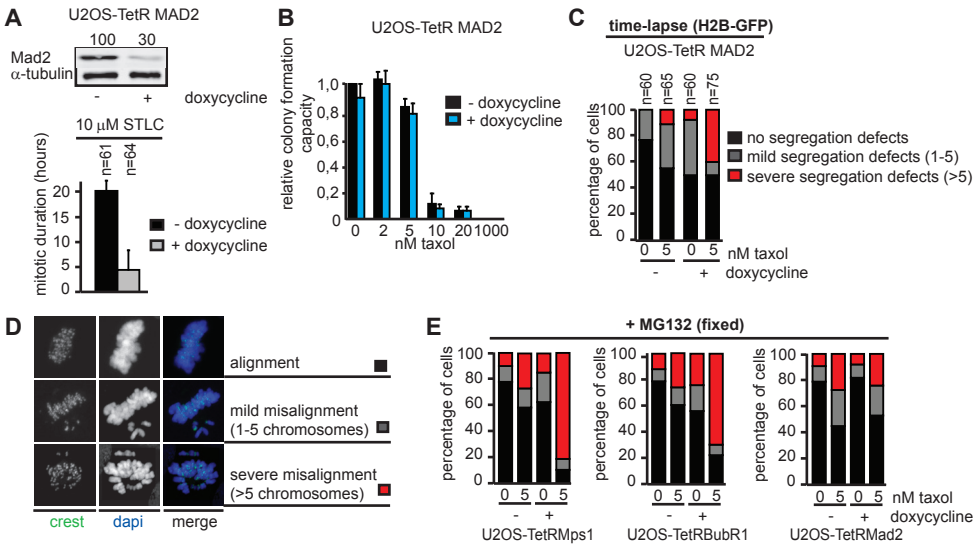

Figure 3. Chromosome alignment dysfunction in Mps1- or BubR1-depleted cells enhances cell death upon taxol [low] treatment.
A) Top: U2OS-TetRMad2 cells that were treated with and without dox were immuno-blotted for Mad2 and α-tubulin. Values indicate relative percentage of Mad2 levels. Bottom: Live cell analysis of the mitotic duration of U2OS-TetRMad2 cells treated and measured as in Fig.1B. B) Quantification of colony formations analyzed as in Fig. 2. C) Quantification of anaphase progression as in Fig. 1E. n=amount of cells filmed. D) Immunofluorescence images of cells with different chromosome alignment phenotypes after 90 minutes addition of MG132. Centromeres (CREST) are in green and DNA (DAPI) is in blue. 'Alignment', 'Mild misalignment' or 'Severe misalignment' indicate cells with 0, 1-5 or more than 5 chromosomes not aligned on the metaphase plate, respectively. E) The indicated cell lines were treated with or without dox for 3 days and 1 hour prior to MG132 addition indicated taxol concentrations were added. n=amount of cells analyzed per condition.

in addition to the mitotic checkpoint. In support of this, when cells were allowed to align their chromosomes for 90 minutes in the presence of the proteasome inhibitor MG132, we found that severe chromosome misalignments were more prevalent in low-taxol-treated populations of cells with diminished BubR1 or Mps1 levels than those with diminished Mad2 (Fig.3D,E). This suggests that reducing Mad2 levels, when weakening mitotic checkpoint activity to a similar extent as partial Mps1 or BubR1 depletion, does not cause sufficient segregation errors in the presence of low doses of taxol to compromise tumor cell viability. These results show that chromosome congression defects play an important role in the synergistic lethality with low doses of taxol. Although congression defects per se are not expected to lead to chromosome missegregations when the mitotic checkpoint is working efficiently, it is formally possible that mere alignment defects are sufficient to cause lethality and that mitotic checkpoint weakening is not required. To address this, we introduced CENP-E siRNA in U2OS-TetRMad2 cells to enhance congression defects in a checkpoint-weakened cell system and thus recapitulate the effects of reducing Mps1 or BubR1 (Fig.S10D, E). The chromosome alignment defects induced by CENP-E siRNA and 5nM taxol treatment led to an increase in segregation errors when compared to control siRNA-treated cells (Fig.S10C -doxycycline), but caused only a minor increase in cell killing (Fig.S10A, B). Importantly, introducing a checkpoint deficiency under these conditions, by partial knockdown of Mad2 (Fig.S10D), clearly increased the level of severe segregation errors and resulted in a significant increase in cell death (Fig.S10A-C +doxycycline). These results support the hypothesis that the synergy in cell killing by low doses of taxol and partial depletion of Mps1 or BubR1 requires significant congression defects combined with a weakened mitotic checkpoint. To rule out that the failure to compromise tumor cell viability by partial depletion of Mad2 was due to selection for cells with higher Mad2 expression during growth in low taxol, we analyzed the ability to delay mitosis in respect to spindle poison (1μM taxol) in U2OS-TetRMad2 cells that

had survived growth for 7 days in the presence of 5nM taxol and doxycycline (Fig.S9D). If the population would have been polyclonal, mitotic checkpoint activity is expected to be restored, at least partially, after elimination of cells with reduced Mad2 levels by synergistic lethality with low taxol. However, the checkpoint response to high taxol was weakened to the same extent in cells with reduced Mad2 levels before or after growth for 7 days in 5nM taxol, indicating that all cells in the U2OS-TetRMad2 clone have similar Mad2 knockdown upon doxycycline addition (Fig.S9D). Based on our studies in cancer cells, we conclude that cell death induced by massive chromosome missegregations can be achieved either by full ablation of the mitotic checkpoint ([292,294] and Fig.S1A) or by simultaneously weakening the mitotic checkpoint and chromosome congression processes.

Mps1 depleted immortalized fibroblasts do not show increased sensitivity towards taxol treatment

We have previously demonstrated that Mps1 inhibition efficiently abrogates the mitotic checkpoint in tumor cells, but not in immortalized fibroblasts [563]. This suggested the possibility that targeting mitotic checkpoint processes required for chromosome segregation may affect tumor cells more severely than untransformed cells. To further investigate this we created an immortalized human fibroblast cell line (VH10-TetRMps1) that stably expressed inducible Mps1 shRNA. Upon doxycycline addition Mps1 levels were reduced to ~20% and colony formation capacity was not affected (Fig.4A). Although the absolute checkpoint responses were incomparable (Fig.4B), the relative reduction in the ability of the VH10-TetRMps1 cells to delay mitosis in response to STLC after reduction of Mps1 was comparable to HCT116 and LS174T-TetRMps1 cells (Fig.S9C). The checkpoint response of untreated VH10-TetRMps1 cells was also comparable to that of the parental VH10 cell line, ruling out the possibility that the relatively short mitotic delay in control cells is due to leakage of Mps1 shRNA (Fig.4B). Despite similar checkpoint inhibition as the tumor cell lines with partial reduction in Mps1, VH10-TetRMps1 cells did not show any increase in taxol-induced cell death after Mps1 knockdown (Fig.4C). This absence of synergy with low doses of taxol in cell death induction correlated with the level of chromosome missegregations observed by live cell analysis of VH10-TetRMps1 cells progressing through mitosis in the presence of 2nM taxol: In about 50% of the cells chromosome missegregations were induced,

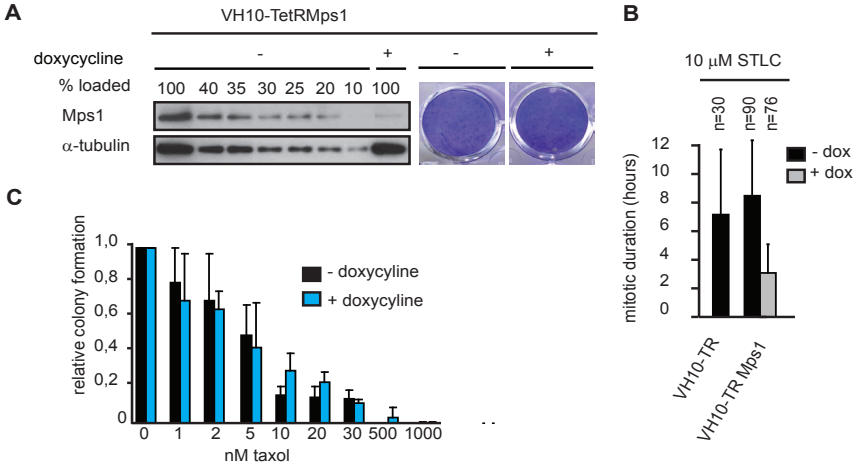

Figure 4. Taxol induced cell death is not enhanced in partial Mps1 depleted immortalized fibroblasts.
A) VH10-TetRMps1 cells that were treated with and without dox for 4 days were immuno-blotted for Mps1 and α-tubulin. Indicated amounts of untreated control sample were loaded to determine knockdown of Mps1 in dox treated sample. B) Live cell analysis of the mitotic duration of indicated cell lines treated and measured as in Fig.1B. C) Quantification of colony formations as in Fig. 2. Average of 3 independent experiments is shown.

however, this amount was not enhanced upon Mps1 reduction (Fig.S10F).
To examine if the correlation between chromosome missegregations, synergistic toxicity with low taxol and karyotype that was observed in the cancer cell lines could be extended to the VH10 cells, we performed karyotyping on the VH10-TetRMps1 cells under the various conditions (Fig. S4B). In agreement with a lack of synergy in cell killing, VH10 cells treated with low doses of taxol did not show a clear increase in aneuploidy when partially depleted of Mps1 (Fig.S4B). Thus, in the two instances in which partial knockdown of a protein did not increase sensitivity to low taxol (VH10-TetRMps1 and U2OS-TetRMad2), no increase in severe chromosome missegregations and no increase in the breadth of distributions of the karyotypes of the cells was observed. Although severe chromosome missegregations occurred upon 2nM taxol treatment in VH10 cells (Fig.S10F), this did not induce an increase in aneuploidy, which suggests that the population selected for near-diploid cells. This result correlates with a previous observation showing that untransformed fibroblasts are able to maintain a diploid population of cells after induction of chromosome missegregations[289]. In agreement with this hypothesis, a decreased growth speed of VH10 cells was observed upon 2nM taxol treatment independent of the absence or presence of Mps1 (Fig.S10G). Our results suggest that tumor cells, (near) diploid, aneuploid as well as CIN, are more sensitive to Mps1 or BubR1 inhibition compared to untransformed cells. As full mitotic checkpoint inhibition is unlikely to be achieved in clinical settings, simultaneous inhibition of processes required for chromosome congression and the mitotic checkpoint may be an efficient way to cause the desired level of segregation errors, especially when used in combination with low doses of taxol. Candidates for inhibition are those involved in both processes, such as Mps1, BubR1, Bub1 and TAO1 [443,564,565]. For an increased understanding of the utility of inhibition of such proteins as an anti-cancer strategy, development of small molecule inhibitors will be extremely valuable.

Materials and Methods

Tissue Culture, Transfections and Treatments

All cell lines were grown in DMEM (Lonza) with 10% Tet-approved FCS (Clontech), supplemented with pen/strep (Invitrogen) and ultraglutamine (Lonza). All DNA transfections were performed using Effectene and siRNA transfections were done using HiPerfect (both from QIAGEN). Taxol, nocodazole, STLC, doxorubicin, MG132 and doxycycline (used at 1ug/ml) were from Sigma. Cell lines stably expressing TetR were infected with retrovirus carrying pSuperior-retro-puro-Mps1, -Mad2 or -BubR1 and selected with 2µg/ml puromycin. Single colonies were selected after replating 1-2 cells/well. Hela-TetRBubR1 cells were infected with retrovirus carrying pBabe Lap-BubR1 (RNAi-insensitive) and selected with blasticidine to perform the rescue experiments.

RNAi

BubR1 [292] and Mad2 [566] shRNA sequences were used to produce pSuperior-retro-puro plasmids using standard cloning procedures (Oligo-Engine.Inc). pSuperiorMps1 [116] was used for creating inducible Mps1 RNAi cell lines and transient transfection. CENP-E siRNA (sequence AACACGGAUGCUGGUGACCUC), Hec-1 siRNA [567] and KIF18A siRNA (Dharmacon) were used.

Antibodies

The following antibodies have been used for Western Blot, Immunofluorescence and FACS analysis: Mps1 (Upstate), BubR1 (a gift from R. Freire), Mad2 (Bethyl), α-tubulin (Sigma), α-actin (TeBu), CENP-E ^{568}, CREST (Cortex Biochem), MPM2 (Upstate), anti-human Alexafluor647, anti-rabbit Alexafluor488, anti-mouse cy-5 (Jackson), anti-Mouse/Rabbit Alexa680/800 (Molecular Probes).

Immuno Blotting

Cells were lysed in Laemmli buffer. Samples were separated by SDS-page and transferred to PVDF (Immobilin FL, Millipore). The membranes were cut in half and blotted with anti-Mps1, Mad2, CENP-E or BubR1, anti-α-tubulin or actin. Western Blot quantification was performed on the Odyssey Infrared Imaging System (LI-COR Biosciences) and quantified using Odyssey application software version 1.2.

Immunofluorescence Microscopy

Cells plated on 12mm coverslips were harvested after 90 minutes MG treatment. Fixation was done using 4% PFA in PEM buffer. CREST was incubated O/N in PBS 3% BSA. Anti-human Alexafluor647 and DAPI were incubated in PBS 0,1% Tween. Stained coverslips were mounted with Vectashield Mounting Medium (Vector). Images were acquired on a Zeiss 510 Meta confocal laser scanning microscope with a 63X/1.4NA Plan-ApoChromat objective using the Zeiss LSM software..

Chromosome spreads

Nocodazole was added for 4 hours to the medium to enrich for mitotic cells. Cells were treated with 0.75 M KCl at 37ºC for 10 minutes, centrifuged at 2000 rpm and fixed for 20 minutes with Methanol: Acetic Acid (3:1). Fixation procedure was repeated 3 times. Samples were collected in Methanol and DAPI to stain for DNA. Chromosome spreads were created by allowing the drops to fall from 30 cm height onto glass slides. Images were acquired as described above for Immunofluorescence Microscopy.

Live cell Imaging

Cells were plated in 2 or 4-well chambered glass bottom slides (LabTek), transfected with H2B-GFP using Effectene and imaged in a heated chamber (37ºC and 5% CO2) using a 40X/1.3NA oil objective on a Zeiss Axiovert 200M microscope equipped with a 0.55NA condenser and controlled by a lambda-DG4 (Roper Scientific) and MetaMorph software. Green fluorescent (80 msec exposure) images were acquired every 3 min using a Photometrics CoolSnap HQ CCD camera (Roper Scientific). Images were processed using MetaMorph software. For cell death analysis, cells were filmed under the same conditions, Propidium Iodide (PI) was added to the medium, DIC and red fluorescent (100 msec exposure) images were acquired every 15 minutes for 64 hours.

Colony formation assays

Cells (+/- 50.000/well) were plated on 6-wells plates (Costar). At day 11, unless stated differently, plates were washed with PBS, fixed 5 minutes with 96% Methanol and stained with 0,1% crystal violet.dH20. Stained colony formations were scanned and quantified for intensity using Metamorph software.

Automated analysis of cell death

Cells were grown in 96 wells plates in 100µl culture medium. 3 days after indicated transfections wells were stained by adding PI and Hoechst to the culture medium. Image acquisition was performed using a Cellomics ArrayScan VTI (Thermo Scientific) using a 20x 0.50 NA objective and 8 images were acquired per well, which contained around 4000 cells in total. Image analysis was performed using Cellomics ArrayScan HCS Reader (Thermo Scientific). The percentage of cell death was calculated by the amount of PI positive cells over the total Hoechst positive cells.

Flow Cytometry

Flow cytometry samples were harvested and fixed using 70% ethanol. α-MPM2 was incubated for 1 hour in PBS-2% BSA-0,1% Tween and α-Mouse Cy5 for 1 hour in PBS-0,1% Tween. Stained cells were collected in PBS containing RNAse and Propidium Iodide. Fluorescence was measured on the FACSCalibur and analyzed with Cell Quest Pro software (BD Biosciences).

Immunofluorescence Microscopy

Cells plated on 12mm coverslips were harvested 2 days after siRNA transfection in the presence or absence of doxycycline. Fixation was done using 4% PFA in PBS. CREST and α–CENP-E were incubated O/N in PBS 3% BSA. Anti-human Alexafluor568, Anti-rabbitAlexafluor488 and DAPI were incubated in PBS 0,1% Tween. Stained coverslips were mounted with Vectashield Mounting Medium (Vector). Images were acquired on a Zeiss 510 Meta confocal laser scanning microscope with a 63X/1.4NA Plan-ApoChromat objective using the Zeiss LSM software. Intensity quantifications were performed using MetaMorph software.

Acknowledgements

The authors thank L. Kleij for technical assistance with confocal and time lapse microscopy, and all members of the Medema, Lens and Kops laboratory for discussions. We thank M. Alvarez and L.Macurek for critically reading the manuscript. We are grateful to M.van de Wetering, M.Timmers and A.G. Jochemsen for providing TetR expressing cell lines to us. This work was supported by the Netherlands Organisation for Scientific Research (NWO) (R.H.M. and A.J.: ZonMw 918.46.616; G.J.P.L.K.: VIDI-91776336), TI Pharma (R.H.M and A.J.: T3-105) and the Dutch Cancer Society (G.J.P.L.K.: UU-2006-3664). R.H.M. was additionally funded by the Netherlands Genomic Initiative of NWO.

Supplemental data

Supplemental figures

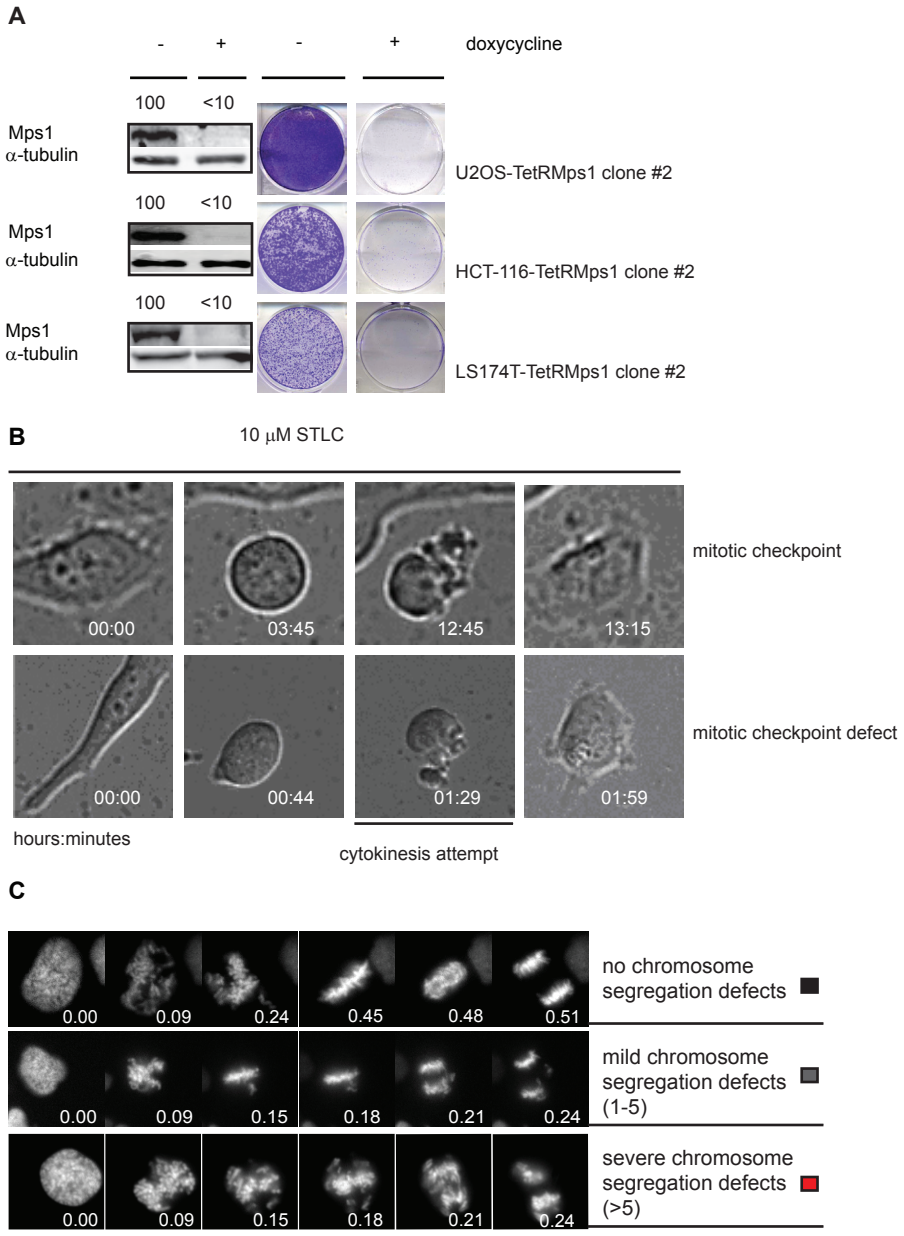

Figure S1.
A) Indicated cell lines were treated with and without doxycycline and immuno-blotted for Mps1 and α-tubulin. Values indicate relative percentage of Mps1 levels. B) Representative image stacks (DIC) of cells treated with 10μM STLC in the presence or absence of a functional mitotic checkpoint. C) Representative images of cells transfected with H2B-GFP and filmed using time-lapse microscopy showing three phenotypes; anaphase without missegregations, mild missegregations (1-5 chromosomes) and severe missegregations (>5 chromosomes). Time indicates minutes after chromosome condensation.

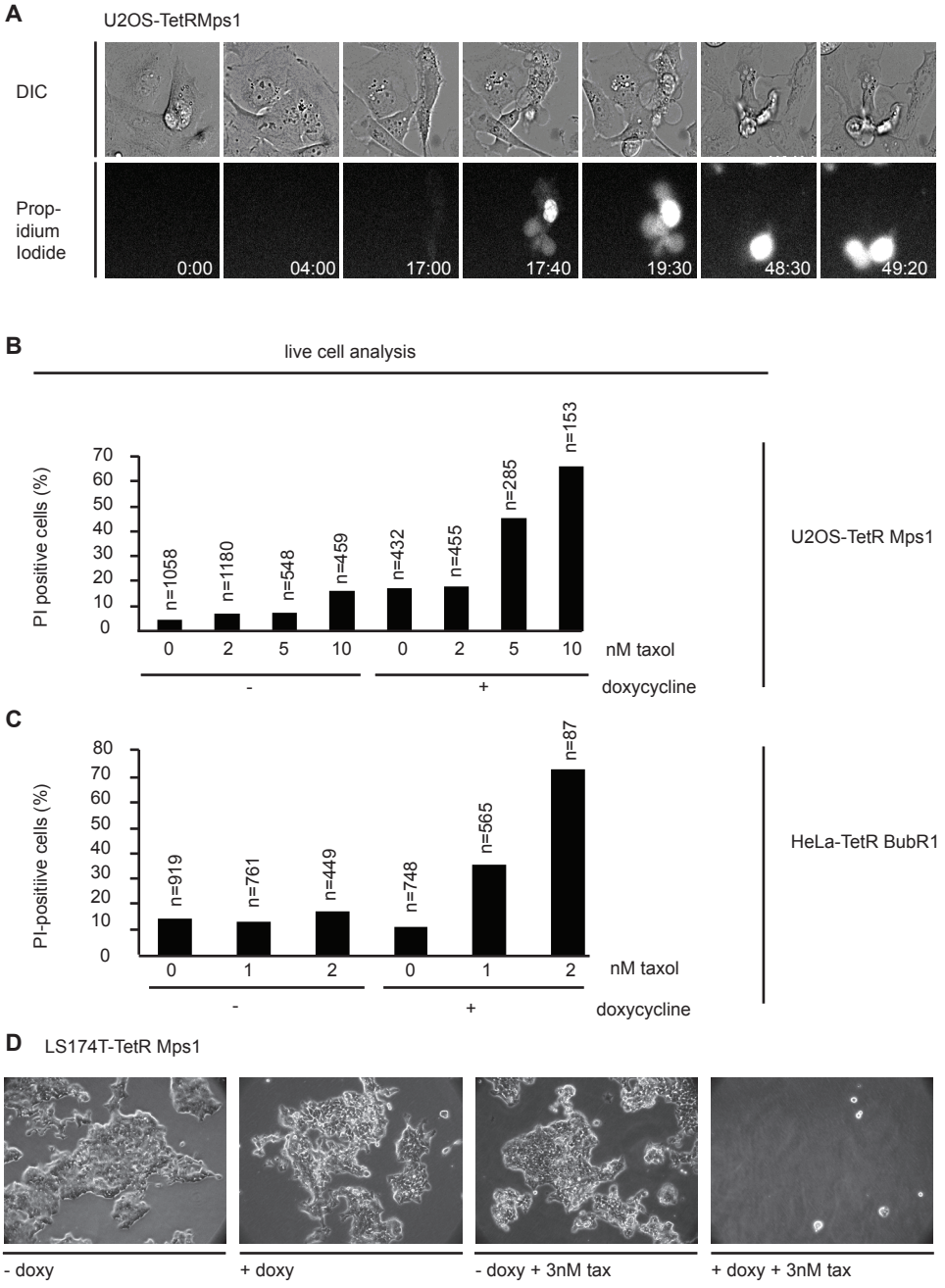

Figure S2.
A) Representative DIC images of U2OS-TetRMps1 cells undergoing cell death after doxycycline and 5nM taxol treatment. Propidium Iodide was added to the culture medium to determine uptake by dying cells. B+C) Quantification of time-lapse analysis performed as in (A) of cell death induction in U2OS-TetRMps1 and Hela-TetRBubR1 cells treated with or without doxycycline and indicated taxol concentrations on day 4, 5 and 6. DIC and PI images were acquired every 15 minutes. The percentage of cell death was measured as the fraction of PI positive cells over the total amount of cells (n) at the end of the experiment. D) Representative images of LS174T-TetRMps1 colonies 11 days after indicated treatments.

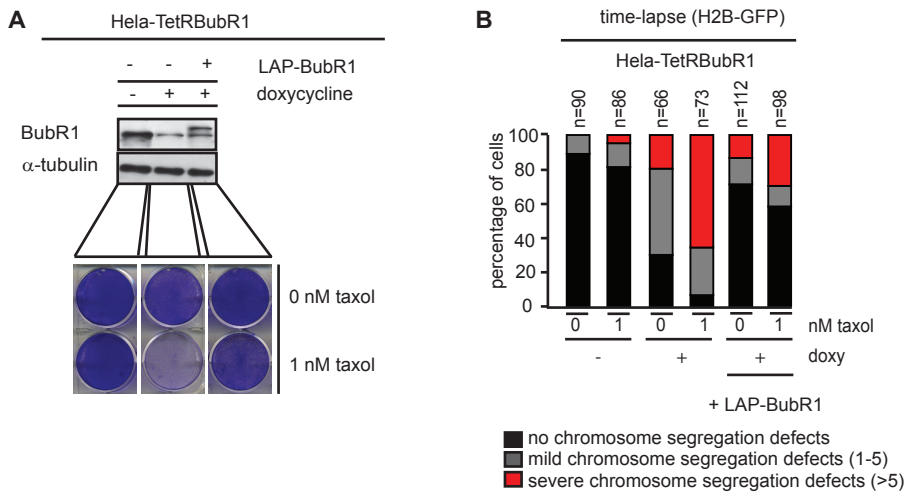

Figure S3.
A) Top: Hela-TetRBubR1 cells with and without stable expression of RNAi insensitive Lap-BubR1 were immuno-blotted for BubR1 and α-tubulin. Bottom: Representative pictures of colony formations treated with or without 1nM taxol. B) Quantification of time-lapse analysis of Hela-TetRBubR1 with or without stable BubR1 expression and doxycycline as in Fig.S1C. n indicates amount of cells filmed.

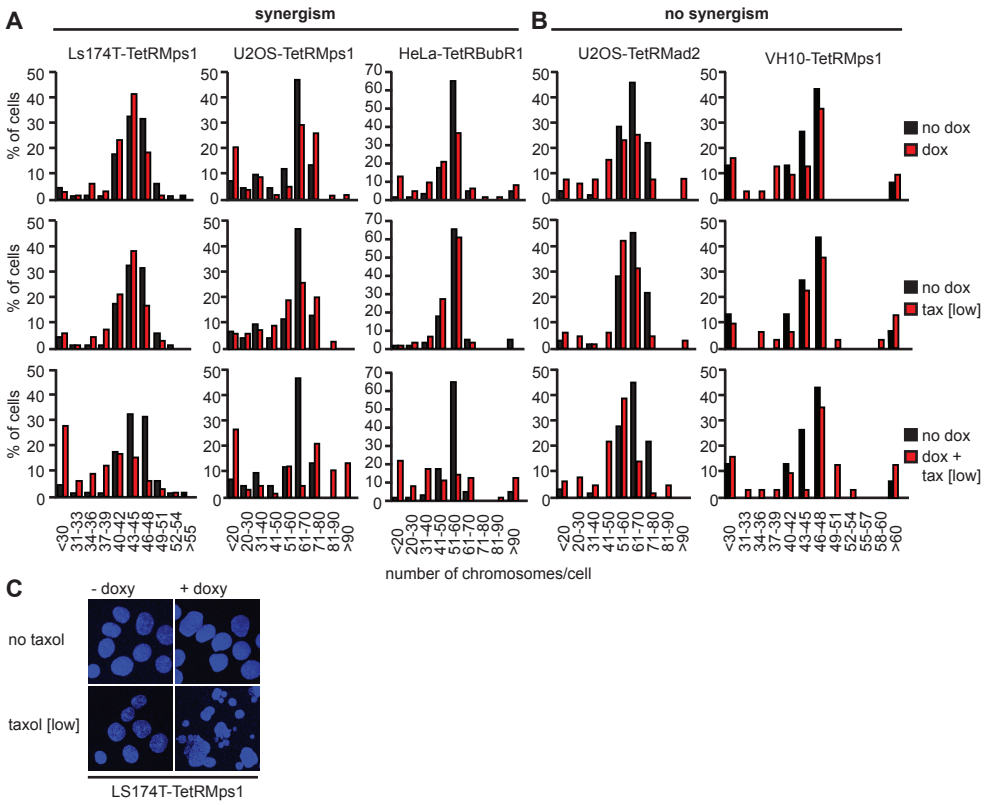

Figure S4.
A+B) Chromosome spreads were performed on cells after 4 days of treatment with or without dox. At least 60 chromosome-spreads were counted per condition. Where indicated taxol was added the last 2 days. Taxol [low] concentrations are: LS174T: 3nM, U2OS: 5nM, Hela: 1nM, VH10: 2nM C) Representative pictures of nuclei of LS174T-TetRMps1 cells after indicated treatments.

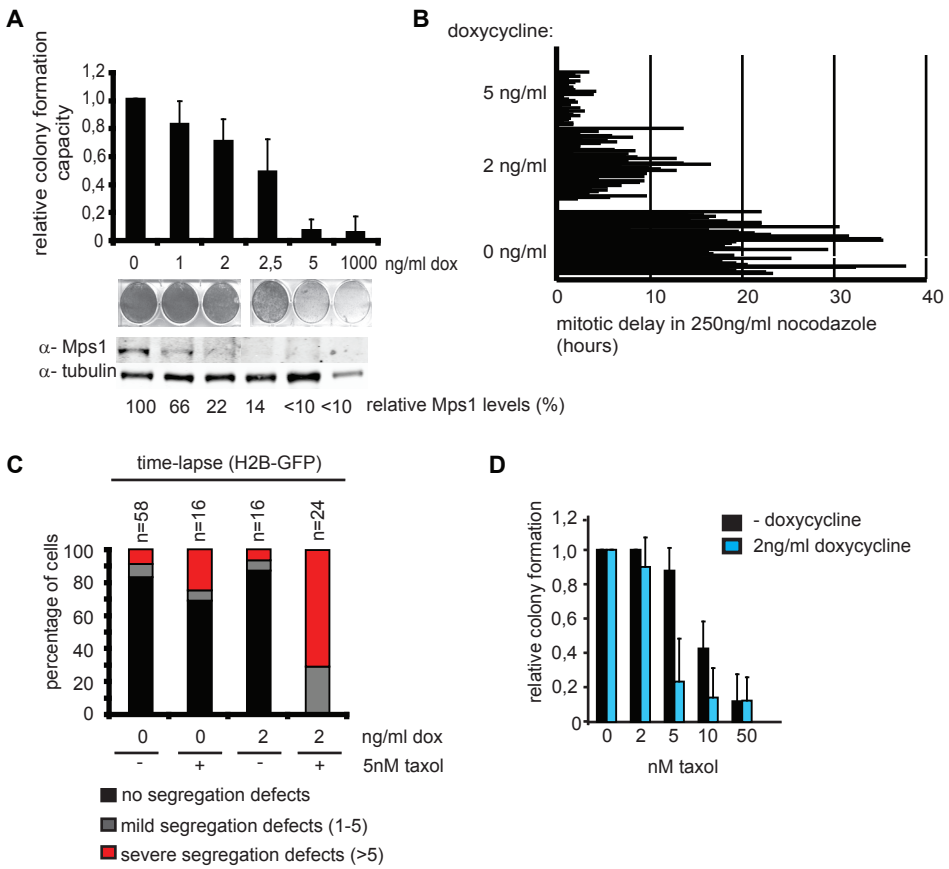

Figure S5.
A) Top: Quantification of colony formations of U2OS-TetRMps1 clone#2 cells that were treated with indicated doxycycline concentrations. Colony formation capacity of non-treated cells (0 μg/ml doxycycline) was set at 1. Bars represent three independent experiments (+SD). Bottom: Immuno-blots of Mps1 and α-tubulin of cells that were treated with indicated doxycycline concentrations for 3 days. Values below immuno-blots represent relative amount of Mps1 protein levels. B) Time-lapse analysis of the duration of the mitotic delay in cells treated with indicated doxycycline concentrations for 3 days and 250ng/ml nocodazole. DIC images were acquired every 15 minutes for 64 hours. Each bar represents a single cell. C) Quantification of anaphase progression as in Fig. 1E of cells that were treated with indicated doxycycline concentrations for 3 days. n indicates amount of cells filmed. Indicated taxol concentrations were added 1 hour prior to filming. D) Quantification of colony formations as in Fig. 2.

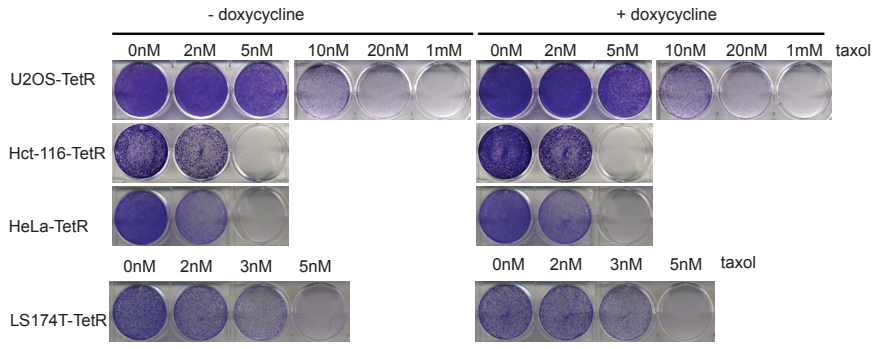

Figure S6.
Colony formations of indicated parental cell lines treated with and without doxycycline (day 0) and indicated taxol concentrations (day 1). Representative pictures are shown.

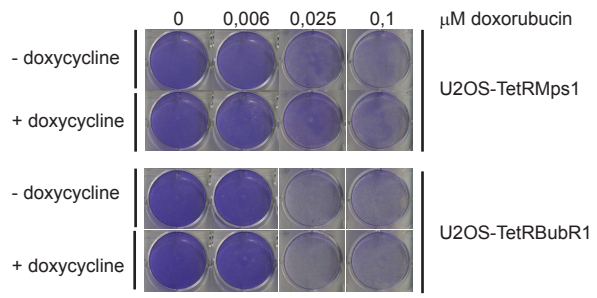

Figure S7
Representative pictures of colony formations of U2OS-TetRMps1 or BubR1 cells treated with or without doxycycline for 11 days and indicated doxorubicin concentrations. Doxorubicin was added one day after doxycycline addition.

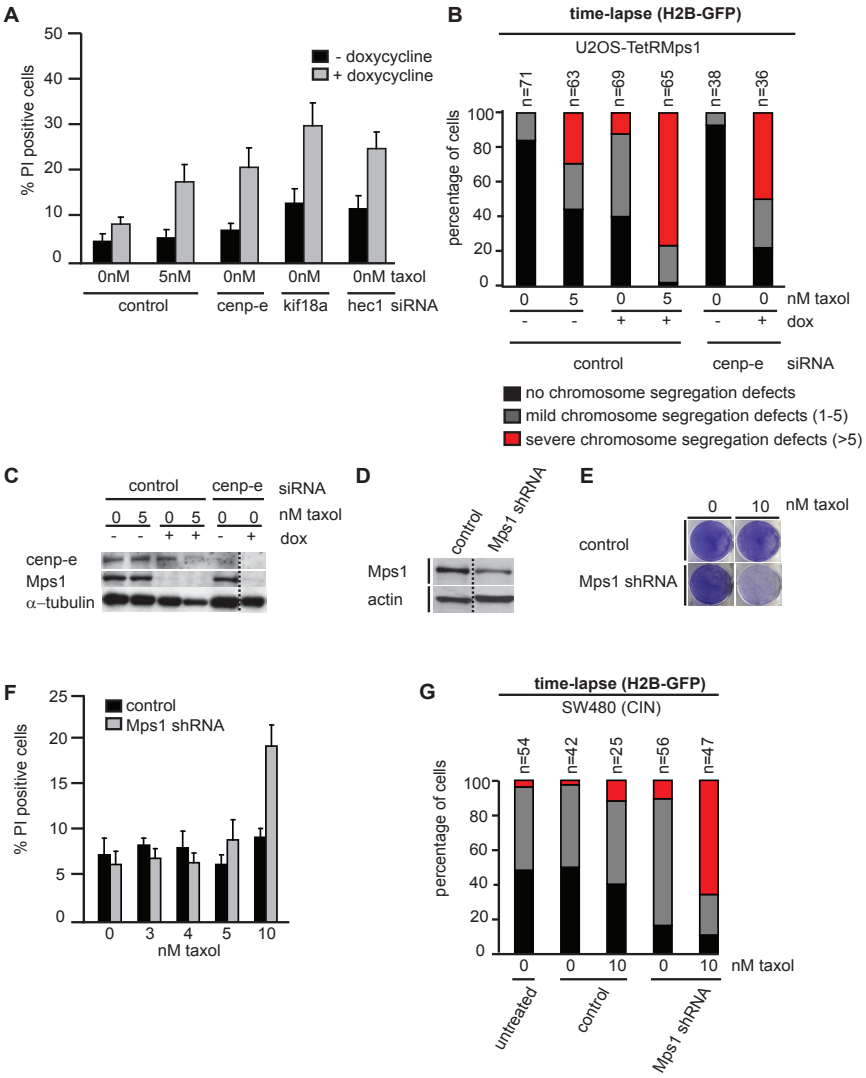

Figure S8
A) Automated analysis of the percentage of PI positive over Hoechst positive U2OS-TetRMps1 cells on day 6, treated with or without doxycycline (day 0), indicated siRNAs (day 2) and 0 or 5nM taxol (day 3). Bars represent the average of 5 independent experiments

(+SEM). B) Quantification of time-lapse analysis of U2OS-TetRMps1cells as in Fig.S1C. siRNA transfections were performed 36 hours prior to filming. Indicated taxol concentrations were added 1 hour prior to filming. C) Immuno-blots of Cenp-E, Mps1 and α-tubulin of U2OS-TetRMps1 cells collected after time-lapse acquisition. D) Immuno-blots of Mps1 and actin of SW480 cells transfected with empty pSuperior (control) and pSuperiorMps1 (Mps1 shRNA) and selected for 2 days with puromycin. E) Representative pictures of colony formations of SW480 cells on day 8. SW480 cells were transfected with pSuperior (control) and pSuperiorMps1 (Mps1 shRNA) (day 0). Cells were selected with puromycin (day 1), replated in 6 wells plates (day 2) and indicated taxol concentrations were added on day 3. F) Automated analysis of the percentage of PI positive over Hoechst positive SW480 cells on day 6 after transfection as in (E). Bars represent the average of 4 independent experiments (+SEM). G) Quantification of time-lapse analysis of SW480 cells as in Fig.S8B. SW480 cells were transfected with H2B-GFP (untreated) or H2B-GFP combined with empty pSuperior (control) or pSuperiorMps1 (Mps1 shRNA). Cells were filmed 2 days after transfection and indicated taxol concentrations were added 1 hour prior to filming. n indicates amount of cells filmed.

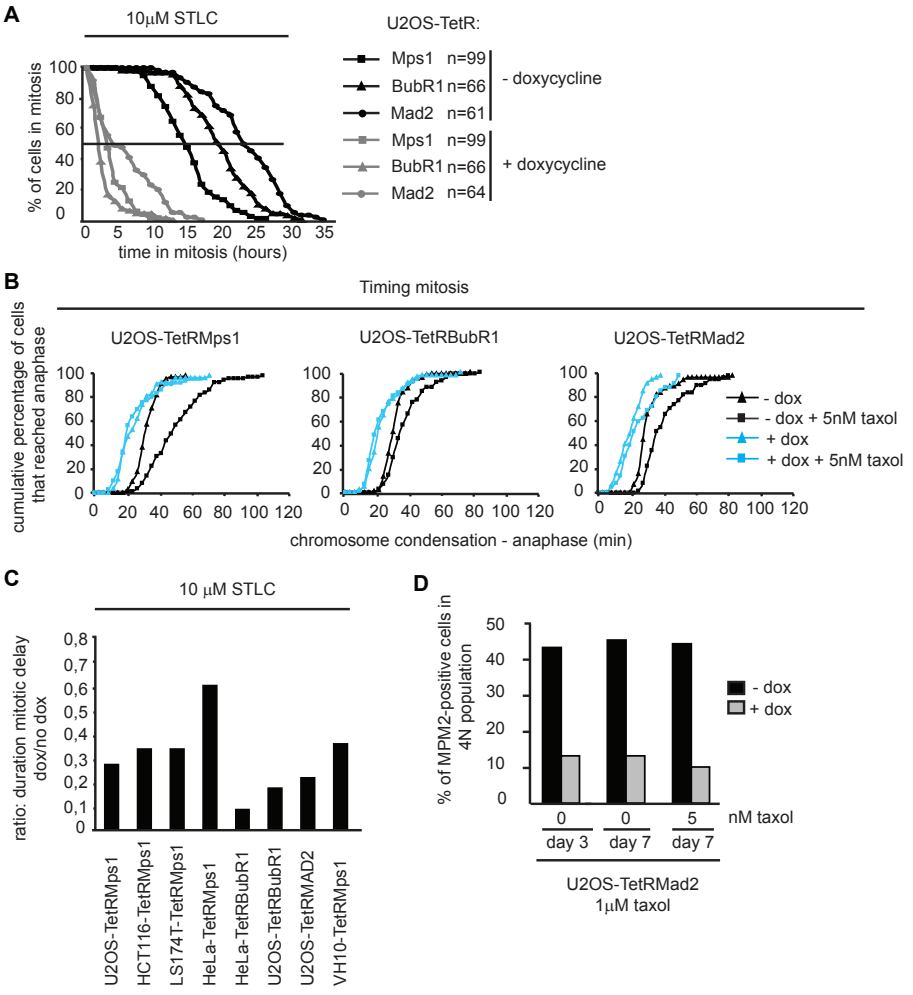

Figure S9.
A) Live cell imaging (DIC) of indicated U2OS cell lines in the presence of 10μM STLC as in Fig. 1B. B) Time-lapse analysis of the duration of mitosis from chromosome condensation until the start of anaphase. Indicated cell lines were treated with and without dox for 2 days and 5nM taxol was added 1 hour prior to filming. At least 30 cells were filmed per condition. C) Ratio of the average mitotic duration of dox treated cell lines divided by the average mitotic duration of control treated cell lines in the presence of 10μM STLC. At least 40 cells were filmed per condition. D) FACS analysis of U2OS-TetRMad2 cells after doxycycline addition for 3 or 7 days. 5nM taxol was added one day after doxycycline administration. After the various treatments cells were treated with 1μM taxol for 18 hours to determine the mitotic checkpoint efficiency. The percentage of mitotic cells was measured as the fraction of cells with 4N DNA content that were positive for MPM2.

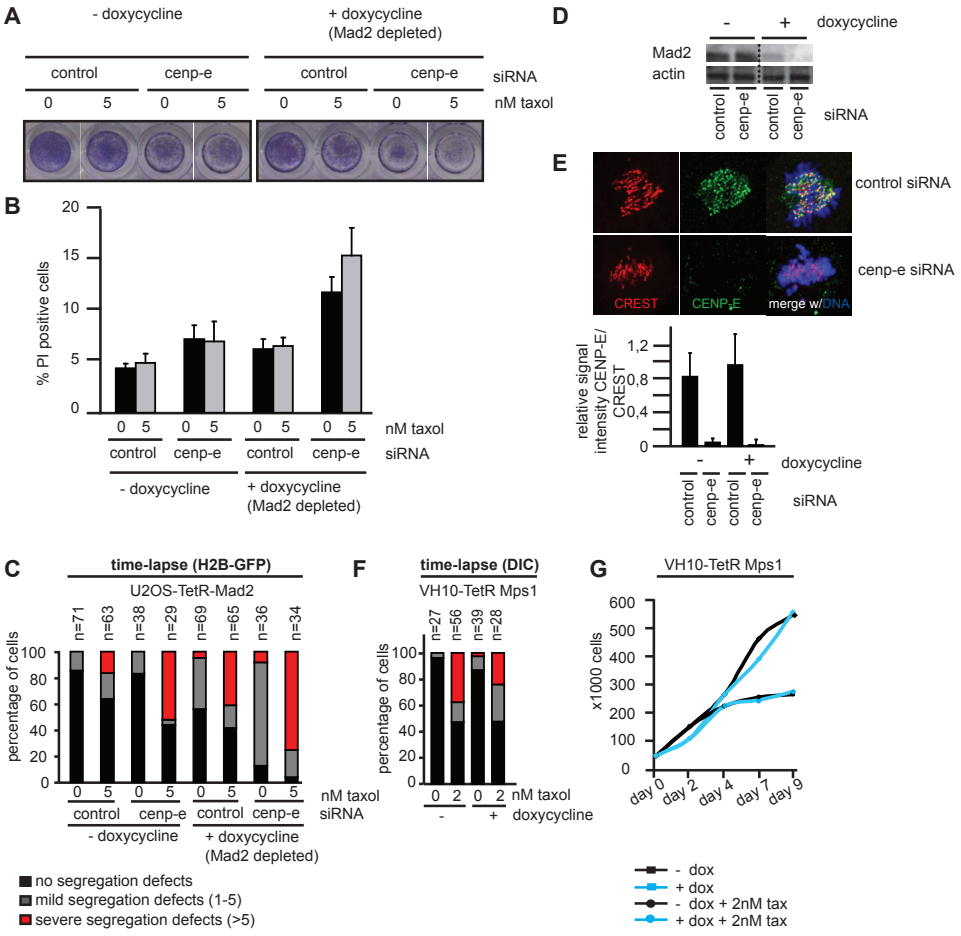

Figure S10.
A) Representative pictures of colony formations of U2OS-TetRMad2 cells on day 6 treated with or without doxycycline (day 0), control or CENP-E siRNA (day 2) and 0 or 5nM taxol (day 3). Luciferase or GAPDH siRNA were used as a control. B) Automated analysis of the percentage of PI positive over Hoechst positive U2OS-TetRMad2 cells on day 6 after treatment as in (A). Bars represent the average of 4 independent experiments (+SEM). C) Quantification of time-lapse analysis as in Fig.S1C. siRNA transfections were performed 36 hours prior to filming. Indicated taxol concentrations were added 1 hour prior to filming. n represents amount of cells filmed. D) Immunoblots of Mad2 and actin of U2OS-TetRMad2 cells treated with and without doxycycline and control or CENP-E siRNA. E) Top: Localization of CENP-E (green) and CREST (red) in mitotic U2OS-TetRMad2 cells transfected with control or CENP-E siRNA. Bottom: Quantification of intensity of CENP-E staining over CREST. Average is shown of 35 kinetochores +SD of 7 analyzed cells per condition. F) Quantification of time-lapse analysis (DIC) of chromosome segregation in anaphase in VH10 cells. n indicates amount of cells filmed. G) Growth curve of VH10-TetRMps1 cells after indicated treatments. On day 0 doxycycline was added, on day 2 2nM of taxol was added where indicated.

Addendum

Targeting the mitotic checkpoint to kill tumor cells.

Aniek Janssen[1,2], Miranda van Amersfoort[1], Geert J. Kops[1,3] and René H. Medema[1,2].

[1] Department of Medical Oncology and Cancer Genomics Center, University Medical Center Utrecht, Universiteitsweg 100, 3584 CG, Utrecht, the Netherlands
[2] Division of Cell Biology, Netherlands Cancer Institute, Plesmanlaan 121, 1066 CX, Amsterdam, the Netherlands
[3] Department of Molecular Cancer Research, University Medical Center Utrecht, Universiteitsweg 100, 3584 CG, Utrecht, the Netherlands

Adapted from:

Horm Cancer. 2011 Apr;2(2):113-6

Abstract

One of the most common hallmarks of cancer cells is aneuploidy, or an abnormal number of chromosomes. This abnormal chromosome content is a consequence of chromosome missegregation during mitosis a defect that is seen more frequently in tumor cell divisions as in normal cell divisions. In fact, a large fraction of human tumors display a chromosome instable phenotype (CIN), meaning that they very frequently missegregate chromosomes. This can cause variegated aneuploidy within the tumor tissue. It has been argued that this hallmark of cancer could be exploited in anti-cancer therapies. Here we test this hypothesis by inactivation of the mitotic checkpoint through RNAi-mediated depletion of an essential checkpoint component, Mps1. The mitotic checkpoint delays segregation of chromosomes during mitosis until all chromosomes are properly attached to the mitotic spindle. Its inactivation will therefore lead to increased segregation errors. Indeed, we show that this can lead to increased cell death in tumor cells. We demonstrate that increased cell death is associated with a dramatic increase in segregation errors. In addition, we show that this can inhibit tumor growth in xenografted tumors in nude mice. This suggests that inhibition of the mitotic checkpoint might represent a useful anticancer strategy.

Introduction

Chromosomal instability (CIN) is a common characteristic of solid tumors that is manifested as gains or losses of whole chromosomes during cell division, leading to aneuploidy 231. This propensity of tumor cells was recognized more than 100 years ago 569, leading to the hypothesis that CIN could be a driving force in tumorigenesis 232. Indeed, several lines of evidence have since suggested a causal role for CIN in tumor formation (reviewed in 570). However, the exact cause of CIN in tumors has remained largely unknown. It has become clear that a broad range of mutations in different cellular processes can result in CIN 282. Defects in mitotic checkpoint function have also been invoked as a causal event for CIN 282. The mitotic checkpoint ensures the fidelity of sister chromatid segregation over the two daughter cells by inhibiting progression to anaphase until all chromosome pairs are bi-oriented on the mitotic spindle (reviewed in 441). In various human cancers mitotic checkpoint function is compromised, and altered expression or mutations of mitotic checkpoint genes have been shown to be related to CIN and aneuploidy (reviewed in 290). Nevertheless, no evidence for checkpoint malfunctions as a direct cause of CIN in tumor cells has been found289,302,342. Moreover, the mitotic checkpoint defects that have been reported (reviewed in 282) may be well tolerated by the tumor cell population. Complete inactivation of the mitotic checkpoint, however, results in gross chromosomal missegregation and is not compatible with cell viability292-294,393. This has led to the suggestion that inhibition of the mitotic checkpoint could have therapeutic potential in cancer treatment 290. Here, we have explored the relationship between chromosome missegregations and tumor cell death by using conditional depletion of the mitotic checkpoint component Mps1.

Results and Discussion

Efficient Mps1 depletion severely compromises viability of tumor cells.

We have previously shown that absence of Mad2, BubR1 or Mps1 causes cell death within 6 cell divisions116,172,292,299. To examine the effect of conditional inactivation of Mps1 in LS174-T colon carcinoma cells, we stably introduced a doxycycline-inducible vector encoding a small hairpin RNA (shRNA) directed against human Mps1. In addition, this line stably expresses a tet-repressor, such that the addition of tetracycline or doxycycline to the culture medium induces the expression of the Mps1 shRNA and a consequent depletion of the endogenous Mps1 protein299. A clone was selected in which expression of Mps1 was reduced by more than 90% upon addition of doxycycline to the culture medium (Fig.1A). This degree of depletion of Mps1 severely compromised the viability of the LS174-T cells, since no colonies grew out in the presence of doxycycline (Fig.1A). Thus, selective inhibition of Mps1 compromises the viability of LS174-T tumor cells.

Mps1 depletion inactivates the spindle checkpoint.

Mps1 is an essential component of the spindle checkpoint, and its inactivation has been shown to override the cellular response to spindle poisons, such as nocodazole and taxol [142] [143]. Therefore, we next tested if RNAi-mediated depletion of Mps1 in the LS174-T cells conditionally expressing the Mps1 shRNA leads to functional inactivation of Mps1. To this end we cultured these cells in the presence or absence of doxycycline for a period of 3 days, and added 1 μM taxol to the culture medium for the last 18 hrs. of the incubation period. Taxol stabilizes microtubules, and perturbs proper spindle assembly. This will normally lead to a mitotic delay and an accumulation of cells in mitosis that is dependent on the mitotic checkpoint. Indeed, in LS174-T cells that are grown in the absence of doxycycline we find a

clear accumulation of cells in mitosis of up to 75% of all cells (Fig.1B). In contrast, depletion of Mps1 by the addition of doxycycline leads to clear inactivation of the mitotic checkpoint, since less than 5% of the cells is mitotic in these cultures (Fig.1B). Addition of doxycycline to the parental LS174 cells did not result in a checkpoint override, indicating that this effect was due to specific depletion of Mps1 (data not shown). These results indicate that conditional depletion of Mps1 from LS174-T tumor cells leads to inactivation of the mitotic checkpoint and a concomitant reduction in cell viability.

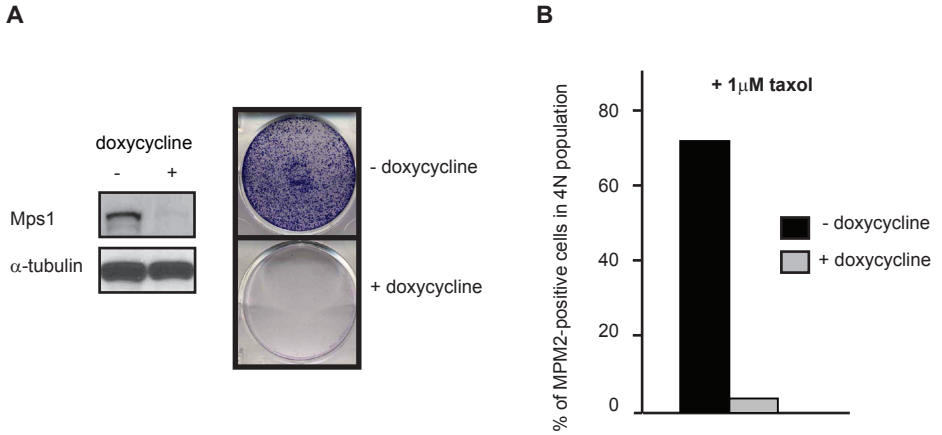

Figure 1: Conditional inactivation of Mps1 causes inactivation of the mitotic checkpoint and tumor cell death.
A) Left: LS174T-TetRMps1, treated without (-) and with (+) doxycycline (dox) for 3 days, were immuno- blotted for Mps1 and α-tubulin. Right: Colony formations of LS174T-TetRMps1 cells treated with and without dox for 11 days. B) FACS analysis of LS174T-TetRMps1 cells treated with or without dox for 3 days and 1μM taxol for 18 hours. The percentage of mitotic cells was measured as the fraction of cells with 4N DNA content that were positive for MPM2.

Mps1 depletion causes severe chromosome alignment defects and enhanced aneuploidy.

Inactivation of Mps1 is expected to compromise a cell's ability to achieve proper chromosome alignment on the mitotic spindle[116]. Therefore we analyzed if conditional depletion of Mps1 compromised the fidelity of chromosome alignment in LS174-T tumor cells. To this end, LS174-T cells grown in the presence or absence of doxycycline for 3 days were incubated with the proteasome inhibitor MG132 for 90 minutes to arrest cells at the metaphase-to-anaphase transition. In control cells grown in the absence of doxycycline, we found that 90% of all mitotic cells had fully aligned their chromosomes (Fig.2A). In contrast, depletion of Mps1 by the addition of doxycycline to the culture medium resulted in a severe reduction, as less than 25% of the cells managed to align their chromosomes in this time (Fig.2A). This increase in segregation errors coincides with a more severe aneuploidy, as evidence by the karyotyping shown in figure 2B (Fig.2B). Taken together, these data show that conditional inactivation of Mps1 compromises the mitotic checkpoint, and results in a severe defect in chromosome alignment. The combination of these two effects results in enhanced segregation errors and as a consequence the karyotype of the tumor cells becomes highly unstable.

Conditional inactivation of Mps1 inhibits tumor growth in vivo.

Our data thus far demonstrate that conditional inactivation of Mps1 inactivates the mitotic checkpoint, increases chromosome alignment defects and compromises cell viability in vitro. We next asked if conditional inactivation of Mps1 could inhibit tumor growth in vivo. For this, we subcutaneously injected LS174-T tumor cells in Balb/c nude mice and monitored tumor growth over time. One third of

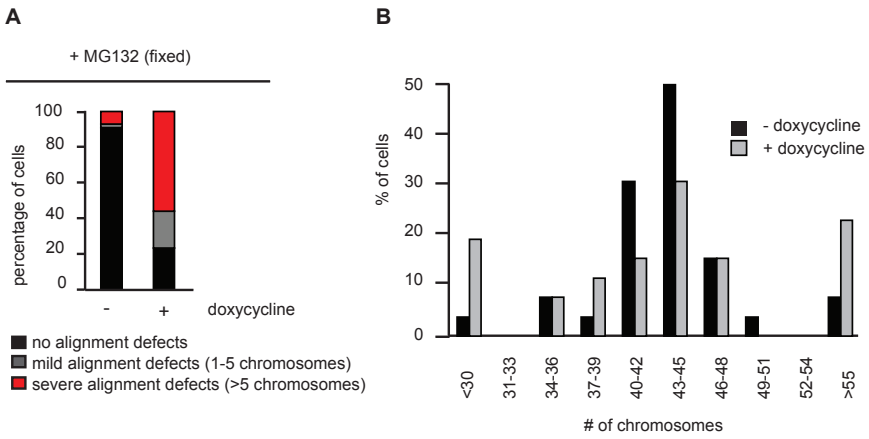

Figure 2: Conditional inactivation of Mps1 causes severe defects in chromosome segregation and severe aneuploidy.
A) LS174T-TetRMps1 cells were treated with or without dox for 3 days and fixed after 90 minutes of MG132 treatment. 'No alignment defects', 'Mild alignment defects' or 'Severe alignment defects' indicate mitotic cells with 0, 1-5 or more than 5 chromosomes not aligned on the metaphase plate, respectively. B) Chromosome spreads were performed on cells after 4 days of treatment with or without dox. At least 60 chromosome-spreads were counted per condition.

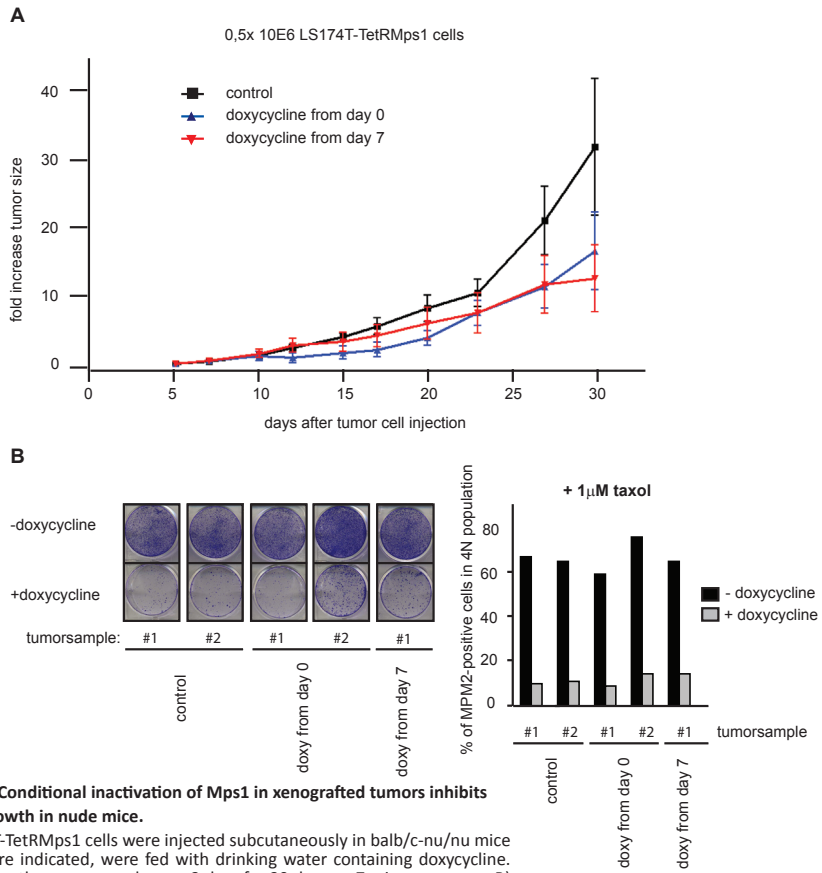

Figure 3. Conditional inactivation of Mps1 in xenografted tumors inhibits tumor growth in nude mice.
A) LS174T-TetRMps1 cells were injected subcutaneously in balb/c-nu/nu mice and, where indicated, were fed with drinking water containing doxycycline. Tumor growth was assessed every 3 days for 30 days. n=7 mice per group. B) Tumor samples were taken from LS174T xenografts on day 35 after tumor cell injection. Left: Cells from indicated tumor samples were cultured and colony outgrowth was determined in the presence or absence of doxycycline addition as in 1A). Right: FACS analysis as in Fig. 1B of LS174T cells of indicated tumor samples.

the mice did not receive any doxycycline, one third of the mice were given doxycycline in their drinking water from day 0 onwards, and one third of the mice received doxycycline in their drinking water from day 7 onwards. Clearly, tumor growth was reduced in the mice that received doxycycline in their drinking water (Fig.3A). Tumor growth was initially most efficiently inhibited in the group that received doxycycline on day 0, but almost all of the mice displayed progressive tumor growth (Fig.3A). Thus, the conditional inactivation of Mps1 that is achieved in this system is capable of slowing down tumor growth, but it is unable to fully arrest tumor growth. Whether this is due to incomplete inactivation of Mps1 in vivo is currently unclear. Alternatively, tumor cells in vivo might be less dependent on Mps1 function for proper chromosome segregation than tumor cells grown in vitro. To analyze if tumors in vivo had lost the ability to shut down Mps1 expression in response to doxycycline, we isolated tumors from the mice that received doxycycline in their drinking water and analyzed their growth in vitro. Importantly, their viability and mitotic checkpoint function was again severely compromised when doxycycline was added to the culture medium, indicating that these cells had not simply lost conditional expression of the Mps1 shRNA (Fig.3B). However, this observation does not discriminate between the possibility that doxycycline does not efficiently reach the tumors in situ, or the possibility that in vivo tumor growth is less dependent on Mps1 function. In order to resolve this we will have to examine the effect of doxycycline on chromosome segregation in vivo. For this purpose we wish to perform intravital imaging of cell division of the xenografted tumor cells. Nonetheless, our data show that inactivation of Mps1 can partially inhibit tumor growth and suggest that targeting Mps1 function might be a useful anti-cancer strategy.

Materials and Methods

Tissue Culture, Transfections and Treatments

LS174T cells were grown in DMEM (Lonza) with 10% Tet-approved FCS (Clontech), supplemented with pen/strep (Invitrogen) and ultraglutamine (Lonza). Taxol, MG132 and doxycycline (used at 1μg/ml) were from Sigma. LS174T cells expressing TetR were infected with retrovirus carrying pSuperior-retro-puro-Mps1 and selected with 2μg/ml puromycin. Single colonies were selected after replating 1-2 cells/well.

Immunofluorescence Microscopy

Cells plated on 12mm coverslips were harvested after 90 minutes MG132 treatment. Fixation was done using 4% PFA in PEM buffer. CREST was incubated O/N in PBS 3% BSA. Anti-human Alexafluor647 and DAPI were incubated in PBS 0, 1% Tween. Stained coverslips were mounted with Vectashield Mounting Medium (Vector). Images were acquired on a Zeiss 510 Meta confocal laser scanning microscope with a 63X/1.4NA Plan-ApoChromat objective using the Zeiss LSM software.

Chromosome spreads

Nocodazole was added for 4 hours to the medium to enrich for mitotic cells. Cells were treated with 0.75 M KCl at 37ºC for 10 minutes, centrifuged at 2000 rpm and fixed for 20 minutes with Methanol: Acetic Acid (3:1). Fixation procedure was repeated 3 times. Samples were collected in Methanol and DAPI to stain for DNA. Chromosome spreads were created by allowing the drops to fall from 30 cm height onto glass slides. Images were acquired as described above for Immunofluorescence.

Flow Cytometry

Flow cytometry samples were harvested and fixed using 70% ethanol. α-MPM2 was incubated for 1 hour in PBS-2% BSA-0,1% Tween and α-Mouse Cy5 for 1 hour in PBS-0,1% Tween. Stained cells were collected in PBS containing RNAse and Propidium Iodide. Fluorescence was measured on the FACSCalibur and analyzed with Cell Quest Pro software (BD Biosciences).

Immuno Blotting and antibodies

Cells were lysed in Laemmli buffer. Samples were separated by SDS-page and transferred to PVDF (Immobilin FL, Millipore). The membranes were cut in half and blotted with anti-Mps1 and anti-α-tubulin. The following antibodies have been used for Western Blot, Immunofluoresence and FACS analysis: Mps1 (Upstate), α-tubulin (Sigma), CREST (Cortex Biochem), MPM2 (Upstate), anti-human Alexafluor647, anti-mouse cy-5 (Jackson)

Colony formation assays

Cells (+/- 50.000/well) were plated on 6-wells plates (Costar). Doxycycline was added at day 0 to allow knockdown of the proteins. At day 11, plates were washed with PBS, fixed 5 minutes with 96% Methanol and stained with 0,1% crystal violet.

Xenografting

0,5 x 10^6 LS174T cells were injected subcutaneously on day 0. Doxycycline (1mg/ml) was added to the drinking water of the mice on indicated days until the end of the experiment. Drinking water was supplemented with 2% sucrose. Tumor growth of LS174T cells was assessed every 3 days for a period of 30 days.

5

Chapter 6

Aneuploid tumor cells are more sensitive to inhibitors of the mitotic checkpoint kinase Mps1

Aniek Janssen[1,2], Husam Alwan[2], Björn ter Horst[2], Ute Boon[3], Rita Maia[1], Joost C.M. Uitdehaag[4], Jos de Man[4], Geert J.P.L. Kops[2,5], Rogier C. Buijsman[4], Jos Jonkers[3], Guido J.R. Zaman[4], René H. Medema[1,2]

[1] Division of Cell Biology, Netherlands Cancer Institute, Plesmanlaan 121, 1066 CX, Amsterdam, the Netherlands

[2] Department of Medical Oncology and Cancer Genomics Center, University Medical Center Utrecht, Universiteitsweg 100, 3584 CG, Utrecht, the Netherlands

[3] Division of Molecular Cell Biology, Netherlands Cancer Institute, Plesmanlaan 121, 1066 CX, Amsterdam, the Netherlands

[4] Netherlands Translational Research Center B.V., P.O. Box 20, 5340 AG, Oss, the Netherlands

[5] Department of Molecular Cancer Research, University Medical Center Utrecht, Universiteitsweg 100, 3584 CG, Utrecht, the Netherlands

Manuscript in preparation

Abstract

Developing anti-tumor therapies that display sufficient tumor selectivity remains a major challenge. We have previously shown that depletion of the mitotic checkpoint kinase Mps1 compromises cell viability and demonstrated that the anti-proliferative effect of Mps1 knockdown is directly correlated with the induction of chromosome segregation errors. In this report, we investigate in the use of Mps1 inhibition as an anti-cancer strategy using a previously unrecognized specific small molecule inhibitor of Mps1 (compound-5). We show that compound-5 compromises cell viability through the induction of severe chromosome segregation errors that subsequently result in excessive aneuploidy and DNA damage. Moreover, we find that transformed cells need more time to establish proper chromosome attachments to the mitotic spindle, resulting in a higher sensitivity to inhibition of Mps1 than non-transformed cells. Further analysis also reveals bioactivity of compound-5 in mice. Our data suggest that Mps1 is an attractive candidate for future anti-cancer studies.

Introduction

Equal segregation of the genetic material to both daughter cells upon cell division depends on the proper functioning of the mitotic checkpoint [441]. The mitotic checkpoint delays mitosis until all chromosomes are attached to the mitotic spindle. Defects in this checkpoint signaling result in chromosome segregation errors, which can cause aneuploidy and DNA damage [389,390,532], two hallmarks of cancer [237]. Mps1, a key player in the mitotic checkpoint, is a kinase originally found to be important in budding yeast spindle pole body duplication [137], spindle formation [571] and the mitotic or 'spindle assembly' checkpoint [140]. In contrast to Mps1 function in centrosome duplication and subsequently bipolar spindle formation[143,146-148], its role in mitotic checkpoint signaling has been confirmed in higher eukaryotes already for over a decade [124,142,143]. Introduction of various mutations in the Mps1 kinase domain of mammalian cells has revealed the essential function of the kinase activity of Mps1 in proper mitotic checkpoint functioning[116-119]. Moreover, in human cells, Mps1 kinase activity is required for proper alignment of the chromosomes at the spindle equator by promoting correction of erroneous kinetochore-microtubule attachments through regulation of Aurora B activity [116,118,123], another important mitotic kinase [572]. Because of its essential roles in the mitotic checkpoint and chromosome alignment, complete absence of Mps1 activity results in cell death within several rounds of cell division [116,118,123,299,573]. Moreover, partial shRNA-based depletion of Mps1 protein levels results in enhanced sensitivity to low doses of the microtubule targeting chemotherapeutic paclitaxel (taxol) in human tumor cells[299], whereas immortalized human fibroblasts display less sensitivity to this combination treatment. Interestingly, Mps1 levels have been found to be strongly elevated in breast cancer cells that harbor an abnormal chromosome count[322]. Reducing Mps1 levels by RNAi specifically killed these cancer cells, but did not affect cell viability of isogenic untransformed breast epithelial cells[324]. These observations have led to a search for more specific Mps1 kinase inhibitors that could be useful in the treatment of cancer. Various small molecule inhibitors have been developed that target Mps1 kinase activity (reviewed in[167,574]). However, some of these inhibitors, such as SP600125, Reversine, staurosporine, Mps1 IN-2 and compound B13, have been shown to have additional targets besides Mps1, which make them less suitable in target validation studies on the role of Mps1 in cancer [123,550,563,575-577]. Other inhibitors, such as Mps1 IN-1, potently inhibit Mps1, but only do so at relatively high doses [123]. Two Mps1 inhibitors, NMS-P715 and MPI-0479605, have been shown to exhibit anti-tumor activity using xenograft studies in mice, but only limited inhibition of tumor growth has been observed [176,578]. These limitations demonstrate the need for more potent and specific Mps1 small molecule inhibitors to assess the utility of Mps1 as a target in anti-cancer treatment. Here, we characterize a previously unrecognized specific small molecule inhibitor of Mps1, compound-5 [579], which potently binds to the ATP binding pocket of Mps1 with a long residence time and is active in mice. Using this inhibitor, we can inhibit Mps1 in cells at extremely low doses and recapitulate the synergistic effects of partial Mps1 depletion and taxol on tumor cell viability[299]. We find that Mps1 inhibition has a more prominent effect on cell viability of transformed cells, compared to healthy, untransformed cells, which makes Mps1 inhibition an interesting candidate for anti-cancer treatment.

Results

Search for a potent and selective compound for Mps1 validation studies

To validate Mps1 as an anti-cancer target, we synthesized and characterized a number of published reference inhibitors of Mps1. Based on activity, selectivity and cellular potency we identified compound-5, which has been described in a patent application of Nerviano Medical Sciences [579], as the most suitable compound for validation studies. We confirmed the *in vitro* inhibitory activity of compound-5 on purified Mps1 in an IMAP enzyme activity assay [44] (IC_{50} of 1,5 nM, Fig.1A). To analyze the selectivity of compound-5, we tested its *in vitro* activity against a panel of 282 purified human kinases in the presence of 5 μM ATP (Fig. 1B). Cross-reactivity with multiple kinases was evident at a concentration of 5 μM compound-5, but this cross-reactivity was clearly reduced when decreasing the concentration to 0.15 μM (Fig. 1B). Furthermore, we tested compound-5 against 93 kinases that are structurally representative for the human kinome (Fig. 1C). 8 out of 93 kinases were significantly inhibited in the presence of 1μM compound-5 (IRKK2, AKT2, SGK1, NUAK1, TSSK1, Chk2, JNK1 and JNK2) (Fig. 1C). However, compound-5 inhibited these 8 kinases with an IC_{50} value of at least 100nM, about 60 times higher than the IC_{50} for Mps1 (~1.5nM) (Fig.

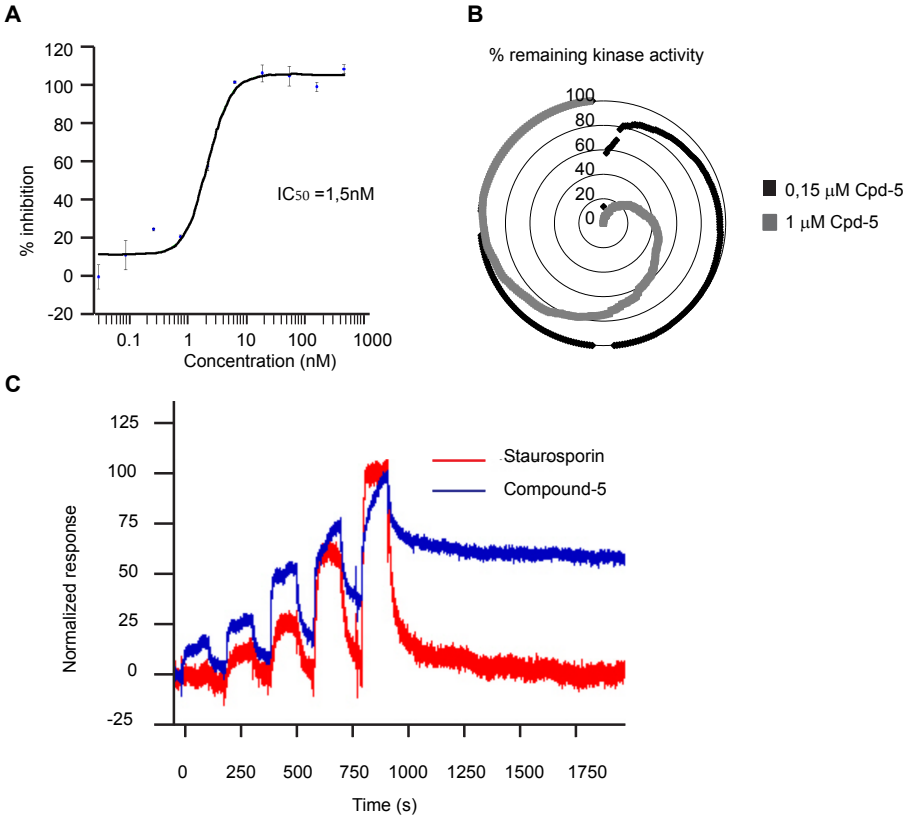

Figure 1. Characterization of compound 5
A) In vitro kinase assay using an IMAP assay was performed to assess the in vitro activity of compound-5 towards Mps1. B) Radar plot depicting the activity of compound-5 towards 282 different kinases at two different concentrations: 0.15μM (blue) and 5μM (purple). Percentage remaining kinase activity is depicted on Y-axis. Each dot represents one kinase. C) Binding assay (BiaCore) of compound-5 (blue line) and staurosporine (red line) binding to full length Mps1. Ka is 2.2 x 10^5 (1/ms), Kd is 4.2 x 10^{-5} (1/s).

S1A, data not shown). Based on these experiments, compound-5 demonstrated a greater than 60 times *in vitro* selectivity towards Mps1 relative to the kinase panel. To determine a quantitative measure of its selectivity, we calculated the selectivity entropy of the compound, which summarizes the result of kinome profiling in a single value [580]. The selectivity entropy of compound-5 is 0.13, which qualifies it as a highly selective kinase inhibitor, compared to other profiled inhibitors [580] . Next, we analyzed the binding properties and residence time of compound-5 to Mps1 using surface plasmon resonance (Biacore) and compared it to the non-specific kinase inhibitor staurosporine, which is an ATP competitor and shown to be active against Mps1 *in vitro*[576]. This analysis revealed that staurosporine dissociated rapidly from the Mps1 coated chip, and the signal dropped back to the initial level within ~50 seconds (Fig.1C). This is in sharp contrast to the compound-5 binding profile, which showed very slow dissociation kinetics (Fig.1C). These Biacore experiments were also used to calculate the true binding constant of compound-5 to full-length Mps1, since the enzyme assay underestimated the affinity of very potent inhibitors due to relatively high concentration of enzyme used (*i.e.,* 5.5 nM in the IMAP assay). The estimated binding constant from Biacore experiments was 190 pM. Collectively, this set of experiments demonstrates that compound-5 is a very potent and selective inhibitor of Mps1 with a long residence time on its target enzyme.

Specific Mps1 inhibition leads to mitotic checkpoint deficiency

Next, we sought to determine the effects of selective Mps1 inhibition on mitotic checkpoint activity. As a measure for mitotic checkpoint activity, we tested the ability of untransformed RPE-1 cells and the tumor cell lines Hela and U2OS to delay mitosis in response to spindle disruption in the presence of compound-5 (Fig.2A). Treatment of RPE-1 cells with compound-5 for 12 hours in the presence of the microtubule destabilizing drug nocodazole resulted in a decrease in the number of mitotic cells from 48% in control cells (nocodazole treated only) to 15% in cells treated with both nocodazole and 20 nM compound-5. Increasing the dose of compound-5 to 100 nM completely abolished the ability of RPE-1 cells to delay mitosis (Fig.2A). Similarly, the capacity of Hela and U2OS cells to delay mitosis upon nocodazole treatment was clearly affected in the presence of 50 nM and 30 nM compound-5, respectively (Fig.2A). In line with the inability to delay mitosis upon treatment with compound-5, low levels of Cyclin B1 and Securin were present in Hela cells simultaneously treated with nocodazole and compound-5 (Fig.2A). Cyclin B1 and Securin are both substrates of the Anaphase Promoting Complex or Cyclosome (APC/C) and their degradation is inhibited in the presence of a mitotic delay imposed by nocodazole (Fig.2B, lane 2). A reduction in Cyclin B1 and Securin protein levels upon simultaneous treatment with compound-5 and nocodazole indicated that the APC/C has been activated and cells have exited mitosis[581,582] (Fig.2B, lane 4-7). In order to assess the intracellular specificity of compound-5 to Mps1, we determined its effect in U2OS cells stably expressing LAP-Mps1 M602Q [123], an Mps1 mutant cDNA which harbors a 'gatekeeper' mutation in the kinase active site. This mutation has previously been shown to affect the inhibitory potential of SP60015, Mps1 IN-1 and Mps1 IN-2 both *in vitro* and intracellularly[123,563]. As expected, simultaneous treatment of parental U2OS cells or U2OS cells stably expressing LAP-Mps1 wildtype (Mps1-WT) with nocodazole and an increasing dose of compound-5 (20nM-500nM) resulted in a decreased number of mitotic cells when compared to nocodazole only treated controls (40-80% reduction in parental U2OS cells and 20-80% reduction in U2OS LAP-Mps1 WT cells respectively) (Fig.2C). Strikingly, stable expression of Mps1 602Q in U2OS cells [123] almost completely abolished the effect of compound-5 treatment in the presence of nocodazole when compared to control U2OS cells (Fig.2C). Together, these data indicate that specific inhibition of Mps1 affects the ability of cells to sustain mitotic checkpoint activity in response to spindle perturbation. Mps1 kinase activity is essential for proper chromosome segregation, owing to its function in both

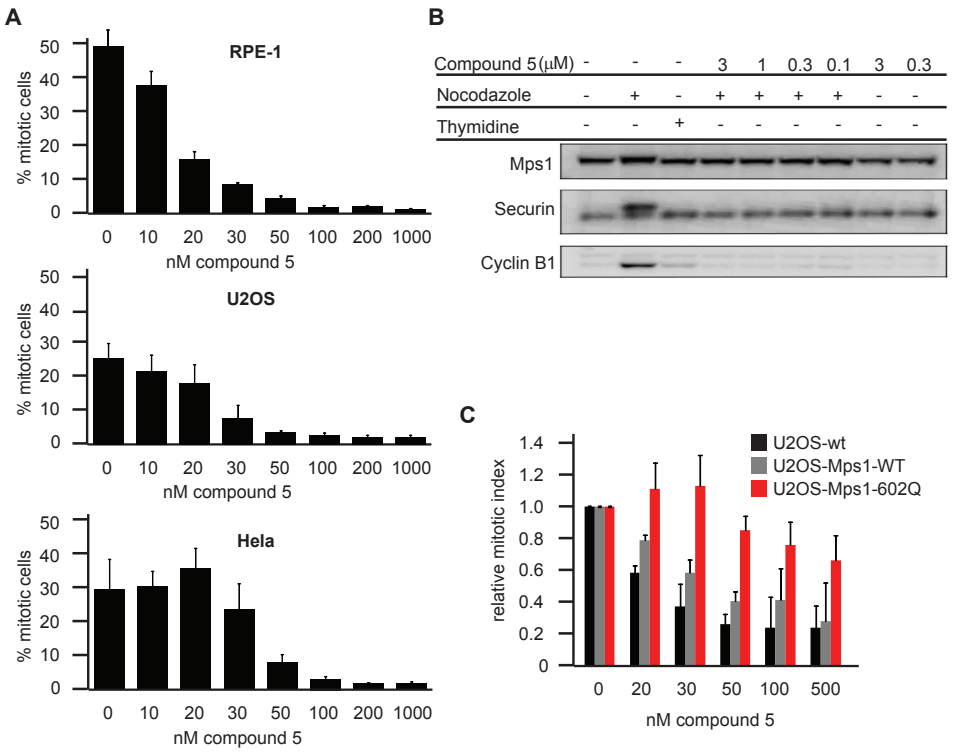

Figure 2. Selective inhibition of Mps1 results in inhibition of mitotic checkpoint signaling
A) Graphs depict the percentage of mitotic cells after treatment of RPE-1 (top), U2OS (middle) and Hela (bottom) cell lines with 250ng/ml nocodazole and indicated concentrations of compound-5 for 12 hours. Percentage of mitotic cells was determined as the number of MPM2 positive nuclei. Average of 3 independent experiments is shown + SD. B) Hela lysates immuno-blotted for Mps1, Securin and Cyclin B-1 after indicated treatments for 18 hours. C) Graph depicts the mitotic index after compound-5 treatment relative to the mitotic index of control treated (0nM compound-5) cells of each individual cell line. Mitotic index was determined as in (A) Average of 3 independent experiments is shown + SD.

mitotic checkpoint signaling and the alignment of chromosomes at the spindle equator (reviewed in [167]).

To examine the effect of compound-5 on the fidelity of chromosome segregation in the absence of microtubule targeting drugs, anaphase progression was followed by time-lapse microscopy (Fig.3A). The percentage of RPE-1, U2OS and Hela cells that displayed either mild or severe chromosome segregation defects in anaphase increased from 5%, 10% and 20% in control cells respectively to 100%, 100% and 98% upon treatment with 100 nM of compound-5 (Fig.3A). In line with these effects on chromosome segregation, U2OS cells also displayed chromosome alignment defects (80% versus 30% in control cells) already when treated with 30nM compound-5 in the presence of the proteasome inhibitor MG132 (Fig.3B). This effect was rescued by expressing the Mps1 gate-keeper mutant in U2OS cells, again confirming the Mps1 specific inhibition (Fig.3B).

Mps1 inhibition selectively kills tumor cells

Partially depleting Mps1 specifically sensitizes tumor cells to the microtubule stabilizing drug taxol[299]. To determine whether we could confirm those effects by partial inhibition, rather than depletion of

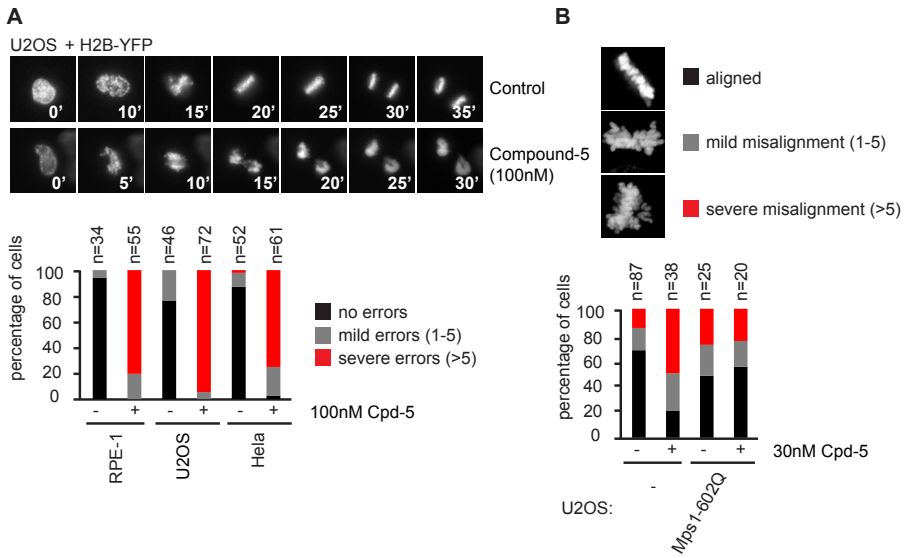

Figure 3. Selective inhibition of Mps1 results in the induction of chromosome misalignments and segregation errors
A) (top) Representative images of U2OS cells stably expressing H2B-GFP undergoing division in the absence or presence of missegregating chromosomes. (bottom) Quantification of time-lapse movies of RPE-1, U2OS and Hela cells stably expressing tagged H2B. Three phenotypes were scored; anaphase without missegregations, mild missegregations (1-5 chromosomes) and severe missegregations (>5 chromosomes). Time indicates minutes after chromosome condensation. N indicates number of cells analyzed. Compound-5 was added 10 minutes prior to filming. B) (top) Representative images of fixed U2OS cells showing no, mild (1-5 misaligned chromosomes) and severe misalignments (>5 misaligned chromosomes). DNA was visualized using DAPI. (bottom) Quantification of chromosome alignment of indicated U2OS cell lines after 30 minutes of treatment with MG132 in the presence or absence of 30nM compound-5.

Mps1, we treated U2OS, Hela and RPE-1 cells with low doses of compound-5 and simultaneously treated them with sub-lethal doses of taxol. Indeed, combined inhibition of Mps1 and treatment with taxol resulted in a synergistic effect on cell viability in both Hela and U2OS cells (Fig.S2A, B) whereas such synergy was not evident in the untransformed cell line RPE-1 (Fig.S2A). Moreover, when we treated various tumor and normal, untransformed cell lines with increasing doses of the Mps1 inhibitor compound-5, we also observed selectivity towards tumor cells with low doses of compound-5 in the absence of taxol (Fig.4A). All tumor cell lines lost the capacity to form colonies upon treatment with 20-30 nM compound-5, whereas viability of both RPE-1 and BJ-Tert cells was not affected in the presence of 50 nM compound-5 (Fig.4A). The effect on cell viability was specifically due to Mps1 inhibition, since the Mps1-602Q mutant could overcome the lethal effects of compound-5 in U2OS cells (Fig.S2C). The difference in sensitivity between cell lines is not due to differences in compound-5 uptake, since treatment of RPE-1 cells with compound-5 affected the ability to delay mitosis in the presence of nocodazole as potently as in U2OS and Hela cells (Fig.2A). We have hypothesized before that untransformed, healthy cells could be less prone to missegregate their chromosomes upon Mps1 depletion or inhibition when compared to aneuploid tumor cells[299,447]. Indeed, when we followed chromosome segregation using time-lapse imaging of various cell lines stably expressing tagged H2B, we observed that tumor cell lines were more prone to missegregate their chromosomes upon low-dose compound-5 treatment (30 nM) when compared to untransformed RPE-1 cells (Fig.4B). In unperturbed anaphases, tumor cell lines showed a chromosome missegregation rate of 20-50% (including both mild and severe segregation errors), which increased to 80-95% when 30 nM compound-5 was added (Fig.4B). In contrast to the tumor cell lines, RPE-1 cells showed mild missegregation events in only 20% of anaphases when treated with low dose compound-5 versus 10% in controls and almost never displayed

severe missegregations in either treated or control anaphases (2% and 1%, respectively) (Fig.4B). Chromosome segregation errors result in aneuploidy and DNA damage[290,389]. To determine whether an increase in DNA damage could be observed specifically in tumor cells treated with the Mps1 inhibitor, we imaged the tumor cell lines MCF-7 and SW480 and the untransformed cell line RPE-1 all stably expressing H2B-RFP and 53BP1-GFP, a marker for DNA damage (Fig.4C). This analysis revealed a clear increase in G1 daughter cells with DNA damage foci after treatment of MCF-7 and SW480 cells with 30 nM compound-5 (18% and 42% respectively with more than 3 foci versus 5% and 21% in controls), whereas RPE-1 cells hardly showed any DNA damage foci formation following mitotic exit (5% versus 0.5% in controls) (Fig.4C). Overall, these data suggest that the deleterious effects of selective Mps1 inhibition specifically on tumor cells are due to the induction of severe chromosome segregation defects, eventually resulting in massive aneuploidy and DNA damage.

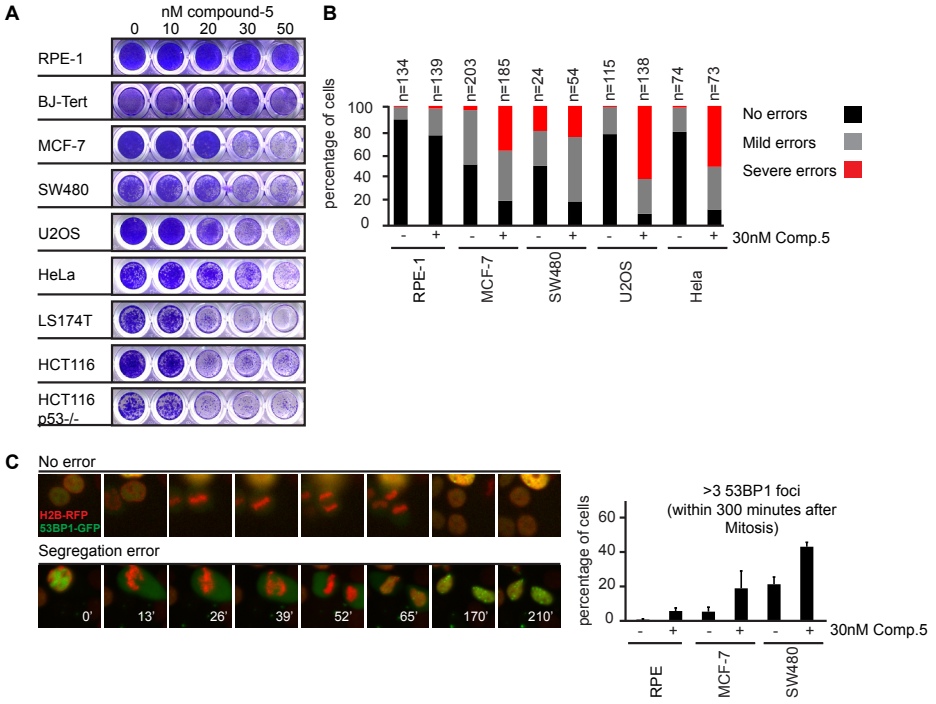

Figure 4. Pharmacological inhibition of Mps1 specifically kills tumor cells
A) Colony formations of indicated cell lines treated with increasing concentrations of compound-5. Cells were harvested 6 days after addition of compound-5. B) Quantification of chromosome segregation performed as in Fig.3A of indicated cell lines expressing tagged-H2B. N indicates number of cells. C) (left) Representative images of MCF-7 cells stably expressing H2B-RFP (red) and 53BP1-GFP (green) undergoing division in the absence or presence of missegregating chromosomes. (right) Graph depicts quantification of percentage of G1 daughter cells having more than three 53BP1 foci within 300 minutes after mitotic exit (3 experiments + SEM, >50 cells/experiment).

Alterations in mitotic progression sensitize tumor cells to Mps1 inhibition

One explanation for the different effects that Mps1 inhibition has on chromosome segregation in transformed versus non-transformed cells could be that aneuploid tumor cells have more difficulties aligning their chromosomes when compared to healthy diploid cells [539] and are therefore more dependent on mitotic checkpoint function to prevent segregation errors. Inhibition of the mitotic checkpoint in combination with problems in chromosome alignment, due to partial Mps1 inhibition, could then lead to a more pronounced defect in the fidelity of chromosome segregation in aneuploid

tumor cells, leaving diploid cells relatively unaffected. In line with this hypothesis, it has been shown that introduction of extra chromosomes in diploid cells directly leads to prolonged mitotic timing, since these cells need more time to congress their chromosomes to the spindle equator [539]. Indeed, time lapse imaging of our panel of cell lines revealed an enhanced timing from nuclear envelope breakdown (NEB) until anaphase in the tumor cell lines when compared to diploid RPE-1 cells (Fig.5A). MCF-7, SW480, U2OS and Hela cells took on average 55, 81, 34 and 55 minutes respectively to complete mitosis, whereas RPE-1 cells only needed ~29 minutes (Fig.5A). As expected[119], treatment with 30 nM compound-5 reduced mitotic timing for all tumor cell lines with more than 15 minutes, whereas RPE-1 cells only reduced their time in mitosis with ~2 minutes on average (Fig.5A). On top of the relatively big effect on mitotic timing, chromosome congression in tumor cells might also be more affected by partial Mps1 inhibition when compared to diploid cells due to Mps1's role in chromosome alignment[116]. Already without the addition of compound-5, tumor cells displayed many more chromosome misalignments (31%-44%) when compared to diploid RPE-1 cells (13%), when we allowed cells to align their chromosomes in the presence of the proteasome inhibitor MG132 (Fig.5B). Addition of 30 nM compound-5 severely enhanced the number of tumor cells with chromosome misalignments (49%-95%), whereas RPE-1 cells were only mildly affected (23%) (Fig.5B).As an alternative of using tumor cells, which could have accumulated non-related defects that render them sensitive to Mps1 inhibition, we also induced transformation in BJ-Tert cells in three consecutive steps [583]. First, we inactivated p53 by introducing stable p53 knockdown. Next, we expressed a mutant form of HRAS (HRASV12) known to induce transformation and finally we combined this with inhibition of the Rb tumor suppressor pathway by transducing

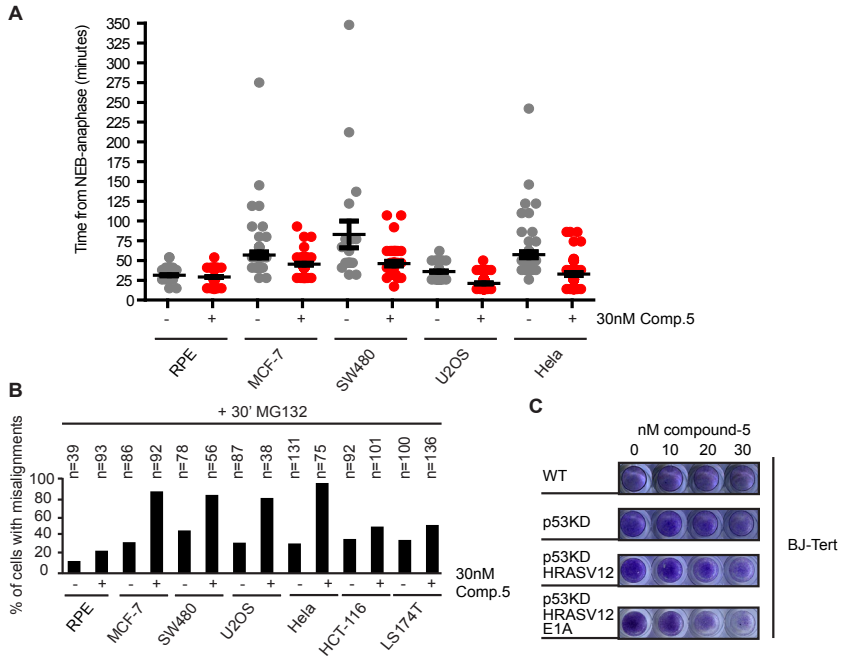

Figure 5. Low dose Mps1 inhibition specifically affects mitotic timing and chromosome alignment in tumor cells
A) Live cell analysis (tagged H2B) of the mitotic duration of indicated cell lines in the presence or absence of compound-5. Mitotic duration was determined as the time in minutes from chromosome condensation (nuclear envelope breakdown (NEB)) to the start of anaphase. Dot plot is shown with each dot representing one cell. Average is indicated +/- SEM. B) Quantification of chromosome alignment of indicated cell lines after 30 minutes of MG132 treatment in the presence or absence of compound-5. N indicates number of cells. C) Colony formations of indicated BJ-Tert cell lines in the presence of increasing concentrations compound-5.

these cells with E1A virus [584]. Strikingly, the transformed BJ-Tert cell line that had undergone all three events was more sensitive to Mps1 inhibition (Fig.5C). While wild-type BJ-Tert cells did not show any decrease in colony formation capacity following treatment with 30nM compound-5, the viability of fully transformed BJ-Tert cells (p53KD, HRASV12 and E1A) was clearly affected (Fig.5C). These data indeed indicate that transformed cells are much more affected by partial Mps1 inhibition compared to healthy diploid cells. These differences are most likely due to more severe effects of partial Mps1 inhibition on mitotic timing and chromosome congression in tumor cells, which eventually lead to chromosome segregation errors, DNA damage and cell death.

High doses of compound 5 lead to deleterious effects on intestinal structures in mice.

Since these and published data suggest that Mps1 inhibition is a possible interesting candidate in specific anti-cancer treatment[176,299,578,585] we plan to test the effect of Mps1 inhibition in a mouse model for spontaneous tumor formation [586]. We tested the bio-availability in Balb/c mice and the maximum tolerated dose (MTD) of compound-5 in wild-type FVB female mice (Fig.6). Pharmacokinetic studies of intravenous and orally delivered compound-5 revealed a long latency time of the inhibitor in the blood of more than 24 hours with a half-time of ~6 hours (Fig.6A). Initial MTD studies (50, 100 and 150 mg kg^{-1} compound-5) resulted in lethality in a very short time-span (~4-5 days). Haematoxylin and Eosin (H&E) staining of the intestines of compound-5 treated mice revealed deleterious effects of the inhibitor on the intestinal structure, as is evident by small villae and unstructured crypts (Fig.6B). Moreover, actively dividing cells were almost completely absent in the intestinal crypts of mice treated with compound-5 as determined with staining for phosphoS10-Histone H3, a mitotic marker, and Ki67, a proliferation marker (Fig.6B). These effects on the intestine indicate that the cell cycle progression of crypt cells in vivo has been affected. In future studies we wish to find well tolerated doses of compound-5 and test the activity in mouse models for spontaneous tumor formation.

Discussion

In this study, we have validated Mps1 as a promising anti-cancer target using a small molecule inhibitor. The inhibitor, referred to as compound-5, binds with subnanomolar affinity to Mps1 and is more than 60-fold selective over a panel of 281 other kinases. Its selectivity entropy, which is a novel quantitative measure of quantifying selectivity from panel screening data [580], is 0.13 and this low value signifies it is an excellently selective inhibitor. In fact there are only three kinase targets on which more selective reference inhibitors were reported so far [587] . Furthermore, the compound has a long retention time on Mps1 (~46 h) (data not shown). The specificity and long latency could make compound-5 useful for *in vivo* tumor studies, since one single administration could inhibit Mps1 molecules for a prolonged period of time, which could decrease the need for multiple rounds of compound-5 administration. Nanomolar concentrations of compound-5 specifically reduced the mitotic timing and affected chromosome alignment of tumor cells, whereas immortalized, diploid fibroblasts were less affected (Fig. 5). This suggests that healthy cells can cope with slight defects in Mps1 activity in contrast to tumor cells, which die at relatively low doses of Mps1 inhibitor (Fig.4A). One explanation for this difference could be that healthy, untransformed cells need less time to align their diploid content of chromosomes and might therefore be less affected by checkpoint inhibition induced by partial Mps1 inhibition when compared to tumor cells that have to cope with the presence of extra chromosomes. This hypothesis is

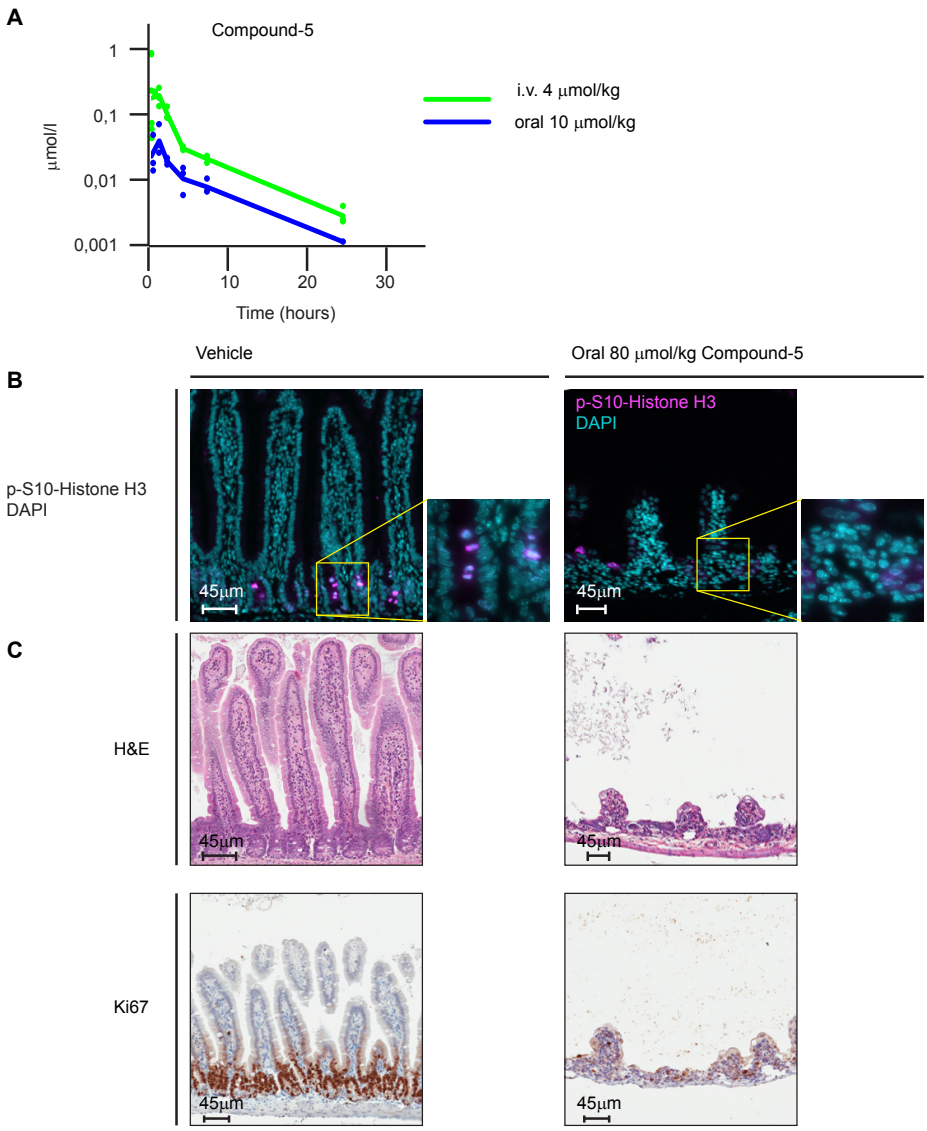

Figure 6. Intestinal toxicity observed with high doses of compound-5 *in vivo*.
A) Concentration of compound-5 measured in venous blood of female balb/c mice treated once with indicated amounts of compound-5. Administration was performed either intravenously (i.v.) or orally (oral). B) Immunofluorescence images of sections made of intestines of female FVB mice 4 days after indicated oral treatments. Phospho-Serine 10-Histone H3 was used as a marker for mitotic cells. DAPI was used to stain nuclei. C) H&E (top) and Ki67 (bottom) immunohistochemistry stainings of intestines of female FVB mice 4 days after indicated oral treatments. Ki67 was used as a proliferation marker.

in line with the fact that mitotic checkpoint abrogation is more detrimental to cells that have obtained extra centrosomes (microtubule organizing centers) and therefore need more time to congress their chromosomes[123,540]. Tumor cells spend more time in mitosis due to the presence of extra chromosomes or centrosomes [539], and as such their chromosome alignment and mitotic timing will be more affected by partial inhibition of Mps1, eventually leading to severe chromosome segregation errors and cell death. Indeed, we observed a significantly prolonged mitotic timing in all tumor lines tested

when compared to diploid untransformed cells. Moreover, partial Mps1 inhibition reduced the mitotic timing by almost two-fold in three out of four tumor cell lines tested, whereas untransformed cells hardly showed a reduction in mitotic timing. Additionally, Mps1 inhibition has also been shown to result in more stable kinetochore-microtubule (KT-MT) attachments [123]. Since chromosome unstable (CIN) tumor cells have been described to have more stable KT-MT attachments when compared to healthy diploid cells [363,364], Mps1 inhibition could specifically enhance chromosome misalignment in CIN tumor cells. Indeed, we observed a striking increase in chromosome congression defects in the CIN tumor cell lines SW480, MCF-7, Hela and U2OS treated with low dose Mps1 inhibition (Fig.5B). In conclusion, two differences: number of chromosomes and KT-MT stability, could make tumor cells more dependent on the chromosome alignment and checkpoint function of Mps1 than healthy, untransformed cells. The enhanced reduction in mitotic timing and increase in chromosome misalignments could very well explain the increase in severe chromosome segregation errors observed specifically in transformed cells. Although two recent studies have employed xenograft mouse models using human cancer cell lines to test the efficacy of Mps1 inhibition *in vivo*[176,578], it will be important in the future to determine the effect of Mps1 inhibition in more relevant mouse models for spontaneous tumor formation, such as mouse models for hereditary breast cancer [586]. Furthermore, it will be important to determine the effects of Mps1 inhibitors on healthy tissues *in vivo.* Although chromosome segregation errors and aneuploidy are generally not well tolerated in healthy diploid cells [431] (Fig.6), it is important to notice that treatment of individuals with Mps1 inhibitors could promote tumor formation in the long run. Future research will hopefully resolve the effects on healthy tissues and determine the value of using Mps1 inhibition in anti-cancer treatment.

Materials and Methods

Kinase assays

IMAP assay was used for assessing (Mps1) kinase activity in vitro. Dilution series of compound-5 were prepared in IMAP reaction buffer containing 10 mM Tris-HCl, 10 mM $MgCl_2$, 0.01% Tween-20, 0.05% NaN3 pH 7.2 and 1 mM freshly added DTT. Subsequently, in 10 µl of IMAP reaction buffer, 2.5 ng (5.5 nM) of full length Mps1 was pre-incubated for 60 minutes at room temperature with the serial dilutions of compound-5. Mps1 substrate used in this assay was fluorescein labeled IMAP synthetic peptide at a final concentration of 50 nM. The reaction was started by adding 5 µM ATP. The reactions were allowed to proceed at room temperature for 120 minutes and finally quenched by adding 30 µl of IMAP progressive binding solution according to manufacturer protocol. Measurement of fluorescein polarization signal was carried out using an Envision 2102 (Perkin Elmer) multi-label reader. Fluorescein labeled IMAP substrate and buffer kit are from Molecular Devices.

Construction of the phylogenetic tree

All protein sequences encoding serine, threonine, and tyrosine kinases used in the selectivity screen were retrieved from Pubmed and stored locally. Based on gene information we identified the boundaries of the kinase domain and generated a list of isolated kinase domains for all kinases. These were used to generate multiple sequence alignments with the help of ClustalX software and the output was used to construct the phylogenetic tree by using Dendroscope package [588] as shown in

Supplemental Figure-1.

Protein biochemistry

For the Biacore experiments all reagents were obtained from GE Healthcare unless stated otherwise. Direct binding experiments were carried out using a Biacore T100 instrument. Full length Mps1 (Invitrogen Cat. No: PV3792) was immobilized on a CM5 sensor chip using common amine coupling: The surface is activated for 900 seconds using a 1:1 dilution of 0.2 M 1-ethyl-3-(3-dimethylaminopropyl) carbodimide hydrochloride (EDC) and 50 mM N-hydroxysuccinimide. Full length Mps1 was injected for 1800 seconds diluted to 45 µg/ml in 10 mM Tris, 10 mM $MgCl_2$, 0.01% Tween-20 and 1 mM DTT at pH 7.2. Remaining active groups on the surface were blocked by a 420 second injection of 1M ethanolamine. A reference surface was generated using a similar procedure without the injection of Mps1. These injections usually result in the immobilization of approximately 10.000 RU (Response Units). Direct binding method: Low molecular weight compounds were diluted in the described buffer resulting in an end concentration of 1% DMSO. An injection series of 5 increasing concentrations (usually: 0.3, 0.9, 2.7, 8.3 and 25 nM –or a series of 10 times higher concentrations) were injected on a freshly immobilized surface as well as a control surface, at a flow rate of 50 µl/min. This method is known as single cycle kinetics. The dissociation after the last injection was monitored for at least 1800 seconds. No regeneration was carried out and each compound was tested on a freshly immobilized surface. Using Biacore T100 evaluation software v. 2.0.1 the measured data were fitted to a simple 1:1 Langmuir binding model, after subtraction of the average of at least two preceding blanks on the blank flow cell subtracted data, a method that is known as double reference subtraction; (FCactive –FCblank) sample - (FCactive –FCblank)blank. The results are evaluated by assessment of the residual plots, the chisquare and U (uniqueness) value of the fit as well as the sensibility of the calculated kinetic values in combination with the tested concentrations.

Western Blot analysis

Cells were lysed in Laemmli buffer. Samples were separated by SDS-page and transferred to PVDF (Immobilin FL, Millipore). The membranes were cut in half and blotted with anti-Mps1, Cyclin B1 and Securin. Peroxidase-coupled secondary antibodies and ECL (GE healthcare) were used to visualize protein bands.

Cell culture, cell lines & reagents

All tumor cell lines were grown in DMEM (Lonza), BJ-Tert and RPE-1 cells were grown in DMEM/F-12 + Glutamax (GIBCO) supplemented with 6% FCS (Clontech), pen/strep (Invitrogen) and ultraglutamine (Lonza). Taxol, nocodazole, thymidine, MG132 and Staurosporine were all from Sigma. SW480, MCF-7 and RPE-1 cells [389] were infected with retrovirus carrying pBabeH2B-RFP (kind gift from Dr. Susanne Lens, University Medical Center Utrecht, The Netherlands) and/or pLNCX2GFP-m53BP1 (kind gift from Dr.Marcel van Vugt, University Medical Center Groningen, The Netherlands). Cell lines were selected with 5µg/ml blasticidine (for H2B-RFP) and 500µg/ml G418 (for GFP-53BP1). Single colonies were selected after replating 1-2 cells/well or using FACS sorting. MCF-7 cells stably expressing 53BP1-GFP were a kind gift from Dr. Marcel van Vugt. BJ-Tert WT, p53KD and p53KD + HRASV12 were all kindly provided by Dr. Roderick Beijersbergen (Netherlands Cancer Institute, Amsterdam, The Netherlands). BJ-Tert stably expressing p53KD and HRASV12 were transduced with retrovirus carrying pBabe-E1A (kind gift from Dr. Benjamin Rowland, Netherlands Cancer Institute, The Netherlands) and selected

with 400μg/ml Hygromycin. U2OS cells stably expressing LAP-Mps1-WT and LAP-Mps1-M602Q were kindly provided by Dr. Nathanael Gray (Dana-Farber Cancer Institute, Boston). Compound-5 is a compound from patent WO 2009/156315 A1 from Nerviano Medical Sciences (Nerviano, Italy) and was synthesized according to the procedures described in the patent.

Live cell imaging

Cells were plated in 8-well chambered glass bottom slides (LabTek) and imaged in a heated chamber (37ºC and 5% CO2) using a DeltaVision RT system (Applied Precision) with a 20x/0.75NA objective (Olympus) using SoftWorx software. Inhibitors were added 10 minutes prior to filming. GFP and/or RFP images were acquired every 10-15 minutes.

Automated analysis of mitotic index

Cells were grown in 96 wells plates in 100µl culture medium. Nocodazole and compound-5 were added for 12 hours and cells were fixed using 5% formaldehyde. Cells were stained with MPM2 and DAPI. Image acquisition was performed using a Cellomics ArrayScan VTI (Thermo Scientific) using a 10x 0.5NA objective. 10 images were acquired per well, which contained around 4000 cells in total. Image analysis was performed using Cellomics ArrayScan HCS Reader (Thermo Scientific). The percentage of mitotic cells was calculated by the amount of MPM2 positive cells over the total DAPI positive cells.

Immunofluoresence microscopy

Cells plated on 12 mm coverslips were harvested after 30 minutes MG132 treatment. Fixation was done using 4% PFA in PBS. DAPI was incubated in PBS for 30 minutes. Stained coverslips were mounted with Prolong Antifade (Invitrogen). Images were acquired on a Zeiss 510 Meta confocal laser scanning microscope with a 63X/1.4NA Plan-ApoChromat objective using the Zeiss LSM software or on a DeltaVision RT system (Applied Precision) with 100x/1.40NA UplanSapo objective (Olympus) using SoftWorx software.

Colony formation assay

Cells (~2500/well) were plated on 96-wells plates (Costar) (day 0). Inhibitors were added on day 1. On day 6, plates were washed with PBS, fixed for 5 minutes with 96% methanol, stained with 0,1% crystal violet.dH20 and scanned for analysis.

Apoptosis assay

Hela cells were plated at a density of 1000 cells/well in a 96 well plate on day 0. On day 1 compounds were added. On day 7 cells were treated with 2.5 µM propidium iodide (PI) for 20 min at 37 ºC followed by Hoechst addition prior to fixation using 0.5% paraformaldehyde for 10 minutes. Images were captured sequentially for the Hoechst and the PI channel. Cells were imaged using an Operetta High Content System with a 20x objective and 200 ms exposure time. The number of cells per well was determined automatically according to manufacturer instructions

In vivo studies

Bioavailability of compound-5 after oral (p.o.) and intravenous (i.v.) application was determined in Balb/c mice. To determine oral bioavailability a single dose of 10 µmol per kg of compound-5 was applied as a suspension in 0.5 % gelatin, 5 % mannitol in H_2O. For the i.v. study the compound was dissolved in 5% DMSO, 5% cremophor, 5% mannitol in H_2O and administered at 4 µmol per kg. For oral administration of 50mg/kg (80 µmol/kg) compound-5, the compound was dissolved at a concentration of 10mg/ml in the vehicle: 10% DMSO 5% Mannitol and 10% Cremophor.H_2O. 5µl/gram mouse was administered orally once a day for 4 consecutive days. On day 4 or 5 mice were euthanized and tissues were isolated and fixed in formaldehyde for 48 hours. Tissues were rehydrated, cut into 4 µm sections and stained with Haematoxylin and eosin. For immunohistochemical staining of ki67, antigen retrieval was performed with citra solution (Biogenex HK086-5K). Before slides were incubated with ki67 primary antibodies, slides were pre-incubated with 1% milk/PBS. Next, slides were incubated with HRP-conjugated Envision (Dako) or stained with biotin-conjugated secondary antibodies and incubated with HRP conjugated streptavidin-biotin complex (Dako). Following detection with 3,3-diaminobenzidine-tetrahydrochloride (DAB; Sigma A-6926), slides were counterstained with Haematoxylin and dehydrated. Pictures were taken using an Aperio ImageScope (Aperio) equipped with a 20x objective and analysis was done using ImageScope software. For immunofluorescence staining of tissues, antigen retrieval was performed by boiling slides in Sodium Citrate dehydrate buffer for 20 minutes. Sections were pre-incubated with TBS-0,1% Tween20 4% BSA for 30 minutes at room temperature. Anti-phospho-Histone H3 (1:250) was incubated for 3 hours in TBS-0,1% Tween20 4%BSA, washed twice with TBS-0,1% Tween20 and secondary antibody was incubated for 45 minutes in the presence of DAPI. Prolong Antifade was used to mount the slides and analysis was done on a DeltaVision RT system (Applied Precision) with 60x or 10x objective (Olympus) using SoftWorx software.

Antibodies

The following antibodies have been used for Western Blot and Immunofluorescence: Mouse anti-Mps1 was from Millipore (05-682). Rabbit anti-Securin was from Abcam (Ab26273), Mouse anti Cyclin B from Santa Cruz and anti-rabbit Alexafluor568, Rabbit anti-Goat-PO, Goat anti-Mouse-PO and Goat anti-Rabbit-PO were all from DAKO. Rabbit anti-Phospho Serine10 Histone H3 and anti-MPM2 were from Upstate.

Acknowledgements

We thank Ellen Mattaar for performing Biacore experiments and data fitting. We thank Antoon van Doornmalen and Judith Haarhuis for performing cellular assays. We thank Livio Kleij from the University Medical Center Utrecht for assistance with the microscopes, the personnel of the animal facilities of the Netherlands Cancer Institute (NKI) for excellent animal husbandry, the NKI animal pathology department for their expertise on immunohistochemical stainings and Anita Pfauth from the NKI FACS facility for sorting cells. We also want to thank all the members of the Medema, Lens, Rowland and Kops labs for helpful discussions. This work was supported by the Netherlands Organisation for Scientific Research (NWO) (R.H.M. and A.J.: ZonMw 918.46.616; G.J.P.L.K.: VIDI-91776336), TI Pharma (G.J.R.Z, H.A., B.H., R.H.M and A.J.: T3-105) and the ERC (G.J.P.L.K.: ERC-StG KINSIGN). R.H.M. was additionally funded by the Netherlands Genomic Initiative of NWO.

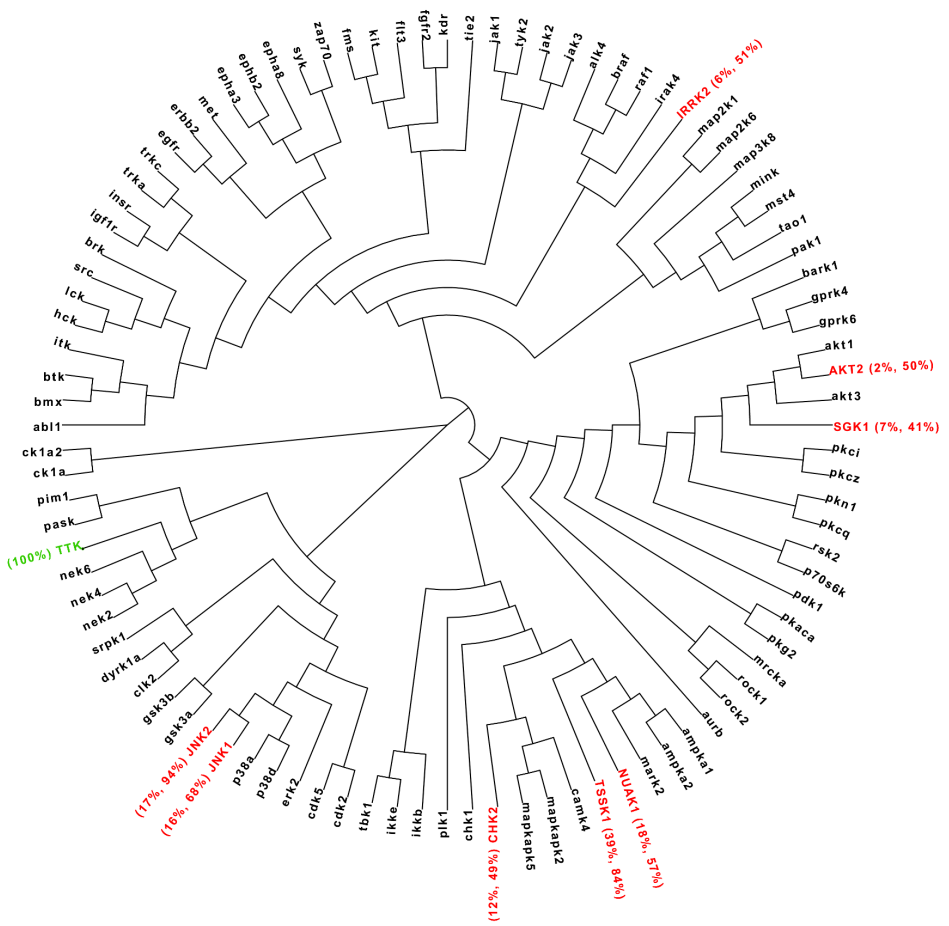

Figure S1
Phylogenetic tree of 93 representative kinases. Kinase assays were performed with the indicated kinases using 100 nM or 1μM compound-5 at Invitrogen (Paisley, U.K.). Cross-reacting kinases are shown in red and Mps1 (TTK) is shown in green. The percentage inhibition of specific kinases at 100 nM and 1μM compound-5 is indicated in between brackets.

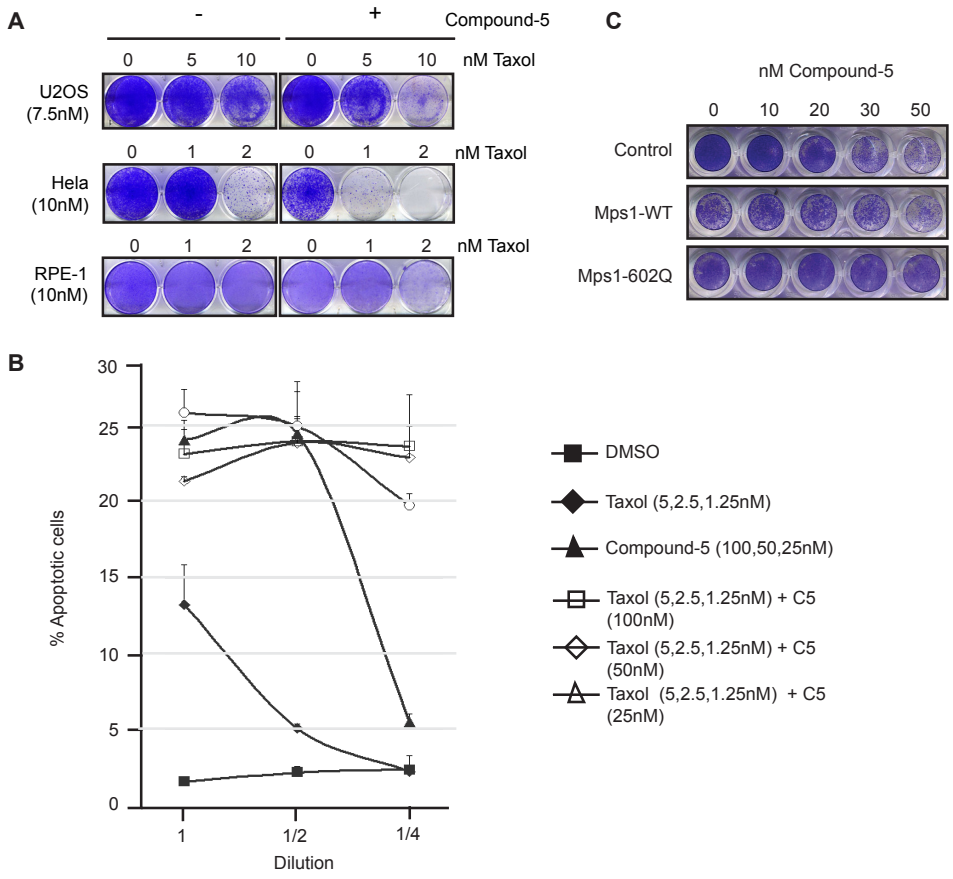

Figure S2
A) Colony formation of U2OS, Hela and RPE-1 cells treated with indicated concentrations compound-5 (in between brackets) and taxol. Taxol and compound-5 were added simultaneously and cells were harvested 6 days later. B) Graph depicting percentage of apoptotic Hela cells 7 days after addition of indicated concentrations of compound-5 and taxol. Apoptosis was determined as the number of propidium iodide positive cells over Hoechst positive nuclei. The highest concentration of each compound is indicated with 'dilution 1' and the lowest with 'dilution 1/4'. C) Colony formation assay of parental U2OS cells, U2OS cells stably expressing Lap-Mps1-WT or Lap-Mps1-602Q in the presence of indicated concentrations compound-5.

Chapter 7

Docetaxel affects *in vivo* tumor cell viability independent of its effects on mitosis

Aniek Janssen[1,2,‡], Evelyne Beerling[3,‡], René Medema[1,2,†,**], Jacco van Rheenen[3,†,*]

[1] Division of Cell Biology, Netherlands Cancer Institute, Plesmanlaan 121, 1066 CX, Amsterdam, the Netherlands.

[2] Department of Medical Oncology and Cancer Genomics Center, University Medical Center Utrecht, Universiteitsweg 100, 3584 CG, Utrecht, the Netherlands

[3] Hubrecht Institute-KNAW & University Medical Center Utrecht, Uppsalalaan 8, Utrecht 3584CT, The Netherlands

[‡] These authors contributed equally

[†] These authors contributed equally

Manuscript submitted

Abstract

Taxanes, such as docetaxel, are microtubule-targeting chemotherapeutics that have been successfully used in the treatment of cancer. Based on data obtained from cell cultures, it is believed that taxanes induce tumor cell death by specifically perturbing mitotic progression. However, recent studies suggest that tumor cell death *in vivo* might not be caused by mitotic perturbations. Here we describe a high-resolution intravital imaging method to simultaneously visualize mitotic progression and the onset of apoptosis. To directly compare *in vitro* and *in vivo* data, we have visualized the effect of docetaxel on mitotic progression in mouse and human colorectal tumor cell lines both *in vitro* and in isogenic tumors in mice. We show that docetaxel-induced apoptosis *in vitro* occurs via mitotic cell death, whereas tumor cells in their natural environment die independently of mitotic defects. Our data demonstrate that docetaxel exerts its anti-tumor effects *in vivo* through means other than mitotic perturbation.

Introduction

Taxanes are among the most widely used chemotherapeutics in the treatment of cancer for over a decade [457]. Taxanes, such as Paclitaxel (Taxol) and its more potent, semi-synthetic analogue Docetaxel (Taxotere) have been shown to bring clinical benefit in various types of cancer[589-591]. However, only half of the cancer patients eventually respond to docetaxel treatment[590], indicating that a better understanding of the specific effects of docetaxel in tumors could help design new combination therapies and improve its efficacy. Taxanes stabilize microtubules by binding to the beta-tubulin subunit of tubulin polymers[592-595]. The clinical efficacy of taxanes has mainly been ascribed to the potent inhibitory effects they have on (tumor) cell proliferation *in vitro* by delaying mitotic progression [460]. Although variation exists in the exact timing of cell death, most tumor cell lines treated with high doses of taxanes form abnormal mitotic spindles, resulting in prolonged mitosis and eventually cell death[342,486,553,596]. Cell death occurs either in mitosis, which is termed mitotic cell death, or in interphase following exit from mitosis in a tetraploid state[342,486]. Low doses of paclitaxel also affect mitotic spindle formation and induce cell death, but do not induce a severe delay in mitotic timing[552,554,555]. These low doses of taxol rather induce aneuploidy (an abnormal chromosome number) in the respective daughter cells which eventually causes cell death [554]. Although various taxane concentrations induce different mitotic perturbations, a clear correlation exists *in vitro* between abnormal mitotic progression and cell death upon taxane treatment. However, data from mice and human patients challenge this idea[590,597-600]. Immunohistological analysis of both mouse and human tumor tissues only revealed small increases in mitotic index (percentage of mitotic cells) following paclitaxel treatment[598-600]. In addition, the minor effect of paclitaxel treatment on mitotic index did not seem to correlate with tumor regression[599,600]. However, a comprehensive comparison between *in vitro* and *in vivo* data in the same tumor model is lacking, and therefore it cannot be excluded that this discrepancy is explained by the use of different cell types. Moreover, even if mitotic perturbations would consistently precede the onset of apoptosis induced by taxanes, it would be impossible to confirm this using immunohistochemistry on fixed tissues. These techniques analyze large, fixed populations of cells and lack crucial information of the history of the individual cells undergoing mitosis and apoptosis at the time of measurement. To overcome these technical limitations, several techniques have been developed to visualize the behavior of individual cells in living mice, a technique often referred to as intravital imaging [601]. Using intravital imaging techniques, changes in individual cell behavior can be visualized during chemotherapy. For example, intravital imaging of tumor cells growing in dorsal skin fold chambers in paclitaxel-treated mice revealed that only a small percentage of tumor cells went through an aberrant mitosis[597]. Nevertheless, it is difficult to link these observations to the induction of apoptosis, since this can only be recognized when cells show the typical late apoptotic morphological changes, such as chromosome condensation and cell fragmentation. This limitation prevents the ability to monitor mitotic progression and the onset of apoptosis in the same cells before and after treatment. Therefore it remains unclear if the (minor) mitotic perturbations are responsible for the tumor regression observed in the same model.

Here, we report the development of high-resolution intravital imaging methods that enable the tracing of individually photo-marked tumor cells before and during docetaxel-treatment in subsequent imaging sessions, and enable the simultaneous visualization of mitosis and the induction of apoptosis before the typical morphological apoptotic changes occur. In our assays we use docetaxel, since this drug is more potent than paclitaxel in inhibiting mitotic progression in tissue culture and is effective in killing paclitaxel-resistant tumor cells [589] . Our comparative study of *in vitro* and *in vivo* imaging data reveals that docetaxel, in contrast to its effects in cell culture, induces apoptosis *in vivo* independent

of mitotic aberrations. These data indicate that the therapeutic potency of taxanes in anti-cancer treatment can be attributed to other, mitosis-independent, detrimental effects on tumor cell viability.

Results

Docetaxel treatment induces cell death both in vitro and in vivo

For our *in vitro* and *in vivo* studies, we chose to use two colorectal tumor cell lines that can be studied *in vitro* and grow tumors upon injection in mice. We used the C26 and SW480 cell lines as a mouse allograft and human xenograft colorectal tumor model respectively. To confirm that both cell lines are sensitive to treatment with the semi-synthetic taxane docetaxel *in vitro*, we determined cell viability after several days of treatment with increasing doses of docetaxel. Colony formation capacity was clearly affected in both cell lines at a dose of 2-3 nM docetaxel, indeed showing the potency of this chemotherapeutic to kill tumor cells in tissue culture (Fig.1A). In order to confirm the docetaxel effect *in vivo*, we subcutaneously injected C26 and SW480 cells in BalbC and immune-compromised SCID mice respectively and allowed the cells to form a tumor within 2-4 weeks. Once tumors were detectable by palpation, we treated animals with the maximum tolerated dose of docetaxel (25mg/kg) and visualized the number of apoptotic cells (defragmented cells) by intravital imaging. In line with our *in vitro* data, we observed a substantial increase in the percentage of apoptotic cells in both tumor models (Fig.1B). From this we conclude that our tumors models are highly sensitive to docetaxel both *in vitro* and *in vivo*.

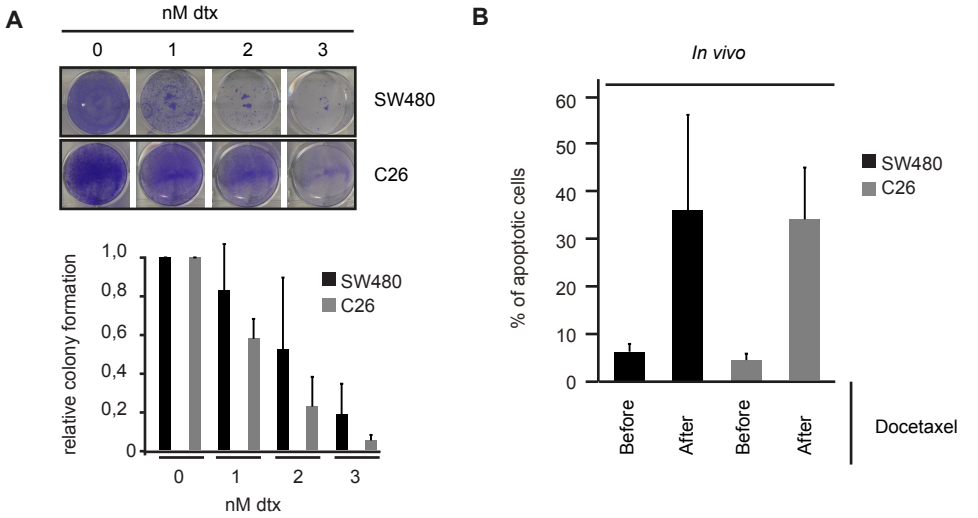

Figure 1. Docetaxel kills tumor cells *in vitro* and *in vivo*
A) Colony formation assay of indicated cell lines treated with increasing doses of docetaxel (Dtx). Colony formation capacity was determined relative to untreated controls 6 days after a single addition of docetaxel. B) Quantification of the number of apoptotic cells before or after (2-4 days) intravenous injection of 25mg/kg docetaxel. Average of 3 independent experiments per cell lines + SEM is indicated.

Simultaneously imaging mitotic progression and the onset of apoptosis

To unequivocally prove that docetaxel-induced apoptosis is mediated through defects in mitotic progression, both processes should be visualized simultaneously in the same cells *in vitro* and *in vivo* before and after docetaxel treatment. Here, we have developed an imaging method to achieve this (Fig 2A, B). Activation of the protease caspase-3 is crucial for apoptosis induction and catalyzes the cleavage of several key cellular proteins. Caspase-3 activation precedes chromosome condensation and cell fragmentation, the typical morphological changes associated with apoptotic cell death [602]. We and others have recently used a caspase-3 Fluorescent Resonance Energy Transfer (FRET) probe to visualize the onset of apoptosis *in vitro* and *in vivo*[601,603-605]. The caspase-3 FRET sensor consists of a CFP and YFP moiety separated by the caspase-3 DEVD cleavage motif and is targeted to the plasma membrane by a C-terminal CAAX sequence [606] (Fig.2A,C). Under normal conditions, caspase-3 is inactive and CFP and YFP are in close proximity, so that CFP can transfer its energy to YFP. As a result of this energy transfer, CFP fluorescence will drop and YFP fluorescence will increase, leading to a low CFP to YFP ratio (referred to as CFP/YFP ratio). Caspase-3-dependent cleavage of the DEVD motif will perturb energy transfer from CFP to YFP and result in a decreased CFP/YFP ratio. We created both C26 and SW480 cell lines stably expressing this apoptosis sensor and, as expected, we were able to visualize apoptosis induction both *in vitro* and *in vivo* using this caspase-3 FRET sensor (Fig 2C).

To follow both caspase-3 activation and mitotic progression before and after docetaxel treatment, we, in addition to the caspase-3 biosensor, also stably introduced Histone 2B tagged to photo-switchable Dendra2 [607] (H2B-D) in C26 and SW480 cell lines (Fig.2B,D). In prior studies, we have used Dendra2 to specifically photo-mark and trace individual cells[608,609]. By switching the color of H2B-Dendra2 (H2B-D) from green to red using a violet laser [607] (Fig.2B, D), we were able to track the same cells both *in vitro* and *in vivo* over multiple imaging sessions (Fig.2D, E). Photo-switching of Dendra2 did not affect caspase-3 FRET measurements and more importantly, FRET levels did not change during mitotic progression, excluding possible effects of the mitotic state on FRET efficiency (Fig.S1A, B). These data show that by imaging the caspase-3 FRET probe and H2B-Dendra2 simultaneously, we are able to visualize mitotic progression and the onset of apoptosis in the same cells both *in vitro* and *in vivo*.

Docetaxel treatment induces caspase-3 activation both in vitro and in vivo

Next, we determined the onset of apoptosis in our cell lines after docetaxel administration *in vitro*. The CFP/YFP ratio clearly increased in mitotic cells after prolonged docetaxel treatment (Fig.3A). Importantly, cells that were morphologically clearly apoptotic showed an even higher CFP/YFP ratio (5.6) when compared to the rest of the mitotic cells treated with docetaxel (3.7). This indicates that we can observe the docetaxel-induced increase in caspase-3 activity well before cells undergo the typical morphological changes associated with apoptosis (Fig.2A,C), which is in line with a recently proposed model in which caspase-3 activity slowly increases during a mitotic delay imposed by treatments with anti-mitotic drugs [342]. To evaluate the effects of docetaxel *in vivo*, H2B-D-expressing cells in the tumor were photo-marked and CFP/YFP ratios of single cells were subsequently determined before, 20 and 48 hours after intravenous docetaxel administration (25mg/kg) (Fig.3B). This analysis revealed a significant increase in the CFP/YFP ratios of both C26 and SW480 tumor cells after docetaxel treatment when compared to the control situation, which indicates that there is an increase in caspase-3 activity (Fig.3B). Before docetaxel treatment, SW480 cells displayed a CFP/YFP ratio of 2.1 on average, which increased to 2.7 and 3.3 after 20 and 48 hours of docetaxel

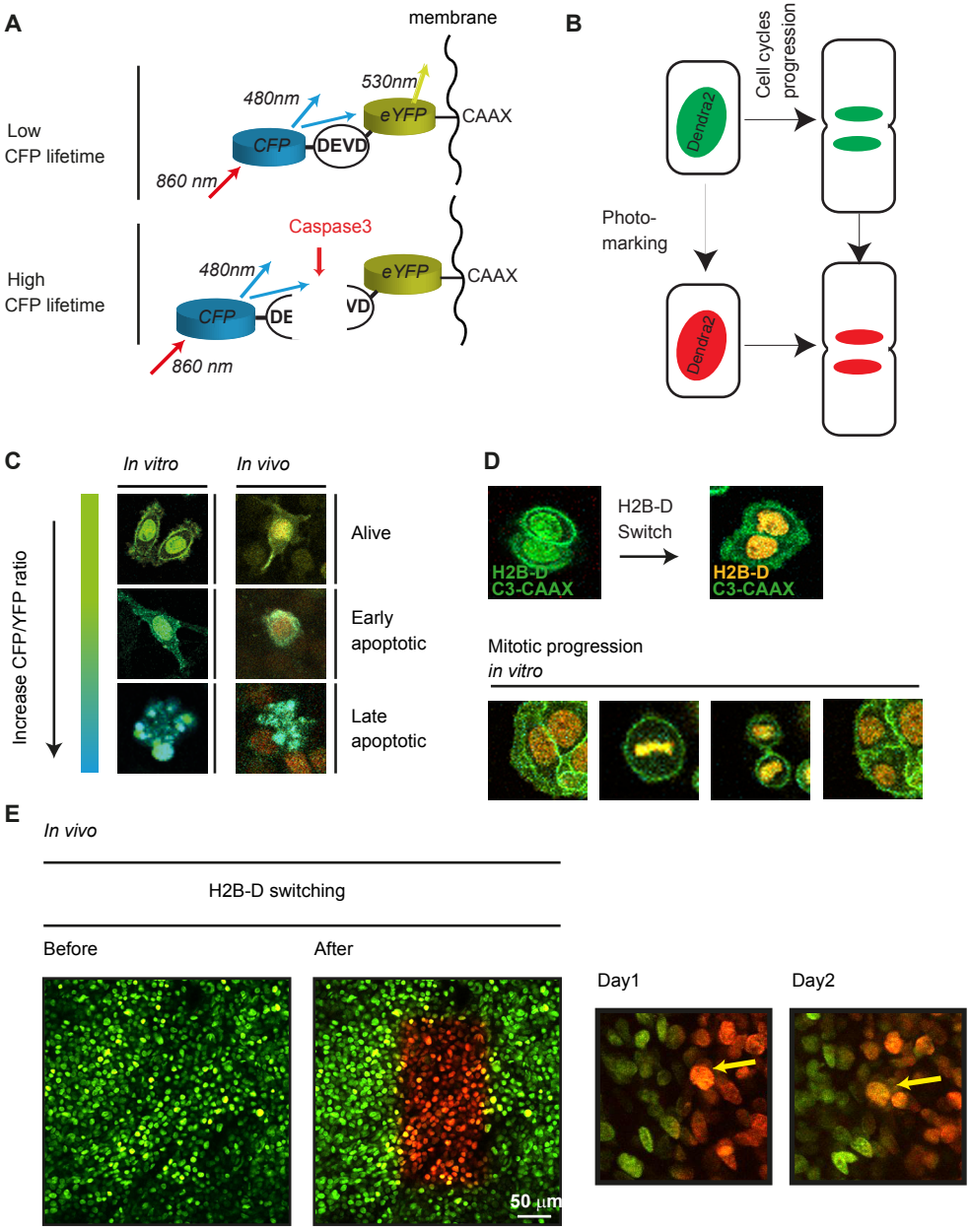

Figure 2. Simultaneous imaging of apoptosis and mitosis
A) Schematic representation of the caspase-3 FRET probe. In the absence of caspase-3 activity, CFP excitation results in the excitation of YFP bound to the membrane (FRET) and a low CFP fluorescence lifetime. A rise in caspase-3 activity, indicative of apoptosis induction, results in the cleavage of the DEVD motif in between the CFP and YFP moieties, which will result in loss of FRET, an increase in CFP-YFP ratio and an increased CFP fluorescence lifetime. B) Schematic representation of photo-marking of H2B-D cells. Switching of H2B-D from green to red enables the tracking of single cells and visualization of mitotic progression. C) Color scheme and representative cells (alive, early apoptotic, late apoptotic) *in vitro* and *in vivo* showing CFP/YFP ratio changes. D) *In vitro* cells representative of H2B-Dendra2 (H2B-D) switching and mitotic progression. E) Left: Representative image of H2B-D photo-switching of SW480 tumor cells *in vivo*. Right: Stills of individual SW480 cell *in vivo* followed for 2 consecutive days.

treatment respectively. In line with these data, C26 cells also showed a significant increase in CFP/YFP ratio following docetaxel treatment (a ratio of 1.0 before and 1.3 and 1.7 after 20 and 48 hours of docetaxel treatment respectively) (Fig.3B). To confirm our FRET results, we also performed fluorescence lifetime imaging microscopy (FLIM) (Fig.3C). Caspase-3 activation results in loss of FRET due to cleavage of the DEVD motif (Fig.2A) and therefore should cause an increase in the CFP fluorescence lifetime [610]. In line with our CFP/YFP ratio measurements, FLIM analysis of C26 cells after docetaxel treatment revealed a significant increase in CFP lifetime from, on average, 1.3 ns before docetaxel treatment to 1.8 ns at two days after docetaxel treatment (Fig.3C, D). The observed increase in caspase-3 activity was not caused by insertion of the imaging window or by light exposure during imaging, since FLIM analysis of tumor sections from within the tumor (not reached by either the window or the laser beam) showed that FRET was even more frequently lost in these areas (Fig.S2A). Together, these data show that caspase-3 activity, and therefore the onset of apoptosis, is induced upon treatment with docetaxel both *in vitro* and *in vivo*.

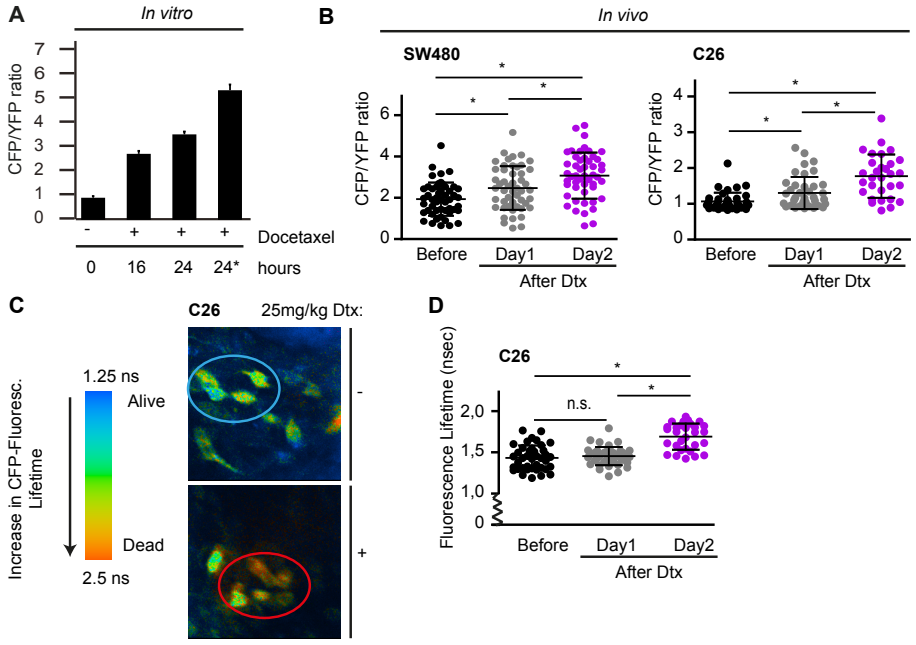

Figure 3. Docetaxel increases caspase-3 activity *in vitro* and *in vivo*
A) Quantification of the CFP-YFP ratio of SW480 cells *in vitro* under indicated conditions. 24* indicates that only apoptotic cells were analyzed, in all other cases (0, 16, 24) mitotic cells were quantified. Apoptotic and mitotic cells were determined according to morphology. Apoptotic: membrane blebbing, fragmented DNA. Mitotic: condensed DNA, rounded membrane morphology. 10 cells were quantified per condition. Average + SEM is shown. B) Quantification of CFP-YFP ratios in single cells *in vivo* of the same tumor fields before, 20 hours (day1) and 48 hours (day2) after 25mg/kg docetaxel treatment (SW480-left, C26-right). Representative experiment of 3 independent experiments per cell line is shown. One dot represents one cell. Line indicates average + SD. n.s.: not-significant (student t-test, paired, P>0.05), *: significant (student t-test, unpaired, p<0.007). C) Left: Color scheme of CFP fluorescence lifetime analysis. FRET: low lifetime (blue), no FRET: increased lifetime (red). Right: Representative images of FLIM analysis of a C26 tumor showing a group of tumor cells before (-) and 20 hours after (+) 25mg/kg docetaxel treatment. D) Quantification of FLIM analysis of C26 cells *in vivo* at indicated time points. One representative experiment is shown of two independent experiments. One dot represents one cell. n.s.: not-significant (student t-test, unpaired, P>0.05), *: significant (student t-test, unpaired, p<0.0001). Line indicates average + SD.

Docetaxel-induced apoptosis depends on the mitotic status of tumor cells in vitro but not in vivo

Next, we followed the effect of docetaxel treatment on mitotic progression using time-lapse imaging of both C26 and SW480 cells expressing H2B-D and the caspase-3 FRET probe (Fig.4A, B). As expected,

docetaxel treatment *in vitro* resulted in a mitotic delay of ~10-20 hours (Fig.4A). Of those mitotic cells, 22% died during this mitotic delay as was evident from the increase in CFP/YFP ratio and clear apoptotic morphology (Fig.4A, gray lines). Treatment of interphase cells with docetaxel *in vitro* did not affect CFP/YFP measurements (Fig.S2B), which indicates that the increase in CFP/YFP ratio is specific for mitotically delayed cells. In line with previous data [342,596], simultaneous imaging of apoptosis onset and mitotic progression shows that *in vitro* docetaxel treatment kills mitotic, but not interphase cells.

To assess the mitotic response to docetaxel *in vivo,* we analyzed the number of mitotic cells following docetaxel treatment in both C26 and SW480 tumors using intravital imaging (Fig.4B). Surprisingly, in contrast to the same cell lines *in vitro*, docetaxel did not induce a significant mitotic delay in their *in vivo* counterparts (Fig.4B). Only a small percentage of mitotic cells were observed in C26 tumors both before and 20 hours after docetaxel treatment (1,4% and 1,2% respectively) (Fig.4B) and we have never observed any mitotic cells in SW480 cells during the intravital imaging sessions (data not shown).48 hours after docetaxel treatment we did observe a slight increase in mitotic cells in C26 tumors to 3.8 % (Fig.4B). A possible explanation for the absence of a clear effect on mitotic index is that only low docetaxel concentrations are able to reach the tumor. Low doses of taxol have been shown to be able to induce chromosome segregation errors upon mitotic exit without inducing a prolonged mitotic duration [554], and therefore we analyzed the number of cells with an abnormal nucleus, which is indicative of earlier mitotic defects (Fig.4C,D). Although low doses of docetaxel treatment *in vitro* did induce the formation of abnormal nuclei, *in vivo* analysis did not reveal striking differences before or after docetaxel treatment (Fig.4C, D). C26 tumors showed a slight increase in cells with abnormal nuclei after docetaxel treatment (12,6% before and 15,2% and 15,6% 20 and 48 hours after docetaxel treatment respectively), but this increase did not correlate with the substantial increase in the percentage of apoptotic cells observed in the same fields (13%,19% and 60% before, 20 and 48 hours after docetaxel treatment respectively) (Fig.4D). The basal number of SW480 cells with abnormal nuclei was higher than that of C26 cells (Fig.4C, D). However, SW480 cells are intrinsically

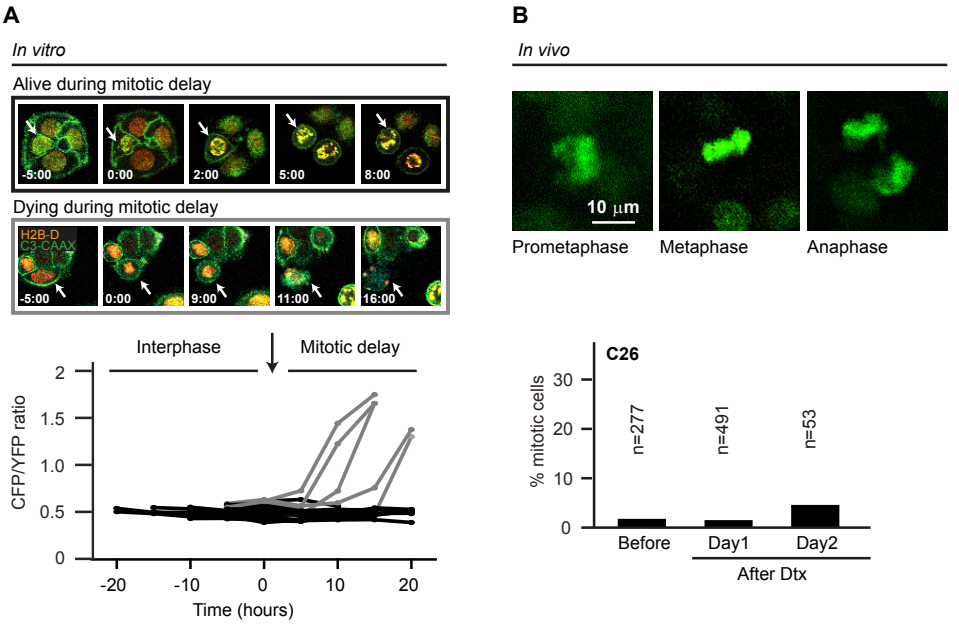

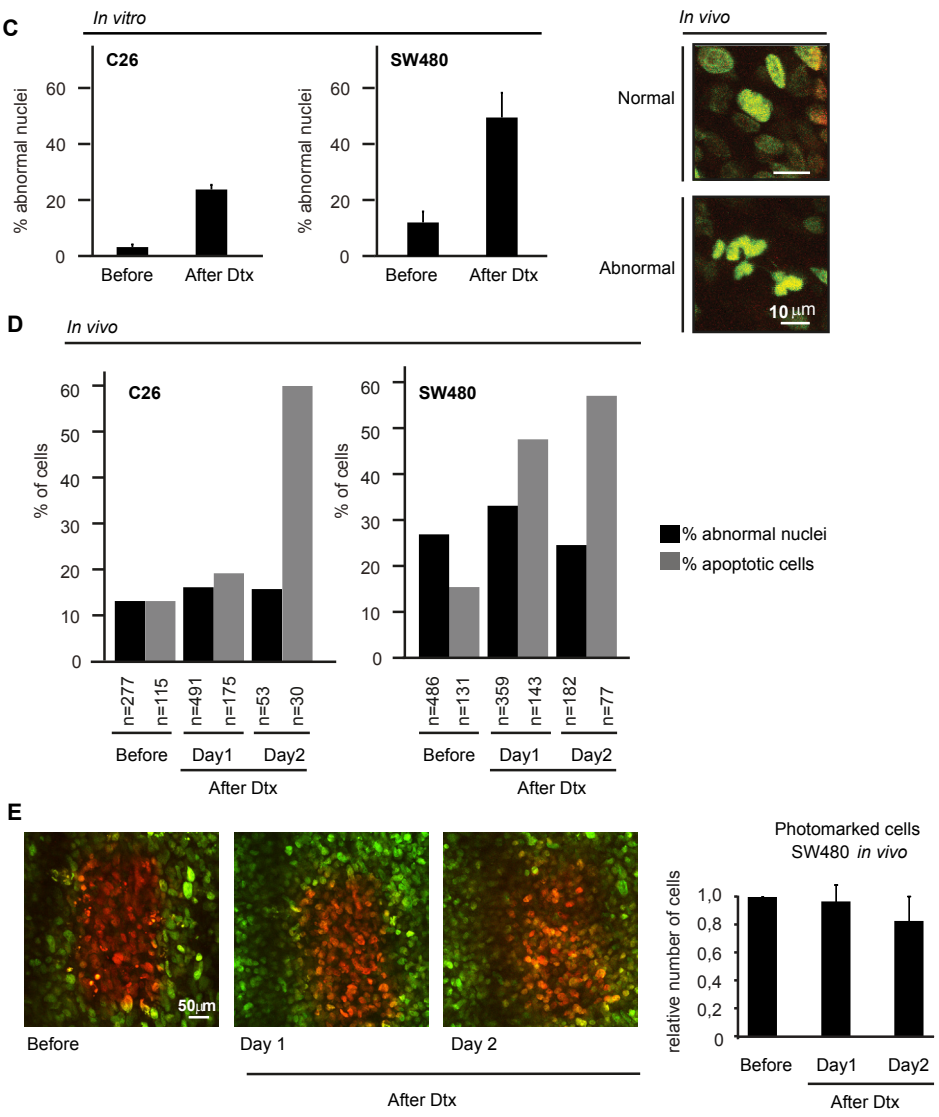

Figure 4. Docetaxel induces apoptosis *in vivo* independent of mitotic defects
A) Representative stills of SW480 cells *in vitro* entering mitosis in the presence of docetaxel resulting in a mitotic delay (top) and eventually apoptosis (bottom). Quantification of CFP-YFP ratios in representative images is shown. Each line represents one cell (black-alive, grey-dying). B) Top: Representative images of mitotic C26 cells *in vivo*. Bottom: Quantification of number of mitotic cells found at indicated time points in C26 tumors. Mitotic cells were determined according to nuclear morphology. C) Quantification of the number of abnormal nuclei in vitro in C26 (left) and SW480 cells (right) before or after treatment with 1nM docetaxel (low dose). D) Left: Representative images of SW480 cells *in vivo* with normal or abnormal nuclear morphology visualized using H2B-D. Right: Quantification of the number of cells with abnormal nuclei (black) and number of apoptotic cells (grey) in SW480 and C26 tumors at indicated time points after docetaxel treatment. Apoptotic cells were determined according to CFP-YFP ratios: 30% more than the average CFP-YFP ratio was used as a cut-off. N indicates number of cells analyzed. E) Left: representative images of photo-marked SW480 cells *in vivo* switched before treatment and imaged on day 1 and 2 after treatment. Right: Quantification of the number of photo-marked (red) H2B-D cells in SW480 tumors *in vivo*. Relative ratio compared to day 0 (before treatment) is

chromosome unstable, which means that they frequently lose and gain whole chromosomes during cell division, already in the absence of any treatment[270,289]. Importantly, neither the number of photo-marked SW480 cells *in vivo* (Fig.4E), nor the number of nuclei with an aberrant morphology (Fig.4D) increased over time upon docetaxel treatment (34% and 25% of cells had an abnormal nucleus 20 and 48 hours after treatment respectively, compared to 27% before treatment) , indicating that these cells have not divided following docetaxel treatment, whereas the percentage of apoptotic cells increased substantially in the same tumor fields (15%, 48% and 57% before, 20 and 48 hours after docetaxel treatment respectively) (Fig.4D).

Taken together, these data show that the onset of docetaxel-induced apoptosis correlates with the number of mitotic defects *in vitro*, but not *in vivo*. From this we conclude that docetaxel, in contrast to its effect *in vitro*, induces apoptosis *in vivo* independent of its effect on mitotic progression.

Discussion

Although Taxanes have been used in the clinic already for over a decade, a discrepancy between in vitro and in vivo data exists on this drug's therapeutic action. In this report, we have used two colorectal tumor models in which we analyze the effect of docetaxel on both mitotic progression and apoptosis induction in in vitro and in vivo models. For this, we have developed intravital imaging techniques that enabled us to track individual cells in multiple imaging sessions, and simultaneously determine mitotic progression and the induction of apoptosis. Our comparison shows that taxanes, as shown before342,486,553,596, affect mitotic progression in vitro, but our in vivo data indicate that other deleterious effects are more likely to be causative in tumor regression. Since we have used the same cell lines in our in vitro and in vivo study, the diverse effects cannot be explained by genetic differences. How can such a striking difference in drug response be explained? To start, tumor cells grown in vitro lack the complex microenvironment provided by neighboring cells, soluble secreted factors, and non-cellular matrix components 602. Surrounding cells include tumor-, stromal-, immune- and endothelial cells, which mutually influence each other. Given that the constantly changing microenvironment controls many signaling pathways in tumor cells, it is not surprising that many in vitro observations do not correlate with in vivo observations 611. For example, cells in culture divide once every day, while cells in primary human breast tumors divide less frequent (40-300 days) 612. Importantly, the cell cycle is well controlled by many signaling pathways and therefore the heterogeneous microenvironment may potentially affect the action of taxanes on tumor cells. Indeed, immunohistological analysis and intravital imaging of mouse and human tumor tissues only revealed small increases in mitotic index following paclitaxel treatment 597-600, supporting our finding that mitotic perturbations are not causative for taxane-induced tumor regression 599,600. Interesting recent data suggest that the microenvironment contributes to drug responses via regulation of vascular permeability and innate immune cell infiltration613. It has indeed been hypothesized that immune cells might elicit an anti-tumor effect upon taxane administration 614 and macrophages can be directly activated by paclitaxel resulting in pro-inflammatory effects 615. Although effects of the innate immune system cannot be excluded, the clear apoptotic effects of docetaxel administration in our human xenograft model using immune-compromised SCID mice indicates that the adaptive immune system is not the main contributor to taxane-dependent cell killing in vivo. The ability of docetaxel to kill tumor cells independent of its effects on mitosis could have important implications for the use and development of mitosis-specific drugs, such as Eg5 or Aurora A inhibitors

(reviewed in 447) and might explain the marginal anti-tumor effects of these drugs in patients until now 471,477. In addition, combination therapies designed in vitro to enhance mitotic defects induced by taxane treatment, should have to be reconsidered299. Nevertheless, tumor-specific traits other than an increased percentage of mitotic cells could still be exploited in future anti-cancer strategies. An example of such a trait is the presence of an abnormal chromosome number, called aneuploidy. More than 80% of all tumors harbor aneuploid cells and recently it was suggested that these cells could be specifically killed by enhancing proteotoxic stress616.

Our findings illustrate that tumor cells in *in vitro* culture systems respond differently to chemotherapy than their *in vivo* counterparts that are located in their natural environment. In addition, our data show how useful intravital imaging techniques are to study the true molecular mechanism of drugs that are frequently being used in the clinic. Therefore, future research in the specific cellular effects of Taxanes and other (anti-mitotic) drugs would benefit from *in vivo* validation with techniques as presented in this study, which hopefully leads to the development of improved combination therapies that will enhance clinical efficacy.

Materials and Methods

Cell culture, cell lines & reagents

SW480 and C26 cell lines were grown in DMEM (Lonza), supplemented with 6% FCS (Clontech), pen/strep (Invitrogen) and ultraglutamine (Lonza). *In vitro* time lapse imaging of cells was performed in Leibovitz medium (Lonza) supplemented with 6% FCS, pen/strep and ultraglutamine. SW480 and C26 cell lines were infected with lentivirus carrying pLV.CMV.puro-c3-CAAX or pWPXLd.c3-CAAX respectively and pLV.CMV.puro.H2B-Dendra. Cell lines were selected with 2μg/ml puromycin (after pLV.CMV.puro infection) and single colonies were selected after replating 1-2 cells/well or using FACS sorting. Puromycin and docetaxel (used in cell culture experiments) were from Sigma.

Plasmids

The caspase-3-CAAX FRET probe [603,606] was ligated in pLV.CMV.puro or pWPXL.d. pLV.CMV.puro was linearized using Pst1 (+ blunt with Klenow) and subsequently cut with EcoR1. pWPXL.d was linearized using BamH1 (+ blunt) and subsequently cut with EcoR1. Caspase-3 CAAX was obtained after restriction of pcDNA3.c3-CAAX with HindIII (+ Blunt) and EcoR1. H2B-Dendra2 was ligated in pLV.CMV.puro. Enzymes were all from NEB. Both pLV.CMV.puro and pWPXL.d were a kind gift from Dr. Patrick Derksen.

Live cell imaging *in vitro*

Cells were plated in 8-well chambered glass bottom slides (LabTek) and imaged in a heated chamber at 37ºC using a Leica TCS SP5 AOBS two-photon microscope (Mannheim, Germany). The stored images were analyzed using LasAF software or ImageJ. Docetaxel was added 10 minutes prior to filming. Fluorescent images were acquired every 30 minutes for duration of 48 hours.

Colony formation assay

Cells (~50.000/well) were plated on 6-wells plates (Costar) (day 0). Docetaxel was added on day 1. On day 6, plates were washed with PBS, fixed for 5 minutes with 96% Methanol, stained with 0,1% crystal violet.dH20 and scanned for analysis. Quantification was performed using ImageJ image analysis.

Window surgery

Window was placed 2-4 weeks after injection of 0,5 -1 million SW480 or C26 cells stably expressing both H2B-Dendra and the caspase-3 FRET probe. All surgical procedures were performed under 2% isoflurane inhalation anesthesia and under aseptic conditions. Before surgery, the tumor area was shaved and the skin was disinfected using 70% EtOH. An incision was made through the skin, where the imaging window was inserted (for details see [608,609]). The window was secured with a non-absorbable, non-woven purse-string suture (4-0 prolene suture). After surgery the mice were kept at 32°C until fully recovered from anesthesia. Mice were closely monitored for a few hours after surgery and food was provided within the cage.

Intravital imaging

Mice were sedated using isoflurane inhalation anesthesia (1.5% to 2% isoflurane/O_2 mixture), and placed with their head in a facemask within a custom designed imaging box. The imaging box and microscope were kept at 32°C using a climate chamber surrounding the complete microscope stage, including the objectives. The mouse vitals were monitored during imaging using the MouseOx system (starr lifescience Corp, Oakmont, PA, USA). Imaging was performed on an inverted Leica TCS SP5 AOBS two-photon microscope (Mannheim, Germany) with a chameleon Ti:Sapphire pumped Optical Parametric Oscillator (Coherent Inc. Santa Clare, CA, USA). Docetaxel obtained from the University Medical Center Utrecht pharmacy was diluted in PBS to a stock concentration of 5mg/ml. 5µl per gram mouse was administered intravenously to obtain a concentration of 25 mg/kg *in vivo*.

All mouse experiments were approved by the animal ethical committee (DEC) of the KNAW (the Netherlands) and animals were kept at the Hubrecht animal facility in Utrecht, the Netherlands. Image analysis was performed using ImageJ software. CFP-YFP ratios of single cells were determined by drawing specific regions of interest (ROIs) around cells and dividing the CFP average intensity by the YFP average intensity. Background levels for CFP and YFP were subtracted prior to ratio calculation.

FLIM analysis

FLIM analysis was carried out using a Leica TCS SP5 inverted microscope (Mannheim, Germany) with a 25x (HCX IRAPO N.A.0.95 WD 2.5mm) water objective, which was adapted for TCSPC (time-correlated single-photon counting) FLIM with a Becker and Hickl SPC 830 card using 64 time channels. The samples were excited using a femtosecond titanium chameleon Ti:Sapphire pumped Optical Parametric Oscillator (Coherent Inc. Santa Clare, CA, USA (80MHz). Images were obtained with a line-scan speed of 400 Hz. Two-photon excitation was carried out using a wavelength of 820nm and fluorescence was detected between 450nm and 480nm. The fluorescence decays obtained were fitted using a single exponential decay model with Becker and Hickl SPCImage software v2,9,9, 29107, and the lifetimes were portrayed in false color maps.

Isolation of tumors

Tissues were isolated and fixed in periodate-lysine-paraformaldehyde (PLP) buffer [601](2,5 ml 4% PFA + 0,0212 g $NaIO_4$ + 3,75 ml L-Lysine + 3,75 ml P-buffer (pH 7.4)) O/N at 4 ºC. On the following day, the fixed tissues were washed twice with P-buffer and placed for at least 6 hours in 30% sucrose at 4 ºC. The tissues were then embedded in OCT tissue freezing medium (Jung) and stored at -20 ºC before sectioning and staining.

Acknowledgements

We want to thank the Hubrecht animal facility for animal husbandry, Stefan van der Elst for help with FACS sorting of the cells and Anko de Graaff of the Hubrecht Imaging Center with imaging help. We are grateful to all the members of the van Rheenen, Medema, Kops and Lens lab for valuable input. This work was supported by the Netherlands Organisation for Scientific Research (NWO) (R.H.M. and A.J.: ZonMw 918.46.61), (E.B. and J.v.R. VIDI 91710330) and TI Pharma (R.H.M and A.J.: T3-105) and equipment grants (NWO 175.01.2007.00 and 834.11.002).

Supplemental figures

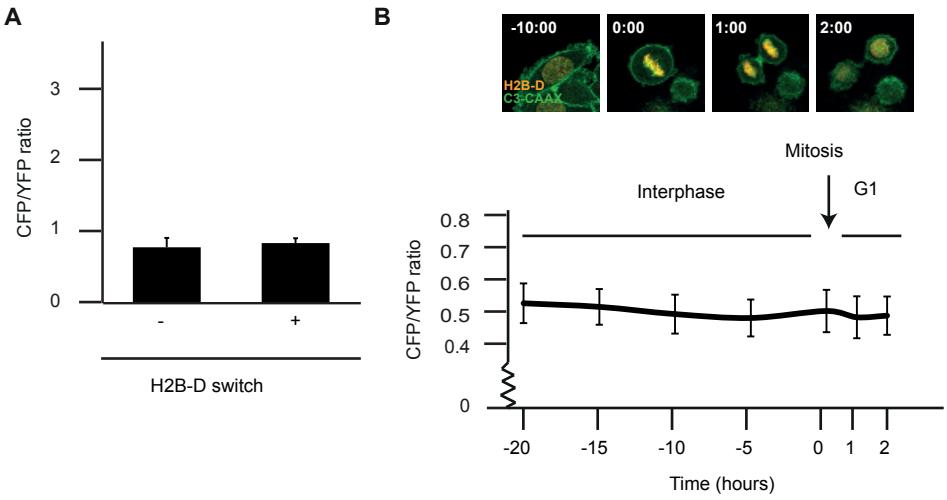

indicated. Average + SD is shown of 3 independent positions.

Figure S1
A) Quantification of CFP/YFP ratio before and after H2B-D switching in vitro. n=10 cells per condition + SEM. B) Top: Representative stills of a SW480 cell stably expressing H2B-D (red) and C3-CAAX (green) progressing through interphase and mitosis without addition of drugs. Time in hours before mitosis is shown. T=0.00 indicates mitotic entry. Bottom: quantification of CFP-YFP ratio of cells progressing through the cell cycle. n=11 cells. Average + SD is shown.

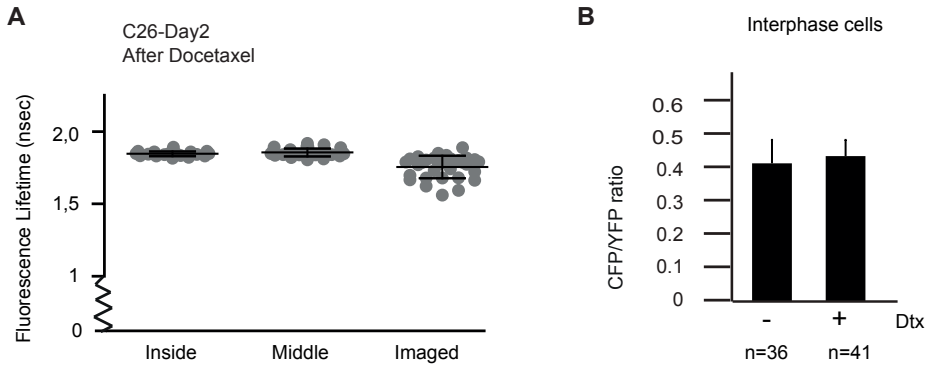

Figure S2
A) FLIM analysis of single cells (dots) in sections of indicated parts of the tumor. Tumor was isolated two days after docetaxel treatment. 'Inside' indicates outer part of tumor (opposite of the imaging window site). 'Middle' indicates middle part of tumor (cross section). 'Imaged' indicates part of tumor that was imaged through the imaging window. Each dot represents one cell. Line indicates average + SD. B) Quantification of the CFP-YFP ratio of interphase SW480 cells in cell culture in the absence or presence of taxanes. N indicates number of cells analyzed. Average + SD is shown.

7

Chapter 8

Summary & Discussion

Thesis summary

Unequal separation of the mother cells' DNA over its two daughter cells upon cell division is a prevalent phenotype found in cancer cells. This imbalanced nuclear division manifests itself as chromosome segregation errors in anaphase and telophase, the final phases of Mitosis. Chromosome unstable (CIN) cancer cells continuously display chromosome segregation errors, which leads to an abnormal chromosome number, termed aneuploidy, in the cancer cells' progeny. Research described in this thesis suggests that CIN is a 'double edged sword'. Although single gains and losses of certain chromosomes could lead to tumor growth promoting effects, severely enhanced levels of CIN unequivocally kills all cells. It is generally hypothesized that single chromosome missegregations can induce gain of certain oncogenes or loss of tumor suppressor genes and thereby stimulate tumorigenesis. **Chapter 2** of this thesis describes another mechanism by which chromosome segregation errors could enhance tumorigenesis. Cleavage furrow ingression in the presence of a single chromosome missegregation event, can lead to double strand breaks when the chromosomes is lagging behind in telophase. These double strand breaks were found to result in structural chromosomal changes in the progeny of the missegregating cells, suggesting that CIN not only enhances tumorigenesis by inducing aneuploidy, but also by introducing breaks in the chromatin. To determine the effects of CIN *in vivo* we developed two mouse models (**Chapter 3**), which each conditionally express a mutant form of the mitotic checkpoint kinase Mps1. Mps1 is essential for the fidelity of cell division and inhibition of its function results in chromosome segregation errors. With the use of these two mouse models, we will be able to to test the influence of various levels of CIN on tumor initiation, progression and, upon induction of severe CIN, also tumor growth inhibition.

The second part of this thesis describes the possibilities of exploiting CIN in anti-cancer strategies (reviewed in **Chapter 4**). Although severe levels of CIN eventually leads to cell death in any cell type, data in **Chapter 5** and **6** demonstrate that partial depletion or inhibition of Mps1 kinase activity could be tumor cell selective. In addition, we show in **Chapter 5** that partial Mps1 depletion synergizes with the clinically used chemotherapeutic Paclitaxel (Taxol) in killing tumor cells. By employing the mouse models described in **Chapter 3** and the Mps1 inhibitor described in **Chapter 6**, we wish to address the question whether Mps1 inhibition *in vivo* also results in tumor cell specific cell death and could therefore, in the future, be used in the clinic. The final experimental chapter, **Chapter 7**, demonstrates the use of intravital imaging as a tool to determine *in vivo* responses to chemotherapeutics. We developed a system to simultaneously image mitotic progression and apoptotic responses in the same cells *in vivo*. Using this system we find, in contrast to the generally accepted idea of Taxane's mode of action, that systemic Docetaxel (a semi-synthetic Taxane) treatment kills tumor cells *in vivo* independently of defects in mitotic progression. These data question the usefulness of anti-mitotic drugs in anti-cancer treatment and are being discussed in light of the recent literature in **Chapter 8** of this thesis, in addition to CIN's 'double edged sword'.

Discussion

1. Chromosome segregation errors & DNA damage

Both structural and numerical chromosomal changes arise in the majority of cancer cells [236,243]. It has been known for several decades that structural chromosomal aberrations can induce chromosome segregation errors during cell division [259]. However, it has only recently been revealed that the opposite also occurs: chromosome segregation errors can indirectly induce structural chromosomal changes through generation of double stranded breaks [388-390] **(Chapter 2)**.

1.1 Mechanisms linking CIN and DNA damage

Duesberg and colleagues observed that the severity of aneuploidy coincides with an increase in structural chromosomal changes [387,617] and several CIN model systems displayed structural chromosomal aberrations as well [332,357,618]. However, until recently, the underlying mechanisms for this correlation remained unknown. By generating 13 aneuploid yeast strains that each harbor an extra single chromosome in addition to the haploid content, it was shown that aneuploidy can directly induce genomic instability [388] (Fig.1A). Aneuploidy of a single chromosome in some cases resulted in chromosome missegregations, whereas in others, the abnormal chromosome numbers induced a high mutation rate. This increased genomic instability is thought to be due to both an increase in DSBs and defects in recombinational repair [388]. The underlying cause of the increase in DSBs remains largely unknown, but could be due to aneuploidy induced stoichiometric imbalances in protein levels [445,446], since diploid yeast strains carrying a single extra chromosome did not display an increase in genomic instability [388]. In addition to defects induced by aneuploidy per se, it was also recently shown that single chromosome missegregation events, the underlying cause of aneuploidy induction, can also directly lead to DNA damage[389,390] (Chapter 2) (Fig.1B,C). Micronuclei, small nuclear compartments that are surrounded by a nuclear envelope, in general contain one or two chromosomes that missegregated in the preceding mitosis [248,263,419]. Through artificial induction of chromosome missegregations [619] it was shown that these micronuclei undergo replication defects in the next S and G2 phase, due to incomplete recruitment of DNA replication factors, such as the DNA helicase components MCM2 and MCM3 and the initiation factor Cdt1 [390]. These replication defects resulted in persistent DNA damage in micronuclei, providing a link between chromosome segregation errors and genomic instability (Fig.1B). Interestingly, on top of DNA damaging events occurring in the next S phase following an aberrant mitosis, we showed that DNA damage can also be directly imposed on lagging chromosomes during telophase **(Chapter 2)**. Following both artificially induced chromosome segregation errors and spontaneous missegregations in CIN cancer cells, we observed the presence of damaged chromatin in telophase and the next G1 phase [389]. The occurrence of these DSBs could be (partially) rescued by inhibiting cytokinesis, suggesting that cleavage furrow ingression causes DNA damage in these cells (Fig.1C). Together, the findings discussed in **Chapter 2** and data from other labs [388,390] reveal new mechanisms by which CIN and aneuploidy could result in genomic instability and structural chromosomal aberrations and can therefore change the genetic make-up of cancer cells (Fig.1).

1.2 How does cleavage furrow ingression damage chromatin?

The question remains how ingression of the furrow could impose such massive force that it damages the lagging chromatin. It could be simply due to mechanical force

exerted through contraction of the actin myosin ring. For that to be true we should first determine whether the furrow is actually in direct contact with the lagging chromatin and subsequently assess whether this physical contact coincides with the observed DNA damage. An interesting hypothesis is that fragile sites present on lagging chromosomes could render them more prone to break when present in the cleavage furrow. It has been shown that fragile sites induced by replication defects are protected from further destabilization and breaking in G1 through the recruitment of 53BP1 [620,621]. Cleavage furrow ingression in the presence of these underreplicated hotspots could promote breakage of lagging chromosomes before 53BP1 has accumulated to protect these loci. Chromatin IP experiments following application of exogenous replication stress also revealed the mere presence of γH2AX and 53BP1 on fragile sites in G1 [620,621]. It would be interesting to determine whether an increase in chromosome segregation errors would specifically increase the association of 53BP1 and γH2AX with fragile sites.

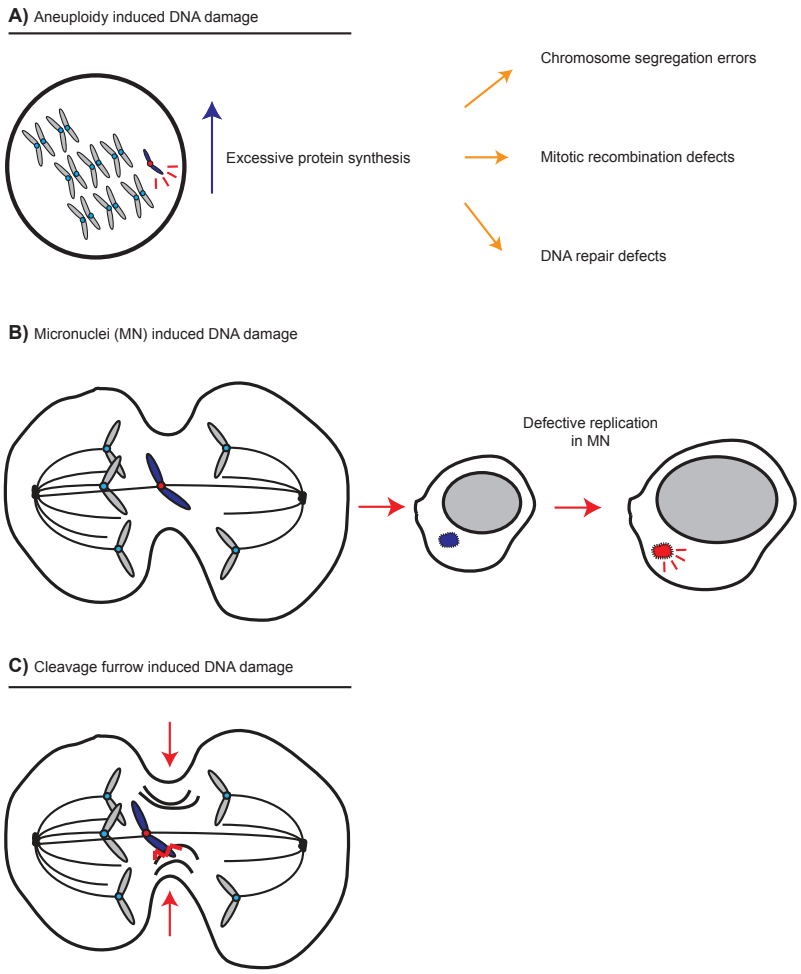

Figure 1. CIN and aneuploidy induce DNA damage
Schematic representation of the proposed links between Chromosomal Instability (CIN), Aneuploidy and genomic instability. A) The presence of an extra chromosome enhances protein synthesis, which can (in) directly lead to chromosome segregation errors, recombination problems and defects in DNA repair. Chromosome segregation errors, associated with CIN, could lead to DNA damage through the formation of replication-defective micronuclei (MN) (B) or cleavage furrow induced chromatin breakage (C).

Since it has been shown that replication stress can induce chromosome segregation errors [379,380], testing the hypothesis that cleavage furrow ingression in the presence of chromosome segregation errors results in fragile site breakage, could reveal a feedback loop which provides a genetically unstable cancer cell with even more possibilities to evolve. Finally, another cause of missegregation-induced damage could be the presence of an increased, centromere localized force imposed by microtubules coming from the two spindle poles. This has also been suggested by an earlier study, in which the authors observed centromere-localized DNA damage foci in interphase CIN cells [622]. To address this point, future studies should determine whether inhibition of this centromere-localized force reduces the DNA damage observed following mitotic exit. In addition, we are currently performing Chromatin-IP experiments using DNA damage specific antibodies to assess where the DSBs are specifically induced at for example centromeres or fragile sites following chromosome segregation errors.

1.3 Chromosome segregation errors & Chromothripsis

The recent discovery of a chromosome shattering phenomenon induced by double-stranded breaks, termed chromothripsis, in 2-3% of all cancer genomes [623], has resulted in the emergence of various hypotheses explaining this striking phenotype. Chromothripsis is defined by the presence of multiple and complex rearrangements, which typically produce a single chromosome, chromosome arm or region that is made up out of fragments from multiple chromosomes[623]. Interestingly, the copy number state in these regions of chromothripsis alternates between one or two copies and does not include multiple copies. It is therefore thought that chromothripsis occurs in one single cellular event, since progressive events would most likely lead to multiple copy number changes [623]. Moreover, chromothripsis is defined by the presence of a high level of breakpoint clustering at one specific chromosomal locus, while progressive, consecutive events would be expected to cause randomly distributed breakpoints [624]. Chromothripsis has been shown to be causative in the development of congenital defects [625]. Moreover, it has been shown to be linked to tumors harboring mutations in the tumor suppressor p53 and is associated with poor prognosis in patients with acute myeloid leukemia and neuroblastoma[626]. In general, chromothripsis seems to be yet another mechanism of creating heterogeneity in cancer cells [624] by for example disruption of tumor suppressor genes [623]. Several underlying mechanisms for chromothripsis have been proposed, such as replication fork stalling or exposure to irradiation during mitosis [624], but direct causes of chromothripsis are still unknown. The finding that micronuclei undergo massive replication-induced DNA damage and that chromatin present in these micronuclei can remain compartmentalized for several cell divisions, led to the hypothesis that chromosome segregation errors could cause chromothripsis through the formation of micronuclei[390]. The induction of multiple DSBs in replication-defective micronuclei and subsequent reintegration of the chromatin from this micronucleus into the main nuclear mass, could lead to the formation of highly localized breaks on only one single chromosome [390]. Alternatively, the presence of highly clustered DSBs has also led to the hypothesis that chromothripsis is induced due to DNA damaging events on condensed chromatin [623]. Since lagging chromosomes can get damaged during cytokinesis while being in a condensed state [389], we propose another hypothesis in which cleavage furrow ingression could cause chromothripsis by inducing multiple breaks on the lagging chromatin. In line with this hypothesis, genome sequencing of patients with congenital disease has revealed that the highly clustered DSBs associated with chromothripsis are often repaired by NHEJ [627], as was to be the preferred mode of repair of cytokinesis-induced damage as well **(Chapter 2)**. To test our hypothesis we have generated single clones following a single chromosome missegregation event and are currently evaluating the presence of chromothripsis in these clones.

1.4 NoCut: preventing the induction of tetraploidy or DNA damage?

The NoCut pathway, initially identified in budding yeast, is thought to protect the chromatin from abscission-induced DNA damage in yeast [197]. The purpose of NoCut pathway activation seems to differ between species, since inhibition of the homologues pathway in human cells resulted in tetraploidy rather than chromatin breakage by the abscission machinery [196]. In addition, we observed that DNA damage on lagging chromosomes occurs already in telophase, before the induction of abscission (Chapter 2). RPE cells do elicit an active NoCut response, since we observed localization of several active NoCut components to the site of abscission in the presence of chromatin bridges (data not shown). These data together indicate that the NoCut pathway in human cells cannot prevent DNA damage from occurring during cytokinesis, which suggests that the NoCut pathway in human cells has indeed primarily been preserved to prevent tetraploidy rather than to inhibit DNA damage induction on chromatin bridges, as in budding yeast [197]. Interestingly, however, a recent report in which the abscission mediator ESCRT III was identified as mediator of the NoCut pathway in human cells, showed that depletion of the ESCRT III subunit CHMP4C resulted in premature chromatin resolution in anaphase and increased DNA damage [628], but did not result in overt tetraploidy. This contradiction raises the question whether the NoCut or abscission checkpoint has been preserved in humans to protect genome stability by inhibiting DNA damage on lagging chromatin, by inhibiting the formation of tetraploid cells or both [196,628].

2. How do chromosome segregation errors contribute to tumorigenesis?

Boveri was the first to postulate that chromosomal aberrations could be a causal factor in the occurrence of cancer [232] after von Hansemann had observed the presence of chromosomal abnormalities and mitotic errors in cancer cells [233]. At present, the impact of structural changes on cancer progression is quite well understood [240], while the effects of numerical changes on tumorigenesis remain highly debated [267,398]. Although some of the CIN mouse models develop spontaneous tumors late in life **(Chapter 1)**, the question remains whether CIN and aneuploidy are causes or consequences of cancer development.

2.1 Chromosomal instability in tumorigenesis

Chromosomal instability (CIN) has been observed in early neoplastic lesions [629] and is thought to be able to cause transformation [397,630,631]. In addition, aneuploidy, one of the common consequences of CIN, can drive evolution by introducing phenotypic variation in several budding yeast strains [632,633]. In line with a role for CIN in tumorigenesis, CIN has been associated with poor prognosis and resistance to chemotherapeutics in human patients [271-280]. Indeed, overexpression of the mitotic checkpoint protein MAD2, which results in CIN [331,332], has also been shown to be able to drive tumor relapse in mice following Kras inhibition, indicating that CIN could overcome oncogene-addiction and affect chemotherapeutic responses[409]. However, not all CIN mouse models develop spontaneous or carcinogen-driven tumors despite clear aneuploidy induction [295,297,300,412,414,415]. Moreover, CIN has also been associated with tumor suppression[286,401,404,405], indicating that the link between CIN and tumorigenesis remains unclear and that multiple factors likely affect the tumor promoting capacity of CIN and aneuploidy.

2.2 Benefits of being CIN

Generally, CIN is thought to be able to promote tumorigenesis by inducing loss of certain tumor suppressor genes or gain of oncogenes. Loss of heterozygosity could reveal certain mutations in tumor suppressor genes and therefore promote a transforming event [634]. In line with this, crossing a CIN mouse model carrying a hypomorphic Bub1 allele with several tumor-prone mouse models resulted in the loss of tumor suppressor genes, such as p53 and APC [286]. Chromosome segregation errors could indeed be quite effective in inducing LOH, since it will immediately induce loss of multiple genes. However, the induction of aneuploidy is very likely to be detrimental to cells[292,294,445,446] and it is therefore thought that coinciding mutations would have to arise in other pathways to render cells insensitive to changes in chromosome number. Examples of such mutations are loss of p53 function [431] or mutations that promote proteasomal degradation in order to circumvent the increases in protein production obtained by gains of chromosomes[538]. These mutations on their turn could allow the induction of other transforming changes, which ultimately could lead to tumorigenesis. Another interesting hypothesis on how CIN and aneuploidy could promote tumorigenesis is through the creation of a mutator phenotype[281,635]. Aneuploidy could, by changing levels of certain DNA repair genes, promote an increase in genomic instability. In line with this hypothesis, aneuploidy was initially found to correlate with genomic instability in cancer cells [617] and has recently been shown to indeed induce genomic instability in budding yeast [388]. Moreover, CIN could itself be a mutator by inducing DNA damage and structural chromosomal changes through micronuclei formation [390] or cleavage furrow ingression in the presence of lagging chromosomes **(Chapter 2)**. Interestingly, crossing a CIN mouse model with a mouse model deficient for the DNA damage checkpoint kinase ATM resulted in accelerated tumor formation[407], suggesting that loss of DNA damage checkpoint activation could promote CIN-induced tumor formation, again supporting a role for CIN in promoting genomic instability. Interestingly, CIN and defects in mismatch repair, which result in microsatellite instability (MIN), were found to be almost always mutually exclusive in colon carcinoma cells [270]. MIN tumor cells are near diploid, indicating that aneuploidy is not simply a bystander of tumor formation [270]. In contrast to MIN cells, CIN cells rarely obtain mismatch repair deficiencies, but are always aneuploid, suggesting that CIN and MIN each support a distinct mutator phenotype driving cancer progression [231]. In summary, CIN and aneuploidy could together create an environment in which cancer cells continuously lose and gain whole chromosomes, but also gain mutations or translocations, which interfere with the function of genes involved in DNA repair, mitotic fidelity and cell cycle progression, therefore promoting transformation of cells or conferring resistance to chemotherapeutics.

2.3 Future of CIN research

The question remains whether CIN is an initiator of tumorigenesis, whether it mainly provides an enhancing effect to promote transformation or if it is a mere consequence of tumor formation. The fact that CIN is a common trait of over 70% of all tumors makes it unlikely to simply be a bystander of tumorigenesis. Whole genome sequencing of early neoplasia in either tumorprone mouse models or human patients in combination with assessment of CIN status could provide answers to the question whether CIN has an initiating or enhancing role in tumorigenesis. The presence of CIN or aneuploidy in early neoplasia in the absence of any other mutations, would suggest that CIN is an initiating event. In contrary, frequent mutations in certain oncogenes or tumor suppressor genes in the absence of any CIN, would suggest that CIN occurs later during tumor development and is rather an enhancer of tumorigenesis. Ideally, mitotic progression or aneuploidy status would be visualized live in mouse models for spontaneous

tumorformation using intravital imaging [636]. Visualizing DNA using fluorescently tagged Histone 2B *in vivo*, as shown in **Chapter 7**, could reveal the presence of chromosome segregation errors already during early mammary neoplasia in for example genetically engineered mouse models for breast cancer. Generation of mouse models in which CIN can be induced during later stages of development, such as our CiMKi mouse model described in **Chapter 3**, will hopefully also provide more knowledge on the effect of CIN in tumorigenesis. In most of the current CIN mouse models, CIN is induced already during embryonic development, which makes it difficult to draw conclusions about tumor development in later life stages. In addition, improving diagnostic tools to visualize CIN in tissues of mouse models, but also human patients, should help in evaluating the various levels of CIN and the impact thereof on tumorigenesis [637]. These tools should help in solving the discrepancies currently found between different mouse models of CIN [398] and improve our understanding of the role of CIN in tumorigenesis.

3. Exploiting CIN as a new therapeutic avenue

Already for over decades, researchers are searching for cancer-specific chemotherapeutics to treat cancer patients. Most of the clinically used anti-cancer strategies involve general cytotoxic agents, such as the DNA damaging agents doxorubicin and cisplatin. In some cases, tumor-specific traits have been used successfully to specifically kill tumor cells, such as treatment of Her2 positive breast cancer with Herceptin [638]. The fact that many tumors are CIN and harbor defects in mitotic progression raises the question whether those traits could provide a window of opportunity in anti-cancer treatment (as discussed in **Chapter 4)**. Exploiting the presence of supernumerary centrosomes [527] or enhancing proteotoxic stress [616] could specifically target CIN and aneuploid tumor cells, while leaving healthy cells unharmed. Alternatively, as discussed in **Chapter 5** and **6**, we have focused on the use of Mps1 as a possible anti-cancer target and have found that its inhibition can specifically kill tumor cells *in vitro*.

3.1 Enhancing CIN kills tumor cells

Employing mouse models with Mps1 mutations (Chapter 3) to investigate in the consequences of CIN in tumorigenesis seems in striking contradiction with the use of Mps1 inhibition in anti-cancer therapy. However, data described in Chapter 5 of this thesis reveal that there might be an optimal level of CIN which could promote tumor growth, whereas excessive CIN will lead to tumor cell death. Indeed, frequency of chromosome segregation errors in CIN tumor cells is rather low, on average 1-3% per chromosome per cell division[270,289]. Inducing excessive CIN, for example by inhibiting mitotic checkpoint signaling [292,299], massively increases the frequency of chromosome segregation errors and is incompatible with cell viability [292,639]. In line with these *in vitro* data, CIN in some mouse models seemed to have an inhibitory effect on tumorgrowth (see Chapter 1-Table I) and enhanced levels of CIN have been shown to correlate with better prognosis than intermediate levels of CIN in several cases of breast, ovarian, gastric, and non-small cell lung cancer [404,405].

3.2 Inhibiting Mps1 as an anti-cancer strategy

Although excessive CIN is lethal to any cell type, Mps1 inhibition seems to induce massive CIN specifically in tumor cells (Chapter 6). The fact that tumor cells generally spend more time in mitosis [539], possibly because they need more time to align their extra sets of chromosomes, is thought to render them more sensitive to Mps1 inhibition. This, together with the fact that partial Mps1 depletion specifically sensitizes cancer cells to the chemotherapeutic taxol [299] (Chapter 5), provides

opportunities for the development of Mps1 inhibitors as tumor-cell specific chemotherapeutics. In addition to determining the effects of CIN on tumorigenesis, the development of our CiMKi mouse models **(Chapter 3)** also provides us with a sophisticated tool to determine the anti-tumor effects of inhibition of Mps1 kinase activity *in vivo*. Crossing our CiMKi^{D637A}/CreER strain with a tumorprone mouse model, such as MMTV-Neu would allow tumor growth in the presence of full Mps1 kinase activity. Subsequently, we could ablate Mps1 kinase activity through (local) addition of tamoxifen, which induces expression of kinase-dead Mps1 (D637A), and determine tumor regression following complete tumor formation. In addition, we could use our CiMKi models to determine effects of Mps1 inhibition on healthy tissues through systemic application of tamoxifen.

3.3 How do anti-mitotic drugs kill tumor cells?

Although *in vitro* experiments show preferential killing of tumor cells following Mps1 inhibition (Chapter 5, 6), the question remains whether similar results will be found *in vivo.* The percentage of mitotic cells in tumors is significantly lower than the percentage found in cell culture [612]. This indicates that drugs, specifically designed to affect mitotic progression of tumor cells, might not be as effective *in vivo* as anticipated from *in vitro* experiments. As described in **Chapter 7**, taxanes induce cell death in tumors *in vivo*, but do this independently of clear effects on mitotic progression. These data are in line with previous results found using intravital imaging in mice and immunohistochemistry analysis of patient tumors treated with taxanes [597-599]. This indicates that taxanes might not be so successful due to their anti-mitotic effects, but rather kill tumor cells through other means. Taxanes might exert anti-tumor effects through activation of the patients' immune system [615] or inhibition of blood vessel formation in the tumor [612] for example. Another hypothesis is that only a handful of cells in the tumor die due to taxane-induced mitotic defects and that their death induces some sort of butterfly effect on the rest of the tumor cells, for example through release of pro-inflammatory cytokines or release of pro-apoptotic signals to their neighbors [612]. In conclusion, data from us **(Chapter 7)** and others [597] indicate that classical anti-mitotic drugs that were initially thought to act by perturbation of spindle assembly could induce tumor cell death in human patients via a different mechanism than what has been observed in cell culture. Nonetheless, two studies have revealed anti-tumor activity of Mps1 inhibitors *in vivo*[176,578] and our data show that extremely low levels of Mps1 inhibitors could be sufficient to specifically kill cancer cells **(Chapter 6)**. Eventually, cancer cells need to divide to form a tumor and at some stage in tumor development these dividing cells should be targetable *in vivo* as well.

4. Concluding remarks

Tumors are extremely heterogeneous, which makes it difficult to determine which cancer cell features are consequences and which are actual initiators of tumorigenesis. Even if CIN turns out to be a mere consequence of cancer progression, we and others have shown that chromosome segregation errors can definitely provide the cancer cell with more evolutionary benefits, which could eventually enhance tumor progression. More importantly, we show that CIN might be useful as an exploitable tumor-specific trait in anti-cancer therapy, since healthy cells are rather insensitive to Mps1 inhibition. Although it remains unknown whether CIN can initiate tumorigenesis, it should be noted that chemotherapeutics that induce excessive CIN in tumors could promote tumorigenesis in healthy cells in the long run. As such, future research in mice should focus on the long-term effects of Mps1 inhibition on healthy cells *in vivo*.

Addendum

&

References

Nederlandse samenvatting

Curriculum Vitae

Publications

Dankwoord

References

1. Pines, J., *The cell cycle kinases.* Semin Cancer Biol, 1994. **5**(4): p. 305-13.
2. Lindqvist, A., V. Rodriguez-Bravo, and R.H. Medema, *The decision to enter mitosis: feedback and redundancy in the mitotic entry network.* J Cell Biol, 2009. **185**(2): p. 193-202.
3. Nasmyth, K., *How might cohesin hold sister chromatids together?* Philos Trans R Soc Lond B Biol Sci, 2005. **360**(1455): p. 483-96.
4. Walczak, C.E. and R. Heald, *Mechanisms of mitotic spindle assembly and function.* Int Rev Cytol, 2008. **265**: p. 111-58.
5. Kirschner, M. and T. Mitchison, *Beyond self-assembly: from microtubules to morphogenesis.* Cell, 1986. **45**(3): p. 329-42.
6. Clarke, P.R. and C. Zhang, *Spatial and temporal coordination of mitosis by Ran GTPase.* Nat Rev Mol Cell Biol, 2008. **9**(6): p. 464-77.
7. Karsenti, E., J. Newport, and M. Kirschner, *Respective roles of centrosomes and chromatin in the conversion of microtubule arrays from interphase to metaphase.* J Cell Biol, 1984. **99**(1 Pt 2): p. 47s-54s.
8. Maiato, H., C.L. Rieder, and A. Khodjakov, *Kinetochore-driven formation of kinetochore fibers contributes to spindle assembly during animal mitosis.* J Cell Biol, 2004. **167**(5): p. 831-40.
9. Tanenbaum, M.E. and R.H. Medema, *Localized Aurora B activity spatially controls non-kinetochore microtubules during spindle assembly.* Chromosoma, 2011. **120**(6): p. 599-607.
10. Brinkley, B.R. and E. Stubblefield, *The fine structure of the kinetochore of a mammalian cell in vitro.* Chromosoma, 1966. **19**(1): p. 28-43.
11. Choo, K.H., *Domain organization at the centromere and neocentromere.* Dev Cell, 2001. **1**(2): p. 165-77.
12. Palmer, D.K., et al., *Purification of the centromere-specific protein CENP-A and demonstration that it is a distinctive histone.* Proc Natl Acad Sci U S A, 1991. **88**(9): p. 3734-8.
13. Allshire, R.C. and G.H. Karpen, *Epigenetic regulation of centromeric chromatin: old dogs, new tricks?* Nat Rev Genet, 2008. **9**(12): p. 923-37.
14. Howman, E.V., et al., *Early disruption of centromeric chromatin organization in centromere protein A (Cenpa) null mice.* Proc Natl Acad Sci U S A, 2000. **97**(3): p. 1148-53.
15. Regnier, V., et al., *CENP-A is required for accurate chromosome segregation and sustained kinetochore association of BubR1.* Mol Cell Biol, 2005. **25**(10): p. 3967-81.
16. Guse, A., M. Mishima, and M. Glotzer, *Phosphorylation of ZEN-4/MKLP1 by aurora B regulates completion of cytokinesis.* Curr Biol, 2005. **15**(8): p. 778-86.
17. Heun, P., et al., *Mislocalization of the Drosophila centromere-specific histone CID promotes formation of functional ectopic kinetochores.* Dev Cell, 2006. **10**(3): p. 303-15.
18. Blower, M.D., B.A. Sullivan, and G.H. Karpen, *Conserved organization of centromeric chromatin in flies and humans.* Dev Cell, 2002. **2**(3): p. 319-30.
19. Cheeseman, I.M. and A. Desai, *Molecular architecture of the kinetochore-microtubule interface.* Nat Rev Mol Cell Biol, 2008. **9**(1): p. 33-46.
20. Gascoigne, K.E. and I.M. Cheeseman, *Kinetochore assembly: if you build it, they will come.* Curr Opin Cell Biol, 2011. **23**(1): p. 102-8.
21. Gascoigne, K.E., et al., *Induced ectopic kinetochore assembly bypasses the requirement for CENP-A nucleosomes.* Cell, 2011. **145**(3): p. 410-22.
22. Schleiffer, A., et al., *CENP-T proteins are conserved centromere receptors of the Ndc80 complex.* Nat Cell Biol, 2012. **14**(6): p. 604-13.
23. Bock, L.J., et al., *Cnn1 inhibits the interactions between the KMN complexes of the yeast kinetochore.* Nat Cell Biol, 2012. **14**(6): p. 614-24.
24. Cheeseman, I.M., et al., *KNL1 and the CENP-H/I/K complex coordinately direct kinetochore assembly in vertebrates.* Mol Biol Cell, 2008. **19**(2): p. 587-94.
25. Desai, A., et al., *KNL-1 directs assembly of the microtubule-binding interface of the kinetochore in C. elegans.* Genes Dev, 2003. **17**(19): p. 2421-35.
26. Goshima, G., et al., *Human centromere chromatin protein hMis12, essential for equal segregation, is independent of CENP-A loading pathway.* J Cell Biol, 2003. **160**(1): p. 25-39.
27. Janke, C., et al., *The budding yeast proteins Spc24p and Spc25p interact with Ndc80p and Nuf2p at the kinetochore and are important for kinetochore clustering and checkpoint control.* EMBO J, 2001. **20**(4): p. 777-91.
28. Wigge, P.A. and J.V. Kilmartin, *The Ndc80p complex from Saccharomyces cerevisiae contains conserved centromere components and has a function in chromosome segregation.* J Cell Biol, 2001. **152**(2): p. 349-60.
29. McCleland, M.L., et al., *The vertebrate Ndc80 complex contains Spc24 and Spc25 homologs, which are required to establish and maintain kinetochore-microtubule attachment.* Curr Biol, 2004. **14**(2): p. 131-7.
30. Bharadwaj, R., W. Qi, and H. Yu, *Identification of two novel components of the human NDC80 kinetochore complex.* J Biol Chem, 2004. **279**(13): p. 13076-85.
31. Cheeseman, I.M., et al., *The conserved KMN network constitutes the core microtubule-binding site of the kinetochore.* Cell, 2006. **127**(5): p. 983-97.
32. Theis, M., et al., *Comparative profiling identifies C13orf3 as a component of the Ska complex required for mammalian cell division.* EMBO J, 2009. **28**(10): p. 1453-65.
33. Welburn, J.P., et al., *The human kinetochore Ska1 complex facilitates microtubule depolymerization-coupled motility.* Dev Cell, 2009. **16**(3): p. 374-85.
34. Raaijmakers, J.A., et al., *RAMA1 is a novel kinetochore protein involved in kinetochore-microtubule attachment.* J Cell Sci, 2009. **122**(Pt 14): p. 2436-45.
35. Daum, J.R., et al., *Ska3 is required for spindle checkpoint silencing and the maintenance of chromosome cohesion in mitosis.* Curr Biol, 2009. **19**(17): p. 1467-72.
36. Hanisch, A., H.H. Sillje, and E.A. Nigg, *Timely anaphase onset requires a novel spindle and kinetochore complex comprising Ska1 and Ska2.* EMBO J, 2006. **25**(23): p. 5504-15.
37. Gaitanos, T.N., et al., *Stable kinetochore-microtubule interactions depend on the Ska complex and its new component Ska3/C13Orf3.* EMBO J, 2009. **28**(10): p. 1442-52.
38. Miranda, J.J., et al., *The yeast DASH complex forms closed rings on microtubules.* Nat Struct Mol Biol, 2005. **12**(2): p. 138-43.
39. Westermann, S., et al., *Formation of a dynamic kinetochore- microtubule interface through assembly of the Dam1 ring complex.* Mol Cell, 2005. **17**(2): p. 277-90.
40. Kops, G.J., A.T. Saurin, and P. Meraldi, *Finding the middle ground: how kinetochores power chromosome congression.* Cell Mol Life Sci, 2010. **67**(13): p. 2145-61.

41. McEwen, B.F., et al., *CENP-E is essential for reliable bioriented spindle attachment, but chromosome alignment can be achieved via redundant mechanisms in mammalian cells.* Mol Biol Cell, 2001. **12**(9): p. 2776-89.
42. Kapoor, T.M., et al., *Chromosomes can congress to the metaphase plate before biorientation.* Science, 2006. **311**(5759): p. 388-91.
43. Cleveland, D.W., Y. Mao, and K.F. Sullivan, *Centromeres and kinetochores: from epigenetics to mitotic checkpoint signaling.* Cell, 2003. **112**(4): p. 407-21.
44. Dujardin, D., et al., *Evidence for a role of CLIP-170 in the establishment of metaphase chromosome alignment.* J Cell Biol, 1998. **141**(4): p. 849-62.
45. Tanenbaum, M.E., et al., *CLIP-170 facilitates the formation of kinetochore-microtubule attachments.* EMBO J, 2006. **25**(1): p. 45-57.
46. Wordeman, L. and T.J. Mitchison, *Identification and partial characterization of mitotic centromere-associated kinesin, a kinesin-related protein that associates with centromeres during mitosis.* J Cell Biol, 1995. **128**(1-2): p. 95-104.
47. Yang, Z., et al., *Kinetochore dynein is required for chromosome motion and congression independent of the spindle checkpoint.* Curr Biol, 2007. **17**(11): p. 973-80.
48. Howell, B.J., et al., *Cytoplasmic dynein/dynactin drives kinetochore protein transport to the spindle poles and has a role in mitotic spindle checkpoint inactivation.* J Cell Biol, 2001. **155**(7): p. 1159-72.
49. Maiato, H., A. Khodjakov, and C.L. Rieder, *Drosophila CLASP is required for the incorporation of microtubule subunits into fluxing kinetochore fibres.* Nat Cell Biol, 2005. **7**(1): p. 42-7.
50. Arnaud, L., J. Pines, and E.A. Nigg, *GFP tagging reveals human Polo-like kinase 1 at the kinetochore/centromere region of mitotic chromosomes.* Chromosoma, 1998. **107**(6-7): p. 424-9.
51. Rattner, J.B., et al., *CENP-F is a .ca 400 kDa kinetochore protein that exhibits a cell-cycle dependent localization.* Cell Motil Cytoskeleton, 1993. **26**(3): p. 214-26.
52. Kitajima, T.S., M. Ohsugi, and J. Ellenberg, *Complete kinetochore tracking reveals error-prone homologous chromosome biorientation in mammalian oocytes.* Cell, 2011. **146**(4): p. 568-81.
53. Tanaka, T.U., et al., *Evidence that the Ipl1-Sli15 (Aurora kinase-INCENP) complex promotes chromosome bi-orientation by altering kinetochore-spindle pole connections.* Cell, 2002. **108**(3): p. 317-29.
54. Hauf, S., et al., *The small molecule Hesperadin reveals a role for Aurora B in correcting kinetochore-microtubule attachment and in maintaining the spindle assembly checkpoint.* J Cell Biol, 2003. **161**(2): p. 281-94.
55. Lampson, M.A., et al., *Correcting improper chromosome-spindle attachments during cell division.* Nat Cell Biol, 2004. **6**(3): p. 232-7.
56. Cimini, D., et al., *Aurora kinase promotes turnover of kinetochore microtubules to reduce chromosome segregation errors.* Curr Biol, 2006. **16**(17): p. 1711-8.
57. Ruchaud, S., M. Carmena, and W.C. Earnshaw, *Chromosomal passengers: conducting cell division.* Nat Rev Mol Cell Biol, 2007. **8**(10): p. 798-812.
58. DeLuca, J.G., et al., *Kinetochore microtubule dynamics and attachment stability are regulated by Hec1.* Cell, 2006. **127**(5): p. 969-82.
59. Welburn, J.P., et al., *Aurora B phosphorylates spatially distinct targets to differentially regulate the kinetochore-microtubule interface.* Mol Cell, 2010. **38**(3): p. 383-92.
60. Liu, D., et al., *Regulated targeting of protein phosphatase 1 to the outer kinetochore by KNL1 opposes Aurora B kinase.* J Cell Biol, 2010. **188**(6): p. 809-20.
61. Kim, Y., et al., *Aurora kinases and protein phosphatase 1 mediate chromosome congression through regulation of CENP-E.* Cell, 2010. **142**(3): p. 444-55.
62. Andrews, P.D., et al., *Aurora B regulates MCAK at the mitotic centromere.* Dev Cell, 2004. **6**(2): p. 253-68.
63. Lan, W., et al., *Aurora B phosphorylates centromeric MCAK and regulates its localization and microtubule depolymerization activity.* Curr Biol, 2004. **14**(4): p. 273-86.
64. Knowlton, A.L., W. Lan, and P.T. Stukenberg, *Aurora B is enriched at merotelic attachment sites, where it regulates MCAK.* Curr Biol, 2006. **16**(17): p. 1705-10.
65. Zhang, X., et al., *Aurora B phosphorylates multiple sites on mitotic centromere-associated kinesin to spatially and temporally regulate its function.* Mol Biol Cell, 2007. **18**(9): p. 3264-76.
66. Liu, D., et al., *Sensing chromosome bi-orientation by spatial separation of aurora B kinase from kinetochore substrates.* Science, 2009. **323**(5919): p. 1350-3.
67. DeLuca, K.F., S.M. Lens, and J.G. DeLuca, *Temporal changes in Hec1 phosphorylation control kinetochore-microtubule attachment stability during mitosis.* J Cell Sci, 2011. **124**(Pt 4): p. 622-34.
68. Li, X. and R.B. Nicklas, *Mitotic forces control a cell-cycle checkpoint.* Nature, 1995. **373**(6515): p. 630-2.
69. Rieder, C.L., et al., *Anaphase onset in vertebrate somatic cells is controlled by a checkpoint that monitors sister kinetochore attachment to the spindle.* J Cell Biol, 1994. **127**(5): p. 1301-10.
70. Rieder, C.L., et al., *The checkpoint delaying anaphase in response to chromosome monoorientation is mediated by an inhibitory signal produced by unattached kinetochores.* J Cell Biol, 1995. **130**(4): p. 941-8.
71. Hoyt, M.A., L. Totis, and B.T. Roberts, *S. cerevisiae genes required for cell cycle arrest in response to loss of microtubule function.* Cell, 1991. **66**(3): p. 507-17.
72. Li, R. and A.W. Murray, *Feedback control of mitosis in budding yeast.* Cell, 1991. **66**(3): p. 519-31.
73. Li, Y. and R. Benezra, *Identification of a human mitotic checkpoint gene: hsMAD2.* Science, 1996. **274**(5285): p. 246-8.
74. Taylor, S.S. and F. McKeon, *Kinetochore localization of murine Bub1 is required for normal mitotic timing and checkpoint response to spindle damage.* Cell, 1997. **89**(5): p. 727-35.
75. Campbell, M.S., G.K. Chan, and T.J. Yen, *Mitotic checkpoint proteins HsMAD1 and HsMAD2 are associated with nuclear pore complexes in interphase.* J Cell Sci, 2001. **114**(Pt 5): p. 953-63.
76. Taylor, S.S., E. Ha, and F. McKeon, *The human homologue of Bub3 is required for kinetochore localization of Bub1 and a Mad3/Bub1-related protein kinase.* J Cell Biol, 1998. **142**(1): p. 1-11.
77. Peters, J.M., *The anaphase promoting complex/cyclosome: a machine designed to destroy.* Nat Rev Mol Cell Biol, 2006. **7**(9): p. 644-56.
78. Yu, H., et al., *Identification of a novel ubiquitin-conjugating enzyme involved in mitotic cyclin degradation.* Curr Biol, 1996. **6**(4): p. 455-66.
79. Aristarkhov, A., et al., *E2-C, a cyclin-selective ubiquitin carrier protein required for the destruction of mitotic cyclins.* Proc Natl Acad Sci U S A, 1996. **93**(9): p. 4294-9.
80. Williamson, A., et al., *Identification of a physiological E2 module for the human anaphase-promoting complex.* Proc Natl Acad Sci U S A, 2009. **106**(43): p. 18213-8.
81. Garnett, M.J., et al., *UBE2S elongates ubiquitin chains on APC/C substrates to promote mitotic exit.* Nat Cell Biol, 2009. **11**(11): p. 1363-9.
82. Kulukian, A., J.S. Han, and D.W. Cleveland, *Unattached kinetochores catalyze production of an anaphase inhibitor that requires a Mad2 template to prime Cdc20 for BubR1 binding.* Dev Cell, 2009. **16**(1): p. 105-17.
83. Suijkerbuijk, S.J., et al., *The Vertebrate Mitotic Checkpoint Protein BUBR1 Is an Unusual Pseudokinase.* Dev Cell, 2012.

22(6): p. 1321-9.
84. Hwang, L.H., et al., *Budding yeast Cdc20: a target of the spindle checkpoint.* Science, 1998. **279**(5353): p. 1041-4.
85. Kim, S.H., et al., *Fission yeast Slp1: an effector of the Mad2-dependent spindle checkpoint.* Science, 1998. **279**(5353): p. 1045-7.
86. Fang, G., H. Yu, and M.W. Kirschner, *The checkpoint protein MAD2 and the mitotic regulator CDC20 form a ternary complex with the anaphase-promoting complex to control anaphase initiation.* Genes Dev, 1998. **12**(12): p. 1871-83.
87. Wassmann, K. and R. Benezra, *Mad2 transiently associates with an APC/p55Cdc complex during mitosis.* Proc Natl Acad Sci U S A, 1998. **95**(19): p. 11193-8.
88. Wu, H., et al., *p55CDC/hCDC20 is associated with BUBR1 and may be a downstream target of the spindle checkpoint kinase.* Oncogene, 2000. **19**(40): p. 4557-62.
89. Hardwick, K.G., et al., *MAD3 encodes a novel component of the spindle checkpoint which interacts with Bub3p, Cdc20p, and Mad2p.* J Cell Biol, 2000. **148**(5): p. 871-82.
90. Tang, Z., et al., *Mad2-Independent inhibition of APCCdc20 by the mitotic checkpoint protein BubR1.* Dev Cell, 2001. **1**(2): p. 227-37.
91. Sudakin, V., G.K. Chan, and T.J. Yen, *Checkpoint inhibition of the APC/C in HeLa cells is mediated by a complex of BUBR1, BUB3, CDC20, and MAD2.* J Cell Biol, 2001. **154**(5): p. 925-36.
92. Fraschini, R., et al., *Bub3 interaction with Mad2, Mad3 and Cdc20 is mediated by WD40 repeats and does not require intact kinetochores.* EMBO J, 2001. **20**(23): p. 6648-59.
93. Millband, D.N. and K.G. Hardwick, *Fission yeast Mad3p is required for Mad2p to inhibit the anaphase-promoting complex and localizes to kinetochores in a Bub1p-, Bub3p-, and Mph1p-dependent manner.* Mol Cell Biol, 2002. **22**(8): p. 2728-42.
94. Poddar, A., P.T. Stukenberg, and D.J. Burke, *Two complexes of spindle checkpoint proteins containing Cdc20 and Mad2 assemble during mitosis independently of the kinetochore in Saccharomyces cerevisiae.* Eukaryot Cell, 2005. **4**(5): p. 867-78.
95. Irniger, S., et al., *Genes involved in sister chromatid separation are needed for B-type cyclin proteolysis in budding yeast.* Cell, 1995. **81**(2): p. 269-78.
96. Sudakin, V., et al., *The cyclosome, a large complex containing cyclin-selective ubiquitin ligase activity, targets cyclins for destruction at the end of mitosis.* Mol Biol Cell, 1995. **6**(2): p. 185-97.
97. King, R.W., et al., *A 20S complex containing CDC27 and CDC16 catalyzes the mitosis-specific conjugation of ubiquitin to cyclin B.* Cell, 1995. **81**(2): p. 279-88.
98. Cohen-Fix, O., et al., *Anaphase initiation in Saccharomyces cerevisiae is controlled by the APC-dependent degradation of the anaphase inhibitor Pds1p.* Genes Dev, 1996. **10**(24): p. 3081-93.
99. Funabiki, H., K. Kumada, and M. Yanagida, *Fission yeast Cut1 and Cut2 are essential for sister chromatid separation, concentrate along the metaphase spindle and form large complexes.* EMBO J, 1996. **15**(23): p. 6617-28.
100. Holloway, S.L., et al., *Anaphase is initiated by proteolysis rather than by the inactivation of maturation-promoting factor.* Cell, 1993. **73**(7): p. 1393-402.
101. Uhlmann, F., F. Lottspeich, and K. Nasmyth, *Sister-chromatid separation at anaphase onset is promoted by cleavage of the cohesin subunit Scc1.* Nature, 1999. **400**(6739): p. 37-42.
102. Luo, X., et al., *The Mad2 spindle checkpoint protein undergoes similar major conformational changes upon binding to either Mad1 or Cdc20.* Mol Cell, 2002. **9**(1): p. 59-71.
103. Sironi, L., et al., *Crystal structure of the tetrameric Mad1-Mad2 core complex: implications of a 'safety belt' binding mechanism for the spindle checkpoint.* EMBO J, 2002. **21**(10): p. 2496-506.
104. Mapelli, M., et al., *The Mad2 conformational dimer: structure and implications for the spindle assembly checkpoint.* Cell, 2007. **131**(4): p. 730-43.
105. Luo, X., et al., *The Mad2 spindle checkpoint protein has two distinct natively folded states.* Nat Struct Mol Biol, 2004. **11**(4): p. 338-45.
106. De Antoni, A., et al., *The Mad1/Mad2 complex as a template for Mad2 activation in the spindle assembly checkpoint.* Curr Biol, 2005. **15**(3): p. 214-25.
107. Lara-Gonzalez, P., et al., *BubR1 blocks substrate recruitment to the APC/C in a KEN-box-dependent manner.* J Cell Sci, 2011. **124**(Pt 24): p. 4332-45.
108. Burton, J.L. and M.J. Solomon, *Mad3p, a pseudosubstrate inhibitor of APCCdc20 in the spindle assembly checkpoint.* Genes Dev, 2007. **21**(6): p. 655-67.
109. Elowe, S., et al., *Uncoupling of the spindle-checkpoint and chromosome-congression functions of BubR1.* J Cell Sci, 2010. **123**(Pt 1): p. 84-94.
110. King, E.M., S.J. van der Sar, and K.G. Hardwick, *Mad3 KEN boxes mediate both Cdc20 and Mad3 turnover, and are critical for the spindle checkpoint.* PLoS One, 2007. **2**(4): p. e342.
111. Pfleger, C.M. and M.W. Kirschner, *The KEN box: an APC recognition signal distinct from the D box targeted by Cdh1.* Genes Dev, 2000. **14**(6): p. 655-65.
112. Tang, Z., et al., *Phosphorylation of Cdc20 by Bub1 provides a catalytic mechanism for APC/C inhibition by the spindle checkpoint.* Mol Cell, 2004. **16**(3): p. 387-97.
113. Klebig, C., D. Korinth, and P. Meraldi, *Bub1 regulates chromosome segregation in a kinetochore-independent manner.* J Cell Biol, 2009. **185**(5): p. 841-58.
114. Warren, C.D., et al., *Distinct chromosome segregation roles for spindle checkpoint proteins.* Mol Biol Cell, 2002. **13**(9): p. 3029-41.
115. Perera, D., et al., *Bub1 maintains centromeric cohesion by activation of the spindle checkpoint.* Dev Cell, 2007. **13**(4): p. 566-79.
116. Jelluma, N., et al., *Mps1 phosphorylates Borealin to control Aurora B activity and chromosome alignment.* Cell, 2008. **132**(2): p. 233-46.
117. Tighe, A., O. Staples, and S. Taylor, *Mps1 kinase activity restrains anaphase during an unperturbed mitosis and targets Mad2 to kinetochores.* J Cell Biol, 2008. **181**(6): p. 893-901.
118. Sliedrecht, T., et al., *Chemical genetic inhibition of Mps1 in stable human cell lines reveals novel aspects of Mps1 function in mitosis.* PLoS One, 2010. **5**(4): p. e10251.
119. Maciejowski, J., et al., *Mps1 directs the assembly of Cdc20 inhibitory complexes during interphase and mitosis to control M phase timing and spindle checkpoint signaling.* J Cell Biol, 2010. **190**(1): p. 89-100.
120. Yamagishi, Y., et al., *MPS1/Mph1 phosphorylates the kinetochore protein KNL1/Spc7 to recruit SAC components.* Nat Cell Biol, 2012.
121. Shepperd, L.A., et al., *Phosphodependent Recruitment of Bub1 and Bub3 to Spc7/KNL1 by Mph1 Kinase Maintains the Spindle Checkpoint.* Curr Biol, 2012. **22**(10): p. 891-9.
122. London, N., et al., *Phosphoregulation of Spc105 by Mps1 and PP1 Regulates Bub1 Localization to Kinetochores.* Curr Biol, 2012. **22**(10): p. 900-6.
123. Kwiatkowski, N., et al., *Small-molecule kinase inhibitors provide insight into Mps1 cell cycle function.* Nat Chem Biol,

2010. **6**(5): p. 359-68.
124. Liu, S.T., et al., *Human MPS1 kinase is required for mitotic arrest induced by the loss of CENP-E from kinetochores.* Mol Biol Cell, 2003. **14**(4): p. 1638-51.
125. Martin-Lluesma, S., V.M. Stucke, and E.A. Nigg, *Role of Hec1 in spindle checkpoint signaling and kinetochore recruitment of Mad1/Mad2.* Science, 2002. **297**(5590): p. 2267-70.
126. Gassmann, R., et al., *Removal of Spindly from microtubule-attached kinetochores controls spindle checkpoint silencing in human cells.* Genes Dev, 2010. **24**(9): p. 957-71.
127. Vanoosthuyse, V. and K.G. Hardwick, *A novel protein phosphatase 1-dependent spindle checkpoint silencing mechanism.* Curr Biol, 2009. **19**(14): p. 1176-81.
128. Habu, T., et al., *Identification of a MAD2-binding protein, CMT2, and its role in mitosis.* EMBO J, 2002. **21**(23): p. 6419-28.
129. Xia, G., et al., *Conformation-specific binding of p31(comet) antagonizes the function of Mad2 in the spindle checkpoint.* EMBO J, 2004. **23**(15): p. 3133-43.
130. Yang, M., et al., *p31comet blocks Mad2 activation through structural mimicry.* Cell, 2007. **131**(4): p. 744-55.
131. Mapelli, M., et al., *Determinants of conformational dimerization of Mad2 and its inhibition by p31comet.* EMBO J, 2006. **25**(6): p. 1273-84.
132. Varetti, G., et al., *Homeostatic control of mitotic arrest.* Mol Cell, 2011. **44**(5): p. 710-20.
133. Westhorpe, F.G., et al., *p31comet-mediated extraction of Mad2 from the MCC promotes efficient mitotic exit.* J Cell Sci, 2011. **124**(Pt 22): p. 3905-16.
134. Teichner, A., et al., *p31comet Promotes disassembly of the mitotic checkpoint complex in an ATP-dependent process.* Proc Natl Acad Sci U S A, 2011. **108**(8): p. 3187-92.
135. Reddy, S.K., et al., *Ubiquitination by the anaphase-promoting complex drives spindle checkpoint inactivation.* Nature, 2007. **446**(7138): p. 921-5.
136. Nilsson, J., et al., *The APC/C maintains the spindle assembly checkpoint by targeting Cdc20 for destruction.* Nat Cell Biol, 2008. **10**(12): p. 1411-20.
137. Winey, M., et al., *MPS1 and MPS2: novel yeast genes defining distinct steps of spindle pole body duplication.* J Cell Biol, 1991. **114**(4): p. 745-54.
138. Poch, O., et al., *RPK1, an essential yeast protein kinase involved in the regulation of the onset of mitosis, shows homology to mammalian dual-specificity kinases.* Mol Gen Genet, 1994. **243**(6): p. 641-53.
139. Lauze, E., et al., *Yeast spindle pole body duplication gene MPS1 encodes an essential dual specificity protein kinase.* EMBO J, 1995. **14**(8): p. 1655-63.
140. Weiss, E. and M. Winey, *The Saccharomyces cerevisiae spindle pole body duplication gene MPS1 is part of a mitotic checkpoint.* J Cell Biol, 1996. **132**(1-2): p. 111-23.
141. Hardwick, K.G., et al., *Activation of the budding yeast spindle assembly checkpoint without mitotic spindle disruption.* Science, 1996. **273**(5277): p. 953-6.
142. Abrieu, A., et al., *Mps1 is a kinetochore-associated kinase essential for the vertebrate mitotic checkpoint.* Cell, 2001. **106**(1): p. 83-93.
143. Stucke, V.M., et al., *Human Mps1 kinase is required for the spindle assembly checkpoint but not for centrosome duplication.* EMBO J, 2002. **21**(7): p. 1723-32.
144. Schutz, A.R. and M. Winey, *New alleles of the yeast MPS1 gene reveal multiple requirements in spindle pole body duplication.* Mol Biol Cell, 1998. **9**(4): p. 759-74.
145. Fisk, H.A. and M. Winey, *The mouse Mps1p-like kinase regulates centrosome duplication.* Cell, 2001. **106**(1): p. 95-
104.
146. Fisk, H.A., C.P. Mattison, and M. Winey, *Human Mps1 protein kinase is required for centrosome duplication and normal mitotic progression.* Proc Natl Acad Sci U S A, 2003. **100**(25): p. 14875-80.
147. Kasbek, C., et al., *Preventing the degradation of mps1 at centrosomes is sufficient to cause centrosome reduplication in human cells.* Mol Biol Cell, 2007. **18**(11): p. 4457-69.
148. Stucke, V.M., C. Baumann, and E.A. Nigg, *Kinetochore localization and microtubule interaction of the human spindle checkpoint kinase Mps1.* Chromosoma, 2004. **113**(1): p. 1-15.
149. Hogg, D., et al., *Cell cycle dependent regulation of the protein kinase TTK.* Oncogene, 1994. **9**(1): p. 89-96.
150. Mills, G.B., et al., *Expression of TTK, a novel human protein kinase, is associated with cell proliferation.* J Biol Chem, 1992. **267**(22): p. 16000-6.
151. Ren, B., et al., *E2F integrates cell cycle progression with DNA repair, replication, and G(2)/M checkpoints.* Genes Dev, 2002. **16**(2): p. 245-56.
152. Palframan, W.J., et al., *Anaphase inactivation of the spindle checkpoint.* Science, 2006. **313**(5787): p. 680-4.
153. Cui, Y., et al., *Degradation of the human mitotic checkpoint kinase Mps1 is cell cycle-regulated by APC-cCdc20 and APC-cCdh1 ubiquitin ligases.* J Biol Chem, 2010. **285**(43): p. 32988-98.
154. Saurin, A.T., et al., *Aurora B potentiates Mps1 activation to ensure rapid checkpoint establishment at the onset of mitosis.* Nat Commun, 2011. **2**: p. 316.
155. Santaguida, S., et al., *Evidence that Aurora B is implicated in spindle checkpoint signalling independently of error correction.* EMBO J, 2011. **30**(8): p. 1508-19.
156. Montembault, E., et al., *PRP4 is a spindle assembly checkpoint protein required for MPS1, MAD1, and MAD2 localization to the kinetochores.* J Cell Biol, 2007. **179**(4): p. 601-9.
157. Howell, B.J., et al., *Spindle checkpoint protein dynamics at kinetochores in living cells.* Curr Biol, 2004. **14**(11): p. 953-64.
158. Jelluma, N., et al., *Release of Mps1 from kinetochores is crucial for timely anaphase onset.* J Cell Biol, 2010. **191**(2): p. 281-90.
159. Pike, A.N. and H.A. Fisk, *Centriole assembly and the role of Mps1: defensible or dispensable?* Cell Div, 2011. **6**: p. 9.
160. Kemmler, S., et al., *Mimicking Ndc80 phosphorylation triggers spindle assembly checkpoint signalling.* EMBO J, 2009. **28**(8): p. 1099-110.
161. Espeut, J., et al., *Phosphorylation relieves autoinhibition of the kinetochore motor Cenp-E.* Mol Cell, 2008. **29**(5): p. 637-43.
162. Wei, J.H., et al., *TTK/hMps1 participates in the regulation of DNA damage checkpoint response by phosphorylating CHK2 on threonine 68.* J Biol Chem, 2005. **280**(9): p. 7748-57.
163. Leng, M., et al., *MPS1-dependent mitotic BLM phosphorylation is important for chromosome stability.* Proc Natl Acad Sci U S A, 2006. **103**(31): p. 11485-90.
164. Huang, Y.F., M.D. Chang, and S.Y. Shieh, *TTK/hMps1 mediates the p53-dependent postmitotic checkpoint by phosphorylating p53 at Thr18.* Mol Cell Biol, 2009. **29**(11): p. 2935-44.
165. Bhonde, M.R., et al., *DNA damage-induced expression of p53 suppresses mitotic checkpoint kinase hMps1: the lack of this suppression in p53MUT cells contributes to apoptosis.* J Biol Chem, 2006. **281**(13): p. 8675-85.
166. Yeh, Y.H., et al., *The cell cycle checkpoint kinase CHK2 mediates DNA damage-induced stabilization of TTK/hMps1.*

Oncogene, 2009. **28**(10): p. 1366-78.
167. Liu, X. and M. Winey, *The MPS1 Family of Protein Kinases.* Annu Rev Biochem, 2012.
168. Chu, M.L., et al., *Crystal structure of the catalytic domain of the mitotic checkpoint kinase Mps1 in complex with SP600125.* J Biol Chem, 2008. **283**(31): p. 21495-500.
169. Wang, W., et al., *Structural and mechanistic insights into Mps1 kinase activation.* J Cell Mol Med, 2009. **13**(8B): p. 1679-94.
170. Mattison, C.P., et al., *Mps1 activation loop autophosphorylation enhances kinase activity.* J Biol Chem, 2007. **282**(42): p. 30553-61.
171. Kang, J., et al., *Autophosphorylation-dependent activation of human Mps1 is required for the spindle checkpoint.* Proc Natl Acad Sci U S A, 2007. **104**(51): p. 20232-7.
172. Jelluma, N., et al., *Chromosomal instability by inefficient Mps1 auto-activation due to a weakened mitotic checkpoint and lagging chromosomes.* PLoS One, 2008. **3**(6): p. e2415.
173. Xu, Q., et al., *Regulation of kinetochore recruitment of two essential mitotic spindle checkpoint proteins by Mps1 phosphorylation.* Mol Biol Cell, 2009. **20**(1): p. 10-20.
174. Dou, Z., et al., *Quantitative mass spectrometry analysis reveals similar substrate consensus motif for human Mps1 kinase and Plk1.* PLoS One, 2011. **6**(4): p. e18793.
175. Tyler, R.K., et al., *Phosphoregulation of human Mps1 kinase.* Biochem J, 2009. **417**(1): p. 173-81.
176. Colombo, R., et al., *Targeting the mitotic checkpoint for cancer therapy with NMS-P715, an inhibitor of MPS1 kinase.* Cancer Res, 2010. **70**(24): p. 10255-64.
177. Glotzer, M., *The 3Ms of central spindle assembly: microtubules, motors and MAPs.* Nat Rev Mol Cell Biol, 2009. **10**(1): p. 9-20.
178. Jiang, W., et al., *PRC1: a human mitotic spindle-associated CDK substrate protein required for cytokinesis.* Mol Cell, 1998. **2**(6): p. 877-85.
179. Mishima, M., S. Kaitna, and M. Glotzer, *Central spindle assembly and cytokinesis require a kinesin-like protein/RhoGAP complex with microtubule bundling activity.* Dev Cell, 2002. **2**(1): p. 41-54.
180. Pavicic-Kaltenbrunner, V., M. Mishima, and M. Glotzer, *Cooperative assembly of CYK-4/MgcRacGAP and ZEN-4/MKLP1 to form the centralspindlin complex.* Mol Biol Cell, 2007. **18**(12): p. 4992-5003.
181. Yuce, O., A. Piekny, and M. Glotzer, *An ECT2-centralspindlin complex regulates the localization and function of RhoA.* J Cell Biol, 2005. **170**(4): p. 571-82.
182. Wolfe, B.A., et al., *Polo-like kinase 1 directs assembly of the HsCyk-4 RhoGAP/Ect2 RhoGEF complex to initiate cleavage furrow formation.* PLoS Biol, 2009. **7**(5): p. e1000110.
183. Neef, R., et al., *Choice of Plk1 docking partners during mitosis and cytokinesis is controlled by the activation state of Cdk1.* Nat Cell Biol, 2007. **9**(4): p. 436-44.
184. Lens, S.M., E.E. Voest, and R.H. Medema, *Shared and separate functions of polo-like kinases and aurora kinases in cancer.* Nat Rev Cancer, 2010. **10**(12): p. 825-41.
185. Neef, R., et al., *Cooperation between mitotic kinesins controls the late stages of cytokinesis.* Curr Biol, 2006. **16**(3): p. 301-7.
186. Vazquez-Novelle, M.D. and M. Petronczki, *Relocation of the chromosomal passenger complex prevents mitotic checkpoint engagement at anaphase.* Curr Biol, 2010. **20**(15): p. 1402-7.
187. Ban, R., et al., *Human mitotic spindle-associated protein PRC1 inhibits MgcRacGAP activity toward Cdc42 during the metaphase.* J Biol Chem, 2004. **279**(16): p. 16394-402.
188. Bement, W.M., H.A. Benink, and G. von Dassow, *A microtubule-dependent zone of active RhoA during cleavage plane specification.* J Cell Biol, 2005. **170**(1): p. 91-101.
189. Nishimura, Y. and S. Yonemura, *Centralspindlin regulates ECT2 and RhoA accumulation at the equatorial cortex during cytokinesis.* J Cell Sci, 2006. **119**(Pt 1): p. 104-14.
190. Matsumura, F., *Regulation of myosin II during cytokinesis in higher eukaryotes.* Trends Cell Biol, 2005. **15**(7): p. 371-7.
191. Castrillon, D.H. and S.A. Wasserman, *Diaphanous is required for cytokinesis in Drosophila and shares domains of similarity with the products of the limb deformity gene.* Development, 1994. **120**(12): p. 3367-77.
192. Severson, A.F., D.L. Baillie, and B. Bowerman, *A Formin Homology protein and a profilin are required for cytokinesis and Arp2/3-independent assembly of cortical microfilaments in C. elegans.* Curr Biol, 2002. **12**(24): p. 2066-75.
193. Watanabe, S., et al., *mDia2 induces the actin scaffold for the contractile ring and stabilizes its position during cytokinesis in NIH 3T3 cells.* Mol Biol Cell, 2008. **19**(5): p. 2328-38.
194. Fededa, J.P. and D.W. Gerlich, *Molecular control of animal cell cytokinesis.* Nat Cell Biol, 2012. **14**(5): p. 440-7.
195. Skop, A.R., et al., *Dissection of the mammalian midbody proteome reveals conserved cytokinesis mechanisms.* Science, 2004. **305**(5680): p. 61-6.
196. Steigemann, P., et al., *Aurora B-mediated abscission checkpoint protects against tetraploidization.* Cell, 2009. **136**(3): p. 473-84.
197. Norden, C., et al., *The NoCut pathway links completion of cytokinesis to spindle midzone function to prevent chromosome breakage.* Cell, 2006. **125**(1): p. 85-98.
198. Hoeijmakers, J.H., *Genome maintenance mechanisms for preventing cancer.* Nature, 2001. **411**(6835): p. 366-74.
199. Ciccia, A. and S.J. Elledge, *The DNA damage response: making it safe to play with knives.* Mol Cell, 2010. **40**(2): p. 179-204.
200. Walker, J.R., R.A. Corpina, and J. Goldberg, *Structure of the Ku heterodimer bound to DNA and its implications for double-strand break repair.* Nature, 2001. **412**(6847): p. 607-14.
201. Kienker, L.J., E.K. Shin, and K. Meek, *Both V(D)J recombination and radioresistance require DNA-PK kinase activity, though minimal levels suffice for V(D)J recombination.* Nucleic Acids Res, 2000. **28**(14): p. 2752-61.
202. Kurimasa, A., et al., *Requirement for the kinase activity of human DNA-dependent protein kinase catalytic subunit in DNA strand break rejoining.* Mol Cell Biol, 1999. **19**(5): p. 3877-84.
203. Costantini, S., et al., *Interaction of the Ku heterodimer with the DNA ligase IV/Xrcc4 complex and its regulation by DNA-PK.* DNA Repair (Amst), 2007. **6**(6): p. 712-22.
204. Nick McElhinny, S.A., et al., *Ku recruits the XRCC4-ligase IV complex to DNA ends.* Mol Cell Biol, 2000. **20**(9): p. 2996-3003.
205. Oliver, F.J., J. Menissier-de Murcia, and G. de Murcia, *Poly(ADP-ribose) polymerase in the cellular response to DNA damage, apoptosis, and disease.* Am J Hum Genet, 1999. **64**(5): p. 1282-8.
206. Lim, D.S., et al., *ATM phosphorylates p95/nbs1 in an S-phase checkpoint pathway.* Nature, 2000. **404**(6778): p. 613-7.
207. Rogakou, E.P., et al., *DNA double-stranded breaks induce histone H2AX phosphorylation on serine 139.* J Biol Chem, 1998. **273**(10): p. 5858-68.
208. Burma, S., et al., *ATM phosphorylates histone H2AX in response to DNA double-strand breaks.* J Biol Chem, 2001. **276**(45): p. 42462-7.
209. Celeste, A., et al., *Histone H2AX phosphorylation is dispensable for the initial recognition of DNA breaks.* Nat Cell Biol, 2003. **5**(7): p. 675-9.

210. Stucki, M., et al., *MDC1 directly binds phosphorylated histone H2AX to regulate cellular responses to DNA double-strand breaks.* Cell, 2005. **123**(7): p. 1213-26.
211. Lee, M.S., et al., *Structure of the BRCT repeat domain of MDC1 and its specificity for the free COOH-terminal end of the gamma-H2AX histone tail.* J Biol Chem, 2005. **280**(37): p. 32053-6.
212. Lou, Z., et al., *MDC1 maintains genomic stability by participating in the amplification of ATM-dependent DNA damage signals.* Mol Cell, 2006. **21**(2): p. 187-200.
213. Schultz, L.B., et al., *p53 binding protein 1 (53BP1) is an early participant in the cellular response to DNA double-strand breaks.* J Cell Biol, 2000. **151**(7): p. 1381-90.
214. Bothmer, A., et al., *53BP1 regulates DNA resection and the choice between classical and alternative end joining during class switch recombination.* J Exp Med, 2010. **207**(4): p. 855-65.
215. Bouwman, P., et al., *53BP1 loss rescues BRCA1 deficiency and is associated with triple-negative and BRCA-mutated breast cancers.* Nat Struct Mol Biol, 2010. **17**(6): p. 688-95.
216. Bunting, S.F., et al., *53BP1 inhibits homologous recombination in Brca1-deficient cells by blocking resection of DNA breaks.* Cell, 2010. **141**(2): p. 243-54.
217. Botuyan, M.V., et al., *Structural basis for the methylation state-specific recognition of histone H4-K20 by 53BP1 and Crb2 in DNA repair.* Cell, 2006. **127**(7): p. 1361-73.
218. Huyen, Y., et al., *Methylated lysine 79 of histone H3 targets 53BP1 to DNA double-strand breaks.* Nature, 2004. **432**(7015): p. 406-11.
219. North, S. and P. Hainaut, *p53 and cell-cycle control: a finger in every pie.* Pathol Biol (Paris), 2000. **48**(3): p. 255-70.
220. Harper, J.W., et al., *The p21 Cdk-interacting protein Cip1 is a potent inhibitor of G1 cyclin-dependent kinases.* Cell, 1993. **75**(4): p. 805-16.
221. Canman, C.E., et al., *Activation of the ATM kinase by ionizing radiation and phosphorylation of p53.* Science, 1998. **281**(5383): p. 1677-9.
222. Banin, S., et al., *Enhanced phosphorylation of p53 by ATM in response to DNA damage.* Science, 1998. **281**(5383): p. 1674-7.
223. Dumaz, N. and D.W. Meek, *Serine15 phosphorylation stimulates p53 transactivation but does not directly influence interaction with HDM2.* EMBO J, 1999. **18**(24): p. 7002-10.
224. Dumaz, N., D.M. Milne, and D.W. Meek, *Protein kinase CK1 is a p53-threonine 18 kinase which requires prior phosphorylation of serine 15.* FEBS Lett, 1999. **463**(3): p. 312-6.
225. Melchionna, R., et al., *Threonine 68 is required for radiation-induced phosphorylation and activation of Cds1.* Nat Cell Biol, 2000. **2**(10): p. 762-5.
226. Ahn, J.Y., et al., *Threonine 68 phosphorylation by ataxia telangiectasia mutated is required for efficient activation of Chk2 in response to ionizing radiation.* Cancer Res, 2000. **60**(21): p. 5934-6.
227. Chehab, N.H., et al., *Chk2/hCds1 functions as a DNA damage checkpoint in G(1) by stabilizing p53.* Genes Dev, 2000. **14**(3): p. 278-88.
228. Shieh, S.Y., et al., *The human homologs of checkpoint kinases Chk1 and Cds1 (Chk2) phosphorylate p53 at multiple DNA damage-inducible sites.* Genes Dev, 2000. **14**(3): p. 289-300.
229. Hirao, A., et al., *DNA damage-induced activation of p53 by the checkpoint kinase Chk2.* Science, 2000. **287**(5459): p. 1824-7.
230. Maya, R., et al., *ATM-dependent phosphorylation of Mdm2 on serine 395: role in p53 activation by DNA damage.* Genes Dev, 2001. **15**(9): p. 1067-77.
231. Lengauer, C., K.W. Kinzler, and B. Vogelstein, *Genetic instabilities in human cancers.* Nature, 1998. **396**(6712): p. 643-9.
232. Boveri, T., *Zur Frage der Entstehung maligner Tumoren vol.1.* 1914.
233. Hansemann, D.P.v., *Ueber patologische Mitosen.* Archiv für pathologische Anatomie and Physiologie und für klinische Medicin, 1891. **119**: p. 299-326.
234. Nowell, P.C., *The minute chromosome (Phl) in chronic granulocytic leukemia.* Blut, 1962. **8**: p. 65-6.
235. Mitelman, F., et al., *Clinical significance of cytogenetic findings in solid tumors.* Cancer Genet Cytogenet, 1997. **95**(1): p. 1-8.
236. Mitelman, F., B. Johansson, and F. Mertens, *Mitelman Database of Chromosome Aberrations and Gene Fusions in Cancer http://cgap.nci.nih.gov/Chromosomes/Mitelman.* 2012.
237. Hanahan, D. and R.A. Weinberg, *Hallmarks of cancer: the next generation.* Cell, 2011. **144**(5): p. 646-74.
238. Obe, G. and M. Durante, *DNA double strand breaks and chromosomal aberrations.* Cytogenet Genome Res, 2010. **128**(1-3): p. 8-16.
239. Obe, G., et al., *Chromosomal aberrations: formation, identification and distribution.* Mutat Res, 2002. **504**(1-2): p. 17-36.
240. Mitelman, F., B. Johansson, and F. Mertens, *The impact of translocations and gene fusions on cancer causation.* Nat Rev Cancer, 2007. **7**(4): p. 233-45.
241. Look, A.T., *Oncogenic transcription factors in the human acute leukemias.* Science, 1997. **278**(5340): p. 1059-64.
242. Nambiar, M., V. Kari, and S.C. Raghavan, *Chromosomal translocations in cancer.* Biochim Biophys Acta, 2008. **1786**(2): p. 139-52.
243. Beroukhim, R., et al., *The landscape of somatic copy-number alteration across human cancers.* Nature, 2010. **463**(7283): p. 899-905.
244. Castro, M.A., et al., *Chromosome aberrations in solid tumors have a stochastic nature.* Mutat Res, 2006. **600**(1-2): p. 150-64.
245. Roschke, A.V., et al., *Karyotypic complexity of the NCI-60 drug-screening panel.* Cancer Res, 2003. **63**(24): p. 8634-47.
246. Abdel-Rahman, W.M., et al., *Spectral karyotyping suggests additional subsets of colorectal cancers characterized by pattern of chromosome rearrangement.* Proc Natl Acad Sci U S A, 2001. **98**(5): p. 2538-43.
247. Davidson, J.M., et al., *Molecular cytogenetic analysis of breast cancer cell lines.* Br J Cancer, 2000. **83**(10): p. 1309-17.
248. Thompson, S.L. and D.A. Compton, *Chromosome missegregation in human cells arises through specific types of kinetochore-microtubule attachment errors.* Proc Natl Acad Sci U S A, 2011. **108**(44): p. 17974-8.
249. Nishizaki, T., et al., *Genetic alterations in lobular breast cancer by comparative genomic hybridization.* Int J Cancer, 1997. **74**(5): p. 513-7.
250. Nishizaki, T., et al., *Genetic alterations in primary breast cancers and their metastases: direct comparison using modified comparative genomic hybridization.* Genes Chromosomes Cancer, 1997. **19**(4): p. 267-72.
251. Natarajan, A.T. and F. Palitti, *DNA repair and chromosomal alterations.* Mutat Res, 2008. **657**(1): p. 3-7.
252. Duker, N.J., *Chromosome breakage syndromes and cancer.* Am J Med Genet, 2002. **115**(3): p. 125-9.
253. Matsuura, S., et al., *Positional cloning of the gene for Nijmegen breakage syndrome.* Nat Genet, 1998. **19**(2): p. 179-81.
254. Ellis, N.A., et al., *The Bloom's syndrome gene product is homologous to RecQ helicases.* Cell, 1995. **83**(4): p. 655-66.
255. Savitsky, K., et al., *A single ataxia telangiectasia gene with a product similar to PI-3 kinase.* Science, 1995. **268**(5218):

p. 1749-53.
256. Miki, Y., et al., *A strong candidate for the breast and ovarian cancer susceptibility gene BRCA1.* Science, 1994. **266**(5182): p. 66-71.
257. Wooster, R., et al., *Identification of the breast cancer susceptibility gene BRCA2.* Nature, 1995. **378**(6559): p. 789-92.
258. Bender, M.A., H.G. Griggs, and J.S. Bedford, *Mechanisms of chromosomal aberration production. 3. Chemicals and ionizing radiation.* Mutat Res, 1974. **23**(2): p. 197-212.
259. McClintock, B., *The Production of Homozygous Deficient Tissues with Mutant Characteristics by Means of the Aberrant Mitotic Behavior of Ring-Shaped Chromosomes.* Genetics, 1938. **23**(4): p. 315-76.
260. McClintock, B., *The Stability of Broken Ends of Chromosomes in Zea Mays.* Genetics, 1941. **26**(2): p. 234-82.
261. Hastie, N.D. and R.C. Allshire, *Human telomeres: fusion and interstitial sites.* Trends Genet, 1989. **5**(10): p. 326-31.
262. Gisselsson, D., et al., *Telomere dysfunction triggers extensive DNA fragmentation and evolution of complex chromosome abnormalities in human malignant tumors.* Proc Natl Acad Sci U S A, 2001. **98**(22): p. 12683-8.
263. Gisselsson, D., et al., *Abnormal nuclear shape in solid tumors reflects mitotic instability.* Am J Pathol, 2001. **158**(1): p. 199-206.
264. Gisselsson, D., et al., *Chromosomal breakage-fusion-bridge events cause genetic intratumor heterogeneity.* Proc Natl Acad Sci U S A, 2000. **97**(10): p. 5357-62.
265. Heim, S. and F. Mitelman, *Numerical chromosome aberrations in human neoplasia.* Cancer Genet Cytogenet, 1986. **22**(2): p. 99-108.
266. Baudis, M., *Genomic imbalances in 5918 malignant epithelial tumors: an explorative meta-analysis of chromosomal CGH data.* BMC Cancer, 2007. **7**: p. 226.
267. Pfau, S.J. and A. Amon, *Chromosomal instability and aneuploidy in cancer: from yeast to man.* EMBO Rep, 2012. **13**(6): p. 515-27.
268. Rehen, S.K., et al., *Constitutional aneuploidy in the normal human brain.* J Neurosci, 2005. **25**(9): p. 2176-80.
269. Duncan, A.W., et al., *The ploidy conveyor of mature hepatocytes as a source of genetic variation.* Nature, 2010. **467**(7316): p. 707-10.
270. Lengauer, C., K.W. Kinzler, and B. Vogelstein, *Genetic instability in colorectal cancers.* Nature, 1997. **386**(6625): p. 623-7.
271. Choi, C.M., et al., *Chromosomal instability is a risk factor for poor prognosis of adenocarcinoma of the lung: Fluorescence in situ hybridization analysis of paraffin-embedded tissue from Korean patients.* Lung Cancer, 2009. **64**(1): p. 66-70.
272. Carter, S.L., et al., *A signature of chromosomal instability inferred from gene expression profiles predicts clinical outcome in multiple human cancers.* Nat Genet, 2006. **38**(9): p. 1043-8.
273. Walther, A., R. Houlston, and I. Tomlinson, *Association between chromosomal instability and prognosis in colorectal cancer: a meta-analysis.* Gut, 2008. **57**(7): p. 941-50.
274. Bakhoum, S.F., et al., *Chromosomal instability substantiates poor prognosis in patients with diffuse large B-cell lymphoma.* Clin Cancer Res, 2011. **17**(24): p. 7704-11.
275. Kuukasjarvi, T., et al., *Genetic heterogeneity and clonal evolution underlying development of asynchronous metastasis in human breast cancer.* Cancer Res, 1997. **57**(8): p. 1597-604.
276. Gao, C., et al., *Chromosome instability, chromosome transcriptome, and clonal evolution of tumor cell populations.* Proc Natl Acad Sci U S A, 2007. **104**(21): p. 8995-9000.
277. Sheffer, M., et al., *Association of survival and disease progression with chromosomal instability: a genomic exploration of colorectal cancer.* Proc Natl Acad Sci U S A, 2009. **106**(17): p. 7131-6.
278. McClelland, S.E., R.A. Burrell, and C. Swanton, *Chromosomal instability: a composite phenotype that influences sensitivity to chemotherapy.* Cell Cycle, 2009. **8**(20): p. 3262-6.
279. Lee, A.J., et al., *Chromosomal instability confers intrinsic multidrug resistance.* Cancer Res, 2011. **71**(5): p. 1858-70.
280. Swanton, C., et al., *Chromosomal instability determines taxane response.* Proc Natl Acad Sci U S A, 2009. **106**(21): p. 8671-6.
281. Kolodner, R.D., D.W. Cleveland, and C.D. Putnam, *Cancer. Aneuploidy drives a mutator phenotype in cancer.* Science, 2011. **333**(6045): p. 942-3.
282. Weaver, B.A. and D.W. Cleveland, *Does aneuploidy cause cancer?* Curr Opin Cell Biol, 2006. **18**(6): p. 658-67.
283. Duesberg, P., R. Stindl, and R. Hehlmann, *Explaining the high mutation rates of cancer cells to drug and multidrug resistance by chromosome reassortments that are catalyzed by aneuploidy.* Proc Natl Acad Sci U S A, 2000. **97**(26): p. 14295-300.
284. Duesberg, P., et al., *The chromosomal basis of cancer.* Cell Oncol, 2005. **27**(5-6): p. 293-318.
285. Duesberg, P., et al., *Cancer drug resistance: the central role of the karyotype.* Drug Resist Updat, 2007. **10**(1-2): p. 51-8.
286. Baker, D.J., et al., *Whole chromosome instability caused by Bub1 insufficiency drives tumorigenesis through tumor suppressor gene loss of heterozygosity.* Cancer Cell, 2009. **16**(6): p. 475-86.
287. Nowak, M.A., et al., *The role of chromosomal instability in tumor initiation.* Proc Natl Acad Sci U S A, 2002. **99**(25): p. 16226-31.
288. Rajagopalan, H., et al., *The significance of unstable chromosomes in colorectal cancer.* Nat Rev Cancer, 2003. **3**(9): p. 695-701.
289. Thompson, S.L. and D.A. Compton, *Examining the link between chromosomal instability and aneuploidy in human cells.* J Cell Biol, 2008. **180**(4): p. 665-72.
290. Kops, G.J., B.A. Weaver, and D.W. Cleveland, *On the road to cancer: aneuploidy and the mitotic checkpoint.* Nat Rev Cancer, 2005. **5**(10): p. 773-85.
291. Michel, L.S., et al., *MAD2 haplo-insufficiency causes premature anaphase and chromosome instability in mammalian cells.* Nature, 2001. **409**(6818): p. 355-9.
292. Kops, G.J., D.R. Foltz, and D.W. Cleveland, *Lethality to human cancer cells through massive chromosome loss by inhibition of the mitotic checkpoint.* Proc Natl Acad Sci U S A, 2004. **101**(23): p. 8699-704.
293. Kalitsis, P., et al., *Bub3 gene disruption in mice reveals essential mitotic spindle checkpoint function during early embryogenesis.* Genes Dev, 2000. **14**(18): p. 2277-82.
294. Michel, L., et al., *Complete loss of the tumor suppressor MAD2 causes premature cyclin B degradation and mitotic failure in human somatic cells.* Proc Natl Acad Sci U S A, 2004. **101**(13): p. 4459-64.
295. Babu, J.R., et al., *Rae1 is an essential mitotic checkpoint regulator that cooperates with Bub3 to prevent chromosome missegregation.* J Cell Biol, 2003. **160**(3): p. 341-53.
296. Dai, W., et al., *Slippage of mitotic arrest and enhanced tumor development in mice with BubR1 haploinsufficiency.* Cancer Res, 2004. **64**(2): p. 440-5.
297. Baker, D.J., et al., *BubR1 insufficiency causes early onset of aging-associated phenotypes and infertility in mice.* Nat Genet, 2004. **36**(7): p. 744-9.
298. Iwanaga, Y., et al., *Heterozygous deletion of mitotic arrest-deficient protein 1 (MAD1) increases the incidence of*

tumors in mice. Cancer Res, 2007. **67**(1): p. 160-6.
299. Janssen, A., G.J. Kops, and R.H. Medema, *Elevating the frequency of chromosome mis-segregation as a strategy to kill tumor cells.* Proc Natl Acad Sci U S A, 2009. **106**(45): p. 19108-13.
300. Kalitsis, P., et al., *Increased chromosome instability but not cancer predisposition in haploinsufficient Bub3 mice.* Genes Chromosomes Cancer, 2005. **44**(1): p. 29-36.
301. Cahill, D.P., et al., *Mutations of mitotic checkpoint genes in human cancers.* Nature, 1998. **392**(6673): p. 300-3.
302. Tighe, A., et al., *Aneuploid colon cancer cells have a robust spindle checkpoint.* EMBO Rep, 2001. **2**(7): p. 609-14.
303. Hanks, S., et al., *Constitutional aneuploidy and cancer predisposition caused by biallelic mutations in BUB1B.* Nat Genet, 2004. **36**(11): p. 1159-61.
304. Matsuura, S., et al., *Monoallelic BUB1B mutations and defective mitotic-spindle checkpoint in seven families with premature chromatid separation (PCS) syndrome.* Am J Med Genet A, 2006. **140**(4): p. 358-67.
305. Wang, X., et al., *Significance of MAD2 expression to mitotic checkpoint control in ovarian cancer cells.* Cancer Res, 2002. **62**(6): p. 1662-8.
306. Wang, X., et al., *Correlation of defective mitotic checkpoint with aberrantly reduced expression of MAD2 protein in nasopharyngeal carcinoma cells.* Carcinogenesis, 2000. **21**(12): p. 2293-7.
307. Kasai, T., et al., *Prevalent loss of mitotic spindle checkpoint in adult T-cell leukemia confers resistance to microtubule inhibitors.* J Biol Chem, 2002. **277**(7): p. 5187-93.
308. Yoon, D.S., et al., *Variable levels of chromosomal instability and mitotic spindle checkpoint defects in breast cancer.* Am J Pathol, 2002. **161**(2): p. 391-7.
309. Minhas, K.M., et al., *Spindle assembly checkpoint defects and chromosomal instability in head and neck squamous cell carcinoma.* Int J Cancer, 2003. **107**(1): p. 46-52.
310. Saeki, A., et al., *Frequent impairment of the spindle assembly checkpoint in hepatocellular carcinoma.* Cancer, 2002. **94**(7): p. 2047-54.
311. Sze, K.M., et al., *Association of MAD2 expression with mitotic checkpoint competence in hepatoma cells.* J Biomed Sci, 2004. **11**(6): p. 920-7.
312. Takahashi, T., et al., *Identification of frequent impairment of the mitotic checkpoint and molecular analysis of the mitotic checkpoint genes, hsMAD2 and p55CDC, in human lung cancers.* Oncogene, 1999. **18**(30): p. 4295-300.
313. Weitzel, D.H. and D.D. Vandre, *Differential spindle assembly checkpoint response in human lung adenocarcinoma cells.* Cell Tissue Res, 2000. **300**(1): p. 57-65.
314. Hempen, P.M., et al., *A double missense variation of the BUB1 gene and a defective mitotic spindle checkpoint in the pancreatic cancer cell line Hs766T.* Hum Mutat, 2003. **21**(4): p. 445.
315. Ouyang, B., et al., *Mechanisms of aneuploidy in thyroid cancer cell lines and tissues: evidence for mitotic checkpoint dysfunction without mutations in BUB1 and BUBR1.* Clin Endocrinol (Oxf), 2002. **56**(3): p. 341-50.
316. Suijkerbuijk, S.J., et al., *Molecular causes for BUBR1 dysfunction in the human cancer predisposition syndrome mosaic variegated aneuploidy.* Cancer Res, 2010. **70**(12): p. 4891-900.
317. Matsuura, S., et al., *Chromosomal instability syndrome of total premature chromatid separation with mosaic variegated aneuploidy is defective in mitotic-spindle checkpoint.* Am J Hum Genet, 2000. **67**(2): p. 483-6.
318. Wang, Q., et al., *BUBR1 deficiency results in abnormal megakaryopoiesis.* Blood, 2004. **103**(4): p. 1278-85.
319. Cahill, D.P., et al., *Characterization of MAD2B and other mitotic spindle checkpoint genes.* Genomics, 1999. **58**(2): p. 181-7.
320. Myrie, K.A., et al., *Mutation and expression analysis of human BUB1 and BUB1B in aneuploid breast cancer cell lines.* Cancer Lett, 2000. **152**(2): p. 193-9.
321. Haruki, N., et al., *Molecular analysis of the mitotic checkpoint genes BUB1, BUBR1 and BUB3 in human lung cancers.* Cancer Lett, 2001. **162**(2): p. 201-5.
322. Yuan, B., et al., *Increased expression of mitotic checkpoint genes in breast cancer cells with chromosomal instability.* Clin Cancer Res, 2006. **12**(2): p. 405-10.
323. Grabsch, H., et al., *Overexpression of the mitotic checkpoint genes BUB1, BUBR1, and BUB3 in gastric cancer--association with tumour cell proliferation.* J Pathol, 2003. **200**(1): p. 16-22.
324. Daniel, J., et al., *High levels of the Mps1 checkpoint protein are protective of aneuploidy in breast cancer cells.* Proc Natl Acad Sci U S A, 2011. **108**(13): p. 5384-9.
325. Tanaka, K., et al., *Mitotic checkpoint protein hsMAD2 as a marker predicting liver metastasis of human gastric cancers.* Jpn J Cancer Res, 2001. **92**(9): p. 952-8.
326. Alizadeh, A.A., et al., *Distinct types of diffuse large B-cell lymphoma identified by gene expression profiling.* Nature, 2000. **403**(6769): p. 503-11.
327. Garber, M.E., et al., *Diversity of gene expression in adenocarcinoma of the lung.* Proc Natl Acad Sci U S A, 2001. **98**(24): p. 13784-9.
328. Manning, A.L. and N.J. Dyson, *pRB, a tumor suppressor with a stabilizing presence.* Trends Cell Biol, 2011. **21**(8): p. 433-41.
329. Ishida, S., et al., *Role for E2F in control of both DNA replication and mitotic functions as revealed from DNA microarray analysis.* Mol Cell Biol, 2001. **21**(14): p. 4684-99.
330. Polager, S., et al., *E2Fs up-regulate expression of genes involved in DNA replication, DNA repair and mitosis.* Oncogene, 2002. **21**(3): p. 437-46.
331. Hernando, E., et al., *Rb inactivation promotes genomic instability by uncoupling cell cycle progression from mitotic control.* Nature, 2004. **430**(7001): p. 797-802.
332. Sotillo, R., et al., *Mad2 overexpression promotes aneuploidy and tumorigenesis in mice.* Cancer Cell, 2007. **11**(1): p. 9-23.
333. Schvartzman, J.M., et al., *Mad2 is a critical mediator of the chromosome instability observed upon Rb and p53 pathway inhibition.* Cancer Cell, 2011. **19**(6): p. 701-14.
334. Iwaizumi, M., et al., *Human Sgo1 downregulation leads to chromosomal instability in colorectal cancer.* Gut, 2009. **58**(2): p. 249-60.
335. Barber, T.D., et al., *Chromatid cohesion defects may underlie chromosome instability in human colorectal cancers.* Proc Natl Acad Sci U S A, 2008. **105**(9): p. 3443-8.
336. Jallepalli, P.V., et al., *Securin is required for chromosomal stability in human cells.* Cell, 2001. **105**(4): p. 445-57.
337. Wang, Z., et al., *Three classes of genes mutated in colorectal cancers with chromosomal instability.* Cancer Res, 2004. **64**(9): p. 2998-3001.
338. Solomon, D.A., et al., *Mutational inactivation of STAG2 causes aneuploidy in human cancer.* Science, 2011. **333**(6045): p. 1039-43.
339. Zhang, N., et al., *Overexpression of Separase induces aneuploidy and mammary tumorigenesis.* Proc Natl Acad Sci U S A, 2008. **105**(35): p. 13033-8.
340. Nasmyth, K. and C.H. Haering, *Cohesin: its roles and mechanisms.* Annu Rev Genet, 2009. **43**: p. 525-58.
341. Remeseiro, S., et al., *Cohesin-SA1 deficiency drives aneuploidy and tumourigenesis in mice due to impaired replication*

of telomeres. EMBO J, 2012. **31**(9): p. 2076-89.
342. Gascoigne, K.E. and S.S. Taylor, *Cancer cells display profound intra- and interline variation following prolonged exposure to antimitotic drugs.* Cancer Cell, 2008. **14**(2): p. 111-22.
343. Cimini, D., et al., *Merotelic kinetochore orientation versus chromosome mono-orientation in the origin of lagging chromosomes in human primary cells.* J Cell Sci, 2002. **115**(Pt 3): p. 507-15.
344. Cimini, D., et al., *Merotelic kinetochore orientation is a major mechanism of aneuploidy in mitotic mammalian tissue cells.* J Cell Biol, 2001. **153**(3): p. 517-27.
345. Cimini, D., et al., *Merotelic kinetochore orientation occurs frequently during early mitosis in mammalian tissue cells and error correction is achieved by two different mechanisms.* J Cell Sci, 2003. **116**(Pt 20): p. 4213-25.
346. Cimini, D., L.A. Cameron, and E.D. Salmon, *Anaphase spindle mechanics prevent mis-segregation of merotelically oriented chromosomes.* Curr Biol, 2004. **14**(23): p. 2149-55.
347. Heneen, W.K., *Kinetochores and microtubules in multipolar mitosis and chromosome orientation.* Exp Cell Res, 1975. **91**(1): p. 57-62.
348. Sluder, G., et al., *The checkpoint control for anaphase onset does not monitor excess numbers of spindle poles or bipolar spindle symmetry.* J Cell Sci, 1997. **110 (Pt 4)**: p. 421-9.
349. Lingle, W.L., et al., *Centrosome amplification drives chromosomal instability in breast tumor development.* Proc Natl Acad Sci U S A, 2002. **99**(4): p. 1978-83.
350. Sato, N., et al., *Correlation between centrosome abnormalities and chromosomal instability in human pancreatic cancer cells.* Cancer Genet Cytogenet, 2001. **126**(1): p. 13-9.
351. Pihan, G.A., et al., *Centrosome defects can account for cellular and genetic changes that characterize prostate cancer progression.* Cancer Res, 2001. **61**(5): p. 2212-9.
352. Ghadimi, B.M., et al., *Centrosome amplification and instability occurs exclusively in aneuploid, but not in diploid colorectal cancer cell lines, and correlates with numerical chromosomal aberrations.* Genes Chromosomes Cancer, 2000. **27**(2): p. 183-90.
353. Nigg, E.A., *Centrosome aberrations: cause or consequence of cancer progression?* Nat Rev Cancer, 2002. **2**(11): p. 815-25.
354. Shi, Q. and R.W. King, *Chromosome nondisjunction yields tetraploid rather than aneuploid cells in human cell lines.* Nature, 2005. **437**(7061): p. 1038-42.
355. Silkworth, W.T., et al., *Multipolar spindle pole coalescence is a major source of kinetochore mis-attachment and chromosome mis-segregation in cancer cells.* PLoS One, 2009. **4**(8): p. e6564.
356. Ganem, N.J., S.A. Godinho, and D. Pellman, *A mechanism linking extra centrosomes to chromosomal instability.* Nature, 2009. **460**(7252): p. 278-82.
357. Fujiwara, T., et al., *Cytokinesis failure generating tetraploids promotes tumorigenesis in p53-null cells.* Nature, 2005. **437**(7061): p. 1043-7.
358. Davoli, T. and T. de Lange, *Telomere-driven tetraploidization occurs in human cells undergoing crisis and promotes transformation of mouse cells.* Cancer Cell, 2012. **21**(6): p. 765-76.
359. Overholtzer, M. and J.S. Brugge, *The cell biology of cell-in-cell structures.* Nat Rev Mol Cell Biol, 2008. **9**(10): p. 796-809.
360. Overholtzer, M., et al., *A nonapoptotic cell death process, entosis, that occurs by cell-in-cell invasion.* Cell, 2007. **131**(5): p. 966-79.
361. Kracjovic, M., et al., *A non-genetic route to aneuploidy in human cancers.* Nature Cell Biol, 2010.
362. Janssen, A. and R.H. Medema, *Entosis: aneuploidy by invasion.* Nat Cell Biol, 2011. **13**(3): p. 199-201.
363. Bakhoum, S.F., G. Genovese, and D.A. Compton, *Deviant kinetochore microtubule dynamics underlie chromosomal instability.* Curr Biol, 2009. **19**(22): p. 1937-42.
364. Bakhoum, S.F., et al., *Genome stability is ensured by temporal control of kinetochore-microtubule dynamics.* Nat Cell Biol, 2009. **11**(1): p. 27-35.
365. Kabeche, L. and D.A. Compton, *Checkpoint-independent stabilization of kinetochore-microtubule attachments by Mad2 in human cells.* Curr Biol, 2012. **22**(7): p. 638-44.
366. Salimian, K.J., et al., *Feedback control in sensing chromosome biorientation by the Aurora B kinase.* Curr Biol, 2011. **21**(13): p. 1158-65.
367. Kinzler, K.W., et al., *Identification of FAP locus genes from chromosome 5q21.* Science, 1991. **253**(5020): p. 661-5.
368. Clevers, H., *Wnt/beta-catenin signaling in development and disease.* Cell, 2006. **127**(3): p. 469-80.
369. Rusan, N.M. and M. Peifer, *Original CIN: reviewing roles for APC in chromosome instability.* J Cell Biol, 2008. **181**(5): p. 719-26.
370. Kaplan, K.B., et al., *A role for the Adenomatous Polyposis Coli protein in chromosome segregation.* Nat Cell Biol, 2001. **3**(4): p. 429-32.
371. Fodde, R., et al., *Mutations in the APC tumour suppressor gene cause chromosomal instability.* Nat Cell Biol, 2001. **3**(4): p. 433-8.
372. Dikovskaya, D., et al., *Loss of APC induces polyploidy as a result of a combination of defects in mitosis and apoptosis.* J Cell Biol, 2007. **176**(2): p. 183-95.
373. Draviam, V.M., et al., *Misorientation and reduced stretching of aligned sister kinetochores promote chromosome missegregation in EB1- or APC-depleted cells.* EMBO J, 2006. **25**(12): p. 2814-27.
374. Zhang, J., S. Ahmad, and Y. Mao, *BubR1 and APC/EB1 cooperate to maintain metaphase chromosome alignment.* J Cell Biol, 2007. **178**(5): p. 773-84.
375. Aoki, K., et al., *Chromosomal instability by beta-catenin/TCF transcription in APC or beta-catenin mutant cells.* Oncogene, 2007. **26**(24): p. 3511-20.
376. Aoki, K. and M.M. Taketo, *Adenomatous polyposis coli (APC): a multi-functional tumor suppressor gene.* J Cell Sci, 2007. **120**(Pt 19): p. 3327-35.
377. Olszak, A.M., et al., *Heterochromatin boundaries are hotspots for de novo kinetochore formation.* Nat Cell Biol, 2011. **13**(7): p. 799-808.
378. Pampalona, J., et al., *Whole chromosome loss is promoted by telomere dysfunction in primary cells.* Genes Chromosomes Cancer, 2010. **49**(4): p. 368-78.
379. Ichijima, Y., et al., *DNA lesions induced by replication stress trigger mitotic aberration and tetraploidy development.* PLoS One, 2010. **5**(1): p. e8821.
380. Chan, K.L., et al., *Replication stress induces sister-chromatid bridging at fragile site loci in mitosis.* Nat Cell Biol, 2009. **11**(6): p. 753-60.
381. Stewenius, Y., et al., *Defective chromosome segregation and telomere dysfunction in aggressive Wilms' tumors.* Clin Cancer Res, 2007. **13**(22 Pt 1): p. 6593-602.
382. Chan, K.L., P.S. North, and I.D. Hickson, *BLM is required for faithful chromosome segregation and its localization defines a class of ultrafine anaphase bridges.* EMBO J, 2007. **26**(14): p. 3397-409.
383. Hu, Z., et al., *The expression level of HJURP has an independent prognostic impact and predicts the sensitivity to*

radiotherapy in breast cancer. Breast Cancer Res, 2010. **12**(2): p. R18.
384. Tomonaga, T., et al., *Overexpression and mistargeting of centromere protein-A in human primary colorectal cancer.* Cancer Res, 2003. **63**(13): p. 3511-6.
385. Van Hooser, A.A., et al., *Specification of kinetochore-forming chromatin by the histone H3 variant CENP-A.* J Cell Sci, 2001. **114**(Pt 19): p. 3529-42.
386. Barnhart, M.C., et al., *HJURP is a CENP-A chromatin assembly factor sufficient to form a functional de novo kinetochore.* J Cell Biol, 2011. **194**(2): p. 229-43.
387. Fabarius, A., R. Hehlmann, and P.H. Duesberg, *Instability of chromosome structure in cancer cells increases exponentially with degrees of aneuploidy.* Cancer Genet Cytogenet, 2003. **143**(1): p. 59-72.
388. Sheltzer, J.M., et al., *Aneuploidy drives genomic instability in yeast.* Science, 2011. **333**(6045): p. 1026-30.
389. Janssen, A., et al., *Chromosome segregation errors as a cause of DNA damage and structural chromosome aberrations.* Science, 2011. **333**(6051): p. 1895-8.
390. Crasta, K., et al., *DNA breaks and chromosome pulverization from errors in mitosis.* Nature, 2012. **482**(7383): p. 53-8.
391. Quevedo, O., et al., *Nondisjunction of a single chromosome leads to breakage and activation of DNA damage checkpoint in G2.* PLoS Genet, 2012. **8**(2): p. e1002509.
392. Foijer, F., V.M. Draviam, and P.K. Sorger, *Studying chromosome instability in the mouse.* Biochim Biophys Acta, 2008. **1786**(1): p. 73-82.
393. Dobles, M., et al., *Chromosome missegregation and apoptosis in mice lacking the mitotic checkpoint protein Mad2.* Cell, 2000. **101**(6): p. 635-45.
394. Baker, D.J., et al., *Early aging-associated phenotypes in Bub3/Rae1 haploinsufficient mice.* J Cell Biol, 2006. **172**(4): p. 529-40.
395. Jeganathan, K., et al., *Bub1 mediates cell death in response to chromosome missegregation and acts to suppress spontaneous tumorigenesis.* J Cell Biol, 2007. **179**(2): p. 255-67.
396. Weaver, B.A., et al., *Centromere-associated protein-E is essential for the mammalian mitotic checkpoint to prevent aneuploidy due to single chromosome loss.* J Cell Biol, 2003. **162**(4): p. 551-63.
397. Weaver, B.A., et al., *Aneuploidy acts both oncogenically and as a tumor suppressor.* Cancer Cell, 2007. **11**(1): p. 25-36.
398. Ricke, R.M., J.H. van Ree, and J.M. van Deursen, *Whole chromosome instability and cancer: a complex relationship.* Trends Genet, 2008. **24**(9): p. 457-66.
399. Ricke, R.M., K.B. Jeganathan, and J.M. van Deursen, *Bub1 overexpression induces aneuploidy and tumor formation through Aurora B kinase hyperactivation.* J Cell Biol, 2011. **193**(6): p. 1049-64.
400. van Ree, J.H., et al., *Overexpression of the E2 ubiquitin-conjugating enzyme UbcH10 causes chromosome missegregation and tumor formation.* J Cell Biol, 2010. **188**(1): p. 83-100.
401. Rao, C.V., et al., *Colonic tumorigenesis in BubR1+/-ApcMin/+ compound mutant mice is linked to premature separation of sister chromatids and enhanced genomic instability.* Proc Natl Acad Sci U S A, 2005. **102**(12): p. 4365-70.
402. Baker, D.J., et al., *Opposing roles for p16Ink4a and p19Arf in senescence and ageing caused by BubR1 insufficiency.* Nat Cell Biol, 2008. **10**(7): p. 825-36.
403. Luongo, C., et al., *Loss of Apc+ in intestinal adenomas from Min mice.* Cancer Res, 1994. **54**(22): p. 5947-52.
404. Birkbak, N.J., et al., *Paradoxical relationship between chromosomal instability and survival outcome in cancer.* Cancer Res, 2011. **71**(10): p. 3447-52.
405. Roylance, R., et al., *Relationship of extreme chromosomal instability with long-term survival in a retrospective analysis of primary breast cancer.* Cancer Epidemiol Biomarkers Prev, 2011. **20**(10): p. 2183-94.
406. Chi, Y.H., et al., *Spindle assembly checkpoint and p53 deficiencies cooperate for tumorigenesis in mice.* Int J Cancer, 2009. **124**(6): p. 1483-9.
407. Li, M., et al., *The ATM-p53 pathway suppresses aneuploidy-induced tumorigenesis.* Proc Natl Acad Sci U S A, 2010. **107**(32): p. 14188-93.
408. Schliekelman, M., et al., *Impaired Bub1 function in vivo compromises tension-dependent checkpoint function leading to aneuploidy and tumorigenesis.* Cancer Res, 2009. **69**(1): p. 45-54.
409. Sotillo, R., et al., *Mad2-induced chromosome instability leads to lung tumour relapse after oncogene withdrawal.* Nature, 2010. **464**(7287): p. 436-40.
410. Garcia-Higuera, I., et al., *Genomic stability and tumour suppression by the APC/C cofactor Cdh1.* Nat Cell Biol, 2008. **10**(7): p. 802-11.
411. Diaz-Rodriguez, E., et al., *Hec1 overexpression hyperactivates the mitotic checkpoint and induces tumor formation in vivo.* Proc Natl Acad Sci U S A, 2008. **105**(43): p. 16719-24.
412. Malureanu, L., et al., *Cdc20 hypomorphic mice fail to counteract de novo synthesis of cyclin B1 in mitosis.* J Cell Biol, 2010. **191**(2): p. 313-29.
413. Li, M., et al., *Loss of spindle assembly checkpoint-mediated inhibition of Cdc20 promotes tumorigenesis in mice.* J Cell Biol, 2009. **185**(6): p. 983-94.
414. Chesnokova, V., et al., *Pituitary hypoplasia in Pttg-/- mice is protective for Rb+/- pituitary tumorigenesis.* Mol Endocrinol, 2005. **19**(9): p. 2371-9.
415. Wang, Z., R. Yu, and S. Melmed, *Mice lacking pituitary tumor transforming gene show testicular and splenic hypoplasia, thymic hyperplasia, thrombocytopenia, aberrant cell cycle progression, and premature centromere division.* Mol Endocrinol, 2001. **15**(11): p. 1870-9.
416. Uren, A.G., et al., *Survivin and the inner centromere protein INCENP show similar cell-cycle localization and gene knockout phenotype.* Curr Biol, 2000. **10**(21): p. 1319-28.
417. Thompson, S.L. and D.A. Compton, *Chromosomes and cancer cells.* Chromosome Res, 2010.
418. Vader, G., R.H. Medema, and S.M. Lens, *The chromosomal passenger complex: guiding Aurora-B through mitosis.* J Cell Biol, 2006. **173**(6): p. 833-7.
419. Cimini, D., *Merotelic kinetochore orientation, aneuploidy, and cancer.* Biochim Biophys Acta, 2008. **1786**(1): p. 32-40.
420. Dalton, W.B., B. Yu, and V.W. Yang, *p53 suppresses structural chromosome instability after mitotic arrest in human cells.* Oncogene, 2010. **29**(13): p. 1929-40.
421. Dalton, W.B., et al., *Human cancer cells commonly acquire DNA damage during mitotic arrest.* Cancer Res, 2007. **67**(24): p. 11487-92.
422. Quignon, F., et al., *Sustained mitotic block elicits DNA breaks: one-step alteration of ploidy and chromosome integrity in mammalian cells.* Oncogene, 2007. **26**(2): p. 165-72.
423. Straight, A.F., et al., *Dissecting temporal and spatial control of cytokinesis with a myosin II Inhibitor.* Science, 2003. **299**(5613): p. 1743-7.
424. Mortlock, A.A., et al., *Discovery, synthesis, and in vivo activity of a new class of pyrazoloquinazolines as selective inhibitors of aurora B kinase.* J Med Chem, 2007. **50**(9): p. 2213-24.
425. Ditchfield, C., et al., *Aurora B couples chromosome alignment with anaphase by targeting BubR1, Mad2, and Cenp-E to kinetochores.* J Cell Biol, 2003. **161**(2): p. 267-80.

426. Giunta, S., R. Belotserkovskaya, and S.P. Jackson, *DNA damage signaling in response to double-strand breaks during mitosis.* J Cell Biol, 2010. **190**(2): p. 197-207.
427. van Vugt, M.A., et al., *A mitotic phosphorylation feedback network connects Cdk1, Plk1, 53BP1, and Chk2 to inactivate the G(2)/M DNA damage checkpoint.* PLoS Biol, 2010. **8**(1): p. e1000287.
428. Petrini, J.H. and T.H. Stracker, *The cellular response to DNA double-strand breaks: defining the sensors and mediators.* Trends Cell Biol, 2003. **13**(9): p. 458-62.
429. Matsuoka, S., et al., *Ataxia telangiectasia-mutated phosphorylates Chk2 in vivo and in vitro.* Proc Natl Acad Sci U S A, 2000. **97**(19): p. 10389-94.
430. Hickson, I., et al., *Identification and characterization of a novel and specific inhibitor of the ataxia-telangiectasia mutated kinase ATM.* Cancer Res, 2004. **64**(24): p. 9152-9.
431. Thompson, S.L. and D.A. Compton, *Proliferation of aneuploid human cells is limited by a p53-dependent mechanism.* J Cell Biol, 2010. **188**(3): p. 369-81.
432. Smith, G.C. and S.P. Jackson, *The DNA-dependent protein kinase.* Genes Dev, 1999. **13**(8): p. 916-34.
433. Szuhai, K. and H.J. Tanke, *COBRA: combined binary ratio labeling of nucleic-acid probes for multi-color fluorescence in situ hybridization karyotyping.* Nat Protoc, 2006. **1**(1): p. 264-75.
434. Kapoor, T.M., et al., *Probing spindle assembly mechanisms with monastrol, a small molecule inhibitor of the mitotic kinesin, Eg5.* J Cell Biol, 2000. **150**(5): p. 975-88.
435. Vassilev, L.T., *Cell cycle synchronization at the G2/M phase border by reversible inhibition of CDK1.* Cell Cycle, 2006. **5**(22): p. 2555-6.
436. Vassilev, L.T., et al., *Selective small-molecule inhibitor reveals critical mitotic functions of human CDK1.* Proc Natl Acad Sci U S A, 2006. **103**(28): p. 10660-5.
437. Saunders, W.S., et al., *Chromosomal instability and cytoskeletal defects in oral cancer cells.* Proc Natl Acad Sci U S A, 2000. **97**(1): p. 303-8.
438. Miyoshi, Y., et al., *Acceleration of chromosomal instability by loss of BRCA1 expression and p53 abnormality in sporadic breast cancers.* Cancer Lett, 2000. **159**(2): p. 211-6.
439. Beheshti, B., et al., *Evidence of chromosomal instability in prostate cancer determined by spectral karyotyping (SKY) and interphase fish analysis.* Neoplasia, 2001. **3**(1): p. 62-9.
440. Kops, G.J., *The kinetochore and spindle checkpoint in mammals.* Front Biosci, 2008. **13**: p. 3606-20.
441. Musacchio, A. and E.D. Salmon, *The spindle-assembly checkpoint in space and time.* Nat Rev Mol Cell Biol, 2007. **8**(5): p. 379-93.
442. Lampson, M.A. and T.M. Kapoor, *The human mitotic checkpoint protein BubR1 regulates chromosome-spindle attachments.* Nat Cell Biol, 2005. **7**(1): p. 93-8.
443. Johnson, V.L., et al., *Bub1 is required for kinetochore localization of BubR1, Cenp-E, Cenp-F and Mad2, and chromosome congression.* J Cell Sci, 2004. **117**(Pt 8): p. 1577-89.
444. Ganem, N.J., Z. Storchova, and D. Pellman, *Tetraploidy, aneuploidy and cancer.* Curr Opin Genet Dev, 2007. **17**(2): p. 157-62.
445. Williams, B.R., et al., *Aneuploidy affects proliferation and spontaneous immortalization in mammalian cells.* Science, 2008. **322**(5902): p. 703-9.
446. Torres, E.M., et al., *Effects of aneuploidy on cellular physiology and cell division in haploid yeast.* Science, 2007. **317**(5840): p. 916-24.
447. Janssen, A. and R.H. Medema, *Mitosis as an anti-cancer target.* Oncogene, 2011. **30**(25): p. 2799-809.
448. Dankort, D., et al., *A new mouse model to explore the initiation, progression, and therapy of BRAFV600E-induced lung tumors.* Genes Dev, 2007. **21**(4): p. 379-84.
449. Ventura, A., et al., *Restoration of p53 function leads to tumour regression in vivo.* Nature, 2007. **445**(7128): p. 661-5.
450. Indra, A.K., et al., *Temporally-controlled site-specific mutagenesis in the basal layer of the epidermis: comparison of the recombinase activity of the tamoxifen-inducible Cre-ER(T) and Cre-ER(T2) recombinases.* Nucleic Acids Res, 1999. **27**(22): p. 4324-7.
451. Soriano, P., *Generalized lacZ expression with the ROSA26 Cre reporter strain.* Nat Genet, 1999. **21**(1): p. 70-1.
452. Reiners, J.J., Jr., S. Nesnow, and T.J. Slaga, *Murine susceptibility to two-stage skin carcinogenesis is influenced by the agent used for promotion.* Carcinogenesis, 1984. **5**(3): p. 301-7.
453. Vasioukhin, V., et al., *The magical touch: genome targeting in epidermal stem cells induced by tamoxifen application to mouse skin.* Proc Natl Acad Sci U S A, 1999. **96**(15): p. 8551-6.
454. Muller, W.J., et al., *Single-step induction of mammary adenocarcinoma in transgenic mice bearing the activated c-neu oncogene.* Cell, 1988. **54**(1): p. 105-15.
455. van der Weyden, L., et al., *Null and conditional semaphorin 3B alleles using a flexible puroDeltatk loxP/FRT vector.* Genesis, 2005. **41**(4): p. 171-8.
456. Truett, G.E., et al., *Preparation of PCR-quality mouse genomic DNA with hot sodium hydroxide and tris (HotSHOT).* Biotechniques, 2000. **29**(1): p. 52, 54.
457. Jordan, M.A. and L. Wilson, *Microtubules as a target for anticancer drugs.* Nat Rev Cancer, 2004. **4**(4): p. 253-65.
458. Manfredi, J.J. and S.B. Horwitz, *Taxol: an antimitotic agent with a new mechanism of action.* Pharmacol Ther, 1984. **25**(1): p. 83-125.
459. Jordan, M.A., D. Thrower, and L. Wilson, *Mechanism of inhibition of cell proliferation by Vinca alkaloids.* Cancer Res, 1991. **51**(8): p. 2212-22.
460. Jordan, M.A., et al., *Mechanism of mitotic block and inhibition of cell proliferation by taxol at low concentrations.* Proc Natl Acad Sci U S A, 1993. **90**(20): p. 9552-6.
461. Rowinsky, E.K., et al., *Microtubule changes and cytotoxicity in leukemic cell lines treated with taxol.* Cancer Res, 1988. **48**(14): p. 4093-100.
462. Goodin, S., *Novel cytotoxic agents: epothilones.* Am J Health Syst Pharm, 2008. **65**(10 Suppl 3): p. S10-5.
463. Yue, Q.X., X. Liu, and D.A. Guo, *Microtubule-binding natural products for cancer therapy.* Planta Med, 2010. **76**(11): p. 1037-43.
464. Rowinsky, E.K., et al., *Clinical toxicities encountered with paclitaxel (Taxol).* Semin Oncol, 1993. **20**(4 Suppl 3): p. 1-15.
465. Tuxen, M.K. and S.W. Hansen, *Neurotoxicity secondary to antineoplastic drugs.* Cancer Treat Rev, 1994. **20**(2): p. 191-214.
466. Harrison, M.R., K.D. Holen, and G. Liu, *Beyond taxanes: a review of novel agents that target mitotic tubulin and microtubules, kinases, and kinesins.* Clin Adv Hematol Oncol, 2009. **7**(1): p. 54-64.
467. Sawin, K.E., et al., *Mitotic spindle organization by a plus-end-directed microtubule motor.* Nature, 1992. **359**(6395): p. 540-3.
468. Blangy, A., et al., *Phosphorylation by p34cdc2 regulates spindle association of human Eg5, a kinesin-related motor essential for bipolar spindle formation in vivo.* Cell, 1995. **83**(7): p. 1159-69.
469. Mayer, T.U., et al., *Small molecule inhibitor of mitotic spindle bipolarity identified in a phenotype-based screen.* Science, 1999. **286**(5441): p. 971-4.

470. Marcus, A.I., et al., *Mitotic kinesin inhibitors induce mitotic arrest and cell death in Taxol-resistant and -sensitive cancer cells.* J Biol Chem, 2005. **280**(12): p. 11569-77.
471. Huszar, D., et al., *Kinesin motor proteins as targets for cancer therapy.* Cancer Metastasis Rev, 2009. **28**(1-2): p. 197-208.
472. Brier, S., et al., *Molecular dissection of the inhibitor binding pocket of mitotic kinesin Eg5 reveals mutants that confer resistance to antimitotic agents.* J Mol Biol, 2006. **360**(2): p. 360-76.
473. Tcherniuk, S., et al., *Mutations in the human kinesin Eg5 that confer resistance to monastrol and S-trityl-L-cysteine in tumor derived cell lines.* Biochem Pharmacol, 2010. **79**(6): p. 864-72.
474. Maliga, Z. and T.J. Mitchison, *Small-molecule and mutational analysis of allosteric Eg5 inhibition by monastrol.* BMC Chem Biol, 2006. **6**: p. 2.
475. Tanenbaum, M.E., et al., *Kif15 cooperates with eg5 to promote bipolar spindle assembly.* Curr Biol, 2009. **19**(20): p. 1703-11.
476. Vanneste, D., et al., *The role of Hklp2 in the stabilization and maintenance of spindle bipolarity.* Curr Biol, 2009. **19**(20): p. 1712-7.
477. Lok, W., R.Q. Klein, and M.W. Saif, *Aurora kinase inhibitors as anti-cancer therapy.* Anticancer Drugs, 2010. **21**(4): p. 339-50.
478. Strebhardt, K. and A. Ullrich, *Targeting polo-like kinase 1 for cancer therapy.* Nat Rev Cancer, 2006. **6**(4): p. 321-30.
479. Carmena, M. and W.C. Earnshaw, *The cellular geography of aurora kinases.* Nat Rev Mol Cell Biol, 2003. **4**(11): p. 842-54.
480. Barr, F.A., H.H. Sillje, and E.A. Nigg, *Polo-like kinases and the orchestration of cell division.* Nat Rev Mol Cell Biol, 2004. **5**(6): p. 429-40.
481. Yao, X., et al., *CENP-E forms a link between attachment of spindle microtubules to kinetochores and the mitotic checkpoint.* Nat Cell Biol, 2000. **2**(8): p. 484-91.
482. Wood, K.W., et al., *Antitumor activity of an allosteric inhibitor of centromere-associated protein-E.* Proc Natl Acad Sci U S A, 2010. **107**(13): p. 5839-44.
483. Schafer-Hales, K., et al., *Farnesyl transferase inhibitors impair chromosomal maintenance in cell lines and human tumors by compromising CENP-E and CENP-F function.* Mol Cancer Ther, 2007. **6**(4): p. 1317-28.
484. Rieder, C.L. and H. Maiato, *Stuck in division or passing through: what happens when cells cannot satisfy the spindle assembly checkpoint.* Dev Cell, 2004. **7**(5): p. 637-51.
485. Brito, D.A. and C.L. Rieder, *Mitotic checkpoint slippage in humans occurs via cyclin B destruction in the presence of an active checkpoint.* Curr Biol, 2006. **16**(12): p. 1194-200.
486. Shi, J., J.D. Orth, and T. Mitchison, *Cell type variation in responses to antimitotic drugs that target microtubules and kinesin-5.* Cancer Res, 2008. **68**(9): p. 3269-76.
487. Brito, D.A. and C.L. Rieder, *The ability to survive mitosis in the presence of microtubule poisons differs significantly between human nontransformed (RPE-1) and cancer (U2OS, HeLa) cells.* Cell Motil Cytoskeleton, 2009. **66**(8): p. 437-47.
488. Stobbe, C.C., S.J. Park, and J.D. Chapman, *The radiation hypersensitivity of cells at mitosis.* Int J Radiat Biol, 2002. **78**(12): p. 1149-57.
489. Westra, A. and W.C. Dewey, *Variation in sensitivity to heat shock during the cell-cycle of Chinese hamster cells in vitro.* Int J Radiat Biol Relat Stud Phys Chem Med, 1971. **19**(5): p. 467-77.
490. Uetake, Y. and G. Sluder, *Prolonged prometaphase blocks daughter cell proliferation despite normal completion of mitosis.* Curr Biol, 2010. **20**(18): p. 1666-71.
491. Allan, L.A. and P.R. Clarke, *Phosphorylation of caspase-9 by CDK1/cyclin B1 protects mitotic cells against apoptosis.* Mol Cell, 2007. **26**(2): p. 301-10.
492. Harley, M.E., et al., *Phosphorylation of Mcl-1 by CDK1-cyclin B1 initiates its Cdc20-dependent destruction during mitotic arrest.* EMBO J, 2010. **29**(14): p. 2407-20.
493. Terrano, D.T., M. Upreti, and T.C. Chambers, *Cyclin-dependent kinase 1-mediated Bcl-xL/Bcl-2 phosphorylation acts as a functional link coupling mitotic arrest and apoptosis.* Mol Cell Biol, 2010. **30**(3): p. 640-56.
494. Vantieghem, A., et al., *Phosphorylation of Bcl-2 in G2/M phase-arrested cells following photodynamic therapy with hypericin involves a CDK1-mediated signal and delays the onset of apoptosis.* J Biol Chem, 2002. **277**(40): p. 37718-31.
495. Wu, L., et al., *Aurora B interacts with NIR-p53, leading to p53 phosphorylation in its DNA-binding domain and subsequent functional suppression.* J Biol Chem, 2010.
496. Ando, K., et al., *Polo-like kinase 1 (Plk1) inhibits p53 function by physical interaction and phosphorylation.* J Biol Chem, 2004. **279**(24): p. 25549-61.
497. Ha, G.H., et al., *p53 activation in response to mitotic spindle damage requires signaling via BubR1-mediated phosphorylation.* Cancer Res, 2007. **67**(15): p. 7155-64.
498. Huang, H.C., et al., *Evidence that mitotic exit is a better cancer therapeutic target than spindle assembly.* Cancer Cell, 2009. **16**(4): p. 347-58.
499. Manchado, E., et al., *Targeting mitotic exit leads to tumor regression in vivo: Modulation by Cdk1, Mastl, and the PP2A/B55alpha,delta phosphatase.* Cancer Cell, 2010. **18**(6): p. 641-54.
500. Rieder, C.L. and R.H. Medema, *No way out for tumor cells.* Cancer Cell, 2009. **16**(4): p. 274-5.
501. Zeng, X., et al., *Pharmacologic inhibition of the anaphase-promoting complex induces a spindle checkpoint-dependent mitotic arrest in the absence of spindle damage.* Cancer Cell, 2010. **18**(4): p. 382-95.
502. Barr, F.A. and U. Gruneberg, *Cytokinesis: placing and making the final cut.* Cell, 2007. **131**(5): p. 847-60.
503. Kaitna, S., et al., *Incenp and an aurora-like kinase form a complex essential for chromosome segregation and efficient completion of cytokinesis.* Curr Biol, 2000. **10**(19): p. 1172-81.
504. Harrington, E.A., et al., *VX-680, a potent and selective small-molecule inhibitor of the Aurora kinases, suppresses tumor growth in vivo.* Nat Med, 2004. **10**(3): p. 262-7.
505. Kaestner, P., A. Stolz, and H. Bastians, *Determinants for the efficiency of anticancer drugs targeting either Aurora-A or Aurora-B kinases in human colon carcinoma cells.* Mol Cancer Ther, 2009. **8**(7): p. 2046-56.
506. Keen, N. and S. Taylor, *Mitotic drivers--inhibitors of the Aurora B Kinase.* Cancer Metastasis Rev, 2009. **28**(1-2): p. 185-95.
507. Wilkinson, R.W., et al., *AZD1152, a selective inhibitor of Aurora B kinase, inhibits human tumor xenograft growth by inducing apoptosis.* Clin Cancer Res, 2007. **13**(12): p. 3682-8.
508. Oke, A., et al., *AZD1152 rapidly and negatively affects the growth and survival of human acute myeloid leukemia cells in vitro and in vivo.* Cancer Res, 2009. **69**(10): p. 4150-8.
509. Uetake, Y. and G. Sluder, *Cell cycle progression after cleavage failure: mammalian somatic cells do not possess a "tetraploidy checkpoint".* J Cell Biol, 2004. **165**(5): p. 609-15.
510. Wong, C. and T. Stearns, *Mammalian cells lack checkpoints for tetraploidy, aberrant centrosome number, and cytokinesis failure.* BMC Cell Biol, 2005. **6**(1): p. 6.

511. Andreassen, P.R., et al., *Tetraploid state induces p53-dependent arrest of nontransformed mammalian cells in G1.* Mol Biol Cell, 2001. **12**(5): p. 1315-28.
512. Ganem, N.J. and D. Pellman, *Limiting the proliferation of polyploid cells.* Cell, 2007. **131**(3): p. 437-40.
513. Doxsey, S., *Re-evaluating centrosome function.* Nat Rev Mol Cell Biol, 2001. **2**(9): p. 688-98.
514. Mazumdar, M., et al., *Tumor formation via loss of a molecular motor protein.* Curr Biol, 2006. **16**(15): p. 1559-64.
515. Olaharski, A.J., et al., *Tetraploidy and chromosomal instability are early events during cervical carcinogenesis.* Carcinogenesis, 2006. **27**(2): p. 337-43.
516. Galipeau, P.C., et al., *17p (p53) allelic losses, 4N (G2/tetraploid) populations, and progression to aneuploidy in Barrett's esophagus.* Proc Natl Acad Sci U S A, 1996. **93**(14): p. 7081-4.
517. D'Assoro, A.B., et al., *Amplified centrosomes in breast cancer: a potential indicator of tumor aggressiveness.* Breast Cancer Res Treat, 2002. **75**(1): p. 25-34.
518. D'Assoro, A.B., W.L. Lingle, and J.L. Salisbury, *Centrosome amplification and the development of cancer.* Oncogene, 2002. **21**(40): p. 6146-53.
519. Basto, R., et al., *Centrosome amplification can initiate tumorigenesis in flies.* Cell, 2008. **133**(6): p. 1032-42.
520. Meraldi, P., R. Honda, and E.A. Nigg, *Aurora-A overexpression reveals tetraploidization as a major route to centrosome amplification in p53-/- cells.* EMBO J, 2002. **21**(4): p. 483-92.
521. Fukasawa, K., *Oncogenes and tumour suppressors take on centrosomes.* Nat Rev Cancer, 2007. **7**(12): p. 911-24.
522. Khodjakov, A., et al., *De novo formation of centrosomes in vertebrate cells arrested during S phase.* J Cell Biol, 2002. **158**(7): p. 1171-81.
523. Uetake, Y., et al., *Cell cycle progression and de novo centriole assembly after centrosomal removal in untransformed human cells.* J Cell Biol, 2007. **176**(2): p. 173-82.
524. Ring, D., R. Hubble, and M. Kirschner, *Mitosis in a cell with multiple centrioles.* J Cell Biol, 1982. **94**(3): p. 549-56.
525. Quintyne, N.J., et al., *Spindle multipolarity is prevented by centrosomal clustering.* Science, 2005. **307**(5706): p. 127-9.
526. Brinkley, B.R., *Managing the centrosome numbers game: from chaos to stability in cancer cell division.* Trends Cell Biol, 2001. **11**(1): p. 18-21.
527. Kwon, M., et al., *Mechanisms to suppress multipolar divisions in cancer cells with extra centrosomes.* Genes Dev, 2008. **22**(16): p. 2189-203.
528. Yuen, K.W., B. Montpetit, and P. Hieter, *The kinetochore and cancer: what's the connection?* Curr Opin Cell Biol, 2005. **17**(6): p. 576-82.
529. Thompson, S.L., S.F. Bakhoum, and D.A. Compton, *Mechanisms of chromosomal instability.* Curr Biol, 2010. **20**(6): p. R285-95.
530. Schvartzman, J.M., R. Sotillo, and R. Benezra, *Mitotic chromosomal instability and cancer: mouse modelling of the human disease.* Nat Rev Cancer, 2010. **10**(2): p. 102-15.
531. Duesberg, P., et al., *Aneuploidy precedes and segregates with chemical carcinogenesis.* Cancer Genet Cytogenet, 2000. **119**(2): p. 83-93.
532. Holland, A.J. and D.W. Cleveland, *Boveri revisited: chromosomal instability, aneuploidy and tumorigenesis.* Nat Rev Mol Cell Biol, 2009. **10**(7): p. 478-87.
533. Schmidt, M. and R.H. Medema, *Exploiting the compromised spindle assembly checkpoint function of tumor cells: dawn on the horizon?* Cell Cycle, 2006. **5**(2): p. 159-63.
534. Torres, E.M., B.R. Williams, and A. Amon, *Aneuploidy: cells losing their balance.* Genetics, 2008. **179**(2): p. 737-46.
535. Cohen, J., *Sorting out chromosome errors.* Science, 2002. **296**(5576): p. 2164-6.
536. Vitale, I., et al., *Chk1 inhibition activates p53 through p38 MAPK in tetraploid cancer cells.* Cell Cycle, 2008. **7**(13): p. 1956-61.
537. Guo, Z., et al., *ATM activation by oxidative stress.* Science, 2010. **330**(6003): p. 517-21.
538. Torres, E.M., et al., *Identification of aneuploidy-tolerating mutations.* Cell, 2010. **143**(1): p. 71-83.
539. Yang, Z., et al., *Extra centrosomes and/or chromosomes prolong mitosis in human cells.* Nat Cell Biol, 2008. **10**(6): p. 748-51.
540. Buffin, E., D. Emre, and R.E. Karess, *Flies without a spindle checkpoint.* Nat Cell Biol, 2007. **9**(5): p. 565-72.
541. Godinho, S.A., M. Kwon, and D. Pellman, *Centrosomes and cancer: how cancer cells divide with too many centrosomes.* Cancer Metastasis Rev, 2009. **28**(1-2): p. 85-98.
542. Cox, C.D., et al., *Kinesin spindle protein (KSP) inhibitors. 9. Discovery of (2S)-4-(2,5-difluorophenyl)-n-[(3R,4S)-3-fluoro-1-methylpiperidin-4-yl]-2- (hydroxymethyl)-N-methyl-2-phenyl-2,5-dihydro-1H-pyrrole-1-carboxamide (MK-0731) for the treatment of taxane-refractory cancer.* J Med Chem, 2008. **51**(14): p. 4239-52.
543. Sakowicz, R., et al., *Antitumor activity of a kinesin inhibitor.* Cancer Res, 2004. **64**(9): p. 3276-80.
544. Gumireddy, K., et al., *ON01910, a non-ATP-competitive small molecule inhibitor of Plk1, is a potent anticancer agent.* Cancer Cell, 2005. **7**(3): p. 275-86.
545. Steegmaier, M., et al., *BI 2536, a potent and selective inhibitor of polo-like kinase 1, inhibits tumor growth in vivo.* Curr Biol, 2007. **17**(4): p. 316-22.
546. Schoffski, P., *Polo-like kinase (PLK) inhibitors in preclinical and early clinical development in oncology.* Oncologist, 2009. **14**(6): p. 559-70.
547. Degenhardt, Y. and T. Lampkin, *Targeting Polo-like kinase in cancer therapy.* Clin Cancer Res, 2010. **16**(2): p. 384-9.
548. LeRoy, P.J., et al., *Localization of human TACC3 to mitotic spindles is mediated by phosphorylation on Ser558 by Aurora A: a novel pharmacodynamic method for measuring Aurora A activity.* Cancer Res, 2007. **67**(11): p. 5362-70.
549. Kitzen, J.J., M.J. de Jonge, and J. Verweij, *Aurora kinase inhibitors.* Crit Rev Oncol Hematol, 2010. **73**(2): p. 99-110.
550. Santaguida, S., et al., *Dissecting the role of MPS1 in chromosome biorientation and the spindle checkpoint through the small molecule inhibitor reversine.* J Cell Biol, 2010. **190**(1): p. 73-87.
551. Heim, S.a.M., F., *Cancer Cytogenetics*1995: Wiley Liss Inc., New York.
552. Horwitz, S.B., *Taxol (paclitaxel): mechanisms of action.* Ann Oncol, 1994. **5 Suppl 6**: p. S3-6.
553. Brito, D.A. and C.L. Rieder, *The ability to survive mitosis in the presence of microtubule poisons differs significantly between human nontransformed (RPE-1) and cancer (U2OS, HeLa) cells.* Cell Motil Cytoskeleton, 2008.
554. Ikui, A.E., et al., *Low concentrations of taxol cause mitotic delay followed by premature dissociation of p55CDC from Mad2 and BubR1 and abrogation of the spindle checkpoint, leading to aneuploidy.* Cell Cycle, 2005. **4**(10): p. 1385-8.
555. Chen, J.G. and S.B. Horwitz, *Differential mitotic responses to microtubule-stabilizing and -destabilizing drugs.* Cancer Res, 2002. **62**(7): p. 1935-8.
556. Fu, Y., et al., *Weakened spindle checkpoint with reduced BubR1 expression in paclitaxel-resistant ovarian carcinoma cell line SKOV3-TR30.* Gynecol Oncol, 2007. **105**(1): p. 66-73.
557. Sudo, T., et al., *Dependence of paclitaxel sensitivity on a functional spindle assembly checkpoint.* Cancer Res, 2004. **64**(7): p. 2502-8.
558. Swanton, C., et al., *Regulators of mitotic arrest and ceramide metabolism are determinants of sensitivity to paclitaxel and other chemotherapeutic drugs.* Cancer Cell, 2007. **11**(6): p. 498-512.

559. Kienitz, A., et al., *Partial downregulation of MAD1 causes spindle checkpoint inactivation and aneuploidy, but does not confer resistance towards taxol.* Oncogene, 2005. **24**(26): p. 4301-10.
560. Lee, E.A., et al., *Inactivation of the mitotic checkpoint as a determinant of the efficacy of microtubule-targeted drugs in killing human cancer cells.* Mol Cancer Ther, 2004. **3**(6): p. 661-9.
561. DeBonis, S., et al., *In vitro screening for inhibitors of the human mitotic kinesin Eg5 with antimitotic and antitumor activities.* Mol Cancer Ther, 2004. **3**(9): p. 1079-90.
562. Mayr, M.I., et al., *The human kinesin Kif18A is a motile microtubule depolymerase essential for chromosome congression.* Curr Biol, 2007. **17**(6): p. 488-98.
563. Schmidt, M., et al., *Ablation of the spindle assembly checkpoint by a compound targeting Mps1.* EMBO Rep, 2005. **6**(9): p. 866-72.
564. Draviam, V.M., et al., *A functional genomic screen identifies a role for TAO1 kinase in spindle-checkpoint signalling.* Nat Cell Biol, 2007. **9**(5): p. 556-64.
565. Meraldi, P. and P.K. Sorger, *A dual role for Bub1 in the spindle checkpoint and chromosome congression.* EMBO J, 2005. **24**(8): p. 1621-33.
566. Lens, S.M., et al., *Survivin is required for a sustained spindle checkpoint arrest in response to lack of tension.* EMBO J, 2003. **22**(12): p. 2934-47.
567. Tanenbaum, M.E., et al., *Dynein, Lis1 and CLIP-170 counteract Eg5-dependent centrosome separation during bipolar spindle assembly.* EMBO J, 2008. **27**(24): p. 3235-45.
568. Brown, K.D., K.W. Wood, and D.W. Cleveland, *The kinesin-like protein CENP-E is kinetochore-associated throughout poleward chromosome segregation during anaphase-A.* J Cell Sci, 1996. **109 (Pt 5)**: p. 961-9.
569. Hansemann, D.P.v., Über asymmetrische Zelltheilung in Epithelkrebsen und deren biologische Bedeutung. Archiv für pathologische Anatomie und Physiologie und für klinische Medicin, 1890. **779**: p. 299-326.
570. Suijkerbuijk, S.J. and G.J. Kops, *Preventing aneuploidy: the contribution of mitotic checkpoint proteins.* Biochim Biophys Acta, 2008. **1786**(1): p. 24-31.
571. Jones, M.H., et al., *Chemical genetics reveals a role for Mps1 kinase in kinetochore attachment during mitosis.* Curr Biol, 2005. **15**(2): p. 160-5.
572. van der Waal, M.S., et al., *Cell division control by the Chromosomal Passenger Complex.* Exp Cell Res, 2012.
573. Janssen, A., G.J. Kops, and R.H. Medema, *Targeting the mitotic checkpoint to kill tumor cells.* Horm Cancer, 2011. **2**(2): p. 113-6.
574. Lan, W. and D.W. Cleveland, *A chemical tool box defines mitotic and interphase roles for Mps1 kinase.* J Cell Biol, 2010. **190**(1): p. 21-4.
575. Amabile, G., et al., *The Aurora B kinase activity is required for the maintenance of the differentiated state of murine myoblasts.* Cell Death Differ, 2009. **16**(2): p. 321-30.
576. Chu, M.L., et al., *Biophysical and X-ray crystallographic analysis of Mps1 kinase inhibitor complexes.* Biochemistry, 2010. **49**(8): p. 1689-701.
577. Miduturu, C.V., et al., *High-throughput kinase profiling: a more efficient approach toward the discovery of new kinase inhibitors.* Chem Biol, 2011. **18**(7): p. 868-79.
578. Tardif, K.D., et al., *Characterization of the cellular and antitumor effects of MPI-0479605, a small-molecule inhibitor of the mitotic kinase Mps1.* Mol Cancer Ther, 2011. **10**(12): p. 2267-75.
579. Caldarelli, M., et al., *pyrazolo-quinazolines.* patent WO 2009/156315 A1, Nerviano Medical Sciences (Nerviano, Italy) 2009
580. Uitdehaag, J.C. and G.J. Zaman, *A theoretical entropy score as a single value to express inhibitor selectivity.* BMC Bioinformatics, 2011. **12**: p. 94.
581. Clute, P. and J. Pines, *Temporal and spatial control of cyclin B1 destruction in metaphase.* Nat Cell Biol, 1999. **1**(2): p. 82-7.
582. Hagting, A., et al., *Human securin proteolysis is controlled by the spindle checkpoint and reveals when the APC/C switches from activation by Cdc20 to Cdh1.* J Cell Biol, 2002. **157**(7): p. 1125-37.
583. Hahn, W.C. and R.A. Weinberg, *Rules for making human tumor cells.* N Engl J Med, 2002. **347**(20): p. 1593-603.
584. Dyson, N., et al., *Cellular proteins that are targetted by DNA tumor viruses for transformation.* Princess Takamatsu Symp, 1989. **20**: p. 191-8.
585. Caldarelli, M., et al., *Synthesis and SAR of new pyrazolo[4,3-h]quinazoline-3-carboxamide derivatives as potent and selective MPS1 kinase inhibitors.* Bioorg Med Chem Lett, 2011. **21**(15): p. 4507-11.
586. Rottenberg, S., M. Pajic, and J. Jonkers, *Studying drug resistance using genetically engineered mouse models for breast cancer.* Methods Mol Biol, 2010. **596**: p. 33-45.
587. Uitdehaag, J.C., et al., *A guide to picking the most selective kinase inhibitor tool compounds for pharmacological validation of drug targets.* Br J Pharmacol, 2012. **166**(3): p. 858-876.
588. Huson, D.H., et al., *Dendroscope: An interactive viewer for large phylogenetic trees.* BMC Bioinformatics, 2007. **8**: p. 460.
589. Bissery, M.C., et al., *Docetaxel (Taxotere): a review of preclinical and clinical experience. Part I: Preclinical experience.* Anticancer Drugs, 1995. **6**(3): p. 339-55, 363-8.
590. Noguchi, S., *Predictive factors for response to docetaxel in human breast cancers.* Cancer Sci, 2006. **97**(9): p. 813-20.
591. Davies, A.M., et al., *Docetaxel in non-small cell lung cancer: a review.* Expert Opin Pharmacother, 2003. **4**(4): p. 553-65.
592. Nogales, E., et al., *Structure of tubulin at 6.5 A and location of the taxol-binding site.* Nature, 1995. **375**(6530): p. 424-7.
593. Schiff, P.B., J. Fant, and S.B. Horwitz, *Promotion of microtubule assembly in vitro by taxol.* Nature, 1979. **277**(5698): p. 665-7.
594. Schiff, P.B. and S.B. Horwitz, *Taxol stabilizes microtubules in mouse fibroblast cells.* Proc Natl Acad Sci U S A, 1980. **77**(3): p. 1561-5.
595. Ringel, I. and S.B. Horwitz, *Studies with RP 56976 (taxotere): a semisynthetic analogue of taxol.* J Natl Cancer Inst, 1991. **83**(4): p. 288-91.
596. Yvon, A.M., P. Wadsworth, and M.A. Jordan, *Taxol suppresses dynamics of individual microtubules in living human tumor cells.* Mol Biol Cell, 1999. **10**(4): p. 947-59.
597. Orth, J.D., et al., *Analysis of mitosis and antimitotic drug responses in tumors by in vivo microscopy and single-cell pharmacodynamics.* Cancer Res, 2011. **71**(13): p. 4608-16.
598. Milas, L., et al., *Kinetics of mitotic arrest and apoptosis in murine mammary and ovarian tumors treated with taxol.* Cancer Chemother Pharmacol, 1995. **35**(4): p. 297-303.
599. Milross, C.G., et al., *Relationship of mitotic arrest and apoptosis to antitumor effect of paclitaxel.* J Natl Cancer Inst, 1996. **88**(18): p. 1308-14.
600. Symmans, W.F., et al., *Paclitaxel-induced apoptosis and mitotic arrest assessed by serial fine-needle aspiration: implications for early prediction of breast cancer response to neoadjuvant treatment.* Clin Cancer Res, 2000. **6**(12): p.

4610-7.
601. Beerling, E., et al., *Intravital microscopy: new insights into metastasis of tumors.* J Cell Sci, 2011. **124**(Pt 3): p. 299-310.
602. Porter, A.G. and R.U. Janicke, *Emerging roles of caspase-3 in apoptosis.* Cell Death Differ, 1999. **6**(2): p. 99-104.
603. Bins, A.D., et al., *Intravital imaging of fluorescent markers and FRET probes by DNA tattooing.* BMC Biotechnol, 2007. **7**: p. 2.
604. Keese, M., et al., *Quantitative imaging of apoptosis commitment in colorectal tumor cells.* Differentiation, 2007. **75**(9): p. 809-18.
605. Keese, M., et al., *Fluorescence lifetime imaging microscopy of chemotherapy-induced apoptosis resistance in a syngenic mouse tumor model.* Int J Cancer, 2010. **126**(1): p. 104-13.
606. van der Wal, J., et al., *Monitoring agonist-induced phospholipase C activation in live cells by fluorescence resonance energy transfer.* J Biol Chem, 2001. **276**(18): p. 15337-44.
607. Gurskaya, N.G., et al., *Engineering of a monomeric green-to-red photoactivatable fluorescent protein induced by blue light.* Nat Biotechnol, 2006. **24**(4): p. 461-5.
608. Kedrin, D., et al., *Intravital imaging of metastatic behavior through a mammary imaging window.* Nat Methods, 2008. **5**(12): p. 1019-21.
609. Gligorijevic, B., et al., *Dendra2 photoswitching through the Mammary Imaging Window.* J Vis Exp, 2009(28).
610. van Munster, E.B. and T.W. Gadella, *Fluorescence lifetime imaging microscopy (FLIM).* Adv Biochem Eng Biotechnol, 2005. **95**: p. 143-75.
611. Ritsma, L., B. Ponsioen, and J. van Rheenen, *Intravital imaging of cell signaling in mice.* Intravital, 2012. **1**(1).
612. Mitchison, T.J., *The proliferation rate paradox in antimitotic chemotherapy.* Mol Biol Cell, 2012. **23**(1): p. 1-6.
613. Nakasone, E.S., et al., *Imaging tumor-stroma interactions during chemotherapy reveals contributions of the microenvironment to resistance.* Cancer Cell, 2012. **21**(4): p. 488-503.
614. Javeed, A., et al., *Paclitaxel and immune system.* Eur J Pharm Sci, 2009. **38**(4): p. 283-90.
615. Fitzpatrick, F.A. and R. Wheeler, *The immunopharmacology of paclitaxel (Taxol), docetaxel (Taxotere), and related agents.* Int Immunopharmacol, 2003. **3**(13-14): p. 1699-714.
616. Tang, Y.C., et al., *Identification of aneuploidy-selective antiproliferation compounds.* Cell, 2011. **144**(4): p. 499-512.
617. Duesberg, P., et al., *Genetic instability of cancer cells is proportional to their degree of aneuploidy.* Proc Natl Acad Sci U S A, 1998. **95**(23): p. 13692-7.
618. Burds, A.A., A.S. Lutum, and P.K. Sorger, *Generating chromosome instability through the simultaneous deletion of Mad2 and p53.* Proc Natl Acad Sci U S A, 2005. **102**(32): p. 11296-301.
619. Cimini, D., C. Tanzarella, and F. Degrassi, *Differences in malsegregation rates obtained by scoring ana-telophases or binucleate cells.* Mutagenesis, 1999. **14**(6): p. 563-8.
620. Harrigan, J.A., et al., *Replication stress induces 53BP1-containing OPT domains in G1 cells.* J Cell Biol, 2011. **193**(1): p. 97-108.
621. Lukas, C., et al., *53BP1 nuclear bodies form around DNA lesions generated by mitotic transmission of chromosomes under replication stress.* Nat Cell Biol, 2011. **13**(3): p. 243-53.
622. Guerrero, A.A., et al., *Centromere-localized breaks indicate the generation of DNA damage by the mitotic spindle.* Proc Natl Acad Sci U S A, 2009. **107**(9): p. 4159-64.
623. Stephens, P.J., et al., *Massive genomic rearrangement acquired in a single catastrophic event during cancer development.* Cell, 2011. **144**(1): p. 27-40.
624. Maher, C.A. and R.K. Wilson, *Chromothripsis and human disease: piecing together the shattering process.* Cell, 2012. **148**(1-2): p. 29-32.
625. Kloosterman, W.P., et al., *Chromothripsis as a mechanism driving complex de novo structural rearrangements in the germline.* Hum Mol Genet, 2011. **20**(10): p. 1916-24.
626. Rausch, T., et al., *Genome sequencing of pediatric medulloblastoma links catastrophic DNA rearrangements with TP53 mutations.* Cell, 2012. **148**(1-2): p. 59-71.
627. Kloosterman, W.P., *Constitutional Chromothripsis Rearrangements Involve Clustered Double-Stranded DNA Breaks and Nonhomologous Repair Mechanisms.* Cell Reports, 2012(doi:10.1016/j.celrep.2012.05.009).
628. Carlton, J.G., et al., *ESCRT-III governs the Aurora B-mediated abscission checkpoint through CHMP4C.* Science, 2012. **336**(6078): p. 220-5.
629. Rajagopalan, H. and C. Lengauer, *Aneuploidy and cancer.* Nature, 2004. **432**(7015): p. 338-41.
630. Pei, L. and S. Melmed, *Isolation and characterization of a pituitary tumor-transforming gene (PTTG).* Mol Endocrinol, 1997. **11**(4): p. 433-41.
631. Zhang, D., et al., *Cre-loxP-controlled periodic Aurora-A overexpression induces mitotic abnormalities and hyperplasia in mammary glands of mouse models.* Oncogene, 2004. **23**(54): p. 8720-30.
632. Pavelka, N., et al., *Aneuploidy confers quantitative proteome changes and phenotypic variation in budding yeast.* Nature, 2010. **468**(7321): p. 321-5.
633. Rancati, G., et al., *Aneuploidy underlies rapid adaptive evolution of yeast cells deprived of a conserved cytokinesis motor.* Cell, 2008. **135**(5): p. 879-93.
634. Cavenee, W.K., et al., *Expression of recessive alleles by chromosomal mechanisms in retinoblastoma.* Nature, 1983. **305**(5937): p. 779-84.
635. Duesberg, P., A. Fabarius, and R. Hehlmann, *Aneuploidy, the primary cause of the multilateral genomic instability of neoplastic and preneoplastic cells.* IUBMB Life, 2004. **56**(2): p. 65-81.
636. Zomer, A., et al., *Real-time intravital imaging of cancer models.* Clin Transl Oncol, 2011. **13**(12): p. 848-54.
637. McGranahan, N., et al., *Cancer chromosomal instability: therapeutic and diagnostic challenges.* EMBO Rep, 2012. **13**(6): p. 528-38.
638. Hudis, C.A., *Trastuzumab--mechanism of action and use in clinical practice.* N Engl J Med, 2007. **357**(1): p. 39-51.
639. Michel, L., R. Benezra, and E. Diaz-Rodriguez, *MAD2 dependent mitotic checkpoint defects in tumorigenesis and tumor cell death: a double edged sword.* Cell Cycle, 2004. **3**(8): p. 990-2.

Nederlandse Samenvatting

Celdeling, het proces waarbij twee 'dochtercellen' ontstaan uit één 'moedercel', is essentieel voor de ontwikkeling van alle organismen. Ook cellen in bijvoorbeeld ons darmstelsel of de huid moeten blijven delen om deze organen goed te laten functioneren. Elke dag worden er in ons lichaam miljarden celdelingen uitgevoerd en het is van cruciaal belang dat al deze delingen goed verlopen.
Het proces van celdeling wordt mitose genoemd. Eén van de meest essentiële onderdelen van de mitose is het splitsen van erfelijk materiaal, het DNA. Het DNA van elke cel is verdeeld over zesenveertig pakketjes, genaamd chromosomen, die zich al vóór de start van mitose verdubbeld hebben. Op het moment dat de moedercel mitose ingaat, heeft deze cel dus twee exacte kopieën van haar 46 chromosomen. Er vormt zich nu een spoelfiguur, bestaande uit twee polen van waaruit een grote hoeveelheid draadjes groeien en zich binden aan de chromosomen (Fig.1). Deze draadjes worden microtubuli genoemd. Door middel van het duwen en trekken van de microtubuli komen uiteindelijk alle chromosomen in het midden van de moedercel te liggen. Op dat moment is de moedercel klaar om te delen en worden de identieke pakketjes chromosomen netjes gedistribueerd over de twee dochtercellen (Fig.1).

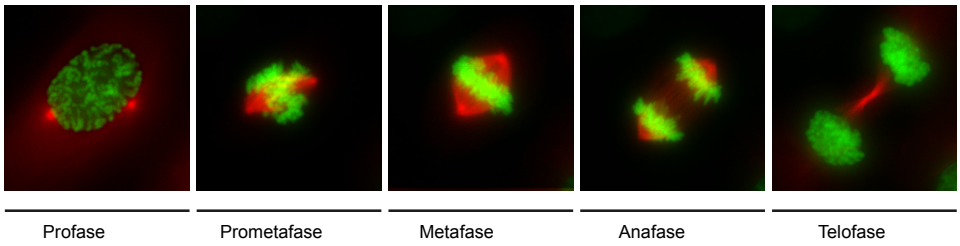

Figuur 1. De verschillende fasen van mitose
In profase beginnen de microtubuli (rood) te groeien vanuit de twee polen. Deze microtubuli binden in prometafase aan de chromosomen (groen), waardoor de chromosomen in het midden van de cel komen te liggen in metafase. In anafase en telofase deelt de cel en wordt het DNA gelijk verdeeld over de twee dochtercellen.

Ongelijke verdeling van het DNA van de moedercel over de twee dochtercellen, kan desastreuze gevolgen hebben. Een van de mechanismen die ervoor zorgen dat het DNA, verpakt in chromosomen, goed verdeeld wordt over het nageslacht, is het 'mitotisch checkpoint'. Dit checkpoint zorgt ervoor dat de cel in mitose blijft totdat alle chromosomen netjes in het midden van de moedercel liggen en allemaal verbonden zijn met de draadjes van de spoelfiguur. Zodra dit het geval is, wordt het mitotisch checkpoint uitgezet en worden de twee identieke chromosoom pakketjes verdeeld over de twee dochtercellen. Wanneer het mitotisch checkpoint niet goed functioneert, gaat het mis tijdens de verdeling van de chromosomen. De chromosomen worden ongelijk gedistribueerd over de twee dochtercellen, wat leidt tot abnormale hoeveelheden chromosomen, dit laatste wordt aneuploidy genoemd.
Veel tumorcellen verdelen hun chromosomen ongelijk tijdens de celdeling en zijn daarom ook vaak aneuploid. Deze continue ongelijke verdeling van chromosomen tijdens de celdeling, wordt chromosoom instabiliteit genoemd. Het wordt geschat dat 70% van alle tumoren chromosoom instabiel is. Het hebben van een ongelijke hoeveelheid chromosomen zou een groeivoordeel kunnen geven aan tumorcellen ten opzichte van gezonde cellen en zou daardoor een rol kunnen spelen bij het ontstaan van kanker. Dit groeivoordeel zou bijvoorbeeld kunnen ontstaan doordat een cel DNA verliest wat codeert voor een groei-remmend eiwit (tumor-suppressor) of anderzijds door DNA te verkrijgen wat codeert voor een groei-stimulerend eiwit (oncogen).

Toch balanceren chromosoom instabiele tumorcellen op de rand van de dood. Een te grote disbalans van het erfelijk materiaal leidt namelijk bijna altijd tot sterfte van cellen. Dit opent deuren voor nieuwe anti-kanker therapieën; kan een ernstige verstoring van de chromosoomverdeling specifiek leiden tot de sterfte van tumorcellen en daarbij gezonde cellen onbeschadigd laten?
Dit proefschrift behandelt deze twee verschillende vraagstukken: Hoe kan chromosoom instabiliteit een groeivoordeel opleveren voor tumorcellen? En hoe kan deze ongelijke verdeling van chromosomen tevens uitgebuit worden in anti-kanker therapie?
In **hoofdstuk 1** wordt een algemene introductie gegeven op het proces van celdeling, alle betrokken eiwitten en de oorzaken en gevolgen van chromosoom instabiliteit. **Hoofdstuk 2** laat zien dat ongelijke splitsing van chromosomen in mitose niet alleen leidt tot aneuploidy, maar ook tot DNA schade. Deze DNA schade ontstaat doordat verkeerd gedeelde chromosomen achterblijven precies op de plek waar de moedercel zich splitst in twee delen (Fig.2). De experimenten beschreven in **hoofdstuk 2** laten daarom zien dat chromosoom instabiliteit niet alleen zou kunnen bijdragen aan het ontstaan van kanker door ongelijke verdeling van het DNA, maar ook door het verkrijgen van DNA schade, wat kan leiden tot blijvende structurele veranderingen in chromosomen.

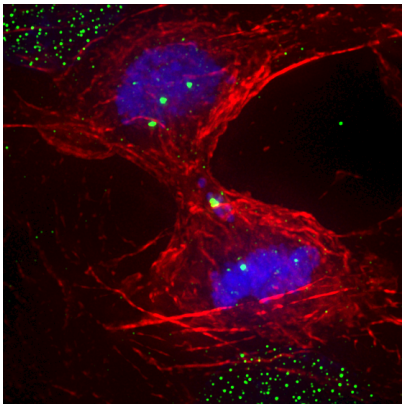

Figuur 2.
Beschadiging van 'achterblijvende' chromosomen tijdens de celdeling
Door ongelijke verdeling van de chromosomen (blauw) tijdens de deling van een tumorcel, kan DNA achterblijven op de plek waar de cel in tweeën splitst (de rode kleur laat zien hoe de cel zich deelt). Deling van de cel op het moment dat er nog chromosomen aanwezig zijn op het delingsvlak kan leiden tot beschadiging (groen) van deze achterblijvende chromosomen.

Om het effect van ongelijke chromosoom verdeling, ook wel chromosoom missegregaties genoemd, te bestuderen in een organisme, hebben we twee muismodellen gegenereerd waarin we op elk gegeven moment tijdens de ontwikkeling van de muis chromosoom missegregaties kunnen introduceren (**Hoofdstuk 3**). Cellen in deze muizen missegregeren hun chromosomen doordat het mitotisch checkpoint verzwakt kan worden door middel van een mutatie in het eiwit Mps1. Mps1 is een eiwit dat essentieel is voor het mitotisch checkpoint en wanneer Mps1 niet volledig functioneert, ontstaan er chromosoom missegregaties. Door middel van deze muismodellen kunnen we bepalen wat het effect is van chromosoom missegregaties op het ontstaan van tumoren, maar ook in het stoppen van tumorgroei en dus als potentiële anti-kanker therapie.
Hoofdstuk 4 geeft een literatuur overzicht van de anti kanker therapieën die momenteel in de kliniek gebruikt worden en ontwikkeld zijn om delende tumorcellen te doden. Verder bespreken we hier nieuwe potentiële anti-kanker strategieën die in de toekomst gebruikt zouden kunnen worden om specifiek tumorcellen te doden door bepaalde eigenschappen van deze tumorcellen uit te buiten. **Hoofdstuk 5** laat zien dat tumorcellen specifiek gedood kunnen worden door het mitotisch checkpoint te ontregelen. Het gedeeltelijk weghalen van het Mps1 eiwit in combinatie met behandeling met het chemotherapeuticum paclitaxel lijkt specifiek tumorcellen te kunnen doden door de chromosoom

verdeling van tumorcellen compleet te ontregelen. Dit leidt tot een ernstige verstoring van de hoeveelheid DNA in de dochtercellen en uiteindelijk celdood. **Hoofdstuk 6** borduurt voort op dit concept door de functie van het Mps1 eiwit te remmen door middel van een Mps1 bindende stof, een inhibitor genoemd. Ook het toevoegen van een lage dosis van deze Mps1 inhibitor leidt tot tumorceldood, terwijl gezonde cellen onbeschadigd blijven. We hypothetiseren dat dit komt doordat tumorcellen meer afhankelijk zijn van de functie van Mps1. Deze afhankelijkheid kan komen doordat tumorcellen een abnormale hoeveelheid chromosomen hebben en hierdoor meer tijd nodig hebben om te delen, terwijl gezonde cellen efficienter door mitose gaan en hierdoor minder afhankelijk zijn van Mps1.

Het laatste experimentele hoofdstuk, **hoofdstuk 7**, beschrijft de ontwikkeling van een systeem waarbij we in muizen 'live' naar tumorcellen kunnen kijken. Door verschillende eiwitten een bepaald kleurtje te geven, kan de beweging van deze eiwitten in tumorcellen gevolgd worden door de camera. We hebben de eiwitten in tumorcellen zo gekleurd dat we zowel de chromosoomverdeling tijdens mitose als het begin van celdood kunnen volgen. Dit systeem is daardoor uiterst geschikt om te kijken naar de manier waarop tumorcellen in het lichaam reageren op bepaalde chemotherapeutica. Na behandeling van muizen met Docetaxel, een chemotherapeuticum dat momenteel in de kliniek gebruikt wordt voor de behandeling van kanker, hebben we gevonden dat tumorcellen in het lichaam anders reageren dan in de celkweek. Docetaxel pakt in de celkweek specifiek de delende cellen aan, terwijl tumorcellen in een levend organisme gedood worden onafhankelijk van de celdeling. Dit hoofdstuk geeft het belang van onderzoek in organismen weer en laat zien dat cellen in de celkweek anders kunnen reageren op chemotherapeutica dan in het lichaam.

In **Hoofdstuk 8** worden de experimentele data van dit proefschrift bediscussieerd in het licht van de relevante literatuur. Tevens worden nieuwe ideeën voor toekomstig onderzoek naar chromosoom missegregaties gesuggereerd.

Curriculum Vitae

Aniek Janssen werd geboren op 19 april 1983 te 's-Hertogenbosch. In 2001 behaalde zij haar Gymnasium diploma aan het Jeroen Bosch College te 's-Hertogenbosch. In hetzelfde jaar startte ze met de opleiding Biologie aan de Universiteit Utrecht, die ze in november 2006 afrondde met de Master Developmental Biology and Biomedical Genetics. Gedurende deze Master begon ze op het Nederlands Kanker Instituut te Amsterdam aan haar stage van negen maanden in het laboratorium van Prof.dr. René Medema onder begeleiding van Dr. Renske van Leuken. Tijdens deze periode verhuisde het lab naar het Universitair Medisch Centrum Utrecht, waar ze haar stage-onderzoek afrondde. Daarna vertrok Aniek voor 6 maanden naar het laboratorium van Prof.dr. Stephen Schoenberger op het La Jolla Institute for Allergy and Immunology te La Jolla, Californië, USA. Na voltooiing van haar master begon ze in december 2006 aan haar promotieonderzoek, beschreven in dit proefschrift, bij de afdeling Medische Oncologie van het Universitair Medisch Centrum Utrecht onder begeleiding van Prof.dr. René Medema en Prof.dr. Geert Kops. In januari 2012 verhuisde het laboratorium terug naar het Nederlands Kanker Instituut te Amsterdam, waar ze haar onderzoek in december 2012 afrondde. Begin 2013 zal Aniek haar onderzoekscarrière voortzetten in het laboratorium van Dr. Gary Karpen aan de University of California te Berkeley, USA.

&

Publications

A. Janssen, R.H.Medema.
Genetic instability: tipping the balance.
Accepted for publication in Oncogene

A. Janssen[‡], E. Beerling[‡], R.H. Medema[†], J. van Rheenen[†]
Docetaxel affects *in vivo* tumor cell viability independent of its effects on mitosis.
[‡] and [†]: equal contributions
Submitted.

A. Janssen, M. van der Burg, K.Szuhai, G.J.P.L. Kops, R.H. Medema.
Chromosome segregation errors as a cause of DNA damage and Structural Chromosome Aberrations.
Science, 30;333(6051):1895-8 (Sep 30, 2011)

A. Janssen, R. H. Medema.
Mitosis as an anti-cancer target.
Oncogene 30, 2799 (Jun 23, 2011).

A. Janssen, G.J.P.L. Kops, R.H. Medema.
Targeting the Mitotic Checkpoint to kill tumor cells.
Horm Cancer 2, 113 (Apr, 2011).

A. Janssen, R. H. Medema.
Entosis: Aneuploidy by Invasion.
Nat Cell Biol 13, 199 (Mar, 2011).

A. Janssen, G.J.P.L. Kops, R.H. Medema.
Elevating the frequency of chromosome mis-segregation as a strategy to kill tumorcells.
Proc Natl Acad Sci U S A 106, 19108 (Nov 10, 2009).

M.E. Tanenbaum, L. Macůrek L, A. Janssen, E.F. Geers, M. Alvarez-Fernández, R.H. Medema.
Kif15 cooperates with Eg5 to promote bipolar spindle assembly.
Curr Biol 19, 1703 (Nov 3, 2009).

Dankwoord

En dan nu eindelijk het dankwoord. Het duurde even voor ik hieraan kon beginnen, misschien wel omdat dit echt het einde van een geweldige tijd betekent. Er is bijna geen dag voorbijgegaan waarbij ik niet met plezier naar het lab ben gegaan en daar ben ik heel veel mensen dankbaar voor.

Allereerst wil ik mijn twee promotoren bedanken, die er voor gezorgd hebben dat ik het beste uit mezelf heb gehaald in de afgelopen zes jaar.

Beste René, bijna mijn hele wetenschappelijke carrière heb ik in jouw lab doorgebracht. Ik weet nog goed hoe erg ik besefte wat een geweldig lab jij wel niet had, op het moment dat ik in San Diego aan mijn stage bezig was. Jij hebt de gave om altijd een enthousiaste en inspirerende groep mensen te behouden en ik ben je heel dankbaar dat ik daar onderdeel van heb mogen zijn. Jouw (meestal) opbouwende, scherpe kritiek en onze discussies hebben me niet alleen als wetenschapper, maar ook als persoon sterker gemaakt en meer zelfvertrouwen gegeven. Daarnaast ben je een hartstikke gezellige vent, altijd in voor een biertje of een praatje, alhoewel je nieuwe functie je dat soms wel moeilijk maakt. Ik wens je heel veel succes en plezier met je voorspoedige carrière en ik hoop dat ik ook in de toekomst van je kan blijven leren!

Beste Geert, je kreeg me er destijds gratis bij, ik weet niet of jij hier zo blij mee was, maar ik in ieder geval wel! Ik ben altijd onder de indruk geweest van jouw kennis en intelligentie en vond het een eer om deel te nemen aan de werkbesprekingen met jou, Nannette en Saskia. Je hebt me geleerd om efficiënt te werken en me laten beseffen dat elk detail ertoe doet. Bedankt voor al je hulp de afgelopen jaren en je begrip tijdens dit laatste, lastige jaar. En niet te vergeten… de gastvrijheid van jou en Martine tijdens de jaarlijkse Bunnik-side BBQ's!

En dan nu mijn twee paranimfen, mijn maatjes in het lab. Ik ben supertrots dat jullie me bijstaan tijdens de verdediging.

Beste Marvin, man, ik mis je nog steeds in het lab! Wat heb ik van jou veel geleerd, jouw onuitputtelijk enthousiasme, intelligentie en kritische vragen hebben mij altijd op scherp gezet. Tot diep in de nacht biertjes drinken en praten over wetenschap, dat is jou op het lijf geschreven. En niet te vergeten je bizarre woordgrapjes, ik probeer het af en toe ook tijdens de lunch, maar zonder succes. Ik heb ontzettend genoten van onze etentjes, wintersport-tripjes en niet te vergeten het geweldige huwelijk van jou en Matilde in Florence, ik zal het nooit vergeten. Bedankt voor je vriendschap. Tot heel snel in SF!

Lieve Nannette, jouw scherpe kijk op het leven en de wetenschap is verfrissend en heeft mij regelmatig verrast en aan het denken gezet. Ik ben heel blij dat ik zoveel van je heb kunnen leren tijdens het maken van CiMKi en vind het super dat je er zulke mooie beurzen mee hebt binnengehaald. Nu nog een beetje geduld en dan kunnen jij en Ajit ook echt aan de bak met de muisjes, ik kan me bijna niet voorstellen dat dat geen succes wordt. De afgelopen twee jaar waren niet makkelijk voor jou en ik heb veel respect voor de manier waarop jij ermee om bent gegaan. Je bent supersterk. Lieve Nannette, bedankt voor al onze gezellige, emotionele en hilarische gesprekken en ik hoop dat we in de toekomst nog vele biertjes en roodjes samen kunnen drinken!

En dan zijn er nu nog een aantal lieve mensen die ik in het bijzonder wil bedanken. Jammer dat ik niet 7 paranimfen kan hebben..
Lieve Jonne, wie had nou gedacht dat we 20 jaar later zouden eindigen als bench-maatjes, toen we in het Rompert Park buskruit aan het spelen waren? Ik ben superblij met onze gezamenlijke Bossche roots, want ik heb daardoor de afgelopen jaren kunnen genieten van je vrolijke en relativerende persoonlijkheid. Naast je gezelligheid, hebben jouw scherpe vragen en opmerkingen mijn tijd in het lab verrijkt. Ik wil je ook heel erg bedanken voor je steun het afgelopen jaar in de vorm van een luisterend oor, auto-tripjes en een iPad. Heel veel plezier met het afronden van je succesvolle AIO periode en kom nou ook gewoon naar Californië, kunnen we daar weer verder lachen!

Lieve Matilde, jij pittige, slimme Italiaanse! Wat ben ik blij dat ik jou ontmoet heb, niet alleen omdat je heerlijk kan koken, maar ook omdat je een hart van goud hebt. Ik vind het heerlijk om met jou sushi of kaasjes te eten en over weten- of vriendschap te praten. Ik heb je het afgelopen jaar gemist en ben heel blij dat we binnenkort lekker samen Pale Ale's en sushi kunnen gaan nuttigen in SF.

Lieve Saskia, wat moet ik nou zonder jou op congres? Achter jouw rustige, lieve persoonlijkheid schuilt een hele wereld van kritische opmerkingen, creatieve ideëen en liefde voor 'het laatste biertje'. Ik heb genoten van onze uitstapjes naar Arcachon, NY, SD en Montpellier en ik hoop dat we er daar in de toekomst nog wat aan toe kunnen voegen. Sas, heel veel plezier en succes in Cambridge, ik bewonder je doorzettingsvermogen en weet zeker dat er een geweldige wetenschappelijke carrière voor jou in het verschiet ligt. Vertrouw er zelf ook op!

Lieve Rens, ik weet nog heel goed hoe erg ik onder de indruk was van je intelligentie en enthousiasme na onze eerste ontmoeting op het NKI. Ik heb zo ontzettend genoten van mijn stage bij jou en zal nooit vergeten hoeveel je mij hebt geleerd. Jouw onuitputtelijke energie en onbevangenheid heb ik altijd bewonderd. Ik wil jou en Ten ook heel erg bedanken voor de gezellige etentjes en wintersport-weekjes, ik zal ze missen. Heel veel geluk in de toekomst met kleine Faye, Fabian en je lieve vent.

Lieve Judith, jij ontzettende enthousiasteling! Wanneer ga je zelf nu eens inzien dat je een supergemotiveerde, slimme AIO bent en dat veel mensen iets van jou kunnen leren?? Ik heb genoten van je als kamergenootje op het UMC, lekker 's ochtends koffie drinken en praten over proeven. En ookal waren we allebei niet zo te spreken over het reizen van en naar het NKI, jij maakte het wel een stuk gezelliger! Bedankt voor je steun (iPad!!) en medeleven het afgelopen jaar en herinner me eraan dat ik op Berkeley nog steeds even moet informeren over die 'package-deal'. Geniet nog van je tijd op het NKI, maak er iets moois van! YOU can Do IT!

Next, I want to thank all the Medema lab-members, which made the lab-life so inspiring and fun. First, the former lab-members: Dear Monica, you were the best roommate ever, I still miss your presence and will never forget the great times we had in and outside the lab. I wish you and Juan all the best in Madrid and hope to see you again! Arne, I enjoyed listening to your models and watching your moves on the dance-floor! All the best in Sweden and good luck with the patterns! Libor, I have never seen anyone work as hard as you, but then again, no one can produce such beautiful blots either. I've always enjoyed your presence in the lab and hope you've put your horse in a safe place. Claudio, was fun having you in the lab, enjoy your second time in Utrecht! Vincent, you sweet guy, all the best in the Heck lab. Andre (Maia), I will never forget your speech and the sugar cookie in between your teeth in Montpellier, thanks for your humor and enthusiasm! All the Spanish girls! Veronica, Tania, Alba and Belen, you really live life to the max! Veronica, too bad we could only enjoy you for a short

period. Tania, congratulations with your PhD, Alba: thanks for the nice conversations and your positive attitude! Don't forget the Medema lab! Belen, you loud Spanish woman! Thanks for the fun we had and remember, think in positive! I will! Bilge, good luck with your PhD and Jolanda, Erica en Anneloes, bedankt!

And of course I also want to thank all the present lab-members, which even make the busy, warm, low-oxygen NKI-offices fun to work at! Wytse, bedankt voor je droge humor en heel veel succes met het afronden van je Tousled-verhaal! Lenno aka Lennie, je hebt naar Monica d'r wijze woorden geluisterd: van teveel-bier-drinkende student naar serieuze OIO, komt helemaal goed met jou! Indra! Ik zal je bizarre vragen missen, altijd lachen met jou, heel veel succes met je (geplande) toekomst! Dear Rita, you're the sweetest person I've ever met. Please, stay like this, don't let those Dutch people make you hard. I'm very proud that you're the one that will keep the ´CIN-soul´ alive in the lab, I'm sure you'll do great! Enjoy Holland! Roy (ke), bedankt voor je enthousiasme, deddel lekker verder in het lab, het gaat je supergoed af tot nu toe! Dear Mihoko, running-queen! Good luck with your cortical Dynein-project and relax once in a while! Dear Melinda, we've been roommates for a long time and I've always enjoyed your happy personality! Keep up the great pipetting! Daniël, bedankt voor je hulp bij mijn zoektocht naar een postdoc plek en natuurlijk je cynische opmerkingen. Beste Rob, wat ben jij een geweldige persoon om in het lab te hebben. Alles onder controle en ondertussen altijd tijd voor een bakkie, wat moet het lab zonder jou? Superbedankt voor al je hulp, vooral tijdens de verhuizing, je bent top! Lieve Femke, wat ben jij al ontzettend gegroeid (wetenschappelijk gezien dan hè) in het afgelopen jaar, dat voorspelt veel goeds! Ik wacht op je Nature paper! Juan, thanks for your sweet personality and all the best in the future, enjoy your family! And of course the two new people in the lab: Andre and Anja, it was fun to meet you, too bad that it was a bit short. Anja, succes met je Xenopus-proeven, supercool dat je dat hier gaat opzetten! Andre, enjoy the lab and don't cheer too hard for your team during WC 2014. En niet te vergeten alle secretaresses, en dat waren er heel wat… Noëline, Claudia, Cristine, Marie Anne, Merel en Marianne, sorry als ik iemand vergeet. Bedankt voor jullie hulp bij alle administratieve rompslomp! En niet te vergeten, mijn twee studenten: Henrike en Nina, ik heb veel van jullie geleerd, ik hoop jullie ook van mij, bedankt!

And…of course the Kopsjes! Thank you for adopting me once in a while and for the great discussions and borrels we had! Adrian, thanks for teaching me how difficult the mitotic checkpoint actually is... And of course for always giving input on my projects. All the best in Dundee together with Joanne and the little one, hope to see you in the future! Tale, bedankt voor je ontzettende vrolijkheid, altijd gezellig met jou, succes met het afronden van je PhD! Mathijs, Mattie, wat moeten Coen en ik nou met een WK zonder jou? Bedankt voor je gezelligheid en succes met al je mooie proeven! Livio, bedankt voor al je hulp met borrelen, dansen, als laatste overblijven op feestjes en natuurlijk de microscopen! Ongelooflijk, waar jij jouw energie vandaan haalt! Heel veel plezier en geluk in de toekomst met Kate en je lieve kids. Ik hoop je nog vaak op feestjes tegen te komen! Wilco, een getrouwd man, nu nog je Dr. titel! Ajit, jammer dat ik niet langer met je heb kunnen werken. Je bent zo'n vrolijke gast, die paar dagen dat ik met je heb gewerkt waren echt kei gezellig! Ik ben blij dat er nu iemand anders is die tegen Nannette kan zeggen dat het zo echt wel goed genoeg is. Succes met je studie en veel plezier in het CiMKi project! And of course.. Banafsheh, Nina, Vincent, Antoinette, Eelco, Merel, Manja, Benedict(in) e and Jasmin: It was great to get to know all of you, maybe we'll meet again in the future!

En het volgende lab op het lijstje! Beste Susanne, ondertussen kennen we elkaar ook alweer een tijdje. Ik vind het heel fijn om te zien dat je altijd zo enthousiast bent over de wetenschap, zelfs als het even niet loopt zoals jij wilt. Bedankt voor al je input in mijn projecten en je hilarische acteerkunsten tijdens

promotie-stukjes! Je bent een voorbeeld voor vrouwen in de wetenschap en ik wens je superveel succes in de toekomst! Lieve Maike, slimmerik! Ik heb genoten van de congressen waar we samen naartoe zijn geweest en je 'Devil's advocate' act op borrels. Ik ben blij dat het allemaal helemaal goed gekomen is met je promotie en je mooie zoontje Beau. Heel veel succes met je sollicitaties! Gerben, bedankt voor je interesse aan het begin van mijn AIO tijd, supertof dat je een positie in Duitsland hebt gevonden, ik wens je veel plezier samen met Barbara en Julia. Beste Martijn, mede-Brabo, bedankt voor alle lol die we op het lab en op borrels hebben gehad! Nu je vader wordt, moet je die laatste trein naar het mooiste stadje van NL echt niet meer missen! Heel veel geluk in de toekomst en hopelijk tot ziens! Beste Rutger (AIO met de gouden handjes), Carin, Amanda, Arianne, Armando, Sanne and Sylvie, thanks for the fun at borrels, retreats and in the lab, good luck in the future!

Beste Benjamin, bedankt voor je hulp bij het schrijven van brieven en grants! Ik heb heel veel geleerd van de manier waarop jij je projecten bedenkt en vind het heel leuk dat jij iedereen altijd bij je ideeën betrekt en vervolgens ook goed naar andermans suggesties luistert, hoe nutteloos die soms ook zijn. Ik heb er vertouwen in dat er hele mooie dingen uit jouw lab gaan komen, al helemaal met die twee kanjers van AIO's! Dear Ahmed, thanks for your positive attitude and your emails during the time I was at home working or recovering, I appreciate that a lot. I wish you all the best with your projects, enjoy! Oh, and thanks for the sandwich.

I also want to thank all the rest of the B5 colleagues for giving us such a warm welcome, too bad I could only enjoy you for a short period. Beste Wolthuisjes, Rob, bedankt voor je kritische vragen en sterkte in deze lastige tijden. Beste Linda: zoals jij geen ander, bedankt voor je gezelligheid op borrels, voor ons leuke tripje naar NY en je interesse in mijn projecten en problemen. Heel veel succes met het vinden van een mooie postdoc plek! Beste Michiel, bedankt voor je enthousiasme, onze fietstripjes van en naar Zuid en je grapjes, als je nog iemand zoekt als sidekick, ik houd me aanbevolen! And of course, the rest of the Wolthuis lab: Erik, Janneke and Connie, thanks for the fun these last months!

En natuurlijk wil ik ook de 2e verdieping-bewoners van het Stratenum bedanken voor alle gezellige retraites, kweekuurtjes en borrels: Onno, Danielle en alle chirurgen (in spe): Winan, Benjamin, Lutske, Frederik, Menno, Ernst en Klaas: ik heb altijd heerlijk met jullie kunnen praten over van alles en nog wat, bedankt voor jullie gezelligheid! Dear Jamila, thanks for the nice conversations we've had, already during my internship, but also later when you came back to the Stratenum. I'm happy to see that you, Onno and your kids are doing so fine, all the best in the future!

En het Voest lab natuurlijk, Emile, naast een goede arts, ook een goede wetenschapper, ik heb altijd genoten van je input tijdens de jaarlijkse retraites. Beste Laura, harde werkster, er zijn maar weinig mensen die zo hard lopen als jij, heel veel succes met je opleiding en het afronden van je promotie. Beste Marlies, Jeanine, Joost, Marco, Julia, Ilse, Martijn, Stephanie, Judith en Rachel, bedankt voor het prettige contact! Beste Sander, bedankt voor de lol die we hebben gehad, haha, wa nou… heel veel succes nog met de laatste loodjes, ik hoop dat je binnenkort op een inspirerende plek verder kan gaan!

Beste Patrick, bedankt voor je hulp aan Nannette en mij bij het bedenken en maken van ons muismodel. En daarnaast voor je poging aanwezig te zijn bij de hoorzitting in Den Haag. Ik heb altijd leuk met je kunnen praten over allerlei zaken, veel succes bij de Pathologie! Lieve Miranda, superbedankt voor al je hulp bij de muizenprojecten, zonder jou was er denk ik helemaal niks van de grond gekomen. Fijn dat je altijd in was voor een gezellig gesprek of een borrel, je bent een topper! Beste Ron, niet altijd even positief, maar wel eerlijk! Succes in de toekomst! Beste Robert en Eva, bedankt voor jullie

gezelligheid bij borrels en in het lab!

I also want to thank the Burgering, Bos, Timmers, Vermeulen, Dansen, Rehmann and Holstege labs for making the Stratenum a great place to work, both scientifically and socially! I especially want to thank Peter, Willem-Jan, Marten, Anna, Astrid, Maaike, David, Hesther, Evi, HarmJan, Marjolein, Diana, Andree, Rik, Maria, Hettie, Marrit, Marieke, Martijn, Lars, Fried, Sarah, Anneke and Holger for joining our borrels, I hope we'll meet in the future again!

Wim en handlangers: bedankt voor jullie hulp bij alle computerproblemen!

Cristina, bedankt voor je gezelligheid, je harde lach en je hulp bij vragen waar onze secretaresses geen antwoord op hadden! En ik raad je aan om niet meer achterin een Fiat 500 te gaan zitten als René achter het stuur zit.

Tobias, Mr. T., wat heb ik genoten van jouw heerlijke kookkunsten, dankjewel daarvoor! En natuurlijk voor je bijdrage aan al onze borrels, feestjes en natuurlijk het CiMKi project. Hoe vaak ik N wel niet heb horen zeggen: ik zat gister met Tobias te denken… Bedankt en veel succes met al je redox-plannen!

Ik wil ook nog een aantal van de mensen bedanken waarmee ik leuke en nuttige samenwerkingen heb gehad:
Het van Rheenen lab, wat een gezellige boel is dat. Dacht ik al in het leukste lab van Nederland te zitten, jullie komen er toch ook wel heel dichtbij in de buurt… Beste Jacco, bedankt voor je onuitputtelijk enthousiasme en je geduld met het uitleggen van alle FLIM/FRET/Multiphoton/etc. dingen. Je hebt zoveel coole projecten lopen, ik ben benieuwd naar al je toekomstige papers! En ook bedankt voor je steun het afgelopen jaar. Lieve Evelyne, wat waren dat toch leuke uurtjes daar in dat donkere hol beneden. Zelfs op oudjaarsdag maken we er nog een dolle boel van met de appeltaart en de vette FRET! Hoe rooier, hoe dooier, zal ik nooit meer vergeten! En nu mooie proeven doen met je TOP muis! En de rest van het van Rheenen lab: Laila, Anoek, Saskia, Anko, Ronny en Nienke, bedankt voor jullie input, lekkernijen, biertjes en gezellige gesprekken!

Frank, Wouter, WJ and Hsin-Yi, thanks for the fun we had in organizing the retreat, all the best of luck in the future.

Dan wil ik ook nog Stieneke en Hugo bedanken voor jullie hulp bij het muizenproject. Wat heb jij alles netjes op orde Stieneke, heel fijn dat Nannette en ik van je expertise gebruik mochten maken, dankjewel. En Hugo bedankt voor je input aan het begin van ons project en veel succes met het opzetten van alle organoid-experimenten op het Stratenum!

Wigard, Eward en Edwin, ik hoop dat jullie de oorzaak van chromothripsis nog gaan vinden, ik zet nog steeds in op chromosoom missegregaties! Succes met alles! Ellen, uiteindelijk geen translocaties gevonden, maar ik wil je wel heel erg bedanken voor je hulp en inzet!

Karoly, thanks for our fruitful collaboration and the nice conversations we had about chromosomes, I learned a lot from you! Beste Marja, bedankt voor al je hulp bij het analyseren van de COBRA's, zonder jou waren we nergens geweest!

En onze samenwerkingen binnen het TiPharma project: Beste Guido, Husam, Björn, Rogier en Joost,

bedankt voor al jullie hulp bij de *in vitro* en *in vivo* proeven. Het is een mooi stuk geworden, hopelijk volgen er nog meer! Heel veel succes in de toekomst! Beste Jos, bedankt voor je input in al onze muizenprojecten, dat hadden we hard nodig! Lieve Ute, superbedankt voor al je hulp met de muisjes, ik heb veel van je geleerd dit laatste jaar!

Tijdens alle gezellige, leerzame labmomenten was ik natuurlijk niks waard geweest zonder mijn lieve vrienden en familie. Lieve Nel, Hel, Sus, Veer, Cor, Maart, Rosa & Margot: Ik ben zo blij met jullie, daar is een dankwoord niet genoeg voor. Ik hoop dat jullie dat wel weten. Toch wil ik jullie ontzettend bedanken voor alles: Gezellige weekendjes weg, hilarische en gestoorde avondjes met wijntjes, biertjes, dansen en lekker eten. En natuurlijk jullie steun en interesse tijdens mijn gehele promotie, maar met name dit laatste jaar, door jullie heb ik het toch nog allemaal weten vol te houden, bedankt lieverds, ik hou van jullie! Lieve Moetoe, we zien elkaar niet vaak, maar als we elkaar zien is het altijd gezellig, bedankt voor je lieve vriendschap en de roti natuurlijk. Lieve Rins, 11 jaar geleden alweer dat we elkaar moesten ondersteunen bij de UBV feestjes en still going strong! Ik heb altijd genoten van onze etentjes en gesprekken tijdens onze promoties en wens je superveel succes bij Jacco! Lieve Lon, Jan & Jas, bedankt voor alle gezellige LAJJM momentjes, ik heb ervan genoten, het heeft me geholpen te relativeren en ontspannen, thnx lieverds!

En mijn lieve familie Lacor, die me het afgelopen jaar nog dierbaarder is geworden. In het bijzonder wil ik Marga en Ellen bedanken: wat zijn jullie sterk! Ik heb ontzettend veel van jullie geleerd en wil jullie bedanken voor al jullie steun en ik wil jullie veel sterkte wensen in deze lastige tijden. En dan wil ik ook nog graag Rik, Wim, Alex, Wendy, Conny, Mieke, Ben en Oma bedanken voor jullie belletjes en steun. Lieve Carine, mijn favoriete nicht, al sinds we klein waren: 2^{e} halte uitstappen en dan heel de dag door het Vondelpark leuren. Ik kan zo heerlijk met jou praten en lachen! Ik wil je ook heel erg bedanken voor je steun deze laatste maanden en wil jou ook heel veel sterkte wensen, ik ben er als je me nodig hebt!

En de grote Suurs-familie: Lieve Marianne, René, Els, Marcel, Agnes, Inge, Pamela, Angela, Sonja, Ronnie, Kim & Mathijs: bedankt voor alle hysterische verjaar- en feestdagen! Ik ben heel blij dat jullie zo lief voor me zijn en ik kan me geen betere (ja nu echt….) schoonfamilie wensen!

Lieve Pap (of Henk, wat jij liever hebt) en Freek, hebben we er ons maar mooi doorheen geslagen hè. Ik ben trots op ons en op jullie en wil jullie bedanken voor alles! Lieve Katherine, bedankt voor je altijd lieve woorden, komt helemaal goed met jou! Heel veel geluk samen met m'n broertje.

And last, but not least…Lieve Coen, wat had ik zonder jou gemoeten deze jaren? Ik ben zo blij met jou en alles wat je me hebt gegeven, ik weet niet hoe ik dat in woorden kan uitdrukken. We hebben ons door lastige tijden heengeslagen en nu gaan we weer eens lekker genieten: Op naar de Golden State! En ik weet het: 'het komt allemaal goed'. Ik hou van jou.

Aniek